



Wrocław University
of Science and Technology

DOCTORAL THESIS

Monitoring of fiber reinforced polymers using fiber Bragg gratings inscribed in highly-birefringent optical fibers

Mgr inż. Karol Wachtarczyk

Supervisor:

Prof. dr hab. inż. Jerzy Kaleta
Department of Mechanics, Materials
and Biomedical Engineering
Wrocław University of Science and Technology

Second supervisor:

Univ-Prof. Dr.-Ing. Ralf Schledjewski
Chair for Processing of Composite Materials
Montanuniversität Leoben

Keywords: highly birefringent fiber,
fiber Bragg grating, carbon fiber
reinforced polymer, manufacturing
process monitoring, structural health
monitoring

WROCŁAW 2023



European Union
European Social Fund



Doctoral thesis co-financed by the European Union under the European Social Fund,
project no POWR.03.02.00-00-I003/16

ACKNOWLEDGEMENTS

This work would not have been possible without the support of other people and opportunities I had.

I am very grateful to my two supervisors: prof. dr. hab. inż. Jerzy Kaleta and Univ-Prof. Dr.-Ing. Ralf Schledjewski for their experience, patience and valuable feedback. Together with them, I am extremely grateful to my informal supervisor dr inż. Paweł Gašior. He introduced me to the world of fiber optic sensors and constantly helped me with his experience and insightful comments.

I would like to thank for the financial support from projects: “InterDok – Interdisciplinary Doctoral Studies Projects at Wroclaw University of Science and Technology” and mobility program “Mobility program financed by the Polish National Agency for Academic Exchange (NAWA) and Austria’s Agency for Education and Internationalisation (OeAD)”, which allowed me conducting interdisciplinary research in cooperation with Chair of Processing of Composites, Montanuniversität Leoben

Many thanks to all the people I’ve met at the Department of Mechanics, Materials and Biomedical Engineering. Special thanks to Przemek who was my guidance in previous years.

I would like to express my gratitude to the whole team at the Chair of Processing of Composites, Montanuniversität Leoben, where all the composite manufacturing took place. Special thanks to, Neha, for all the help related to ATL and for the conversations we had. Thanks also to Marcel for his help with the RTM.

I’d like to thank the teams at the Institute of Electronic Systems, Faculty of Electronics and Information Technology, Warsaw University of Technology, and the Institute of Chemical Sciences, Faculty of Chemistry, Maria Curie-Skłodowska University, for giving me access to the fiber optic sensors, which were an essential part of the whole research.

Last but not least, I would like to thank my family. In particular, I would like to thank my wife Joanna for her incredible patience and constant support, and my daughter Jadwiga for her heart-warming smiles.

ABSTRACT

The main objective of the dissertation was to investigate the feasibility of effective use of embedded fiber Bragg gratings inscribed in highly-birefringent optical fiber (HB FBG) to measure strain during the manufacturing and exploitation stages of continuous fiber reinforced polymers and composite structures. Meanwhile, **the application goal** was to present ways to use HB FBG sensors in two selected modern composite manufacturing processes, namely resin transfer molding (RTM) and automated tape layup (ATL).

A thesis was stated, that the proposed generation of HB FBG sensors would allow the monitoring of the manufacturing processes of thermoset and thermoplastic matrix composites, as well as allow the measurement of the complex state of strain within the composite structure, both under quasi-static and time-varying loading conditions. It was concluded that the **following key tasks** were necessary to achieve the main objectives and prove the thesis of the dissertation:

- Building of a measurement system with fiber Bragg grating inscribed in a side-hole (SH) birefringent fiber,
- Application of HB FBG type fiber optic sensors for monitoring of a composite curing during the RTM process and for testing composites under bending conditions,
- The application of HB FBG sensors for monitoring composite fabricated by ATL process.

A review on the state of the art in fiber-reinforced composite monitoring, the sensors used for this reason and their integration techniques was conducted. The literature emphasizes that the anisotropic nature of composites, the diversity of their manufacturing techniques, and complex operating conditions make it challenging for monitoring systems to assess the service life, current health state and failure prediction in composite structures. Therefore, there is an observable trend towards the development of dedicated structural health monitoring (SHM) of the composite manufacturing process and the subsequent operation of composite structures. Moreover, it is known that advanced SHM systems consist of sensors deployed both on the surface and embedded inside the composite. Since the sensor are embedded at the composite production stage, the same sensors can also be used for process monitoring. There are various types of sensors, which can be used for SHM. Among them are fiber optics sensors, which shape and size allow them to be integrated into the structure without compromising the mechanical properties of the composite. Fiber optic sensors capable to measure strain, monitoring various phases of the manufacturing process were studied in more details. Among the various types of fiber optic sensors, fiber Bragg grating (FBG), including the continuously improving HB FBG, were considered particularly useful in composites research. As a result of the conducted literature review, a research program was formulated.

In the next step, the own research was conducted. The first part described the building of a measurement system with a sensor inscribed in a highly birefringent optical fiber. The required optical fiber was obtained and Bragg gratings were inscribed into it using the phase mask technique. These steps were possible thanks to the support of two research facilities in Lublin and Warsaw. Next, the sensitivity of the manufactured HB FBG sensor was determined, which required the construction of an original test setup and supporting software. Known parameters of a commercial sensor were used to calibrate the custom sensor. As a result, the full usefulness of the measurement system with the original HB FBG sensor for measuring strain along its length and across its diameter was demonstrated. The novel HB FBG had a significantly higher sensitivity to transverse force than sensors inscribed in a commercial fiber.

The second part focused on the application of HB FBG fiber sensors to monitor the thermoset composite curing kinetics during the RTM process and to test the manufactured composites under bending loads. First, it was necessary to investigate the effect of the compression occurring in the RTM steel mold on the sensor embedded in the reinforcing fibers and to evaluate the possible degradation of the sensor reflection spectrum. The next step was to study the curing kinetics of the RTM process by identifying the gel point and determining the complex strain state due to the resin curing process. The manufactured composite plates were then tested under quasi-static bending loads to demonstrate the ability of the HB FBG sensors to measure the complex strain state. As a result, it was demonstrated that embedded HB FBG sensors can be used to monitor the RTM process and measure the strain of thermoset composites produced by this process.

The third part dealt with the application of HB FBG sensors to monitor a thermoplastic composite produced by the ATL process. First, the effect of process temperature and roller compaction force on the measurement performance of FBG sensors had to be evaluated. Then, the residual strain state was measured in the plane of the composite plate, and in the perpendicular direction, both during the layup of subsequent composite layers and after the entire production process. It was thus possible to observe the cumulation of strain during the ATL process. In addition, strain was measured under cyclic loading conditions. It was shown that HB FBG sensors can be applied to observe the change in material stiffness and measure the area of the mechanical hysteresis loop. This allowed the study of local fatigue processes in composite structures.

In the final part of the dissertation, conclusions and remarks were formulated and directions for further research were identified.

STRESZCZENIE

Głównym celem rozprawy była możliwość efektywnego wykorzystania zintegrowanych światłowodowych siatek Bragga na światłowodzie o wysokiej dwójłomności (HB FBG) do pomiaru odkształceń na etapie wytwarzania oraz eksploatacji kompozytów i konstrukcji kompozytowych wzmacnianych włóknami ciągłymi. **Celem aplikacyjnym** z kolei było zaprezentowanie sposobów wykorzystania czujników HB FBG w dwóch wybranych współczesnych technologiach polimerowych, a mianowicie resin transfer molding (RTM) oraz automated tape layup (ATL).

Przyjęto tezę, iż zaproponowana generacja czujników HB FBG umożliwi monitorowanie procesów wytwarzania kompozytów z matrycą duroplastyczną oraz termoplastyczną, pozwoli na pomiar złożonego stanu odkształceń, w tym wewnątrz struktury kompozytu, zarówno w warunkach obciążenia quasi-statycznego jak również zmiennego w czasie

Uznano, iż osiągnięcie celów pracy i udowodnienie tezy rozprawy, wymagało **podjęcia następujących zadań o znaczeniu kluczowym**:

- Wytworzenie układu pomiarowego ze światłowodem dwójłomnym typu side-hole (SH) na który wpisano siatkę Bragga,
- Zastosowanie czujników światłowodowych typu HB FBG do monitorowania kinetyki procesu wytwarzania kompozytów technologią RTM oraz badania kompozytów w warunkach zginania,
- Zastosowywanie czujników HB FBG w zakresie monitorowania kompozytu wytworzonego metodą ATL.

Dokonano przeglądu stanu wiedzy głównie z zakresu monitorowania kompozytów wzmocnionych włóknami, stosowanych do tego czujników i technik ich integracji. W literaturze przedmiotu podkreśla się, iż anizotropowość kompozytów, różnorodność technologii ich wytwarzania, złożone warunki eksploatacji powodują, iż ocena żywotności, dalszej przydatności i przewidywania awarii w strukturach kompozytowych jest wyzwaniem dla systemów monitorowania. Dlatego widoczny jest trend do tworzenia dedykowanego strukturalnego monitorowania (SHM) procesu wytwarzania kompozytów oraz późniejszej eksploatacji konstrukcji kompozytowych. Wiadomo przy tym, iż zaawansowane systemy SHM składają się z czujników rozmieszczonych zarówno na powierzchni jak i wewnątrz kompozytu, co wymaga ich integracji z kompozytem. Ponieważ integracja odbywa się na etapie produkcyjnym, można czujniki również wykorzystać do monitorowania procesu technologicznego. Istnieje wiele rodzajów czujników, które mogą być używane do monitorowania SHM. Przeanalizowano dokładniej literaturę przedmiotu dotyczącą czujników światłowodowych, które są w stanie mierzyć odkształcenie, monitorować różne fazy procesu produkcyjnego, a ich kształt i rozmiar umożliwiają zintegrowanie ich ze strukturą bez uszczerbku dla właściwości mechanicznych kompozytu. Spośród różnych rodzajów czujników światłowodowych za szczególnie przydatne w badaniach kompozytów uważane są fiber Bragg grating (FBG), w tym także i te ostatnio rozwijane typu HB FBG. Przeprowadzona analiza literatury ułatwiła w rezultacie sformułowanie programu badań własnych z uwzględnieniem aktualnego state of the art.

Przeprowadzono następnie badania własne. Pierwsza część dotyczyła wytworzenia układu pomiarowego ze światłowodem dwójłomnym. Pozyskano niezbędny światłowód i wpisano nań siatki Bragga przy użyciu techniki maski fazowej. Działania te możliwe były dzięki wsparciu dwóch ośrodków naukowych w Lublinie i w Warszawie. Następnie wyznaczono czułość wytworzonego czujnika HB FBG, co wymagało budowy oryginalnego

stanowiska badawczego i oprogramowanie wspomagające. Do kalibracji wytworzonego czujnika wykorzystano znane parametry czujnika komercyjnego. W rezultacie wykazano pełną przydatność układu pomiarowego z oryginalnym czujnikiem HB FBG do pomiaru odkształceń przy obciążaniu czujnika wzdłuż jego długości i w poprzek średnicy oraz o czułości na odkształcenia poprzeczne znacznie większej jak w czujnikach na włóknie komercyjnym.

Druga część dotyczyła zastosowania czujników światłowodowych typu HB FBG do monitorowania kinetyki procesu wytwarzania kompozytów na osnowie duroplastycznej technologią RTM oraz badania otrzymanych w ten sposób kompozytów w warunkach zginania. Na wstępie niezbędne było zbadanie wpływu ściskania występującego w formie stalowej do RTM na czujnik zagrzebany we włóknie wzmacniającym i ocenienie możliwej degradacji widma odbicia. W kolejnym kroku zbadano kinetykę utwardzania kompozytu w czasie procesu RTM przez identyfikację punktu żelowania, oraz wyznaczenia złożonego stanu odkształceń w następstwie procesu utwardzania żywicy. Wytworzone w ten sposób kompozytowe płyty były następnie badane w warunkach zginania, w celu wykazania możliwości pomiaru odkształceń w badaniach quasi-statycznych. Wykazano w rezultacie, iż zagrzebane czujniki HB FBG mogą służyć do monitorowania procesu technologicznego RTM oraz pomiaru odkształceń kompozytów wykonanych tą metodą.

Trzecia część dotyczyła zastosowania czujników HB FBG do monitorowania kompozytu na osnowie termoplastycznej wytworzonego metodą ATL. Zadanie wymagało najpierw oceny wpływu temperatury procesu i siły nacisku rolki na właściwości pomiarowe czujników FBG. Następnie zmierzono stan odkształceń resztkowych w płaszczyźnie płyty kompozytowej i w kierunku prostopadłym, zarówno w trakcie nakładania kolejnych warstw kompozytu jak i po zakończeniu procesu. Możliwa była zatem obserwacja kumulowania się odkształceń w trakcie procesu ATL. Dodatkowo przeprowadzono pomiar odkształceń w warunkach obciążeń cyklicznych. Wykazano możliwość wykorzystania czujników HB FBG do badania zmiany sztywności materiału oraz pomiaru pola pętli histerezy mechanicznej, co pozwala badać lokalnie proces zmęczenia struktur kompozytowych.

W części końcowej rozprawy sformułowano wnioski i uwagi oraz wskazano kierunki dalszych badań.

TABLE OF CONTENTS

Acknowledgements	i
Abstract	ii
Streszczenie	iv
Table of contents	vi
List of acronyms	viii
List of symbols	x
1. Introduction	1
1.1. Challenges in monitoring of fiber reinforced composites, applied sensors and their integration techniques	1
1.2. Optical fiber sensors used for the composite monitoring	2
1.2.1. Types of fiber optic sensors used for structural health Monitoring	3
1.2.2. Composite production and exploitation monitoring with fiber optic sensors ..	13
1.3. Fiber Bragg gratings inscribed in highly-birefringent optical fibers	23
1.3.1. Highly-birefringent optical fibers with inscribed FBGs	23
1.3.2. FBG in a single-mode fiber and response to strain and temperature	25
1.3.3. HB FBG's response to the mechanical load	27
1.3.4. Strain sensing in composites with HB FBG	31
1.4. Aim and scope of thesis	34
2. Manufacturing and calibration of FBG inscribed in highly-birefringent fibers	36
2.1. Side-hole fibers and inscription of FBG sensors	36
2.1.1. Bragg Gratings inscription and exemplary FBG spectrum	37
2.2. Review of HB FBG mechanical calibration devices and device used in the thesis	38
2.3. Software supporting the sensitivity testing of the HB FBGS and Bragg wavelengths determination	42
2.4. Mechanical testing of FBG inscribed in HB fibers and temperature calibration	46
2.5. Determination of fiber orientation with diffraction patterns	49
2.6. Summary	52
3. Resin transfer molding (RTM). Process monitoring with HB FBG sensors	53
3.1. Compaction tests of dry textiles with attached optical fibers	54
3.1.1. Compression of textiles on rig for sensor testing	55
3.1.2. Compaction using the textile compaction setup	57
3.1.3. Spectrum changes due to textile compaction	62
3.1.4. Summary of the study of textile-sensor interaction during compression	64
3.2. Resin curing monitoring	65
3.3. RTM process monitoring	68
3.3.1. RTM conditions and measurement setup for process monitoring	68

3.3.2. RTM process monitoring with SMF FBG sensors	71
3.3.3. Process monitoring with HB FBG sensors	72
3.3.4. Summary of RTM process monitoring with FBG and HB FBG sensors	76
3.4. Multi-axial strain measurement in a plate element.....	77
3.4.1. Four point bending of a composite plate with embedded HB FBG	77
3.4.2. Analysis of the effect of load configuration and HB FBG sensor location on strain measurement sensitivity	79
3.4.3. Summary on the application of FBG (HB FBG) sensors to plates produced by the RTM process	83
3.5. Summary on the application of HB FBG sensors for monitoring RTM process kinetics and determination of strain state in plate components.....	84
4. Automated tape layup (ATL). Monitoring with fiber optic sensors.....	86
4.1. Influence of the ATL processing parameters on FBG sensors performance.....	86
4.1.1. Investigation of the compaction force on the spectrum of regular FBGs.....	87
4.1.2. Monitoring of ATL process with SMF FBG sensors	89
4.1.3. Calibration of integrated FBG sensors	91
4.1.4. Summary of tests on ATL processing parameters on FBG sensor performance.....	94
4.2. Monitoring of residual strain in the ATL process with HB FBG sensors	95
4.2.1. ATL process conditions and measurement setup for process monitoring.....	95
4.2.2. In-plane and out-of-plane residual strain measured with HB FBG sensors	96
4.2.3. Summary of ATL process monitoring with HB FBG sensors	97
4.3. Quasi-static and cyclic testing of composite manufactured in ATL process	98
4.3.1. Quasi-Static tests of ATL samples with integrated HB FBG sensors	99
4.3.2. Monitoring of composite plates with integrated HB FBG sensors during cyclic four-point bending test	102
4.3.3. Summary of the application of HB FBG to monitor the plate produced in the ATL process in terms of quasi-static and cyclic bending	109
4.4. Summary of the application of HB FBG sensors for monitoring a composite manufactured by ATL process	110
5. Conclusions and future perspectives	112
5.1. future perspectives.....	115
List of tables	122
References	123

LIST OF ACRONYMS

Acronym	Description
BVID	Barely visible impact damages
NDT	Non-destructive testing
SHM	Structural health monitoring
RTM	Resin transfer molding
TRL	Technology readiness levels
FBG	Fiber Bragg grating
HB	Highly-birefringent
HB FBG	Fiber Bragg grating inscribed in highly-birefringent optical fiber
SMF	Single mode fiber
SMF FBG	FBG inscribed in single mode fiber, in terms of this thesis also referred as conventional or standard FBG
SH	Side-hole optical fiber
SH2 FBG	FBG inscribed in the side-hole ² optical fiber
PMMA	Poly(methyl methacrylate)
FOS	Fiber optic sensor
FPI	Fabry-Perot interferometer
CTE	Coefficient of thermal expansion
MZI	Mach-Zehnder interferometer
LPG	Long-period grating
PCF	Photonic crystal fibers
MI	Michelson interferometer
RIU	Refractive index unit
MMF	Multi-mode fiber
SOFO	Surveillance d'Ouvrages par Fibres Optiques
RMS	Root mean square
SI	Sagnac interferometer
TFBG	Tilted fiber Bragg grating
OTDR	Optical time-domain reflectometry
OBR	Optical backscatter reflectometry
SWI	Swept wavelength interferometry

SRI	Surrounding refractive index
CLPG	Chirped long-period grating
EFS	Etched fiber sensor
DSC	Differential scanning calorimetry
MOF	Microstructured optical fiber
PDL	Polarization-dependent loss
FEA	Finite element analysis
CFRP	Carbon fiber reinforced polymer
PCA	Principal component analysis
HDPE	High-density polyethylene
DSHF	Dual side-hole fiber
ATL	Automated tape layup
FWHM	Full width at half maximum
CCA	Cross-correlation algorithm
SH	Side-hole
FVF	Fiber volume fraction
NCF	Non-Crimp Fabric
LVDT	Linear Variable Differential Transformer
SNR	Signal to noise ratio
DC	Direct current
DEA	Dielectric analysis
ASTM	American Society for Testing and Materials
PEEK	Polyether ether ketone
PP	Polypropylene
TC	Thermocouple
UTM	Universal Testing Machine

LIST OF SYMBOLS

Symbol	Unit	Description
$\mu\varepsilon$	-	Microstrain (10^{-6} strain)
n	-	Refractive index
λ_B	nm	Bragg wavelength
ε	-	Strain
T	°C	temperature
Λ	Nm	Period of the FBG grating
G	-	Group birefringence
B	-	Phase birefringence
s_f/s_s	pm/(N/mm)	Sensitivity to the linear transversal force of fast/slow axis of HB FBG
s_{eff}	pm/(N/mm)	Sensitivity to the linear transversal force of peak separation of HB FBG
k_f/k_s	pm/ $\mu\varepsilon$	Sensitivity of fast/slow axis of HB FBG for transversal strain
k_{SEP}	pm/ $\mu\varepsilon$	Sensitivity of HB FBG peak separation for transversal strain
F	N	Force
φ	°	Orientation angle of optical fiber
θ	°	Angle between the optical fiber and reinforcing fibers
$K_{\varepsilon/T}$	pm/ $\mu\varepsilon$	Sensitivity of FBG for strain/temperature
N/N_f	-	Number of cycles/number of cycles to failure
E	GPa	Young modulus

1. INTRODUCTION

1.1. CHALLENGES IN MONITORING OF FIBER REINFORCED COMPOSITES, APPLIED SENSORS AND THEIR INTEGRATION TECHNIQUES

Composite materials have received increasing attention in recent decades [1,2]. For example, current aircraft (e.g. Boeing 787 or Airbus A350 XWB) consist of more than 50% composites by weight [2]. In this case, the use of fiber-reinforced composites makes it possible to improve energy efficiency (reduction of fuel consumption) and reduce emission [2,3]. Another key challenge is the urgent need for an energy transformation of the global economy. To give just two examples in this area, one can point to the widespread use of composites for wind turbine blades [4], but also pressure vessels for hydrogen storage for vehicles and stationary applications [5].

However, the use of anisotropic fiber-reinforced polymers is more challenging than that of metals. They are composed of two or more different materials, which is one reason for their less predictable failure mechanism [3]. For example, aerospace composites are exposed to moisture, which can cause microcrack growth through cyclic freezing and melting. Bird strikes, gravel, and dropped tools can cause, so-called barely visible impact damage (BVID), which can be points where the crack propagation begins. They are difficult to detect and may be omitted from routine pre-flight inspections. Even if a defect is detected, its propagation is difficult to predict because it depends not only on the material composition but also on the composite layup sequence [6].

The two most common methods of ensuring the operational safety of a structure are non-destructive testing (NDT) and structural health monitoring (SHM). NDT requires periodic general inspection of the structure. This can be done using ultrasound, X-ray, etc. [6]. NDT is based on scheduled technical inspections, which is not always technically and economically justified.

On the other hand, continuous monitoring of a structure with a dedicated SHM system increases the probability of damage detection [1] and also predicts the service life or maintenance schedule. This can be achieved with a dedicated SHM system. It consists of sensors distributed throughout the structure and the data processing system that supports the maintenance decision. The SHM system does not require a lot of human resources, because after the sensors are installed and the system is deployed, the monitoring is done online during the whole lifetime.

The composite manufacturing process also needs to be monitored. Cost optimization in composite manufacturing is driving processes to reduce fill and cure time. At the same time, variations in material batches affect the reproducibility of the process. To avoid filling errors, uncured products, and degradation of mechanical properties due to residual stresses, process monitoring can be a viable solution [7].

SHM and production monitoring typically use different sensors. SHM requires sensors that can be integrated or attached to the structure and measure the response on-line. Because they are attached to the structure, in many cases they cannot be reused. Composite manufacturing process monitoring, on the other hand, prefers sensors that can measure the process without requiring extensive preparation of each composite structure, so they do not affect process efficiency. The best solution for molding processes, such as resin transfer molding (RTM), is to use sensors integrated into the mold. [7].

SHM of composites can be performed with surface-mounted sensors, but this makes them vulnerable to accidental external damage [8]. Moreover, they cannot be used to monitor the material state inside the material. In this case, a good approach is to integrate them into the composite. Since the integration is done at the manufacturing stage, they can also be used for manufacturing monitoring [9,10].

There are numerous types of sensors that can be used for SHM and process monitoring (piezoelectric [11–13], piezoresistive sensors [14–16], fiber optic sensors [3,8,17]). Piezoelectric sensors can detect damage at a distance from the sensor due to the propagation of vibrational waves. On the other hand, due to their size, they cannot be integrated into the structure [12]. Recently, attention has been paid to carbon nanotube materials. They can be formed in a layer (buckypaper/film) [18] or braided together with textile [16]. This type of sensor is very promising, but work is still at a low technology readiness level (TRL) [3]. This technology still needs more research to mature. Fiber optic sensors are able to accurately measure strain, monitor various composite manufacturing processes, and their shape and size allow them to be integrated into the structure without compromising the mechanical properties of the host material.

Among the various types of fiber optic sensors, Fiber Bragg Gratings (FBG) are probably the most popular. They can be multiplexed along a single optical fiber, allowing for coverage of multiple hot spots in the final structure. The response of FBG sensors based on single-mode fiber (SMF) is affected by strain along the optical fiber and temperature variations. For strain measurements, temperature can be compensated for with additional sensors or another FBG placed nearby. However, if the FBG sensor is inscribed in a highly birefringent optical fiber instead of a single-mode fiber, it can also be successfully used to measure strain in the transverse direction. Highly birefringent FBG sensors are not widely available, and their application is more challenging than SMF FBG sensors. For these reasons, there are few application examples in the literature and they are limited to thermosetting composites [19–23].

In view of the above, it can be concluded that the following topics:

- monitoring of the manufacturing process and exploitation of composite materials and structures,
- new generations of fiber optic sensors applicable for composites monitoring,
- methods for embedding these sensors into the composite material

are current research problems of great scientific, economic and social importance.

1.2. OPTICAL FIBER SENSORS USED FOR THE COMPOSITE MONITORING

An optical fiber is a small diameter (typically 125 μm), light-transparent fiber, which can guide light along its length. A scheme of basic optical fiber is shown in Figure 1-1. The central part of the optical fiber - a core - has slightly higher refractive index than surrounding part (cladding). As a consequence, light that arrives to the core-cladding interface at angles θ smaller than critical angle ($\theta_c = \arcsin(n_{core}/n_{clad})$) are subjected to the total internal reflection. Due to reflections light is transmission through the fiber with very low losses. An optical fiber is mechanically protected with layer of coating [24,25]. An optical fiber is in most cases made out of silica or glass, but some of them are also made from polymers, e.g. PMMA or CYTOP [26].

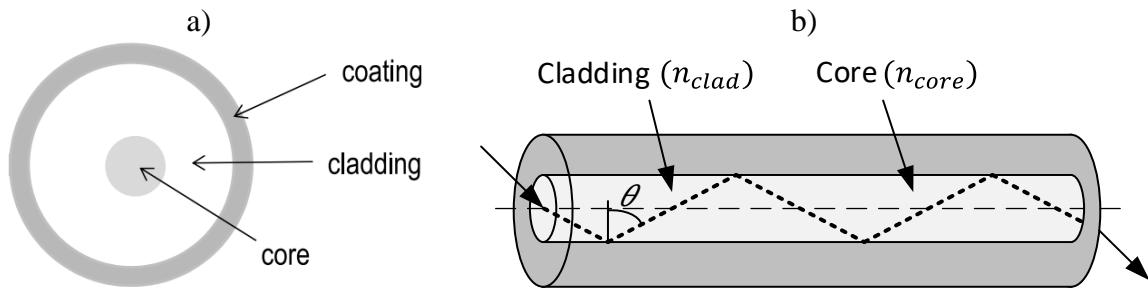


Figure 1-1: An optical fiber, a) Basic cross section [3],
b) working principle (based on [27]).

Fiber optical sensors (FOS) have many advantages for composite applications; they are compact, lightweight, are insensitive to the electromagnetic interference. Moreover, many fiber optical sensors can be multiplexed, thus reduce the amount of wiring. Shape of optical fibers makes them good option to be embedded into composites. It was shown that if FOS are properly integrated, they can have only small influence on the mechanical performance of the host structure [28]. Because of this reason, from decades many researchers used them for the embedded sensing applications.

1.2.1. Types of fiber optic sensors used for structural health Monitoring

Fiber optic sensors used for composites monitoring can be separated into three groups depending on the type of sensing method: interferometric, grating-based and distributed sensors (Figure 1-2). Interferometric sensors are single-point sensors, grating-based sensors have the capability to be multiplexed for multi-point sensing. Distributed sensors are based on analysis of the backscattering of an optical fiber, which technique allows measurement along whole fiber [2]. Characterization of these types will be provided in next sections.

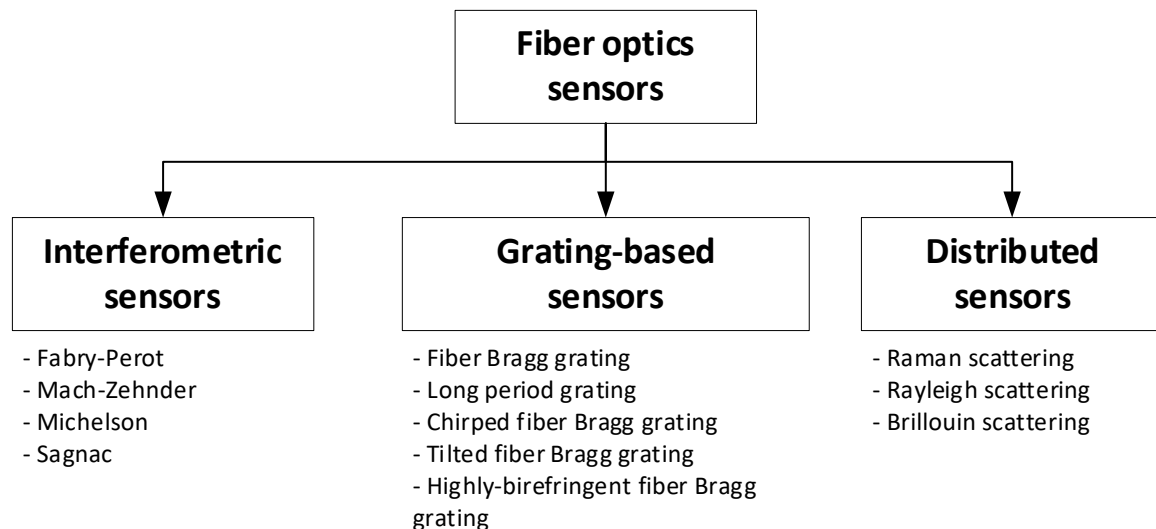


Figure 1-2: A classification of optical fiber sensors by sensing method used for the SHM (based on [2]).

A. Interferometric sensors

The working principle of interferometric fiber optic sensors is based on the light phase difference between the reference and measurement laser beams. If the length of one of the beam paths is changed, one of the beams is delayed, causing a phase difference between the two signals. There are few configurations of interferometers used in fiber optics, namely Fabry-Perot, Mach-Zehnder, Michelson, and Sagnac interferometer [2,24]. Basic schemes of these types are presented in Figure 1-3.

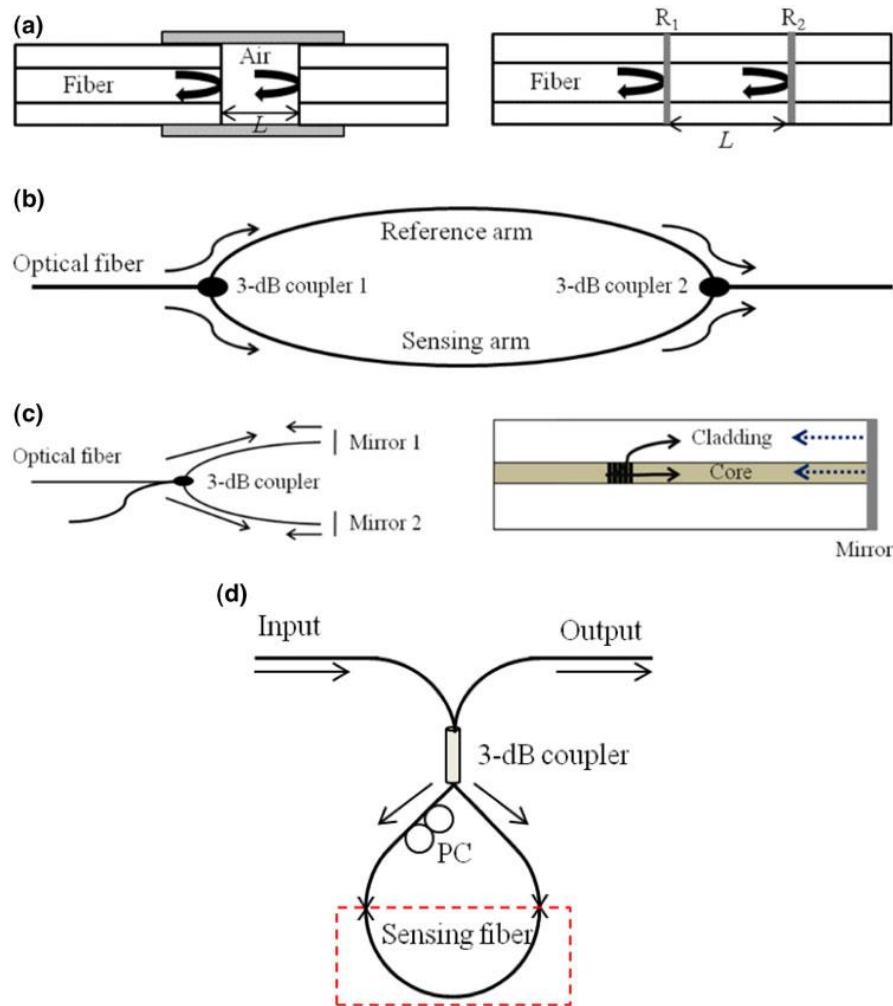


Figure 1-3: A diagram of different interferometric optical fiber types; a) Fabry-Perot, b) Mach-Zehnder, c) Michelson, d) Sagnac [29,30].

Fabry-Perot interferometer

One of the most popular types is Fabry-Perot interferometer (FPI) (Figure 1-3a). It is formed as a cavity with parallel reflecting surfaces. If coherent light is guided through a single optical fiber and approaches the cavity, some part of the light is reflected from both side of the cavity [31]. If distance between surfaces changes, phase between light beam reflected from both sides of the cavity changes as well.

FPI can have a form of an extrinsic FPI or intrinsic FPI. In the case of extrinsic FPI cavity is outside of the first optical fiber. A cavity can be formed by a second section of the fiber which is inserted in-line with first fiber into a quartz capillary (Figure 1-3a left) [31]. In the case of

intrinsic FPI cavity is formed inside the fiber itself (Figure 1-3a right). It can be made with e.g. chemical etching or laser micromachining/discharge [29,30].

To measure the external perturbation applied to the FPI, a length of the cavity has to be measured. For this reason, one has to count the number of fringes from the reflection spectrum over a specified wavelength range. Length of the cavity can be later calculated from the equation [31]:

$$L = \frac{m\lambda_1\lambda_2}{2(\lambda_2 - \lambda_1)} \quad (1.1)$$

where L is a length of the cavity, phase difference at wavelength λ_1 and λ_2 is $2m\pi$, and m is an integer.

The cavity length depends on the strain and temperature variations. The cavity's length change can be calculated as:

$$\Delta L = L\varepsilon + A\Delta T \quad (1.2)$$

where ε – strain, ΔT – temperature variation, A – temperature sensitivity, given as $A = L(\alpha_q - \alpha_f)$. $\alpha_{q,f}$ – coefficients of thermal expansion of a capillary and a fiber. If the extrinsic FPI is formed in a quartz tube, it is insensitive to the temperature, because coefficient of thermal expansion (CTE) of quartz and glass fiber is almost equal [31]. In this case ($A = 0$), strain can be calculated by:

$$\varepsilon = \frac{\Delta L}{L} \quad (1.3)$$

FPI-based sensors were reported to measure various measurands, among them strain, pressure (also on acoustic levels), refractive index and temperature [31,32]. One example of FPI sensor application for strain is temperature measurement was presented in paper [33]. Two SMF ends spliced together in such a way they form a rectangular air-bubble allowed measurement of strain with sensitivity of 43 pm/ $\mu\varepsilon$ with temperature sensitivity on the level of 2.0 pm/ $^\circ\text{C}$ [33] (Figure 1-4).

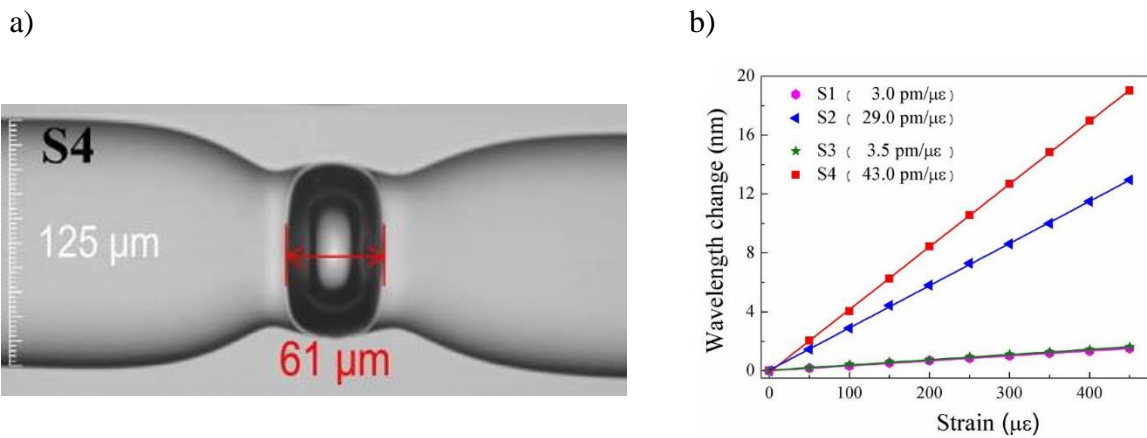


Figure 1-4: A FPI formed in fiber, a) Microscopic view; b) Wavelength shift of the interferometric fringe around 1550 nm to strain [33].

Another examples of FPI can be found in papers [32,34] A FPI dedicated for temperature measurement depending on the configuration can be used for the range up to 800 °C with sensitivity of 29.9 pm/°C [32]. An acoustic sensor based on the FPI measured the pressure with sensitivity of 198.3 nm/Pa, and minimum detectable sound level of $-1.54 \text{ dB}/\sqrt{\text{Hz}}$ (sensors was more sensitive than human ear) [34]. A gas pressure was measured with sensitivity of 4147 pm/MPa in range of 0-1.52 MPa. Extensive review of various uses of FPI is given in [32].

Mach-Zehnder interferometer

A basic Mach-Zehnder interferometer (MZI) contains two independent fibers, namely reference and sensing arms (Figure 1-3b). Incident light is first split into two beams, one – guided through the reference fiber, second – guided though the measuring arm. Both beams are recombined at the end of the fibers. The reference arm is isolated from the perturbation, only the sensing arm is exposed to it. When measuring arm is subjected to some perturbation which changes its optical path length, phase of the recombined signal changes. Counting of the interferometric fringes can be later calculated into the perturbation [29].

There are methods to form an MZI out of a single optical fiber. To achieve it, a part of the light from the core is coupled to the cladding modes and later recombined back into the core. A split of light can be achieved with various methods, long-period fiber grating (LPG) [35], air hole made with a femtosecond laser, connecting of photonic crystal fibers (PCF) or multi-mode fiber to the single mode fiber [30], connecting fibers with a core mismatch (offset, diameter difference) or fiber tapering [29].

Light propagates in the cladding of an optical fiber due to the total internal reflection at the cladding edge. A regular single mode fiber (SMF) is coated with a material with refractive index higher than the cladding, so total internal refraction doesn't take place and light escapes from the cladding. As a consequence, an MZI cannot be formed inside such a fiber. If a double-cladding fiber is used, a cladding beam travels in the internal cladding [29]. This is possible to measure the refractive index variations on the outside of MZI, because the total internal reflection is affected by the refractive index of the surrounding [29,36,37].

Measurands which are possible to be sensed with an MZI depend on the construction of the interferometer. A twin-core fiber based MZI allowed to measure strain and temperature with resolution of 1.2°C and 25.8 $\mu\epsilon$ [38]. In the case of an MZI in an asymmetric, two-core PCF connected with SMF simultaneous measurement of torsion, strain, temperature was performed with resolution of 1.88°, 47.61 $\mu\epsilon$ and 1.24°C (in the case of 1pm wavelength reading resolution) [39]. Another design was a segment of four-core fiber was spliced between sections of SMF fibers creating an MZI (Figure 1-5). Such an interferometer was reported to have a sensitivities of 209 pm/°C, 1.78 pm/ $\mu\epsilon$, 20.18 nm/m⁻¹ and 91.39 nm/RIU (reflection index unit) for strain, temperature, curvature and refractive index respectively [40].

a)

b)

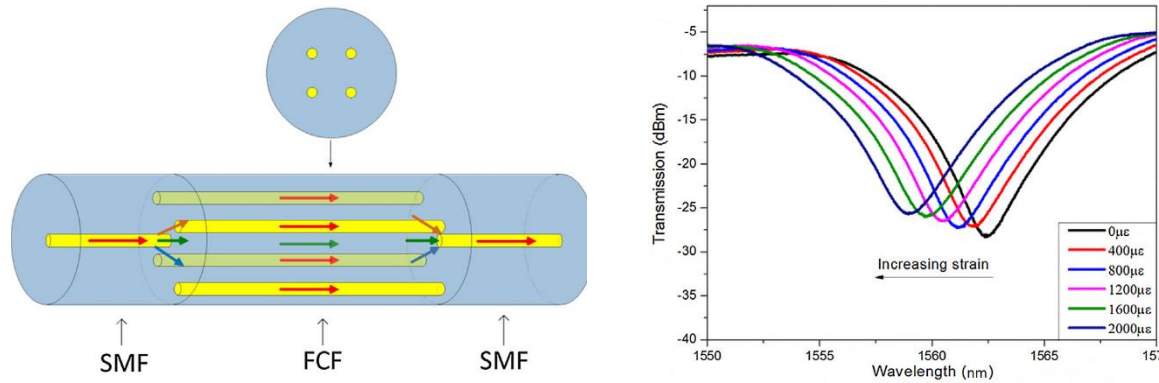


Figure 1-5: A Mach-Zehnder interferometer formed with a sections of SMF and four-core-fiber; a) schematic build; b) Response of interferometric fringe to axial strain [40].

An another sensing application can be found in paper [41]. A core-offset MZI for humidity measurement was constructed from sections of SMF, where a middle one was covered with graphene oxide. This sensor was capable to measure humidity with resolution of 0.0272 nm/%RH (percent of relative humidity) [41].

Michelson interferometer

A fiber Michelson interferometer (MI) has a similar working principle as MZI does. A scheme of an MI is shown in (Figure 1-3c). A light beam is split in two arms, but beams are reflected at the ends for the fibers. In these terms, an MI is almost like a half of MZI, but it analyses the reflection light instead of transmission. The reflection mode operation allows more compact design and easier handling than MZI. A MI can be also manufactured as an in-line configuration, with usage of methods used in MZI [29,30], e.g. a long-period grating, which couples a part of the light beam to the cladding (Figure 1-3c, right).

Possibilities of MI for measurement of various quantities were reported in the literature. MI is often used to measure temperature and refractive index of surrounding material [29]. Two single-mode optical fibers with core offset of 50 μm allowed measurement of humidity and temperature with -0.83 dB/%RH and 9.5 $\text{pm}/^\circ\text{C}$ resolution respectively [42]. A temperature variation dependency in the RIU measurement was reduced through fabrication of MI with a photonic crystal fiber (PCF) with a silica rod at the end. This setup measured variations of RI, with 850 nm/RIU [43]. A quasi-Michelson interferometer, which consisted of two sections of SMF and MMF in the middle, with an end surface covered with silver, shown a response to the variations of refractive index and temperature with sensitivities of -574.6 (pm/mm)/RIU and 61.26 $\text{pm}/^\circ\text{C}$ [44].

A popular sensor used for the structural health monitoring, namely type SOFO (fr. “Surveillance d’Ouvrages par Fibres Optiques”, structural monitoring by optical fibers [45]) is based on MI. The SOFO sensor consist of a pair of single-mode fibers. The measurement fiber is in contact with the structure, while the reference fiber is placed near this fiber, but it is loose. Proximity of both fibers causes compensation of temperature variations, so only strain is measured [45].

To achieve an absolute strain measurement, a low-coherence MI in tandem configuration is used (Figure 1-6). First MI is a SOFO sensor, and second MI is integrated into the data collecting unit. The interferometer in the unit is equipped in the moving scanning mirror, which allows introduction of length unbalance between sensor arms, which allows absolute

measurements [45]. This type of sensor measures strain with precision of $2 \mu\epsilon$ RMS (root mean square), while the sampling rate doesn't exceed 1 Hz [46].

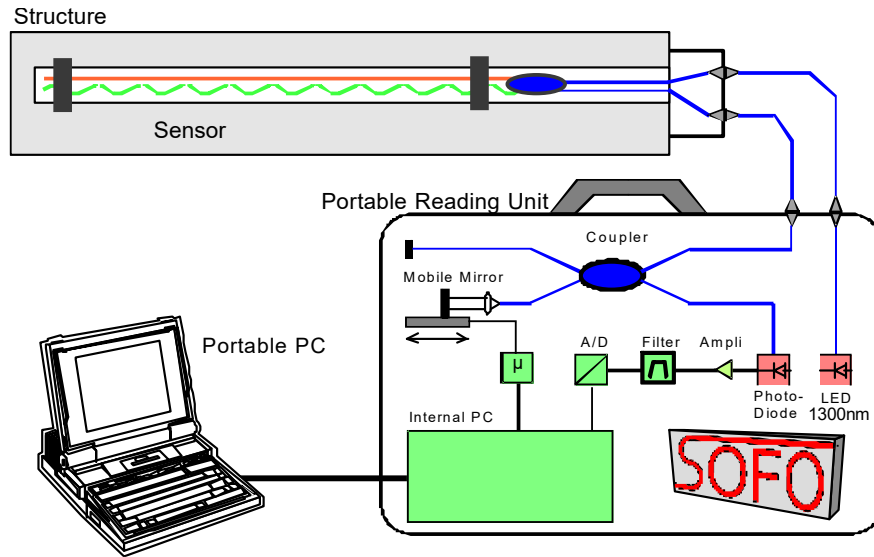


Figure 1-6: Setup of the SOFO system [45].

Sagnac interferometer

A Sagnac interferometer (SI), consist of a loop of fiber, where two light beams are guided in opposite directions (Figure 1-3d). Beams in both directions are orthogonally polarized [32]. An input light is split with a coupler into two beams. After travelling through the loop, they are recombined with the same coupler. Variations in optical path are caused by to difference in the propagation speed of light for both polarizations. The state of polarization is controlled with a polarization controller (PC). To enhance the polarization dependency, sensing part of a loop is made out of polarization maintaining or highly-birefringent optical fiber [29,30,32].

A SI is used in the temperature, strain and pressure sensing. Paper [47] presents a interferometer using a few-mode fiber (PANDA) for strain and temperature measurement. Sensitivities to these effects are $1.97 \text{ pm}/\mu\epsilon$, and $0.123 \text{ nm}/^\circ\text{C}$ respectively. Another paper describes a similar interferometer (also HB PANDA fiber in a sensing loop) used as a pressure sensor. The reported sensitivity was $2330 \text{ pm}/(\text{N}\cdot\text{m})$ [48].

B. Grating-based sensors

Grating-based fiber optic sensors are made as a modulation of the refractive index on certain length of the fiber's core [49]. Such a modulation can be in-written with laser and phase mask, or with a point-by-point laser method. Depending on the distance between modulation and angle between the core has different working principle and spectral response. Variations of the grating types are shown in Figure 1-7.

It is also worth to mention, that gratings can be inscribed not only in single-mode optical fibers, but also different fiber types to change their sensing properties. Use of fiber Bragg gratings to measure transversal strain will be described in terms of this dissertation

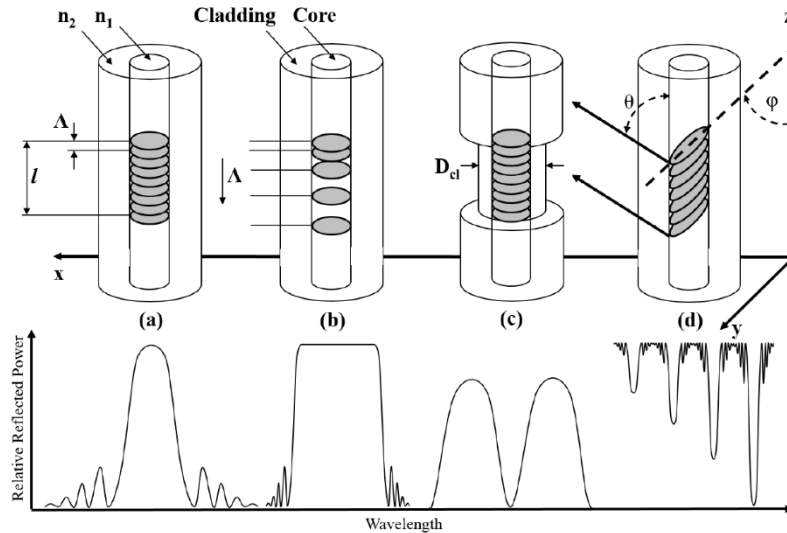


Figure 1-7: Fiber grating types, a) standard, b) chirped, c) birefringent, d) tilted, and exemplary reflection spectra [50].

The most basic grating-based FOS is a fiber Bragg grating (FBG). In this case, the modulation is periodic and regularly spaced. It is usually inscribed with a phase mask and laser. An FBG causes only a very narrow band of light to be reflected from the sensor when broadband light is passed through the fiber. An FBG inscribed in regular single-mode fibers is affected by strain and temperature with sensitivities of $0.84 \mu\epsilon/\text{pm}$ and $0.11 \text{ }^\circ\text{C}/\text{pm}$ [51]. A working principle of an FBG is described in section 1.3.2. An FBG sensor inscribed in a single mode fiber is the most common commercially available type of FBG. Therefore, it is also referred to as a conventional FBG or standard FBG in the context of this thesis.

A long period grating is similar to a regular FBG, but distance between the periodic changes is greater than $100 \mu\text{m}$. An LPG causes that, part of the light is coupled into cladding modes where it is absorbed. As a result, in the reflection spectrum a whole set of reflection peaks is visible. An LPG inscribed in phase-maintaining fiber was reported to measure simultaneously strain and temperature with repeatability of $15.6 \mu\epsilon$ and $0.7 \text{ }^\circ\text{C}$ respectively [52]. An LPG inscribed in phase-maintaining PANDA fiber as a multi-parameter sensors achieved resolution of $4 \cdot 10^{-4}$, $0.1 \text{ }^\circ\text{C}$ and $5 \mu\epsilon$ for surrounding refractive index, temperature and strain respectively [53].

A chirped grating (Figure 1-7b) has a varying period along the length of the grating. This results in the much broader peak in reflection spectrum. In the case of a chirped FBG, if a grating period changes monotonically (Figure 1-8b), the Bragg wavelength changes as well. In this case, a specific wavelength from the spectrum is reflected in the location along the sensor. In the case of any perturbation along the sensor, it is visible as the variations in this broad peak. Because of this feature, this a chirped FBG was shown to be useful for the crack and delamination detection [54,55].

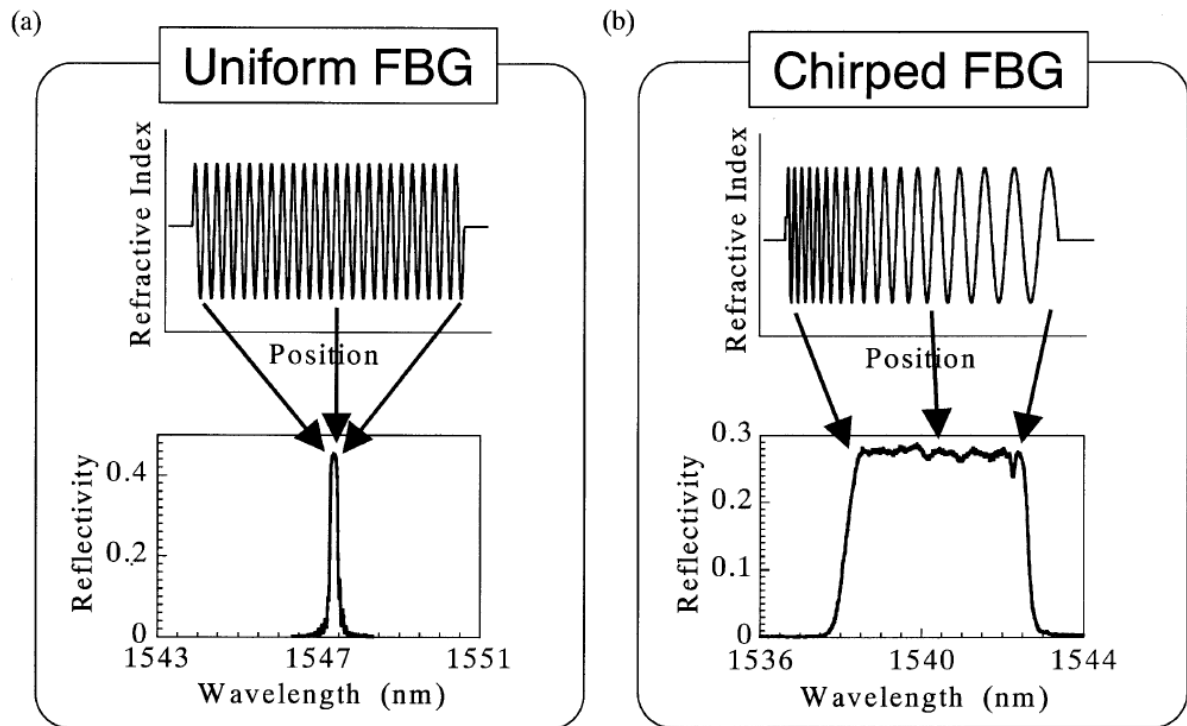


Figure 1-8: Comparison of refractive index variations along the a) regular FBG; b) A chirped [54].

A tilted fiber grating (Figure 1-7d) is similar to regular FBG, but it is written at some angle to the fiber's axis. Because of this reason, some of the light from the core modes is coupled with cladding modes [56,57]. This type of FBG is mostly used for the spectrometers and optical interrogators [50], but there are few applications for other measurements. In the paper [56], a tilted FBG was used for the simultaneous measurement of strain and temperature. The coupling of core-cladding modes in the TFBG causes the transmission spectrum to contain peaks of the core-core mode (as in a regular FBG) and the core-cladding mode. Both have different sensitivities to temperature, but are comparable to strain, allowing separation of strain and temperature. The measurement error was reported to be $7\mu\epsilon$ and 1°C , respectively.

FBG sensors can be inscribed in different types of optical fibers. For example, an FBG can be inscribed in highly-birefringent (HB) optical fiber. This fiber has different refractive index for light travelling in both polarization axes. In this case, a broadband light passed through the optical fiber will be reflected in the form of two separated peaks (Figure 1-7c). Since birefringence in the core is dependent on the stress state in the core of the optical fiber [58], applying of the lateral force to the optical fiber will change the birefringence, so also – peak separation. HB FBG were thus be used for the lateral force [59] and strain [21,60] with resolution of $5\mu\epsilon/\text{pm}$ [19]. This type of sensor is described in the section 1.3.

C. Distributed sensing

Distributed sensing method originated from the Optical time-domain Reflectometry (OTDR), which is used in fiber telecommunication industry for optical cable testing. In this technique a signal is sent through the fiber and device listens to echoes from obstacles along the optical fiber (defects, welds, connectors). Time elapsed to response is calculated to the location of the local defect [61].

In distributed sensing there is no strictly engraved optical sensor on the length of a fiber. Light guided through the cable is backscattered along the length of the fiber. Disturbances along the fiber cause changes in the scattered light's spectrum from each fiber's section. The time delay is used to determine the location of the perturbation. In the fiber optics sensing, mostly three types of scattering are used, namely: Rayleigh, Brillouin and Raman [2]. Their appearance in backscattered radiation spectrum is shown in Figure 1-9.

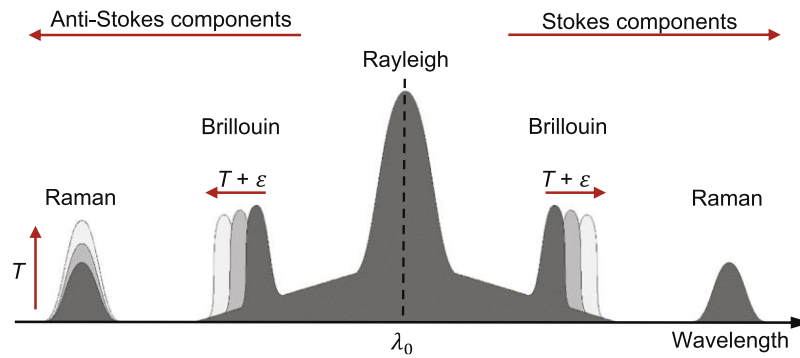


Figure 1-9: Light scattering spectrum in optical fiber [4].

Rayleigh scattering is associated with variations in the refractive index of a fiber, due to fluctuations of density and chemical composition along the fiber. This scattering component has the same wavelength as a laser pulse and can be used to find defects along the fiber (OTDR method) [24]. It has highest amplitude and is in the center of the scattering spectrum. The Rayleigh peak divides spectrum to Stokes (higher wavelengths) and anti-Stokes (lower wavelengths) components.

Brillouin scattering is a result of an interaction of laser light with acoustic waves present in the fiber. The mass oscillations (due to acoustic waves propagation and the photoelastic phenomenon) cause the Doppler shift of light wavelength. The Brillouin peaks are shifted on both sides of Rayleigh peak and depend on the strain and temperature changes [24].

A small portion of photons is scattered with molecules in such a way, that the laser frequency is shifted by the characteristic vibrational frequency of atomic bond of silica [62]. This effect is called Raman scattering. If temperature varies, the anti-Stokes component changes its amplitude, while the Stokes peak remains stable. The power ratio of both peaks is used to calculate temperature [24,63].

The optical backscatter reflectometry (OBR) uses the swept wavelength interferometry (SWI) to measure the Rayleigh backscattering with sub-millimeter spatial resolution along the optical fiber. A diagram showing the idea is shown in Figure 1-10. A tunable laser light is split into measurement and reference path of interferometer. The reference light beam is split evenly into orthogonal polarization states with a polarization beam splitter and a polarization controller. The interference for each polarization states of measurement and reference arms is performed. A Fourier transform and cross-correlation with baseline state is used to calculate strain and temperature [2,64,65].

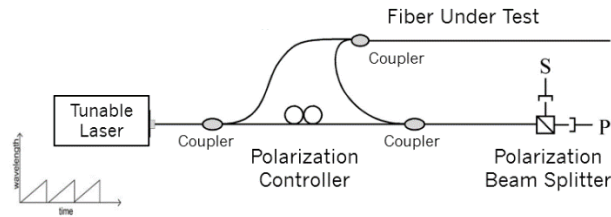


Figure 1-10: A diagram of Optical Backscatter Reflectometry [64].

Commercial devices for the distributed sensing can measure thousands of measurement sections with various ranges. The QuantX distributed acoustic sensing interrogator (OptaSense, LUNA Innovations) dedicated for long range applications can measure multiple thousands of sections (theoretically – 50,000) along 100 km range. Gauge length varies from 2.05 to 205.4 m. Maximum sampling rate is 5 kHz which can be achieved for 20 km long fiber [66]. ODiSI optical Distributed Sensors Interrogators (LUNA Innovations) can measure with as small spatial resolution as 0.65 mm. In this configuration, whole fiber sensing length is 2.5 m with sampling rate of 250 Hz. Resolution of the system for strain and temperature are $0.1 \mu\epsilon$ and 0.1°C respectively. Uncertainty of measurement in 0.65 mm spatial resolution are $\pm 5\mu\epsilon$ and $\pm 2.2^\circ\text{C}$ for strain and temperature respectively [67].

D. Comparison of fiber optic sensors

All the fiber optic sensors are compact, lightweight, robust and immune to the electromagnetic fields [2,3,32], however, each group of sensors presented here has some key use cases and features.

The interferometric sensors are dedicated for precise measurements. They have strain sensitivity in range of $0.1 \mu\epsilon$ [32,33]. They can be adopted to measurement of various measurands (not only strain and temperature [32]). Depending on the interferometer design, they can measure point-wisely (cavity in intrinsic FPI has length $< 1\text{mm}$), or average measurand on the section of optical fiber (Sagnac, Michelson, SOFO). Their main drawback is poor multiplexing ability [2].

In the case of fiber Bragg gratings, multiple sensors can be inscribed in single optical fiber. This allows quasi-distributed sensing with well-defined sensor location, so they can be integrated in the specific, targeted points in the composites structure (e.g. hot-spots). Since the measurement method is based on the Bragg wavelength changes, allows absolute measurements with resolution of around $1\mu\epsilon$ with high sampling rate (sampling rate can be as high as 1 MHz [2], depending on the reading unit properties). Proper distribution of sensors allows them to detect defects in the vicinity of the sensors.

Distributed sensing covers the monitored structure with much higher number of sensing points, thus this method is more likely to find any defects during the exploitation stage. On the other hand, sampling rate is limited to range of hundreds to few kHz, which is not enough e.g. for in-flight control of aerospace structures [2]. An optical fiber is not expensive, but the measurement unit costs in the range 100,000-200,000 Euro, which is few times more than unit for FBGs [24].

Different characteristics of sensors causes that each of them has place to be used in monitoring of composite manufacturing and exploitation. Depending on the exact structure, accuracy of measurements, other methods should be used. In the following chapter the applications of different types of sensors for composite sensing will be shown.

1.2.2. Composite production and exploitation monitoring with fiber optic sensors

Quality of final composite structure is determined by the manufacturing process. Errors in filling with resin and curing process can cause dry spots, under-curing, which weaken the structure, thus threatens the integrity of the final part [7]. Variations in the batch-to-batch properties of half-products makes repeatable production challenging. Quality of the final product can be increased by application of some monitoring method. In the terms of high-volume production composite production, manufacturing can be monitored with sensors integrated into tooling. For example, in resin transfer molding (RTM) sensors are a part of the mold and they monitor process inside the mold's cavity. Usage of integrated sensors, which would require placement in the mold increases the overall production time of each structure, so usage of in-mold sensors is preferred.

In some application (e.g. aviation), structural parts have to be monitored to detect any damages that can threaten its integrity. One approach is to periodically examine its state with non-destructive testing, but other approach is to equip the structure with dedicated SHM system, which monitors structure during the operation. Sensors are spread across the structure and measure response of a structure. The supervising algorithm constantly monitors occurrence of damage in the structure. In SHM systems sensors can be attached on the surface or be embedded into the composite. The second approach protects them from external damage, which also increases their lifetime [8]. In this group fiber optic sensors attracted a lot of attention.

Sensors dedicated to be used in SHM are integrated into the composite along with reinforcing fibers, so they can be used not only for their main use in exploitation measurement, but also for the composite manufacturing monitoring. Fiber optic sensors were shown to be useful for both stages. Because of this reason use of FOS for the manufacturing process and exploitation monitoring will be shown in this section.

A. Challenges in terms of thermoset composite production

In the manufacturing process, optimization is focused on the increasing of quality of the manufactured parts along with reduction of the production cost, while both directions have different challenges [68–70]. In both cases sources of errors in the production environment have to be characterized [68]. Source of uncertainties are textiles, resin system, tool-part interactions and processing parameters.

Variations in the batch-to-batch properties of the reinforcing textiles, which may include tow misalignment, incorrect fiber orientation, missing yarns, etc., result in uneven infiltration of the preform. In such a situation, the flowing resin may not infiltrate some parts of the preform, resulting in the so-called dry spots, or vice versa, at the locations with missing fibers, resin reach locations may be formed [68].

In the case of resin system, chemical composition of the supplied resin and hardener can differ between batches, which can lead to the uncertainty of the curing time. During the injection resin has to be mixed with hardener. Depending if mixing is done manually or automatically some errors can happen. During the manual mixing - weighing, pouring, stirring they all can lead to errors. In the case of automatic mixing heads - residua from previous injections can incorporate imperfections to the resin system. In both cases, component ratio and properties of substrates cause variations of the curing process [68].

Tool-part interaction can lead to non-uniform infiltration of the produced part. Between the edge of the part and tool preferential flow path can appear (due to gap or uniformity of

reinforcing fibers). If gaps are present, filling with higher velocity can appear in the area (so-called race tracking). Moreover, if fiber volume content is not uniform on the whole surface of the part, flow front can be also disturbed.

Some batch-to-batch variations or errors with the textile or resin can be detected prior the manufacturing. Textiles can be monitored with vision system to find defects [71]. For the resin it was shown that some of basic tests (density, melt flow, heat deflection) done for each batch of a resin can keep production in comparable conditions [68]. However, even if these errors are reduced, still better results can be achieved with additional monitoring of the process.

Another defect occurring during the production is residual stress. Residual stress is caused by difference in the coefficient of thermal expansion of reinforcement, matrix and tool. Residual stress influences the geometry and mechanical properties of the final product [72]. It affects dimension accuracy, can cause spring-in and warpage. If residual stress exceeds allowable limits, it can even cause delamination and matrix cracking. Residual stress appears in few levels: microscopic (constituent) level – expansion between fibers and matrix, macroscopic – due to a difference in CTE between plies, global – gradients in the temperature over thickness of composite, e.g. because by toll and part difference in thermal expansion [73–77]. To prevent them many studies were focused on their characterization. It was shown that fiber optic sensors can be used for their formulation during the manufacturing [78–83].

During the process itself, temperature is a crucial parameter. The curing of an epoxy resin an exotherm reaction, which speeds up when temperature increases. The tool temperature can be controlled e.g. with water cooling, but in the case of thicker composites some temperature gradients through-thickness can appear. These gradients lead to variations in the curing speed, which can cause distortions and matrix degradation [68].

B. Sensors application for thermosetting processes monitoring

For in-line monitoring of the infiltration and curing of the composite, various sensors are used. Their summary is given in the review [7]. The infiltration changes the characteristics of the reinforcement textile. First, flowing resin changes its resistance and impedance, which can be measured with electric sensors. Second, if resin has different temperatures than the tool, various temperature sensors can also be used to track the flow. The flow of the resin causes variations in the pressure inside the mold, which can be measured with pressure sensors [7]. The main challenge in the filling monitoring is the detection of so-called dry spots. Sensors can be integrated in hot spots to detect if dry spots did not occur in these locations, but they cannot still cover every location of the textile. There are also trials with the usage of area sensors for flow-front detection [84].

As epoxy resin cures, chemical reactions convert the liquid resin to a solid state. Curing is a polymerization process in which compounds in the resin system bond together to form macromolecules. This transition can be observed using Raman spectroscopy [85]. Polymerization changes the viscosity of the resin, which can be detected with fiber optic sensors. The formation of larger molecules changes the electrical impedance, which can be observed using dielectric analysis (DEA) or direct current (DC) sensors [7,85,86]. In addition, curing of an epoxy resin is an exothermic reaction, so heat flow measurements can be used to monitor the process.

In the case of fiber optic sensors, their ability to monitor the curing process can be divided by the resin properties measured with the sensor. First, chemical reactions cause an increase in the refractive index of the resin. This approach is generally used for sensing with a Fresnel

refractometer [23,87], but also with tilted FBG [88]. The second approach to curing monitoring is the result of deformation (shrinkage) of the resin. When resin is liquid, it is too soft to transfer any stresses to the optical fiber, but from the moment of gelation, resin is capable of transfer the strain from the epoxy to the optical fiber. This allows the use of FOS for the detection of gel point [9,86–89]. Since gelation, FOS can measure residual strain buildup. For monitoring based on strain, mostly FBG sensors are used, but there is also an example of distributed sensing [72].

In papers [83,84] the Fresnel reflectometer was used for the degree of cure determination. A Fresnel refractometer is basically a cleaved end of an optical fiber inserted into the tested medium. When light guided through the optical fiber arrives at the end, some part of the light is reflected (Figure 1-11). The fraction of the reflected power depends on the variations of the surrounding refractive index (SRI) [23]. Another example is a tilted fiber Bragg grating (TFBG). TFBG is capable of measuring SRI because it couples the light mode from the core to the cladding modes [88] that are affected by SRI. TFBG were shown to be capable of measuring SRI along with strain [88], but also SRI, strain, and temperature at the same time [89]. A chirped long period grating (CLPG) was used to measure the direction of flow and cure monitoring [90]. The direction of flow could be detected because the shape of the reflection spectrum was different in the case when CLPG was impregnated along increasing or decreasing grating period. Cure monitoring was measured due to the fact that the coupling of the LPG core-cladding mode is affected by variation of SRI.

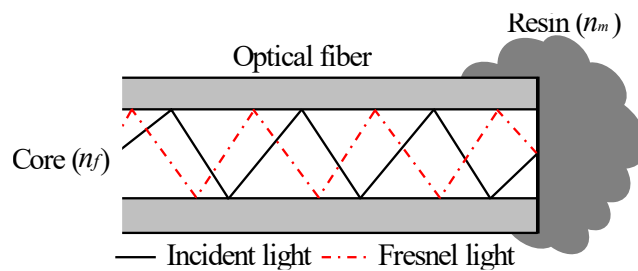


Figure 1-11: Scheme of a Fresnel refractometer applied for measurement of resin refractive index variations [91].

The strain sensing approach with FBG sensors was a topic of numerous papers [9,78,81,92–98]. In papers [92–94] Fiber Bragg gratings were used along with etched fiber sensors (EFS) to monitor the flow front and the curing process in transparent mold in RTM process. EFS is a simple sensor, where a short distance of fiber's cladding is etched. When resin arrives to EFS, variation in the surrounding refractive index changes the transmission through the fiber causing variation in the guided light power. EFS sensors were placed in few locations so the flow front could be tracked, while after the filling of a mold, data from FBG were used to monitor the process. FBG sensors were successfully used for the monitoring of complex composite structures. A full-scale aerospace part (a hinge arm droop nose mechanism for an Airbus A380 aircraft) was monitored using integrated FBG and capacitive sensors [95,96]. It was shown that FBG sensors were able to show infiltration with resin, vitrification and measure the residual strain after curing, and strain after cooling down of a whole structure. Capacitive sensors were used as additional reference method. A full-size, one-piece tail cone of regional jet aircraft [23] was monitored with FBG sensors inscribed in single mode and highly-birefringent FBG sensors, but also with Fresnel refractometers. Combination of sensors allowed assessment of degree of cure and also strain in axial and transversal direction.

Apart from regular FBG, other types of fiber optical sensors were used for strain-related cure monitoring. In a paper [72] distributed sensing method was used to measure the development of curing process by measurement of the strain build-up during the curing.

In order to increase the reproducibility of monitoring the liquid composite molding process with FBG sensors, some researchers have isolated the influence of the textile on the curing process. In the paper [97], the researchers placed an FBG in a small elastic container (latex glove finger) together with a thermocouple, and also a thermocouple outside of the container (Figure 1-12a). Since curing of the resin is an exothermic reaction, as long as the heat of reaction is released from the resin, continues. An FBG was used to find a gel point, based on strain measurement (Figure 1-12b). Another paper [9] focused on monitoring the RTM process of a natural fiber composite. In this case, the FBG sensors were placed in locations where they were surrounded by neat resin. To achieve this, two approaches were used - sensors were installed in holes punctured in the textiles and in specially designed capillaries.

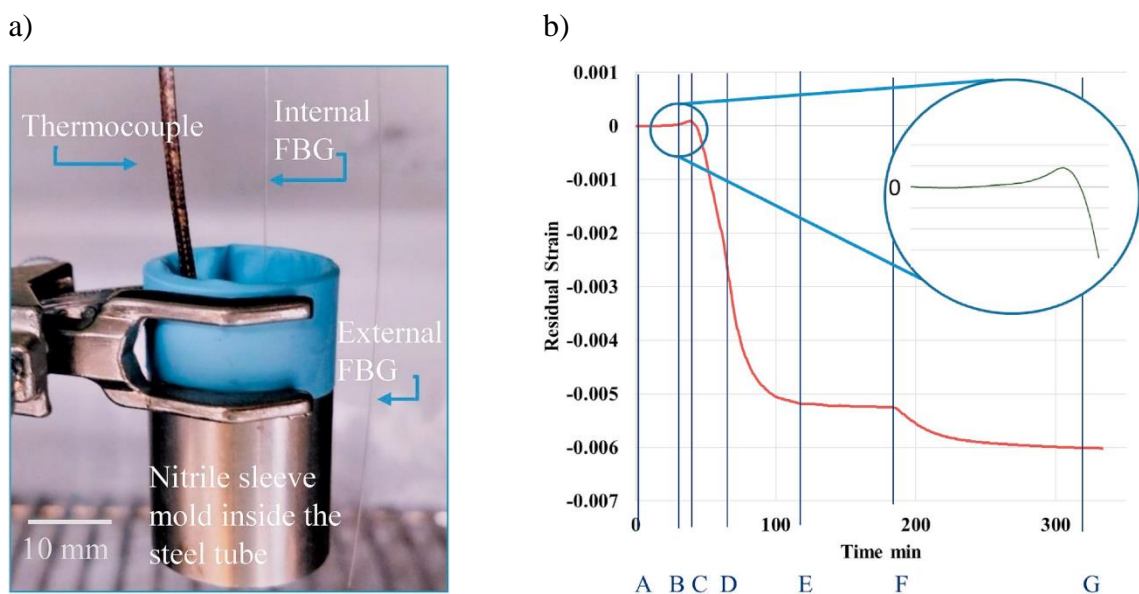


Figure 1-12: An application of FBGs along with thermocouple to measure the curing of neat resin; a) location of FBG sensors, b) identified stages of the process: A – start of the cure, B – gelation, C – curing, D – end of curing, E – sample cooled down, F - oven shut off, G – room temperature reached [97].

The examples presented so far have focused mainly on axial/in-plane strain measurement. On the other hand, curing shrinkage has a higher amplitude in the out-of-plane direction than in the in-plane direction [72]. Transversal strain-based monitoring was done with FBG sensors inscribed in regular (single-mode), and highly-birefringent optical fiber.

The most self-explaining method to measure through-thickness strain is presented in paper [99] where FBG sensor was inserted in out-of-plane to the thick composite plate (Figure 1-13). Sensor was used for the gel point determination and residual strain measurement. Differential scanning calorimetry (DSC) tests confirmed the gelation time. Disadvantage of this solution is that it cannot be used in closed-mold processes and can be used only for relatively thick composites.

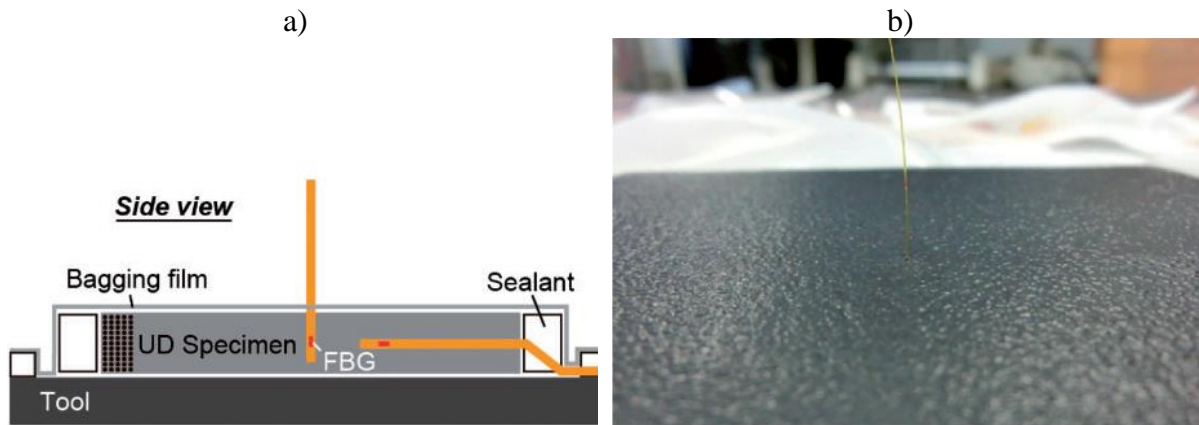


Figure 1-13: Through thickness measurement of strain during the curing the process; a) Scheme of a sample, b) Sample with an inserted FBG [99].

Another method of assessing out-of-plane strain is based on the birefringence phenomenon. Mechanics of birefringence dependence on the external load is described in section 1.3.3. In this approach an optical fiber is integrated in-plane of composite, but during curing of the composite, out-of-plane stresses cause transverse compression of the optical fiber. Due to photoelasticity phenomenon, this transversal compression causes variation of refractive indices of the fiber (in-plane and out-of-plane). The influence on FBG spectra is presented in Figure 1-14. If FBG is inscribed in highly-birefringent fiber (two peaks are already in spectrum), transversal strain causes changes in the separation of peaks. A single-mode fiber has low birefringence, so reflection spectrum consists of single peaks. In this case, transversal stress causes splitting of FBG peak into two separate ones.

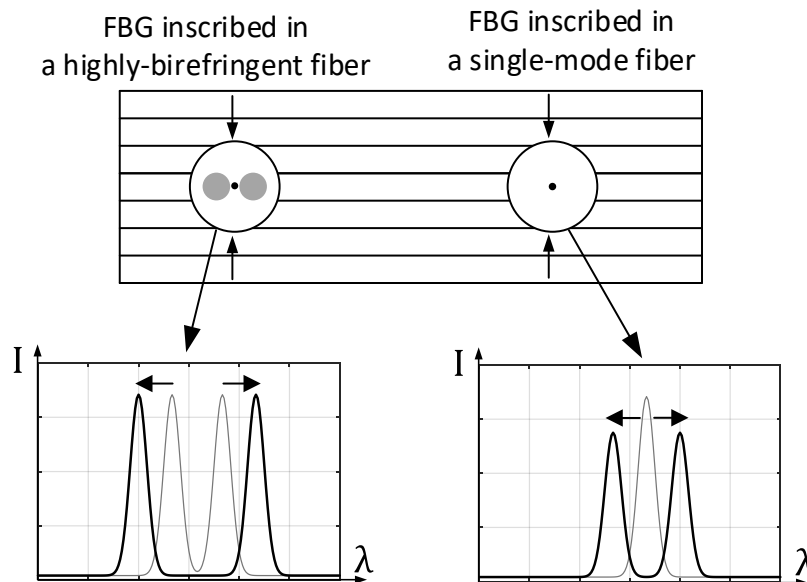


Figure 1-14: Spectra of FBG sensors inscribed in highly-birefringent and single-mode fibers changed by the transversal shrinking of the composite laminate.

Highly-birefringent optical fibers were used to monitor the manufacturing process in papers [23,100–102]. In paper [100] is presented the first attempt to cure monitoring of an unidirectional glass fiber/epoxy composite with FBG sensors inscribed in bow-tie fiber. FBG sensors were placed in various conditions: along reinforcing fibers, transversal to them and into

neat resin. Transversal strain measurement caused by the chemical reaction were monitored. FBGs inscribed in bow-tie fibers were also used in paper [23] to measure the transversal strain in the resin infusion manufacturing of aircraft tail cone.

Another group of highly-birefringent fibers is microstructured fibers (photonic crystal fibers), which shows much higher sensitivity to the transversal load than previously mentioned fibers. An FBG inscribed in microstructured fiber (MOF) was used to monitor the autoclave process (Figure 1-15). It was shown the peak separation (so also transversal strain) changes significantly only during the curing phase. Besides that MOF FBG was used to measure residual strain during the cooling of the composite after the process (thermal through-thickness shrinking of the composite) [102]. In the paper [101] the MOF FBG was one of type of sensors used for the autoclave process monitoring. It also shown the variations in peak separation on the stage of curing and cooling down of composite structure.

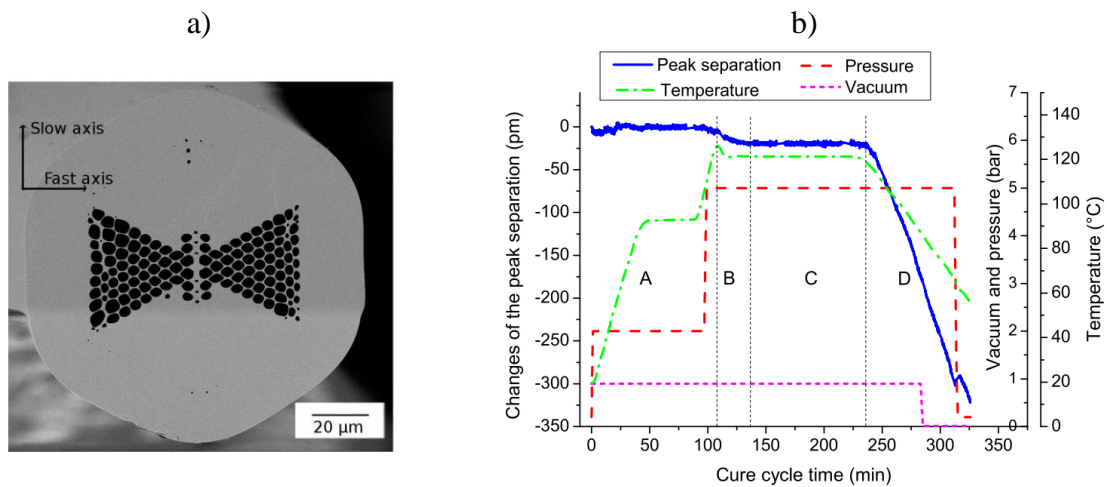


Figure 1-15: The microstructured FBG used for the autoclave process monitoring; a) The microstructured optical fiber cross-section, b) peak separation changes due to curing stages [102].

An issue with application of FBG inscribed in highly-birefringent fibers have orientation-dependent load sensitivity, which causes that FBG sensors require precise integration into the composite. However, paper [83] shows application of a regular FBG sensor to measure the transversal strain in the autoclave process, which does not require orienting of a fiber. During the curing of cross-ply composite, transversal shrinkage causes splitting of the FBG peak [83,103]. Measurement of peak separation could be used to calculate transversal strain, but typically it requires that peaks separate enough to distinguish peaks. For this reason, authors supported peak wavelengths determination with the polarization-dependent loss (PDL) measurement. This parameter describes the ratio between maximum and minimum transmission losses in all polarization stages for a certain wavelength [83]. The composite curing caused a transverse load, which resulted in the PDL variations around the peak wavelength. In this way, even a very small transverse strain could be observed, which did not result in the separation of the spectrum peaks into two. This method, however, required optical vector analyzer, which operates at sampling rates less than 1 Hz.

C. Monitoring of composite materials and composite structures with optical fiber sensors

Damage in composite structures can occur due to exploitation loadings and environmental influence. Potential failures of structures such as aircrafts can lead to massive cost or even to losses of human life [104]. To examine any abnormalities in the structures, two basic approaches are used: non-destructive testing (NDT) and structural health monitoring (SHM). In NDT methods, structure health state is examined in periodically scheduled maintenances with methods such as ultrasound, X-ray, etc. In SHM structure is examined online with some supervision system, which uses sensors attached to the structure [1].

Structures made of composites can be lighter than metallic ones, but have a much more complex mechanics and failure mechanism. Metals isotropy allows prediction of damage progress, but in composites, failure mechanism depends on the multiple variables. The composite fails differently if it works under tension or compression. A fatigue performance depends not only on reinforcement and matrix materials but also on the lay-up sequence [3]. Another issue is that the composites are prone to barely visible impact damage (BVID), which could be caused by bird strikes, gravel, hail, or tool drops. BVIDs can cause damage such as delamination, cracks in the matrix, and fiber breakage [3,30,104]. Due to the size of BVIDs, they can be omitted by the human eye. To maintain safety standards, structures have to be over engineering, which counteracts the advantage of use of composite to reduce mass of the structure [3]. A way to keep the safety in this environment is use of a SHM system, which can constantly control the structure.

Sensors are a fundamental element of SHM systems. They measure critical parameters such as strain and temperature variations, which are input to decide about the need for maintenance. In SHM systems, various types of sensors are used, but due to the ability of FOS to be integrated into a composite without significantly influencing the integrity of the structure, they have received a lot of attention [3,104] in various industries: aerospace [2,3,23,105], automotive [5,106], and renewable energy [4,5,107,108].

Research on the application of FOS for strain measurement and damage detection can be divided into two main groups, focusing on material degradation and monitoring of the entire composite structure. Material degradation and strain monitoring research focuses on the application of novel sensors and the investigation of the possibility of detecting single defects in the composite. Structural health monitoring of composite structures focuses on multi-point strain sensing and detection techniques to find defects in large data sets collected by sensors.

Monitoring of composite material state

In the material scale, FOS were successfully used for detection of delamination [55], measurement of crack growth [109], and localization of impact events [105,110–112]. An article [55] shows the use of chirped FBG to investigate the fatigue and decohesion of the carbon fiber reinforced polymer (CFRP) patch used for repair of damage in the host structure. Crack growth measurement in paper [109] used FBG and analysis of spectrum degradation. Occurrence of crack caused non-uniform strain along the optical fiber causing degradation of the spectrum, which was later correlated to the progression of crack.

Research focused on the localization of impacts are investigating various data processing methods to detect damage or impact. Modifications of the PCA method are developed to extract valuable data from the huge sets of data produced by the SHM systems [113–115]. For detection algorithms based on pattern recognition and machine learning, they are receiving a lot of attention [116].

In terms of multiaxial strain measurement, FOS can also be incorporated. For in-plane measurements, FBG sensors can be arranged in the form of rosettes [111], similar to strain gauges. However, this approach still does not allow measurement of out-of-plane strain, which is important from the delamination monitoring point of view. This strain can be measured with FBG sensors inscribed in highly-birefringent optical fibers. They were used in strain measurement in the past; however, the number of applications for composites is limited [19,20,23,117–119] in comparison to FBG sensors inscribed in single-mode fibers.

HB FBG sensors were used to measure quasi-static [19] and dynamic strain [118], and delamination progress [20]. Multiaxial (3-D) strain was measured with use of two FBGs inscribed in microstructured optical fibers achieving $5\ \mu\epsilon$ resolution [19]. The same type of MOF FBG was integrated into an adhesive layer in single lap joint. This approach allowed to measure shear strain with resolution of $50\ \mu\epsilon$, which allowed observation of delamination growth [20].

In terms of dynamic strain measurement, two MOF FBGs in 3-D configuration were used to measure the strain caused by a composite coupon under impact [118]. Another use case is a MOF FBG to distinguish symmetric from antisymmetric lamb waves [119]. A single paper investigated the variations of the integration angle of HB FBGs in a laminate and their sensitivity to various loading cases, potentially to distinguish the type of defects occurring in the structure [120].

Few studies tried to use FBG inscribed in single-mode fibers for multi-axial strain measurement, which were embedded in the composite in such a way that the composite during production caused birefringence in the fiber. This approach allowed measurement of multicomponent strain [121], or axial strain and temperature [103]. The drawback is the lower sensitivity than that achieved by novel MOF HB FBGs dedicated for this purpose.

Structural health monitoring of composite structures

FOS were used for structural health monitoring of composite structures. Few examples will be presented. An example of application in aircraft was described in a paper [105]. A small aircraft wing structure (Jabiru UL-D) was monitored with six FBG sensors glued to the surface of the wing. The structure was impacted with low velocities. Using fast data collection ($f_s=100\text{kHz}$) and sophisticated processing method allowed reproduction of the localization of impacts. The second application of FBGs of aerospace composites is tail cone assembly for a regional jet aircraft (Figure 1-16) [23]. This structure was equipped with integrated multiplexed FBG sensors inscribed in single mode and highly-birefringent optical fibers. The structure was manufactured in an autoclave process. FBG sensors inscribed in single-mode fibers measure the axial strain, while highly-birefringent ones were used for measurement of transversal deformation.

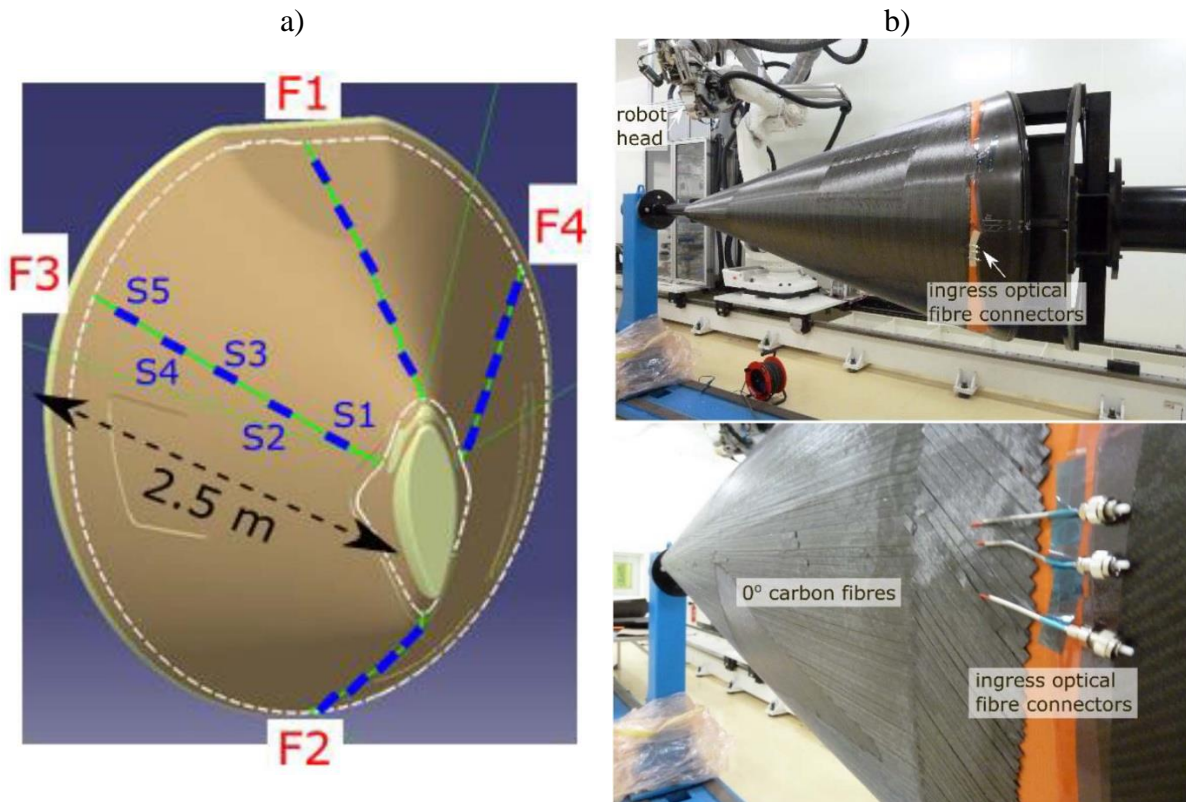


Figure 1-16: View of the tail cone of a commercial aircraft monitored with FBG sensors; a) Scheme with localization of sensors, b) View of the composite cone during the production [23].

Another example of use in aircrafts is a hinge arm of the droop-nose mechanism of the Airbus A380 [106]. FBG sensors were integrated in the RTM process and used for the determination of vibration characteristics Figure 1-17.

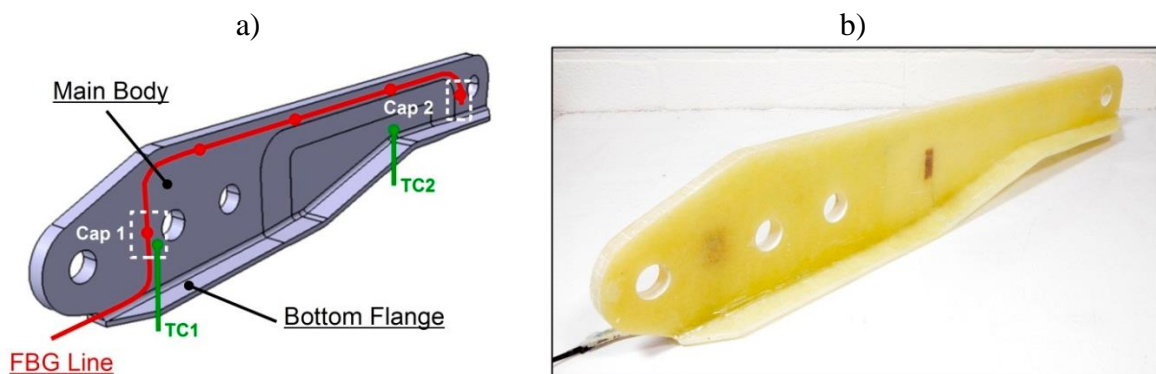


Figure 1-17: The Airbus A380 hinge arm; a) Concept diagram with shown sensors locations, b) Manufactured part [95].

The paper [122] describes landing gear for aircrafts monitored with 10 FBG sensors glued to the surface of a structure (Figure 1-18). The location of the measurement points was based on finite element analysis (FEA), and mechanical validation was performed in quasi-static mechanical testing.

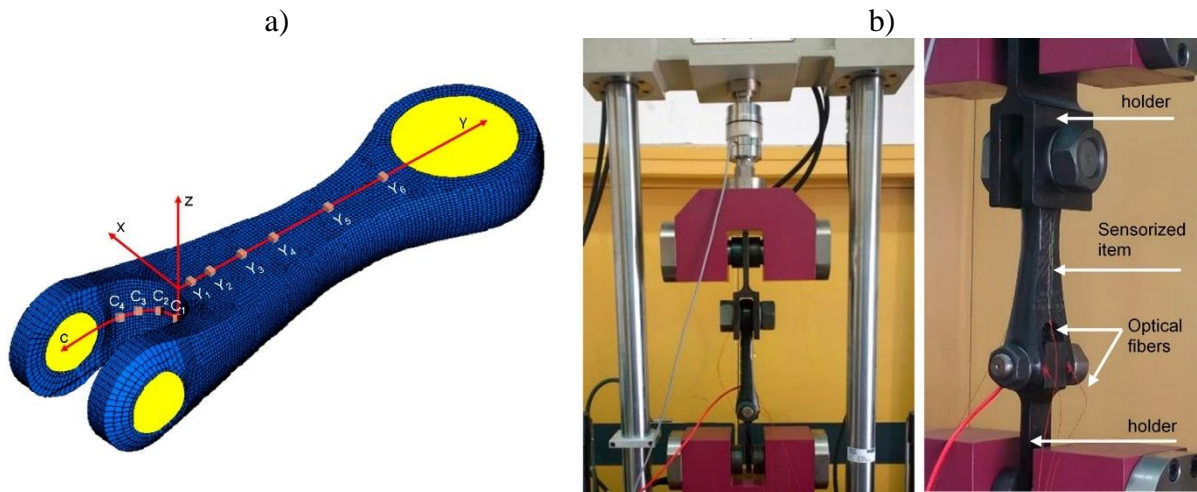


Figure 1-18: A composite drag strut monitored with FBG sensors, a) FEA model with sensors locations, b) The drag strut in the testing machine [122].

Climate changes pushes forward the development of green energy generation and storage methods. Research is focused on the health monitoring of wind turbine blades. Paper [4] describes the use of FBG sensors and distributed optical fiber sensors (OBR) integrated into a 13.5m long composite blade. Sensor data are processed with principal component analysis (PCA) and based on the statistics created defects in the structure were detected.

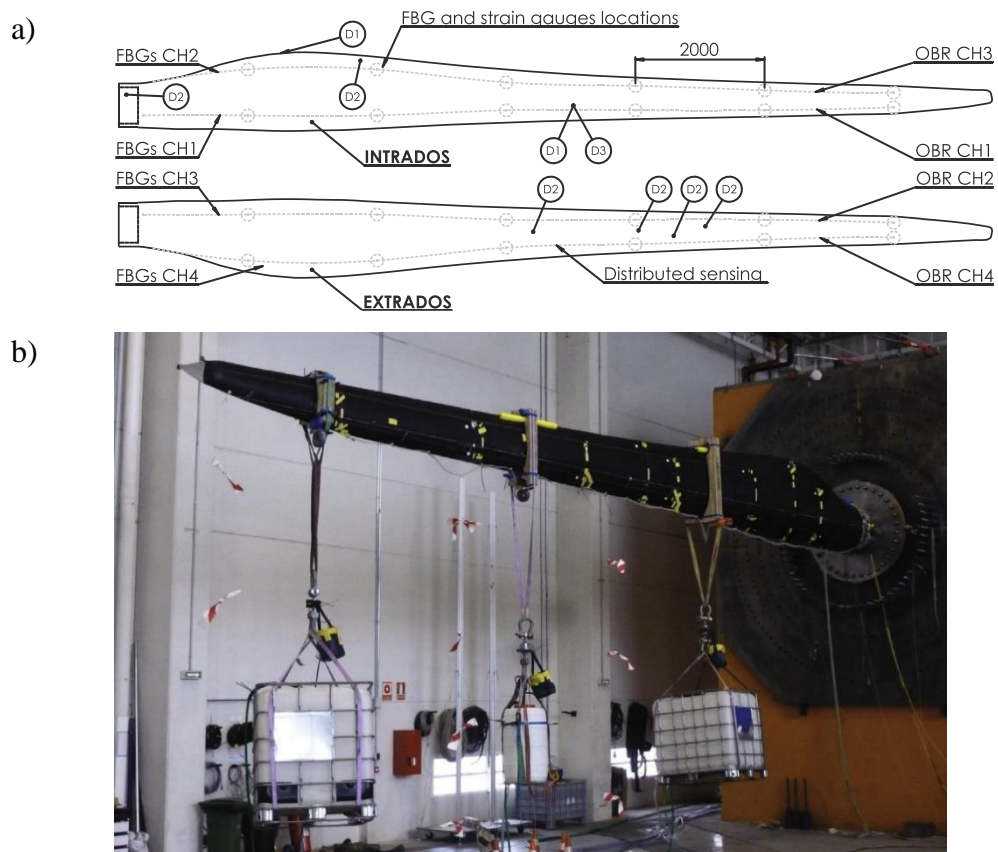


Figure 1-19: Composite wind turbine blade with FOS; a) Locations of sensors, b) View of the loaded blade [4].

Hydrogen is going to play an important role in the green transformation. A promising method for storage is to keep it in the gas state in high-pressure composite vessels. Such structures can be monitored with fiber optic sensors. The articles describe the use of FBG sensors glued on the surface [108] of the vessel and embedded before winding [5] for strain analysis. The FBG sensors were able to detect vessel failure during pressure testing [5] and the appearance of the damage in the shell [108] (Figure 1-20). FBG sensors were also used for strain analysis of the high-density polyethylene (HDPE) liner, which is an internal part of composite pressure vessel [123].

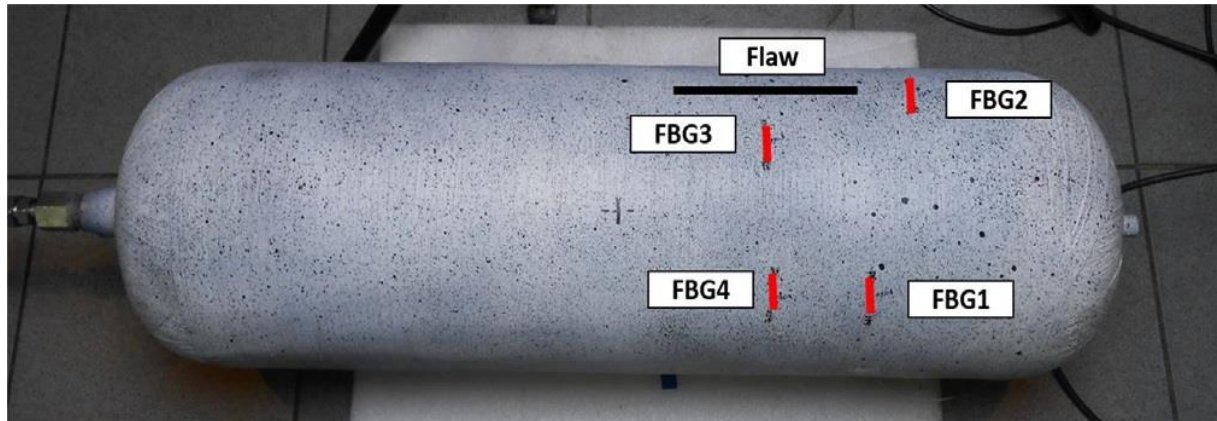


Figure 1-20: A composite pressure vessel with attached FBG sensors for detection of artificial defects in the vessel. Surface of the vessel is sprayed with a pattern for DIC strain analysis [108].

1.3. FIBER BRAGG GRATINGS INSCRIBED IN HIGHLY-BIREFRINGENT OPTICAL FIBERS

Various applications of FOS have been shown in the previous sections. In this group, HB FBG sensors, which can measure lateral strain, have not been widely studied. In this section, a detailed explanation of their measurement principles and capabilities will be elaborated. For this reason, a basic explanation of birefringence in optical fibers is given. Later, the response of the FBG sensor inscribed in the HB fiber is explained. At the end of this section, the application of HB FBG sensors for strain measurement is given.

1.3.1. Highly-birefringent optical fibers with inscribed FBGs

Birefringence is a phenomenon in materials in the case where the refractive index depends on the polarization state and the direction of propagation of light [124]. This effect can be observed in calcite mineral. If object is observed through the crystal, it appears to be doubled (Figure 1-21). Glass and silica are photoelastic materials, which means that stress changes refractive index of the material. This is the origin of use of photoelasticity to investigate the residual stresses in the transparent materials [124].

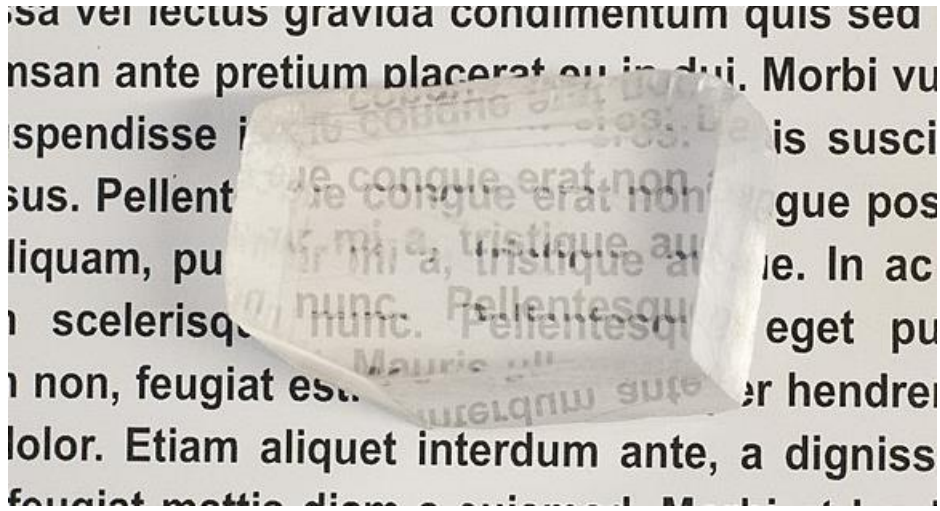


Figure 1-21: A text viewed through the birefringent crystal (calcite) [125].

In a perfect optical fiber, there is no birefringence, and light propagates without changing the polarization state. Real fibers, however, have some manufacturing stresses or ellipticity in the core causing nonzero birefringence. As a consequence, orthogonally polarized modes travel at various velocities, leading to dispersion. To maintain the linear polarization state of the light, birefringence is intentionally introduced into a fiber. It can be achieved by using an elliptic core or the introduction of stress-applying parts with the use of other types of glass in the cladding. Differences in CTE of glass cause formulation of stresses in the core. Such fibers are called highly-birefringent (HB) fibers or phase-maintaining optical fibers [27,126,127]. The cross section of few HB fibers is shown in Figure 1-22.

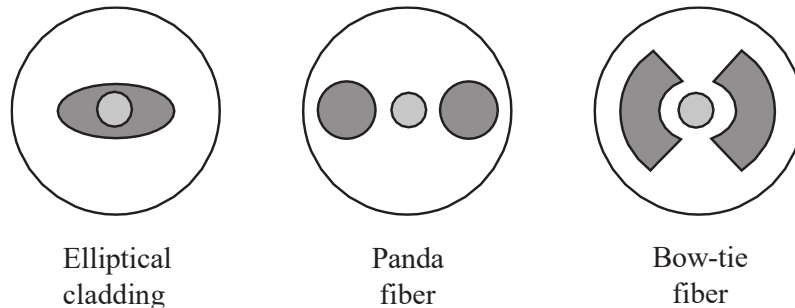


Figure 1-22: Cross-sections of highly-birefringent optical fibers [27].

A basic parameter describing the HB optical fiber is phase birefringence B . Phase birefringence is a difference between the refractive indices for polarization modes x and y :

$$B = n_{eff}^x - n_{eff}^y \quad (1.4)$$

In single-mode fibers it has value of around 10^{-7} , for bow-tie highly-fibers often used in load sensing it is around 10^{-4} [59], for optical fibers optimized for strain sensing it is in range of 10^{-3} [128,129]. Birefringence of the fiber can also be characterized by beat length L_B , which is the length of the optical fiber, which causes the phase variations of 2π . It can be calculated by:

$$L_B = \frac{\lambda}{B} \quad (1.5)$$

Group birefringence G is however calculated as:

$$G = B - \lambda \frac{\partial B}{\partial \lambda} \quad (1.6)$$

This type of optical fiber was shown to be capable of measuring transverse strain in composites, but the breakthrough was the introduction of air channels into the fiber's cross section to form a microstructured optical fiber (MOF). Microstructured optical fibers can exhibit much higher birefringence and can also be optimized for higher sensitivities to pressure and strain. Cross-sections of few MOFs used in load sensing are shown in Figure 1-23. The first MOF (Figure 1-23a) is first MOF shown to measure transversal strain with in-written FBG. The second one (Figure 1-23b) is a MOF that exhibits high sensitivity to the transversal strain, outperforming typical HB with stress applying parts. The third one (so called side-hole, SH, fiber) is an optical fiber used in terms of this dissertation, which could be used thanks to researchers from UMCS in Lublin.

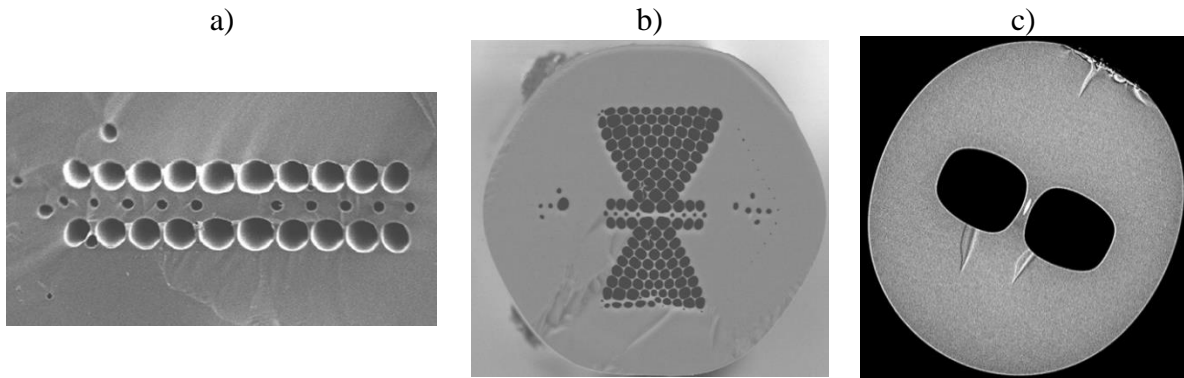


Figure 1-23: Cross-sections of highly-birefringent microstructured optical fibers used for pressure and strain sensing; a) With two rows of holes, [130], b) With triangular sections with air channels (Butterfly) [131] ; c) With two big holes on both side of the core (Side-hole) [128].

1.3.2. FBG in a single-mode fiber and response to strain and temperature

If broadband light is transmitted through a single-mode optical fiber with an inscribed FBG, a narrow band of light is reflected (so-called Bragg wavelength). This wavelength depends on the period of the FBG and the properties of the fiber. The other part of the light will travel through the fiber and will not be affected by FBG. The basic working principle is shown in Figure 1-24.

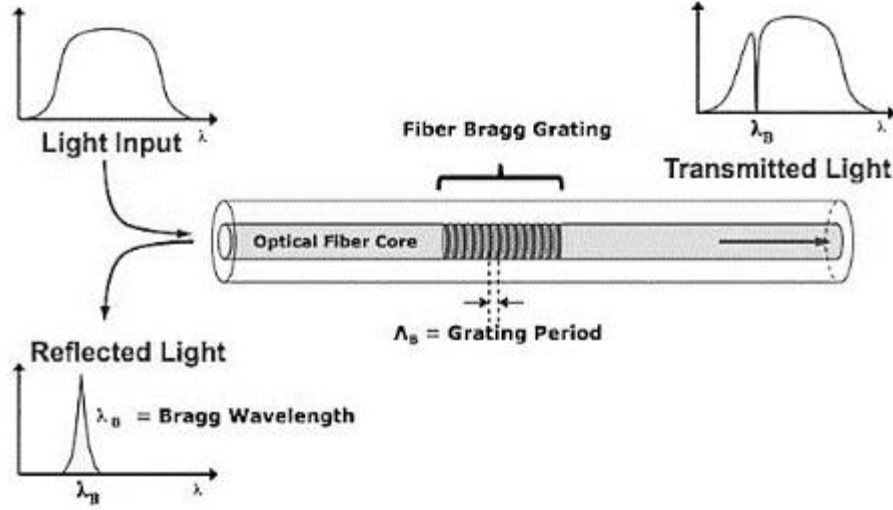


Figure 1-24: Fiber Bragg grating's operation principle [2].

For an FBG inscribed in the low-birefringent (SMF) fiber, Bragg wavelength is expressed by a equation:

$$\lambda_B = 2n_{eff}\Lambda \quad (1.7)$$

where n_{eff} is an effective refractive index of the fiber and Λ is a grating period. Both parameters (n_{eff} and Λ) depend on the strain and temperature. Because of this reason, shift of the Bragg wavelength can be generally expressed as [132]:

$$\Delta\lambda_B = 2 \left(n_{eff} \frac{\partial\Lambda}{\partial\varepsilon} + \Lambda \frac{\partial n_{eff}}{\partial\varepsilon} \right) \varepsilon + 2 \left(n_{eff} \frac{\partial\Lambda}{\partial T} + \Lambda \frac{\partial n_{eff}}{\partial T} \right) \Delta T \quad (1.8)$$

In the case of isothermal measurement, strain dependence can be expressed as:

$$\frac{\Delta\lambda_B}{\lambda_B} = (1 - p_e)\varepsilon \quad (1.9)$$

where p_e is a fiber's photo-elastic parameter expressed as:

$$p_e = \frac{n_{eff}^2}{2} [p_{12} - \nu(p_{11} + p_{12})] \quad (1.10)$$

and p_{11} , p_{12} are components of photo-elastic tensor and ν is Poisson's ratio. For silica fibers ($p_e = 0.22$) and Bragg wavelength of 1550 nm, it gives strain sensitivity of around $1.2 \text{ pm}/\mu\varepsilon$ [2].

In terms of temperature, FBG is affected by change in the refractive index of the optical fiber because of thermo-optic coefficient ξ and change of the physical length due to thermal expansion (α_f). In no-strain case Bragg wavelength shift due to temperature is given by:

$$\frac{\Delta\lambda_B}{\lambda_B} = (\xi + \alpha_f)\Delta T \quad (1.11)$$

For silica optical fibers $\xi \approx 5 - 10 \cdot 10^{-6} \text{ } ^\circ\text{C}^{-1}$ and $\alpha_f \approx 5.2 \cdot 10^{-7} \text{ } ^\circ\text{C}^{-1}$ [132]. For a commercially available FBG in SMF fiber (Sylex, FFA-01), sum of these parameters is,

$\xi + \alpha_f = 5.86 \cdot 10^{-6} \text{ }^\circ\text{C}^{-1}$. For an FBG with $\lambda_B=1550\text{nm}$, it results in temperature sensitivity is $0.91 \text{ pm}/^\circ\text{C}$.

When both influences are considered together, the equation 1.8 gets a form:

$$\frac{\Delta\lambda_B}{\lambda_B} = (1 - p_e)\varepsilon + (\xi + \alpha_f)\Delta T = K_\varepsilon\varepsilon + K_T\Delta T \quad (1.12)$$

Sensitivity to both strain and temperature causes, that if FBG is used to measure in non-isothermal environment, temperature influence has to be compensated [2]. It can be done either with a second FBG which is not loaded, or with another temperature sensor.

1.3.3. HB FBG's response to the mechanical load

In highly-birefringent optical fibers, difference in the refractive index in x and y causes the equation 1.7 should be considered separately for both polarization modes. It is assumed that coordinate system as shown in Figure 1-25. xy plane is in cross-section of the fiber, while z axis is along a fiber.

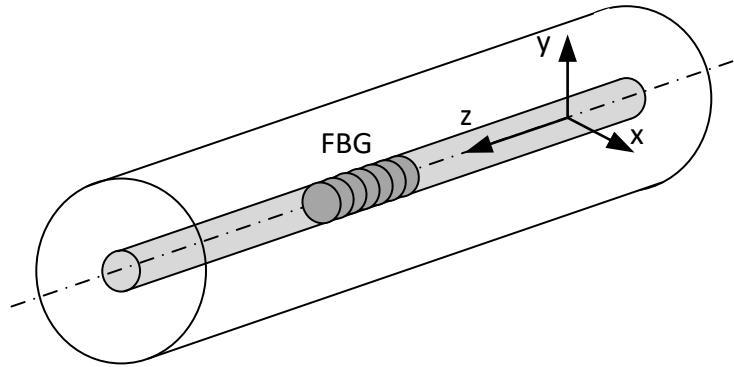


Figure 1-25: A coordinate system of a highly-birefringent optical fiber.

In this case, equation 1.7 can be expressed as:

$$\begin{cases} \lambda_{B,x} = 2\Lambda n_{eff,x} \\ \lambda_{B,y} = 2\Lambda n_{eff,y} \end{cases} \quad (1.13)$$

As a consequence, the reflection spectrum contains two peaks, the separation of which is dependent on the birefringence of the fiber. The peak with lower wavelength is referred as a fast axis peak, while higher wavelength – slow axis. This is associated with the speed of the propagation in both polarization modes. Birefringence causes that when FBG is inscribed for reflection in the 1550 nm window, the unloaded FBG in bow tie fiber has a peak separation of 0.35 nm, comparable to PANDA (0.34nm) [59]. FBG inscribed in MOF has separation few times higher. For the ‘butterfly’ fiber (Figure 1-23b) it is 2.17 nm, while for side-fiber with an elliptical core (Figure 1-23c) it is 1.20 nm.

The birefringence is the effect of the photoelasticity and ‘frozen’ stress in the fiber, so by applying the external load to the optical fiber, refractive index of a fiber will change.

If refractive index tensor is given by [58]:

$$[n] = \begin{bmatrix} n_1 & n_6 & n_5 \\ n_6 & n_2 & n_4 \\ n_5 & n_4 & n_3 \end{bmatrix} \quad (1.14)$$

Both of silica and glass can be considered as an isotropic material, Photoelastic effect on the refractive index tensor can be calculated from the equation [58]:

$$\begin{bmatrix} \Delta\left(\frac{1}{n_1^2}\right) \\ \Delta\left(\frac{1}{n_2^2}\right) \\ \Delta\left(\frac{1}{n_3^2}\right) \\ \Delta\left(\frac{1}{n_4^2}\right) \\ \Delta\left(\frac{1}{n_5^2}\right) \\ \Delta\left(\frac{1}{n_6^2}\right) \end{bmatrix} = \begin{bmatrix} p_{11} & p_{12} & p_{12} & 0 & 0 & 0 \\ p_{12} & p_{11} & p_{12} & 0 & 0 & 0 \\ p_{12} & p_{12} & p_{11} & 0 & 0 & 0 \\ 0 & 0 & 0 & \frac{p_{11} - p_{12}}{2} & 0 & 0 \\ 0 & 0 & 0 & 0 & \frac{p_{11} - p_{12}}{2} & 0 \\ 0 & 0 & 0 & 0 & 0 & \frac{p_{11} - p_{12}}{2} \end{bmatrix} \begin{bmatrix} \varepsilon_x \\ \varepsilon_y \\ \varepsilon_z \\ \gamma_{xy}/2 \\ \gamma_{xz}/2 \\ \gamma_{yz}/2 \end{bmatrix} \quad (1.15)$$

where p_{11} , p_{12} are photoelasticity coefficients of the fiber and $\varepsilon_{x,y,z}, \gamma_{xy,xz,yz}$ are strain tensor components

Since this matrix equation is valid for the isotropic material, it is assumed that coordinate system strain and birefringence tensors is the same. Shear components ($\gamma_{xy,xz,yz}$) don't influence the refractive indices [133]. Variations in refractive indices are given as:

$$\begin{aligned} \Delta\left(\frac{1}{n_x^2}\right) &= p_{11}\varepsilon_x + p_{12}(\varepsilon_y + \varepsilon_z) \\ \Delta\left(\frac{1}{n_y^2}\right) &= p_{11}\varepsilon_y + p_{12}(\varepsilon_x + \varepsilon_z) \end{aligned} \quad (1.16)$$

To calculate the response of an FBG subjected to the multiaxial strain, above variations are incorporated into the equation 1.8. As result peak shifts of an FBG are given as:

$$\begin{cases} \frac{\Delta\lambda_{B_x}}{\lambda_{B_x}} = \varepsilon_z - \frac{1}{2}n_x^2[p_{11}\varepsilon_x + p_{12}(\varepsilon_y + \varepsilon_z)] \\ \frac{\Delta\lambda_{B_y}}{\lambda_{B_y}} = \varepsilon_z - \frac{1}{2}n_y^2[p_{11}\varepsilon_y + p_{12}(\varepsilon_x + \varepsilon_z)] \end{cases} \quad (1.17)$$

It can be seen the peak separation is dependent on the transversal strain and since $n_x \approx n_y$, peak separation is approximately insensitive to the axial strain.

Sensitivity to the transversal strain is dependent on the photoelastic coefficients. For a pure bulk silica they are $p_{11} = 0.121$ and $p_{12} = 0.270$ [134], however their final value can vary between fibers, due to the presence of dopants. Even for low-birefringent (SMF) fibers photoelastic coefficients were measured as $p_{11} = 0.113$ and $p_{12} = 0.252$ [134]. In HB fibers not only various doped materials are used, but also microstructure can influence the final

sensitivity. Because of this reason, the final sensitivity of the optical fiber has to be determined experimentally [59,129,135–137] or with support of finite element analysis [131,136,138,139].

Moreover, HB fibers have an anisotropic cross section, so depending on the angle of loading of the fiber, they will result in different sensitivity. This behavior can be observed in the results of the stress analysis of some HB optical fiber (Figure 1-26).

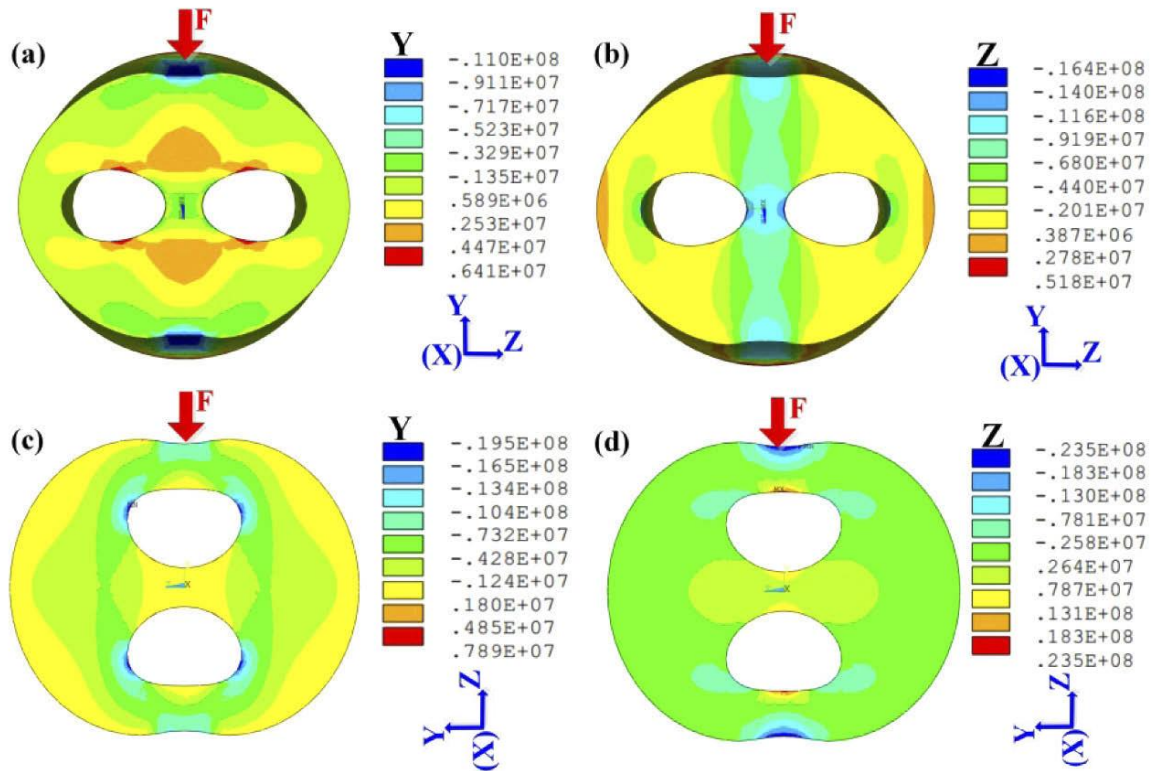


Figure 1-26: Stress distribution calculated with FEA of the dual side-hole fiber (DSHF) under transversal load applied along: (a, b) slow axis, and (c, d) fast axis. Diagrams present distribution of stress in (a, c) y direction and (b, d) z direction [136].

In the case of loading along slow axis (Figure 1-26a, b), stress in y direction in the vicinity of the core is positive, while stress for z axis is negative. On the other hand, when load is applied along fast axis (Figure 1-26c, d), both y and z stress components are positive. As a consequence, Bragg peaks will shift differently depending on the loading direction.

The cross-section of DSHF fiber is similar to the side-hole fiber, which is subject of this research. However, birefringence of DSHF fiber is much lower phase birefringence than used optical fiber (DSHF - $B = 1 \cdot 10^{-5}$ [136], side-hole2 (SH2) - $B = 1 \cdot 10^{-3}$ [128]).

Because of this reason, FBGs inscribed in HB fibers have to be mechanically pre-tested under transversal load at various angles, to determine the most efficient integration angles [59,136,137,140]. For this purpose, FBG sensors are tested the way shown in Figure 1-27.

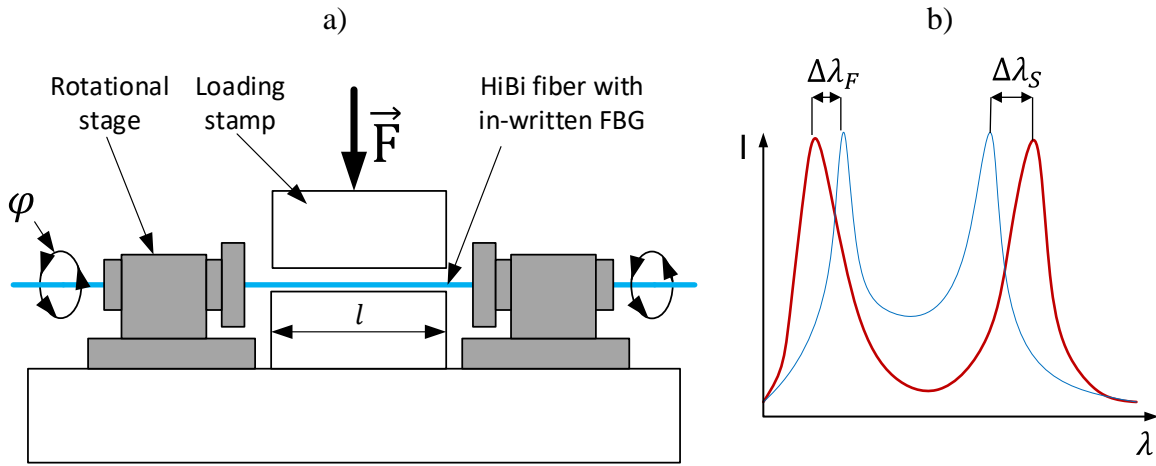


Figure 1-27: Concept of the mechanical testing rig for an HB FBG; a) testing scheme; b) An exemplary spectrum change due to transversal loading.

In this loading setup, an optical fiber with inscribed FBG is fixed on both ends with rotational stages. This allows a precise rotation of the fiber. A load stamp is used to apply force on some length of the optical fiber. The load causes variations in the wavelengths of the peaks, which are later calculated in force sensitivity with an equation [59]:

$$s_{s,f} = \frac{\Delta\lambda \cdot l}{F} \quad (1.18)$$

where, $\Delta\lambda_{s,f}$ – Bragg wavelength shift due to the external force for one polarization axis, l – length of the loaded fiber, F – force applied to the fiber

The procedure of determining this sensitivity is performed for the 180° range and the sensitivity curve for the transverse load is determined. An example of the angle dependence of sensitivity found for a bow tie fiber with in-written FBG is shown in Figure 1-28 [59].

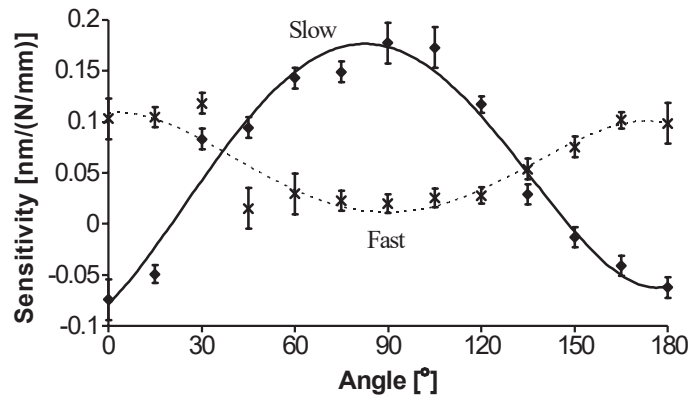


Figure 1-28: A sensitivity dependency of a bow-tie fiber to the transversal load applied at varying load to the optical fiber [59].

This sensitivity curve shows that if compression is applied at a 90° angle, the wavelength of the slow peak increases, while the fast peak almost does not change its wavelength. As a consequence, the overall peak separation increases. On the other hand, when load is applied at 0° transversal load causes increasing the fast peak wavelength, and also decreasing slow peak wavelength. As a consequence, such a loading condition results in decreased peak separation. It is also worth to mention that from the previous figure one can see that when an optical fiber

is loaded on the angle 35° , transversal compression will cause parallel shift of both peaks without changing the peak separation. It means that it will not be distinguishable from the axial strain of the optical fiber.

1.3.4. Strain sensing in composites with HB FBG

In the 1980s, first applications of HB for pressure sensing were shown [141], however, the first case of directional load measurement was presented in 1997 by Lawrence et al. [117]. An FBG inscribed in a phase maintaining fiber was compressed transversally between two plates at various angles to measure its sensitivity. Using the FEA, the strain sensitivity over the angles was calculated. In a later Lawrence paper [139], the strain-sensing ability was validated by loading the FBG placed in a V-groove loading fixture.

The first research on directional load sensing investigated the response of a bare sensor, but when an optical fiber is embedded, its response is affected by the stress transfer of a surround material. In 2003 the response of an embedded FBG to transversal load was investigated [60]. The sensor was integrated into the epoxy form, which could be loaded in two-axial loading tests (Figure 1-29).

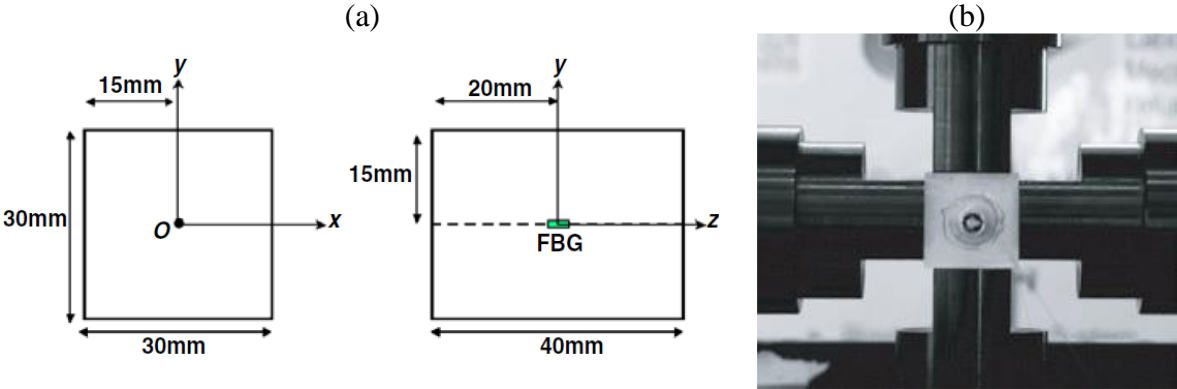


Figure 1-29: HB FBG integrated into the neat resin; a) Geometry of the specimen with FBG, b) Specimen in loading fixture for bi-axial loading tests [60].

An HB FBG integrated into epoxy samples was also subject of another research. In the paper [142] FBG was integrated in the middle of an epoxy roller (Figure 1-30). This approach was used to investigate the influence of the host material on the angular sensitivity of FBG.



Figure 1-30: An epoxy roller with an integrated compressed FBG on the testing machine [142].

Further work in this field focused on increasing measurement sensitivity and discerning additional strain components. HB FBG is cross-sensitive to axial and transversal strain. In papers [22,137] use of two FBG sensors was proposed to measure multiaxial strain. To change the sensitivity to transverse load of an FBG, it was inserted into a steel capillary, which prevents one sensor from being transversely compressed. This approach shows the possibility of determination of the three-dimensional principal strain in the location of sensor with determination of temperature.

An increase in strain-sensing abilities was achieved by the use of microstructured optical fibers [21]. Fiber optimized for strain use was presented in [135]. The FBG inscribed in presented fiber outperformed previous phase-maintaining fibers (fiber shown in Figure 1-23b) by increasing the transverse force sensitivity to about $-370 \text{ pm}/(\text{N}/\text{mm})$, which is twice that measured for bow tie fiber. Furthermore, the peak separation for an FBG was 2.17 nm at $\lambda_B=1550 \text{ nm}$, so six times more than for the bow tie fiber reported, e.g. in [59]. This significantly increased the range of measurement of this method.

In next papers, this MOF was used to measure the three-dimensional principle strain [19]. In this approach, variation in the angular sensitivity to the transversal load was used. Two MOF FBGs were placed in such a way that both fibers were parallel, but their polarization axes were orthogonal (Figure 1-31). Due to this approach, sensitivity to measure principal strain was increased. The use of this kind of sensors along with FEA to calculate the transfer matrices allowed the measurement of the strain with a resolution of around $5\mu\epsilon$ in the transverse direction. Subsequently, the same sensor configuration was used to measure the 3D dynamic strain during impact load to the composite coupon [118].

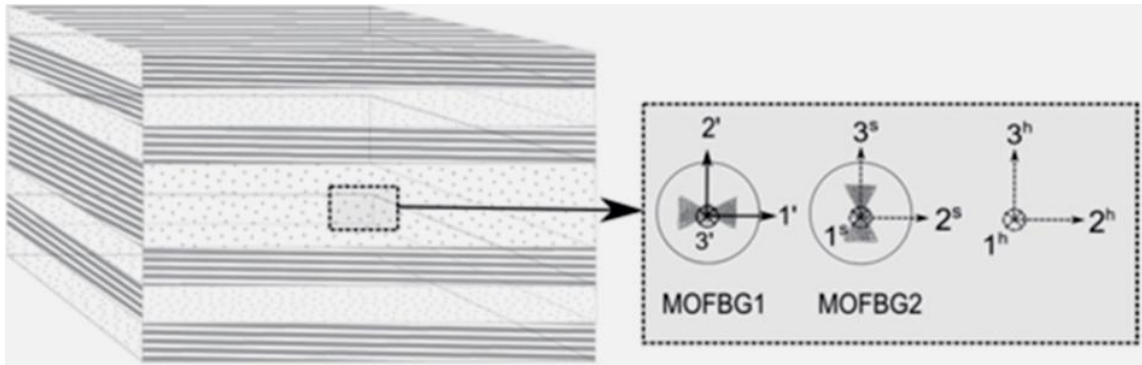


Figure 1-31: Placement of MOF FBGs in a form of 3D strain sensor [19].

Another approach was to optimize the embedding angular orientation of the optical fiber in order to achieve highest sensitivity to measure some specific structure state, e.g. a MOF FBG integrated at the 45° angle (Figure 1-32) was able to detect transverse shear load, which was associated with the progress of delamination in the joint.

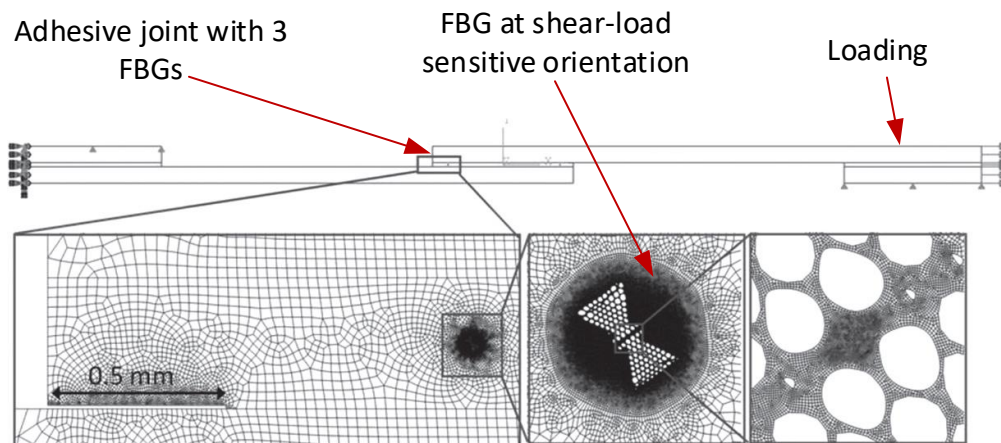


Figure 1-32: Single lap joint monitored with MOF FBGs in shear-sensitive measurement orientation [20].

1.4. AIM AND SCOPE OF THESIS

Considering the presented above state of the art, covering the fields of: optical fiber sensors and current challenges in the area of monitoring of composites and composite structures during manufacturing and operation, the following main assumptions and goals of the dissertation were stated.

The scientific goal of the dissertation is the demonstration of the suitability and determination of the scope of application of integrated Bragg gratings inscribed in highly-birefringent optical fiber (HB FBG) for strain measurement at the stage of manufacturing and exploitation of continuous fiber-reinforced polymers.

The application goal of the dissertation is to present ways to use HB FBG sensors in two selected modern composite manufacturing technologies, namely resin transfer molding (RTM) and automated tape layup (ATL).

The main theses of the dissertation are:

- HB FBG sensors can be used to monitor the manufacturing processes of thermoset and thermoplastic matrix composites (to the best of the author's knowledge, application for thermoplastic matrix composites has been addressed for the first time in the literature).
- HB FBG sensors can be used to measure the complex state of strain inside the composite.
- HB FBG sensors can be used for monitoring of composite under quasi-static as well as time-varying loading

In order to achieve the objectives and prove the thesis, the following **key research tasks** had to be planned and performed:

1. Obtaining and calibrating a unique HB FBG sensor, including:
 - a. Obtaining of a side-hole optical fiber and inscription of the FBG sensor,
 - b. Mechanical calibration of the HB FBG under the transversal force applied to the optical fiber with sensor,
 - c. Identification of hazards to the optical fiber during composite manufacturing processes, independently for two processes (RTM and ATL).
2. Detection of gel point and the measurement of residual strain in RTM process.
3. Quasi-static mechanical testing of composite samples fabricated by RTM process with embedded sensors used for detection of complex strain state.
4. Measurement of residual strain during composite fabrication by ATL process.
5. Measurement of strain of composite produced by ATL process with integrated HB FBG sensor under cyclic loading.

Additional assumptions:

The implementation of the above interdisciplinary tasks required the use of the competence and technical resources of the following research institutions:

1. Department of Mechanics, Materials and Biomedical Engineering, Faculty of Mechanical Engineering, Wrocław University of Science and Technology in the field of: performing of mechanical tests of composites and calibration of HB FBG sensors. Task performed by the PhD student.
2. Chair of Processing of Composites, Leoben University (Austria) in the field of: fabrication of composites by two technologies (RTM and ATL) with simultaneous embedding of fiber optic sensors. Task performed by the PhD student.

3. The Institute of Electronic Systems, Faculty of Electronics and Information Technology, Warsaw University of Technology (WUT) on: inscription of FBG sensors in side-hole optical fibers using WUT's original systems for writing of Bragg gratings. Task performed under contract without participation of a PhD student.
4. Laboratory of Optical Fibers Technology, Institute of Chemical Sciences, Faculty of Chemistry, Maria Curie-Skłodowska University in Lublin in the scope of: production of original highly-birefringent side-hole optical fiber. Task performed under contract without the participation of a PhD student.

Financial support:

The main costs of the works were covered by two sources, namely:

1. Main project: InterDok – Interdisciplinary Doctoral Studies Projects at Wroclaw University of Science and Technology, project no, POWR.03.02.00-00-I003/16, co-financed by the European Union under the European Social Fund.
2. Mobility project: Mobility program financed by the Polish National Agency for Academic Exchange (NAWA, project no. PPN/BIL/2018/1/00058) and Austria's Agency for Education and Internationalisation (OeAD, No. PL 05/2019).

2. MANUFACTURING AND CALIBRATION OF FBG INSCRIBED IN HIGHLY-BIREFRINGENT FIBERS

The FBG sensor written on a birefringent optical fiber and the possibility of its application in selected composite technologies were crucial for achieving the goals set in the dissertation and confirming the main hypothesis.

Difficulties related to the lack of access to a commercial product forced the need to obtain a dedicated solution in cooperation with recognized research institutions in Poland. Thus, in particular, it was necessary to:

- Obtain a highly-birefringent optical fiber with the required properties,
- Inscribe a fiber Bragg grating,
- Build a measurement system to study the sensitivity of the sensor as a function of the applied transverse force, its angle of application and temperature,
- Write software for the processing of optical signals,
- Perform tests to determine sensor sensing parameters.

The implementation of the tasks and the results obtained are described below, supplemented by references from the literature.

2.1. SIDE-HOLE FIBERS AND INSCRIPTION OF FBG SENSORS

In this research, a highly-birefringent optical fibers manufactured in Poland in Laboratory of Optical Fibers Technology, Institute of Chemical Sciences, Maria Curie-Skłodowska University in Lublin and previously described in the literature were used [143–145]. The optical fiber, which had two large side-holes and elliptical core positioned in a thin glass bridge between the holes (Figure 2-1). The fibers preform was composed of pure silica rods and tubes and a cylindrical core preform. Central part of the preform was heavily doped with germanium (~22% m/m) and contained a thin pad of pure silica. The preform was thermally bonded and fiber was drawn at a temperature of about 2175°C with drawing speed around 20 m/min. The elliptical core was formed by the elevated pressure inside the side holes, causing compression of the glass bridge and enlarging of side-holes. While both fibers were produced from the same preform, the pressure variation was used to influence the fibers geometries. Fiber manufactured with lower pressure was labeled side-hole fiber 1 (SH1), while with higher side-hole fiber 2 (SH2) [128]. For both fibers selected geometry features were measured; fiber cladding diameters (2R), side hole sizes (D), thickness of the glass bridge (c), as well as core diameters (a and b), and core ellipticity (e). The sizes of the geometric features were measured directly from the SEM images and are summarized in Table 2-1.

Higher pressure applied to the holes caused higher ellipticity of SH2 fiber, and therefore, higher birefringence [127]. The phase birefringence value measured at 1550 nm with wavelength scanning method [146], combined with the lateral force method [147] equals to 10.5×10^{-4} and 4.4×10^{-4} for SH2 and SH1, respectively [128].

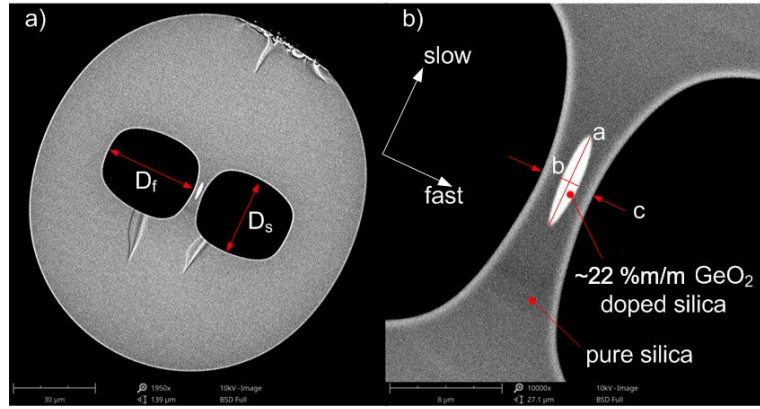


Figure 2-1: SEM image of side-hole 2 optical fiber, a) An entire fiber's cross-section, b) Zoom of a glass bridge between holes with visible fiber's elliptical core [128].

Table 2-1: Geometrical features of the side-hole fibers [128].

Fiber	Core			Glass bridge	Side hole		Cladding	
	a	b	e	c	D _s	D _f	2R _s	2R _f
	[μm]	[μm]	[-]	[μm]	[μm]	[μm]	[μm]	[μm]
SH1	4.6	1.8	2.6	5.7	23.4	32.5	128.9	120.0
SH2	6.9	1.5	4.6	4.0	27.4	33.8	131.7	120.0

2.1.1. Bragg Gratings inscription and exemplary FBG spectrum

Fiber Bragg gratings used in research were inscribed in the Institute of Electronic Systems, Faculty of Electronics and Information Technology, Warsaw University of Technology. Both SH1 and SH2 fibers were photosensitive due to a high concentration of GeO₂ in the cores. This means that no hydrogen loading, which would increase photosensitivity was required. To ensure compatibility with the optical interrogator, pieces of a regular SMF-28 optical fibers were spliced to the both ends of the SH fibers. Difference in shapes and sizes of the mod fields of the combined fibers caused coupling losses of less than 3 dB. Although this value is significantly larger than the coupling losses in the SMF welding, it did not have a significant impact on the measurement capabilities during operation of the HB FBG sensor.

Fiber Bragg gratings were written using a phase mask technique. This technique provides the best repeatability of all FBG writing methods [127]. A KrF excimer laser operating at 248 nm was used for inscription. It emitted z short pulses of 20 ns duration with a repetition rate of 200 Hz. The UV beam was focused on an optical fiber through a cylindrical lens with a focal length of 17.5 cm, producing fiber Bragg gratings with a length of a few mm. To obtain Bragg wavelength peaks at approximately 1550 nm, a phase mask with a period of 1069 nm was used [128].

During laser illumination, the grating inscription was monitored. The transmission spectrum was monitored using an optical spectrum analyzer with 20 pm resolution. The optical fiber was connected to a broadband superluminescent diode. In order to achieve an equal excitation of both polarization modes, a polarization controller was used. The free ends of the

fiber were fixed to prevent bending or changes in fiber position. Such polarization control allowed the two peaks to be balanced during FBG labeling. It was found that the relative arrangement of the air holes and the illumination beam did not affect the quality of the grating. The writing was stopped when the transmission minima exceeded -2 dB. In addition, the quality of the FBGs was not compromised because the UV pattern was only affected by two air-glass interfaces in the fiber. In the case of microstructured fibers with multiple holes, the interference pattern behind the phase mask may be degraded, blocking the FBG formulation [148].

An exemplary transmission spectrum from the FBG inscribed in SH2 fiber is shown in Figure. Birefringence of the fiber resulted in two well distinguishable minima, for both fast and slow fiber axes. For the unloaded Bragg grating in the room temperature, Bragg wavelength were 1547.1 nm and 1548.3 nm, so the peak separation was 1.2 nm. This separation corresponds to the birefringence of 11.2×10^{-4} [128].

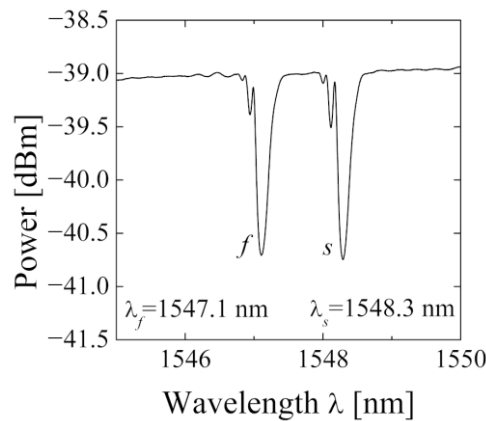


Figure 2-2: An exemplary transmission spectrum of fiber Bragg gratings written in SH2 optical fiber [128].

2.2. REVIEW OF HB FBG MECHANICAL CALIBRATION DEVICES AND DEVICE USED IN THE THESIS

The sensitivity to the transverse load of an FBG inscribed in high-birefringent fibers depends on the angular orientation [22,59]. This causes the need to find the sensitivity to the transverse force depending on the angular orientation of the fiber. For this reason, load is applied to the optical fiber on some angle, response to the transversal load is measured, and later, fiber is rotated by some angle and loaded again. The procedure is repeated until half on an optical fiber was tested. The basic concept of the measurement basis is shown in Figure 1-27.

In literature, two basic concepts of the fiber loading are present [149]. One is based on the leverage arm to apply load to the fiber, second – directly applying force. Detailed overview of the testing setups is provided in dissertation [149], here only examples explaining the concept will be shown.

Lever designs are based on the one-sided lever, which transfers the load through the pin to the stamp which compressed tested fibers. Example of such a test setup is shown in Figure 2-3. Lawrence et al. [140] proposed a setup with a lever supported by the steel pin, which pushes the stamp to compress two fibers: tested HB fiber and supporting one. Force is adjusted by the changes of a mass hanging on the end of a lever. Use of two fibers placed symmetrically to the steel pin ensures uniform compression of both fibers.

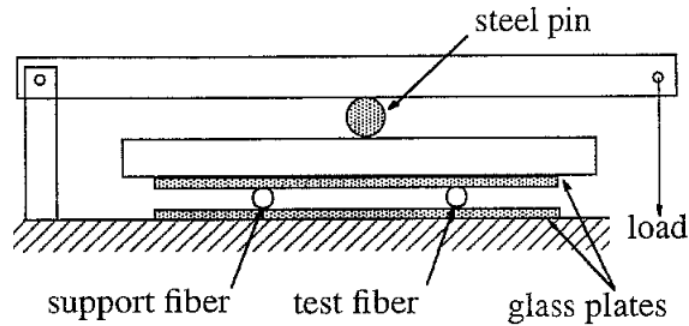


Figure 2-3: Mechanical test stand based on the lever-design [133].

In the case of direct load design [59,150], the fibers (tested and supporting) are placed underneath the stamp, but the load is applied with a rotating screw (Figure 2-4). The stamp moves along the guiding pins, ensuring linear movement. The force is measured with a load button, which is located between the stamp and the screw.

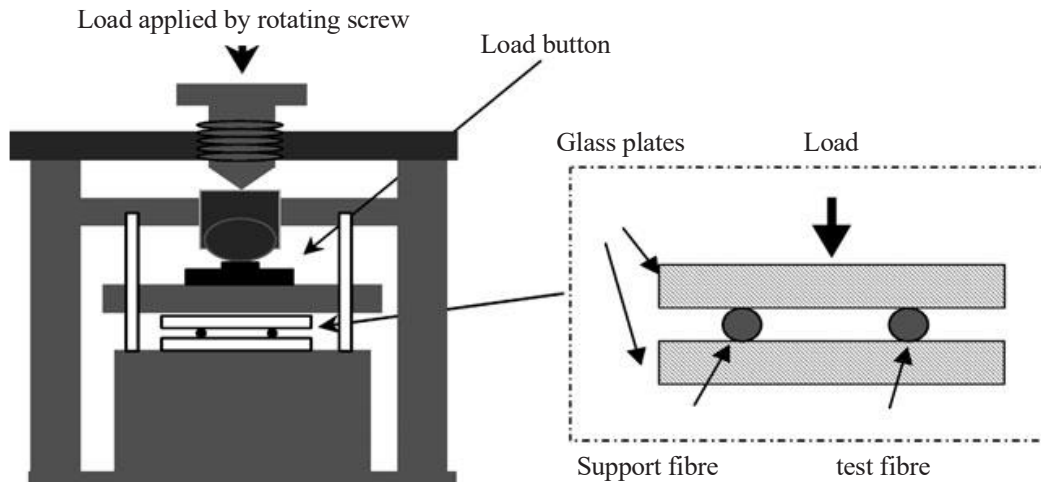


Figure 2-4: Mechanical testing rig design, using the rotating screw to load fibers [59].

On the other hand, in the if the stamp is guided by pins and both glass plates are not perfectly parallel, fibers will be compressed uneven, because no compensation is possible. Additionally, friction of the guiding pins can influence force readings, since measurement was performed between the loading screw and the upper part of the stamp.

Guemes [133] proposed a simple setup in which two fibers with FBG sensors were placed between glass plates and compressed (Figure 2-5). The use of two sensors allowed the compensation of misalignment in the applied load to both sensors. The lack of guiding pins compensated for the load distribution and eliminated friction; however, optical fibers could work as rollers, which could cause their rotation.

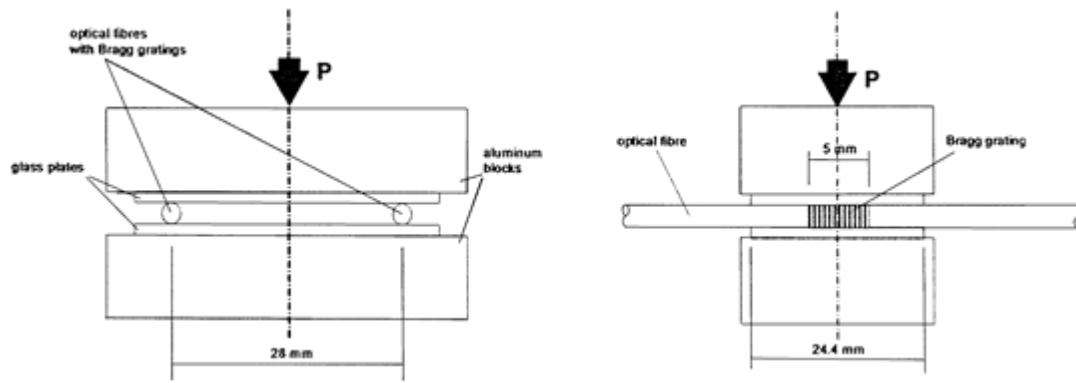


Figure 2-5: The testing design directly loading optical fibers [133].

The design presented in [149] dealt with the rotation and friction problems by designing the fixture to the testing machine (Figure 2-6). In this approach, two fibers with inscribed FBG sensors were fixed in rotational stages on each side. As a support, a steel base with a glass plate inserted underneath the fibers was used. Force was applied through the polished steel stamp and compensation of the loading direction was ensured by the use of a ball joint. To increase the repeatability of applying force stamp, the release mechanism was lifted with four pins pushed out simultaneously. The use of two FBGs was explained to be a method to better compensate the nonuniform load applied to the fibers. It was assumed that since both FBGs are from the same batch, they should have comparable sensitivity. Therefore, when sensitivity will be determined at the same time for both FBGs, the final proper sensitivity is the average of the results obtained for both sensors.

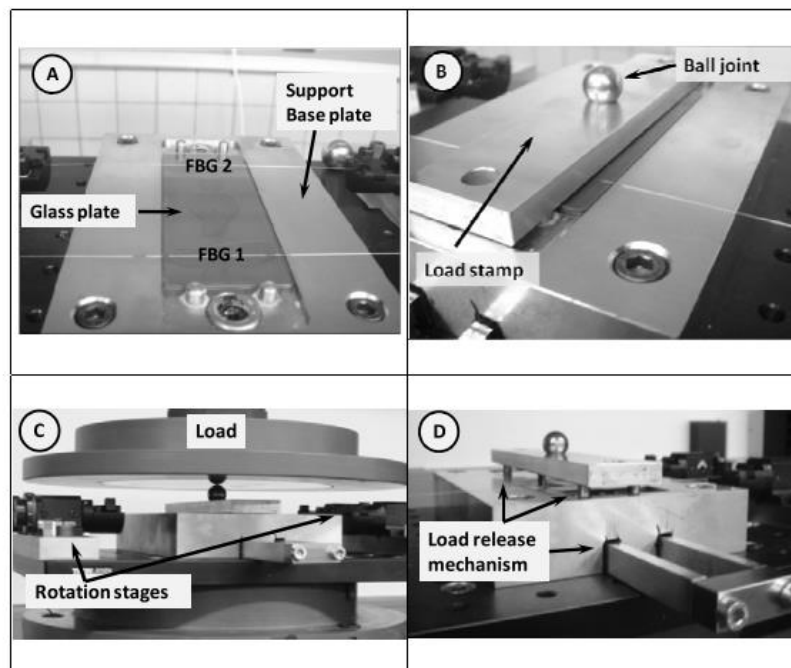


Figure 2-6: The fixture used to measure sensitivity of HB FBGs in a universal testing machine [149].

On the basis of the solutions presented, a modified test setup of our own was proposed (Figure 2-7). In this design, the load is applied directly on three optical fibers (one – with written FBG and two supporting fibers). Fiber with an FBG is placed in the middle, and supporting

fibers are fixed symmetrically on both sides. Force is applied with a loading screw, which pushes the stamp down. A steel ball between the bolt the pushing pin and rubber joint between the pushing pin and the upper stamp allow the compensation of misalignment. When the fibers are not loaded, the upper stamp is lifted by a spring pushing the guiding pin to the top.

The fibers are placed on the top of the lower stamp, which is fixed to the force transducer (1kN range, Erichsen, Iserbach, Germany). This way the exact force applied to the fibers can be measured. The tested optical fiber is rotated with fiber rotators (HFR007, Thorlabs Sweden AB, Mölndal, Sweden). Bragg wavelengths for both polarizations are derived from the reflection spectrum acquired with the optical interrogator (SI405, HBM, Darmstadt, Germany). The detection method is described in the further sections.

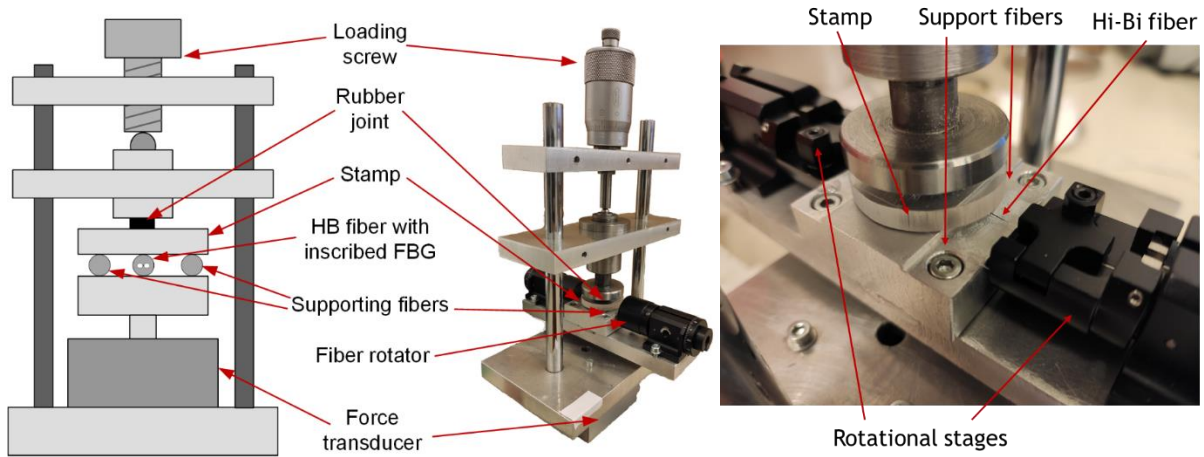


Figure 2-7: Testing device used for the mechanical testing of the HB optical fibers with in-written FBG [128].

In this design, the load was distributed along the three fibers on the length of 20 mm (width of the lower part of the stamp). Due to the compensation mechanism, it was assumed that the force is uniform along the three optical fibers, so the linear loading force was calculated by dividing the measured force by the sum of the length of the compressed part of the fiber, so the force applied to the fiber was in the range $[0; 100] N$ ($[0; 1.67] N/mm$). The whole sensitivity characteristics of a fiber is measured along half of a revolution in 15° steps. For each angle characteristics of $\lambda_{FBG}^s = (F, \varphi)$ and $\lambda_{FBG}^f = (F, \varphi)$ were collected. Regression lines were fitted to the results $\lambda_{FBG}^{s,f} = (F, \varphi)$. Slopes of lines are final sensitivities of both polarization modes to the external transverse load.

The changes in the peak separation of the fiber subjected to external load are described by effective sensitivity (s_{eff}). It can be calculated either by subtracting the sensitivity for the slow axis and the fast axis:

$$s_{eff} = s_s - s_f \quad (2.1)$$

or by the fitting of the line to the separation for each sample point peaks, which is:

$$s_{eff} = \frac{\Delta SEP \cdot l}{F} \quad (2.2)$$

where ΔSEP is variation of peak separation. The effective sensitivity describes if peaks of the FBG are getting closer ($s_{eff} < 0$) or further from each other ($s_{eff} > 0$).

The whole procedure to obtain the mechanical response is shown in Figure 2-8.

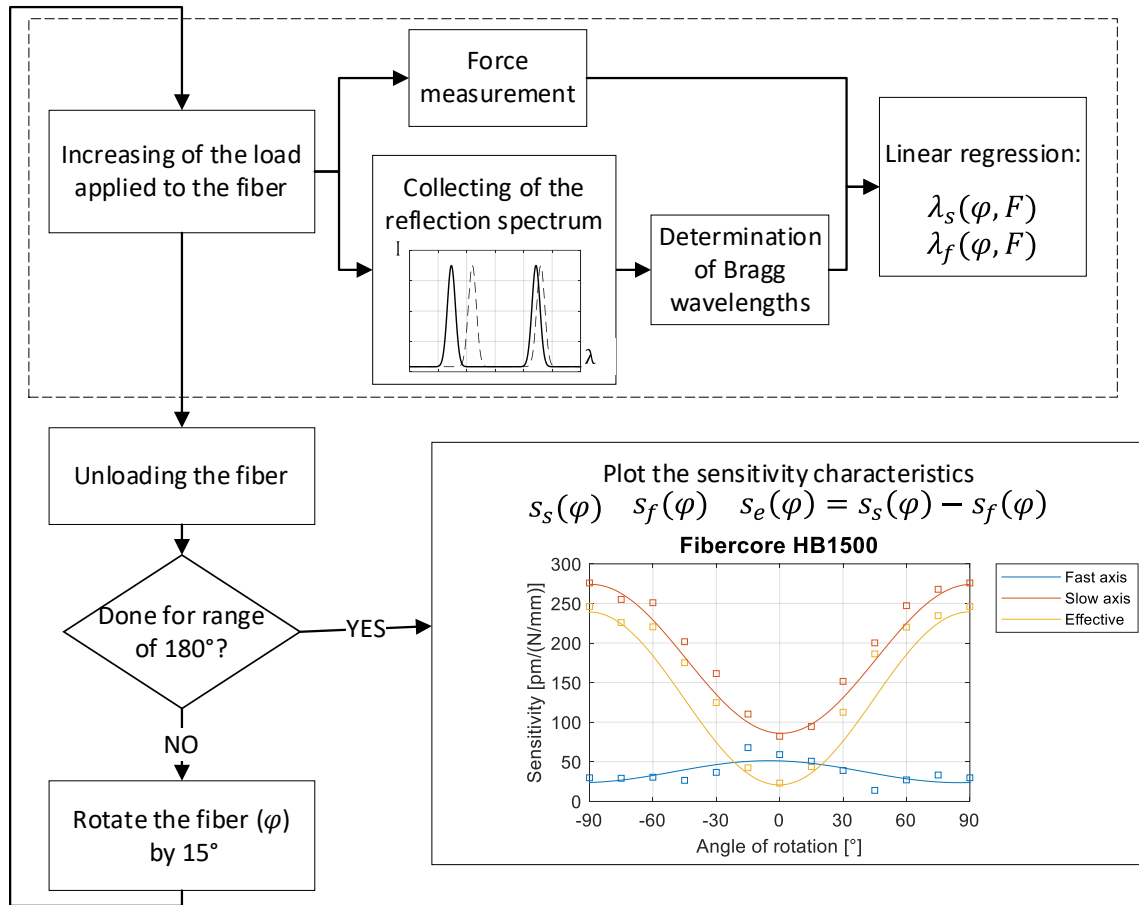


Figure 2-8: Procedure for the determination of the mechanical properties of HB FBG.

When the calibration curve is done, it is possible to find the orientation that results in the highest sensitivity to the transverse force. When the fiber is placed in this orientation, small droplets of glue are placed on both ends of the optical fiber. After curing, the flat bottom surface of the droplets fixes the optimum orientation of the optical fiber.

2.3. SOFTWARE SUPPORTING THE SENSITIVITY TESTING OF THE HB FBGS AND BRAGG WAVELENGTHS DETERMINATION

During the testing of the sensors force was applied at various angles to the fiber. In each orientation during applying of the force, Bragg wavelengths in the function of force had to be determined. To help in this process, the software and scripts to automatically determine the sensitivity curve was developed.

During the testing, spectra along with force measurement were collected. Scheme of data collection is shown in Figure 2-9. Each spectrum from HBM SI405 was saved in separated txt files with HBM Catman software. Filename were rotation angle and a timestamp. Force logging software written in C# and .NET was run on the same computer. It used the RS232 connection to the Rinstrum R320 measurement module, which was reading force applied to the fibers.

Force logger collected timestamps and force. For each rotation angle force-spectra results were placed into separated catalogs. Procedure of collecting spectra and force was performed for all required angular orientations.

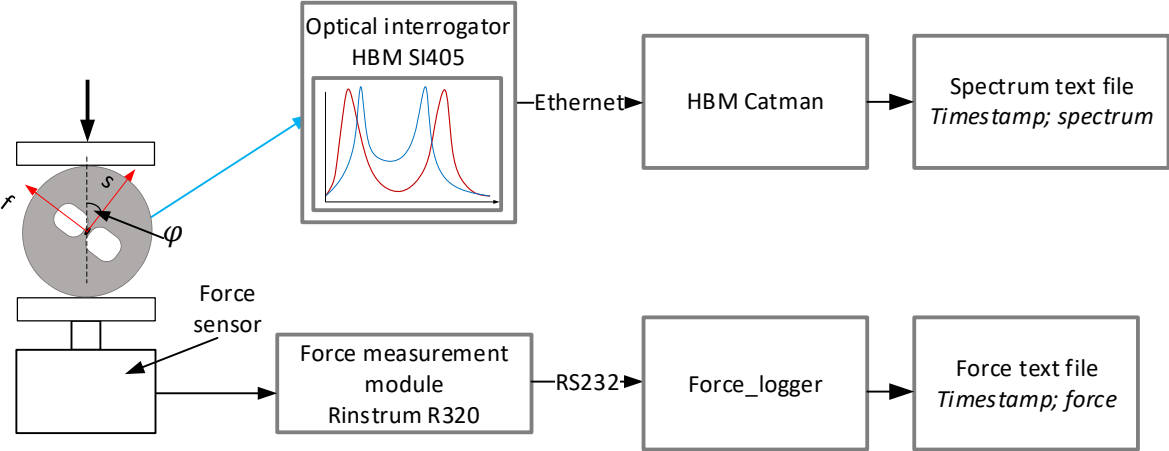


Figure 2-9: Scheme of measurement results flow.

After testing of the whole fiber, hundreds of output spectra files were collected. They were renamed with another program, which combined spectra with corresponding force. As an output new files named by the angle and force were produced (eg. Filename for $\varphi = 135^\circ$ angle and $F = 1.123N$: FBG_135degrees_1.123N.txt). Such files were imported into the MATLAB environment and further processing was performed to detect Bragg peaks. Bragg wavelengths are plotted against the force and regression is made to get sensitivities for fast and slow axis. Script does this to all orientation and plots the resulting sensitivity curve. Dataflow and example fitting processes is shown in Figure 2-10.

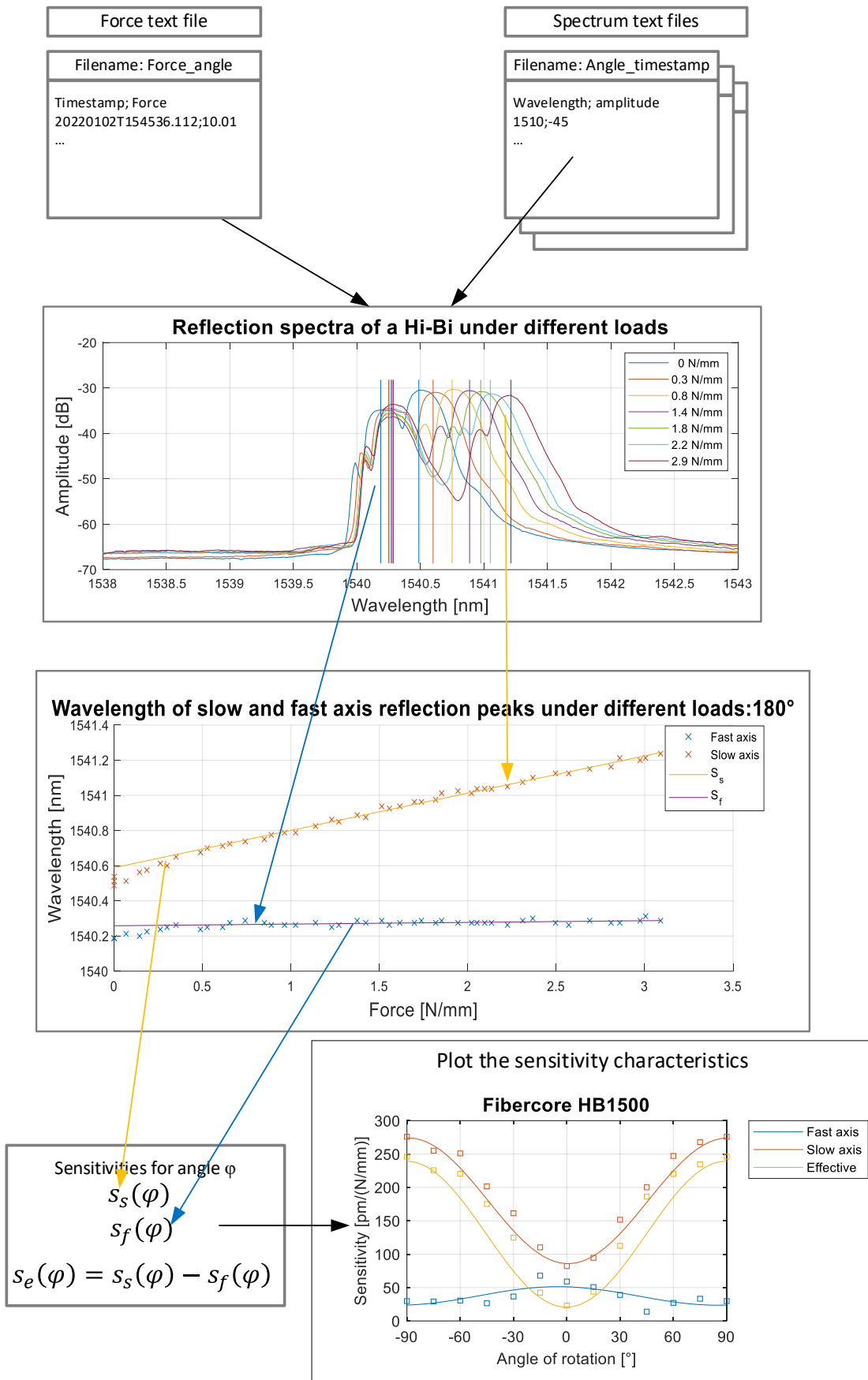


Figure 2-10: Determination of sensitivities of HB loaded in some angular orientation.

Reflection spectra under the transversal load had to be processed manually because tested spectra were often distorted, so the automatic determination method implemented into the interrogator couldn't provide reliable data. To find the exact Bragg wavelengths for both axes, different methods of Bragg wavelength determination were tested [151–153], namely:

- Maximum detection algorithm – wavelength which corresponds to the maximum reflection power in spectrum
- Full width at half maximum (FWHM) – middle point between points when amplitude dropped by 3dB
- Centroid detection algorithm – geometrical centroid of the reflection spectrum
- Polynomial fitting – uses least-square method to fit polynomial (in most cases 3rd order) to the surround of the Bragg peak
- Cross-correlation algorithm (CCA) – calculation of the correlation between the two spectra gives a Gauss distribution, which peak is related to the shift of a Bragg wavelength [152]
- Fast phase correlation algorithm – first, Fourier transform is calculated on two spectra and the differences in phases for spectral lines is calculated into the peak shift [151]

In the simple test with stretching of an FBG inscribed in low-birefringent (regular SMF fiber), it was found that for the nondegraded spectrum, all methods gave approximately good results. For the maximum detection algorithm, the resolution was the lowest, since it is limited to the resolution of the measurement points in spectrum. All the other methods shown consistency on the sub-resolution level.

The test performed on the transverse force compression of HB fibers (data from the mechanical test of HB fibers) showed that for distorted spectra, methods based on correlation performed best among all of them, which was also found in the literature [151]. For this reason, the cross-correlation method has been used for peak determination in all Bragg wavelength measurements described in this thesis, unless otherwise stated.

2.4. MECHANICAL TESTING OF FBG INSCRIBED IN HB FIBERS AND TEMPERATURE CALIBRATION

The method explained in previous points will be applied to assess sensitivity of the HB FBGs to the transversal load. The results of the mechanical tests of the fibers shown in this section are part of a published paper [128].

First, to ensure that the measurement results are valid, the procedure was validated by testing the bow-tie fiber (HB1500, Fibercore House, Southampton, UK), which was often used in previous tests [22,59,60,100,137,142,154]. A cross-section diagram of this fiber is shown in (Figure 1-22). Validation of the method was performed by testing four FBGs. Since all the fibers were from the same batch of optical fiber, average sensitivities were used. The results are shown in Figure 2-11.

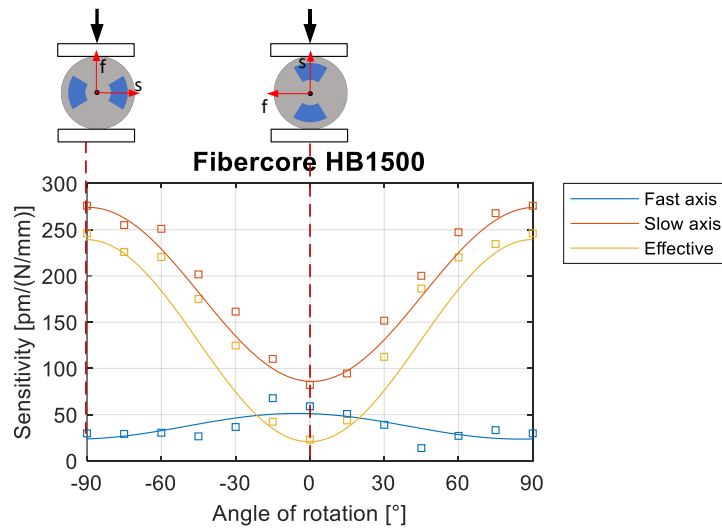


Figure 2-11: Transverse sensitivity of HB15000 fiber to the transversal load for varying fiber orientation [128].

The maximum effective sensitivity of $s_{eff} = 230 \text{ pm}/(N/mm)$ was observed when force was applied along the fast axis of the fiber ($\varphi = 90^\circ$). In this orientation, the sensitivity of the slow axis was $s_s = 260 \text{ pm}/(N/mm)$ and $s_f = 30 \text{ pm}/(N/mm)$. The shape of a curve was similar to shown in the literature (sine-like) [22,59].

The validated testing method was used to determine the transversal load sensitivity of side-hole fibers with an elliptical core (SH1 and SH2).FBG inscribed in side-hole fibers were tested accordingly to the method described previously. Obtained sensitivity curves are shown in Figure 2-12:

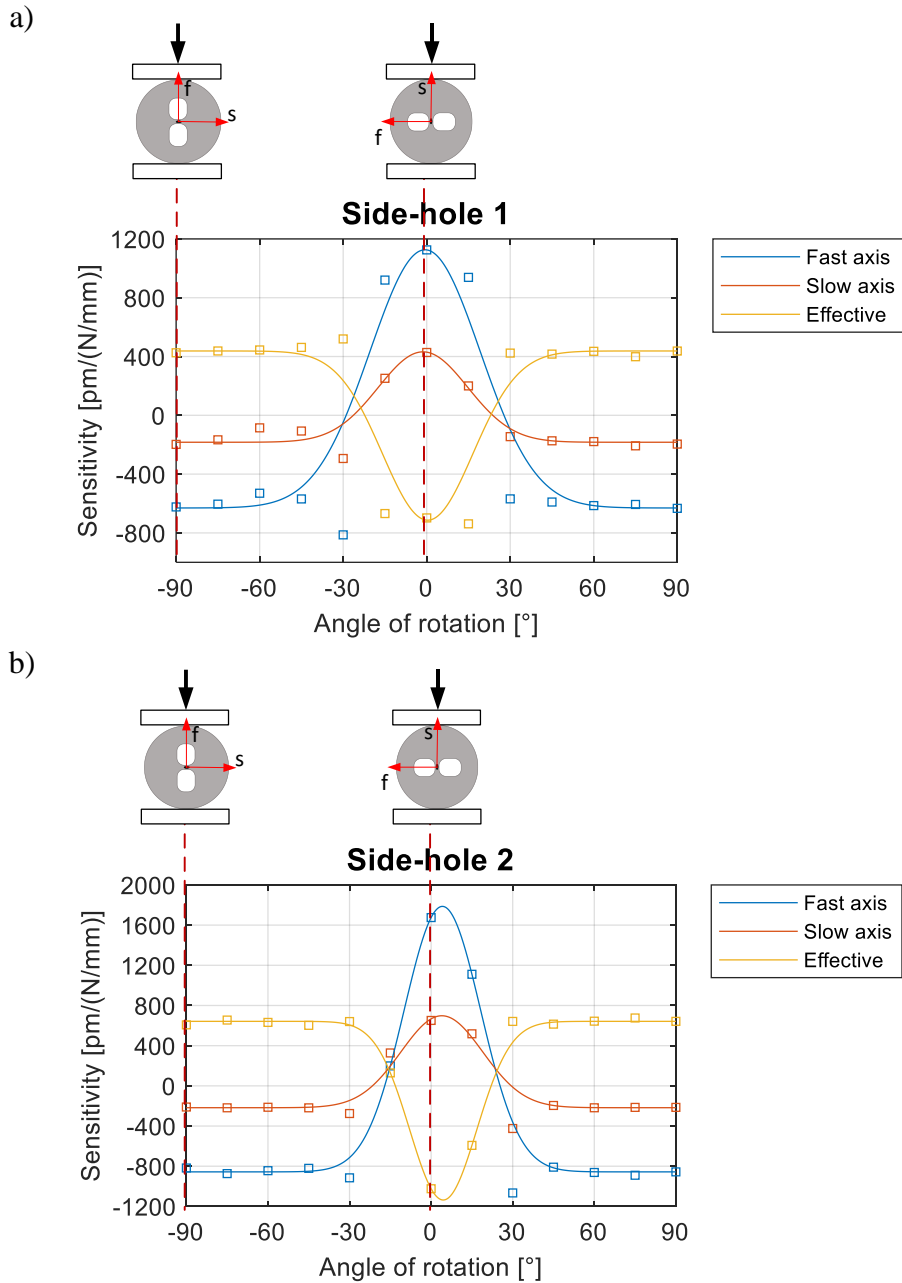


Figure 2-12: The transversal force sensitivity curves for fibers: a) Side-hole 1 (SH1)
b) Side-hole 2 (SH2).

Sensitivity curve of the side-hole fibers consist of a wide and relatively constant sensitivity in the long range in angular orientation of $\pm(30-90)^\circ$. In the range of $\pm(0-30)$ sensitivity rapidly changes. When load is applied along the slow axis ($\varphi = 0^\circ$), s_{eff} is negative and achieves maximum amplitude of the sensitivity.

The fact that the sensitivity curve has a wide flat part of the curve can be very useful with the integration into materials, because even if the orientation of the fiber during integration changes, the sensitivity for the strain measurement should not change significantly. Paper [19] shows FEA results showing that even misalignment of 25-30 degrees for the microstructured optical fiber (butterfly type) did not significantly influence the strain-sensing abilities [135].

The effective sensitivity of fibers subjected to the transversal load is achieved when load is applied along the slow axis of the fiber ($\varphi = 0^\circ$). In this orientation the effective sensitivity of SH1 $s_{eff} = -700$ pm/(N/mm) while SH2 $s_{eff} = -1150$ pm/(N/mm). When load is applied in range of $\pm(30-90)^\circ$ sensitivity has stable sensitivity of $s_{eff} = 410$ pm/(N/mm) $s_{eff} = 650$ pm/(N/mm) for SH1 and SH2 respectively. Sensitivities of these fibers are compared with other fibers found in the literature and presented in the Table 2-2.

Table 2-2: Peak separation and effective sensitivity to the transversal load [128].

Optical Fiber	Peak Separation [nm]	Effective Sensitivity to the Transverse Force [pm/(N/mm)]	Ref.
Panda	0.34	-210	[59]
MOF	0.85	100	[21]
MOF (Butterfly)	2.17	-370	[135]
Dual side-hole fiber	0.07	699	[155]
Bow-tie-literature	0.35	160	[22,59]
Bow-tie-measured	0.32	230	Thesis/[128]
Side-hole 1 (SH1)	0.54	410 ($\varphi = 90^\circ$), -700 ($\varphi = 0^\circ$)	Thesis/[128]
Side-hole 2 (SH2)	1.16	650 ($\varphi = 90^\circ$), -1150 ($\varphi = 0^\circ$)	Thesis/[128]

Sensitivity to the transversal force of SH2 fiber is higher than sensitivities of other fibers presented the literature. A different side-hole fiber presented in [155] has similar sensitivity to SH1 fiber, but it has much smaller birefringence, thus almost no peak separation. This reason limits usage of this fiber for small loads with regular optical interrogators, because low force applied to the fiber will only broaden the reflection peak.

For the SH2 fiber the basic peak separation of 1.16 nm allows to measure even loads around zero point. The higher peak separation was reported for the MOF butterfly fiber [135], which could extend the range of usefulness for higher load measurements, but with lower sensitivity than for SH1 and SH2 fibers.

Fiber Bragg gratings inscribed in both side-hole fibers were tested in terms of temperature sensitivity in 25-100 °C range [128]. Four FBG sensors inscribed in SH1 and SH2 were tested in the oven. Data were collected at 25°C, later for 30-100 in 10°C steps. Shifts were measured for each step giving the following sensitivities:

- For side-hole 1: 10.75 pm/°C (fast axis), and 10.63 pm/°C (slow axis);
- For side-hole 2: 10.41 pm/°C (fast axis), and 10.24 pm/°C (slow axis).

The difference in sensitivities for SH1 and SH2 fibers does not exceed 4%. For each fiber, sensitivities for slow and fast axis are almost the same (<2% difference). Separation of peaks changes by 0.12 pm/°C (SH1); 0.17 pm/°C (SH2), which is 60-80 times less than shift of a single Bragg peak due to temperature. It means measurement of transversal load is almost temperature insensitive.

2.5. DETERMINATION OF FIBER ORIENTATION WITH DIFFRACTION PATTERNS

Location of fiber axes using the mechanical testing method is time consuming. For the half of rotation transversal force has to be applied to the fiber and later based on the sensitivity curve axes of an optical fiber are determined. However, the location of axes of highly-birefringent fibers can be determined by observation of the diffraction view of the laser passed through the side of an optical fiber [59,100,156] or just side-view of a fiber [157]. This approach is faster and doesn't require mechanical loading.

In paper [156] an optical fiber was fixed in a chuck rotation possibilities in such a way that the optical fiber was hanging vertically. On the end of the optical fiber, a small weight was attached. This way, the fiber was hanging straight. A stripped part of the optical fiber was illuminated with a laser. The diffraction pattern was compared with the diffraction pattern obtained for a short optical fiber, the optical axes of which had been determined with a short piece of an optical fiber, by the microscopic view of the cross section of the fiber. The fiber was rotated until the diffraction view matched the reference one.

An orientation of the optical fiber can also be detected by the side-view of an optical fiber seen by the camera. Work [157] describes a procedure for determining the axes of the fiber of a HB fiber (PANDA) based on the width of stripes associated with various parts of the fiber. If fiber was rotated, some of the stripes remained stationary, but those caused by the stress rods has changed. When particular width of strips was achieved, fiber was aligned along known axis. Idea is shown in Figure 2-13.

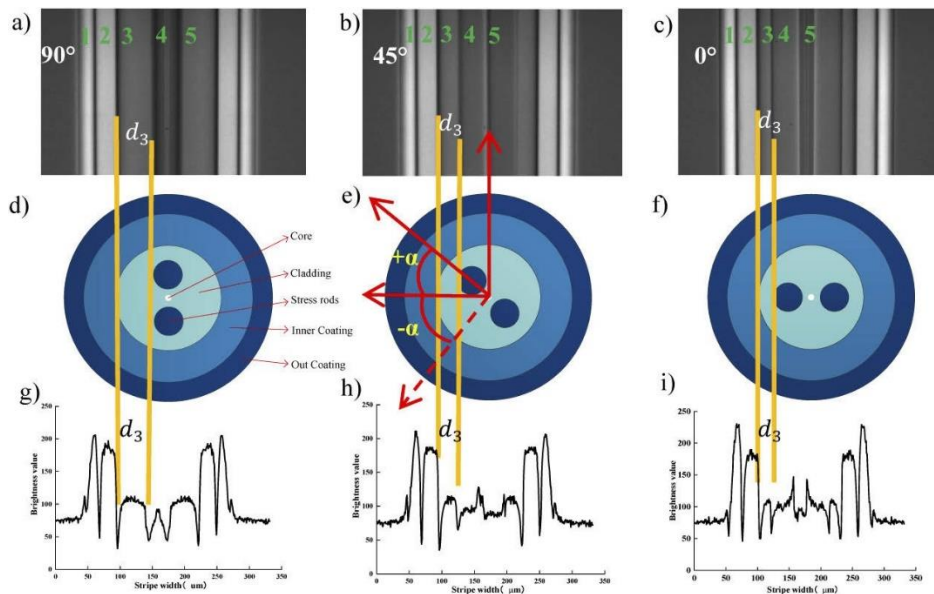


Figure 2-13: Determination of the PANDA fiber orientation based on the stripes widths [157].

Alignment of the fibers in the automatic splicers for phase-maintaining optical fibers is done with the use of a method called Polarization Observation by the Lens-effect Tracing. This

method uses the phenomenon that the circular optical fiber acts as a lens for light that illuminates the optical fiber from its side [158]. The camera is placed in a distance from the fiber, which results in maximum light contrast. Later on, camera is still and fiber is rotated. Rotation causes changes in image contrast because the refractive index of the HB fiber varies with rotation. An angle-contrast profile is characteristic for the fiber and can be used for polarization axes determination.

The setup used in this thesis is shown in Figure 2-14. It is based on the diffraction pattern method, but both sides of an optical fiber are clamped in fiber rotators. Beneath the fibers, there is a supporting table, which makes space to put droplets of glue on both sides of calibrated fiber. The laser illuminates the side of the fiber, resulting in the diffraction pattern visible on the screen behind the fiber.

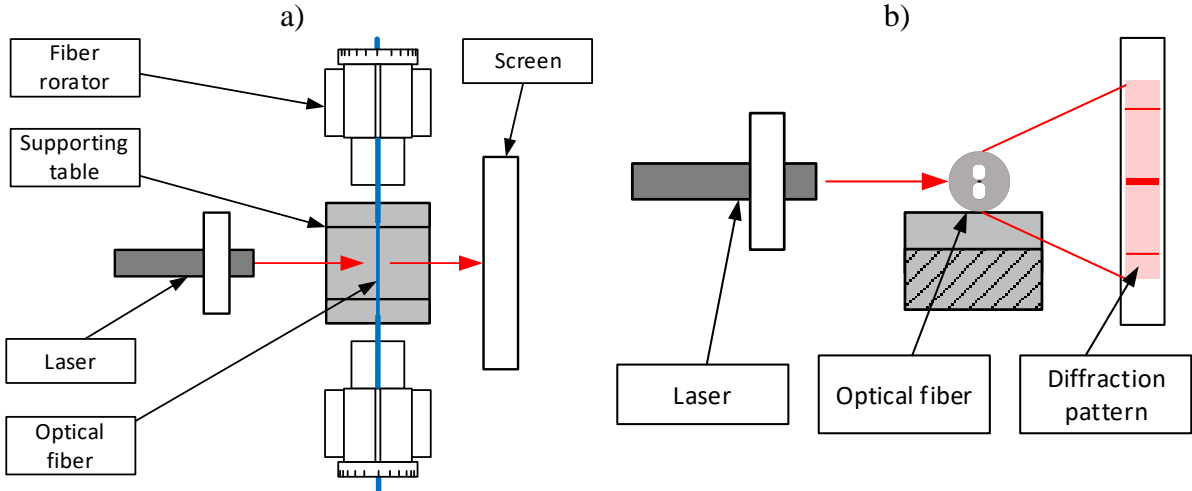


Figure 2-14: Scheme of testing setup, a) top view, b) side view.

First, to correlate diffraction pattern with mechanical sensitivity and axes orientation, FBG inscribed in side-hole fiber was tested with the mechanical loading method. Fiber was fixed in orientation along one of the optical axes. In the next step, the optical fiber was illuminated along this known orientation and diffraction patterns for this and orthogonal orientation were obtained (Figure 2-15).

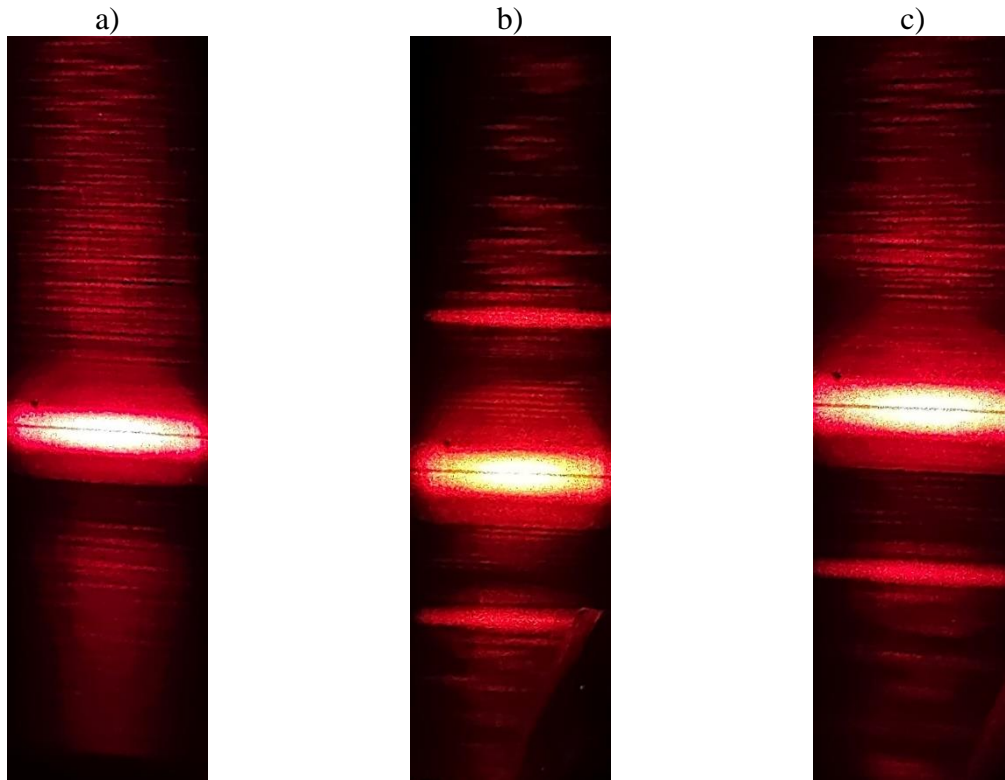


Figure 2-15: A diffraction pattern from the side-hole fiber when illuminated with a laser diode. a) along the fast axis; b) along the slow axis; c) not perfectly aligned with slow axis.

When the side-hole fiber was illuminated along its fast axis (a) – uniform background of diffraction image was observed. If it was illuminated along the slow axis (b) – two distinct lines show up on both sides of the optical fiber. If fiber was not aligned perfectly (c), one of line was blurred. Thus, to align an optical fiber, it was fixed in the setup and rotated until both diffraction side lines were well visible. Alignment was performed on both ends of a stripped section of a fiber to ensure there is no fiber rotation along this length. Finally, depending which orientation of alignment is required for further testing (e.g. highest sensitivity should be in plane or out-of-plane), it was either fixed or rotated accordingly.

This method is better from the mechanical testing, because of higher accuracy, possibility to align fiber rotation along stripped section of the fiber and is less time-consuming. Moreover, a diffraction pattern is changing when fiber is rotated even by 5 degrees (testing steps every 15° [22,60,135]). Moreover, two independent fiber rotators allow to align whole length of the stripped part, because any rotation along the fiber can be corrected with one of them. Method doesn't require manual loading at each step and orientation is visible on the screen immediately. In the case of mechanical loading, a calibration curve first has to be drawn.

On the other hand, this method cannot be used to assess the mechanical properties of the fiber, so pre-testing to find the diffraction patterns for this particular fiber type is still required. Because of this reason, this method can effectively help in use of FBG sensors and speed up the preparation process after their sensitivity curve is determined.

2.6. SUMMARY

Following the work described above, the following main results were obtained:

1. A highly birefringent fiber with two side holes and an elliptical core, manufactured in Poland, was obtained. Different fabrication pressures made it possible to obtain two fibers with different geometrical characteristics and different phase birefringence.
2. Fiber Bragg gratings were inscribed in the fibers using the phase mask technique. By controlling the grating writing process, high-quality gratings with equal excitation of both polarization modes were manufactured.
3. A test stand was built to determine the sensitivity of the sensor to load, in which the force is applied directly to three optical fibers (one - with written FBG and two supporting fibers). The stand was verified by conducting tests on a commercial fiber of known sensitivity.
4. Original software was developed to support testing the sensitivity of HB FBGs, which facilitated the operation of recording and processing a large amount of measurement data.
5. Various methods of determining Bragg wavelengths for both sensor axes (so-called fast and slow) were tested. The method of determining peaks using the cross-correlation method was considered particularly useful and was stashed in further studies.
6. It was shown that the sensitivity of the applied fibers to the transverse force was higher than that of fibers known from the literature. In the case of the SH2 fiber, the sensitivity to transverse force was 60% higher than the best birefringent fibers found in the literature

In addition, a wider application of FBGs inscribed in side-hole fibers requires a faster method for rotational alignment of each FBG. Therefore, an optical method instead of mechanical was proposed. It uses the diffraction pattern of an optical fiber illuminated from the side. This method was faster and less invasive than mechanical testing.

Based on this, it was concluded that the FBG inscribed in SH2 fiber could be approved for testing the determination of the strain field in composites manufactured by the two selected methods, namely resin transfer molding (RTM) and automated tape layup (ATL).

3. RESIN TRANSFER MOLDING (RTM). PROCESS MONITORING WITH HB FBG SENSORS

The next chapter describes the key issue of monitoring resin transfer molding (RTM) process using tested FBG fiber optic sensors. Own results are preceded by a broader description of technological considerations that have a significant impact on the effectiveness of the measurements, including the use of information from the literature.

One of the most popular manufacturing processes for the mass production of composite parts is resin transfer molding. The basic scheme of a process is shown in Figure 3-1. The RTM process begins with the inserting of a preform into the stiff mold. Later, resin is injected and infiltrates the preform. When it overflows, the injection stops and the resin cures. After a certain time, when the product is cured, it is removed from the mold [159].

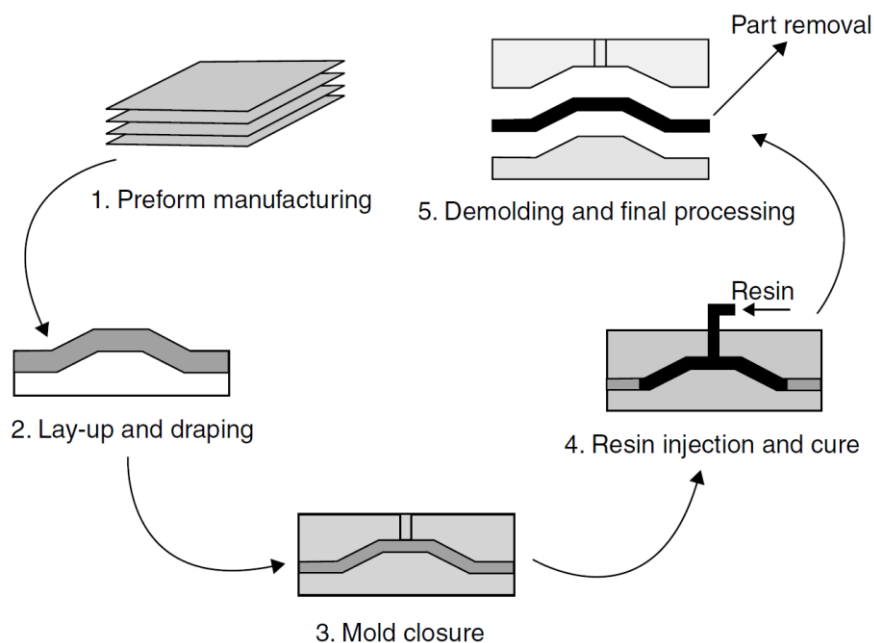


Figure 3-1: Scheme of the resin transfer molding (RTM) process [160].

FBG sensors were applied in the RTM process for residual strain measurement [7,9,70,94,95], gel point [7,70,95], and degree of cure measurement [70,90], but also flow front determination [94]. However, the process can damage or cause a negative impact on the performance of embedded FBG sensors [8,149]. Because of this reason, before sensors installation in RTM, process conditions should be analyzed.

One of the factors that limits the application of FBG in the RTM process is the interaction with the preform during the mold closure. FBG sensors must be embedded with preform, which is compressed during mold closure. The perfect case is that the reinforcement fibers are arranged exactly along the optical fiber. In this case, they surround the optical fiber and protect it. On the other hand, if FBG is placed on some angle to the fibers, nonuniform compression can cause strain gradients along the optical fiber, which can compromise performance of sensors.

In some cases, optical fibers can be arranged along the reinforcement, but often the stacking of the textiles is fixed by the design, which can limit the placement along the reinforcement. In

even the case of a cross-ply laminate, an optical fiber can be parallel to the bottom textile, but will be perpendicular to the reinforcing fibers above it. In the case of twill, the interaction mechanism will be even more complex.

The second part to be analyzed is the process of curing the resin. During the injection, resin causes the local influence on the FBG sensors; resin during the injection, flows through the preform and later is being cured with reinforcing fibers to the final product in the cavity. The liquid resin goes from the liquid state through the gel to the solid state, and the measurement of the neat resin is an important step before the monitoring of the actual RTM process.

The identification of the process conditions which could result in degradation of sensors performance will be tackled in two next subchapters; compression of textiles with FBG sensors in section 3.1, while curing of a neat resin in section 3.2. Later, after an overview of the parts of the manufacturing process, RTM monitoring is done (section 3.3).

3.1. COMPACTION TESTS OF DRY TEXTILES WITH ATTACHED OPTICAL FIBERS

The RTM process is performed in a closed and stiff mold. After inserting the reinforcing textiles, when a mold is closed, the preform is compressed. If FBG sensors are integrated along with the preform, the compacting force compresses the preform and also rearranges the preform to fit FBG inside. If an optical fiber is placed parallel to reinforcement fibers, it will be surrounded by fibers and protected from external load, so even a high force should not cause any problems [28,161]. However, FBG sensors cannot always be placed along the reinforcement. If strain has to be measured in different directions or the preform stacking sequence does not allow them to be fit along the fibers, a compressive force can cause spectrum degradation.

A compressive force that pushes the reinforcing fibers to an FBG can cause small undulations of an optical fiber. As a consequence, the length of the longitudinal FBG strain will vary. This leads to the degradation of the reflection spectrum (broadening/splitting of a peak). Strain gradients along the fiber cause local changes in the period of the grating. This effect does not change the birefringence of an optical fiber, and thus it is not possible to reduce this degradation with polarized light.

However, if textile fibers are packed and their diameter is small in comparison to optical fiber, after curing a composite, they can cause uniform compression along the FBG. As a consequence, this will induce birefringence in the optical fiber [103,121]. In the case of HB fibers, such compression will simply change the peak separation, so measurement will still be possible. In the case of usage of regular (SMF) fibers, this aspect can cause errors in the measurement if unpolarized light is used or require polarization control to reduce this effect.

Induced birefringence does not degrade measurement possibilities of HB FBG, however microbending can lead to interrogation issues, because of the degradation of peaks shape. To find what reinforcement stacking can be used for measurement, compaction tests with optical fibers with dry fabrics were performed, and degradation of the spectrum was analyzed.

Main goal of the tests was to investigate what should be position of FBG and in what stacking conditions (sequence/maximum fiber volume fraction) which would not influence the sensor. Additionally, since birefringence doesn't induced birefringence doesn't compromise functionality of HB FBG sensors, if they can be used in wider range of positions.

A first stage was investigating the interaction of FBG sensors with textiles on the test rig used for mechanical calibration, to see the spectrum changes under various conditions. On the

next stage, the maximum fiber volume fraction (FVF) that can be used in the RTM process, which will not damage the negatively influence of the stripped fibers during the closure of the mold, was determined. In the second stage, the FBG was compacted using the compaction test rig used for textile testing.

3.1.1. Compression of textiles on rig for sensor testing

The issue of the effect of the compressive load on the quality of the signal from the FBG sensor embedded between the reinforcing textiles required dedicated research prior to the main RTM process monitoring tests. A mechanical testing rig used for HB FBG could be used to reconstruct the effects of various textiles and the interaction of FBG. In this case, the FBG sensor is fixed on the test rig, alike during the mechanical tests of bare fibers (Figure 2-7), but additionally piece of various sheet materials or textiles can be placed. Compression of such a stack will reproduce the load application and allow the investigation of potential degradation of spectra. In Figure 3-2 FBG test setup is shown.

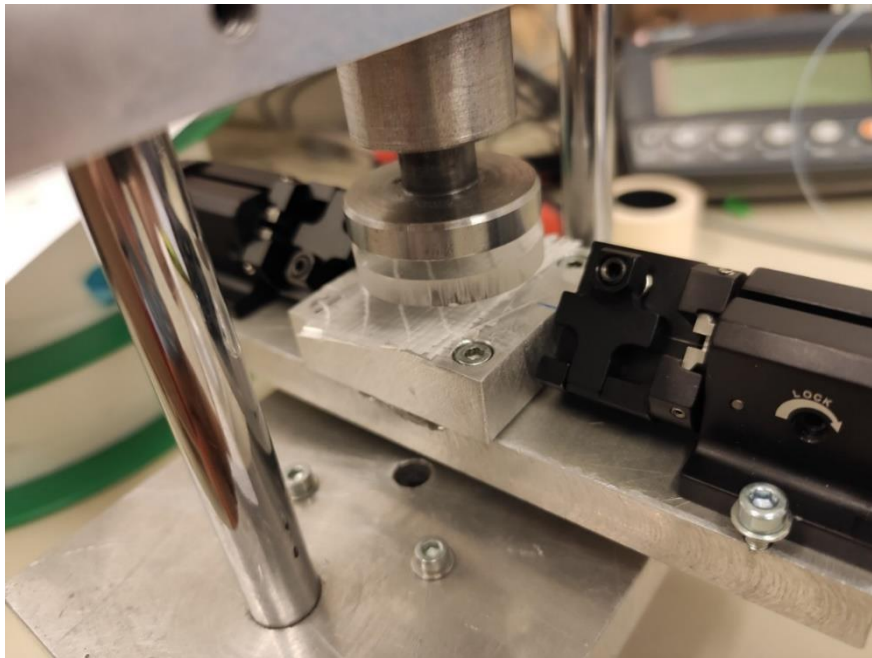


Figure 3-2: Testing of FBG sensors compressed indirectly through various materials.

HB FBG sensor (SH-1) was fixed typically in the testing rig, in the orientation which results in peak separation increase along with the compression force. During the compression, spectra along with force were collected. An FBG was placed on the top of the aluminum stamp, but on the top of the FBG various materials reflecting uniform and non-uniform load were placed, namely:

- Uniform: Paper – regular thick paper sheet (aerial weight 150 g/m²),
- Non-uniform: Fiber reinforcement - EBX400 (SELCOM SRL Multiaxial Technology, Fregona, Italy) glass-fiber non-crimp fiber ([0/90], 400 g/m²)

In the case of the non-uniform reinforcement (glass-fiber NCF), textile sheets were placed on the fiber in three cases: reinforcing fibers along the FBG ($\theta = 0^\circ$), perpendicular to the optical fiber ($\theta = 90^\circ$) and at $\theta = 45^\circ$ to the optical fiber.

Reflection spectra collected during the uniform load applied through the paper are shown in Figure 3-3.

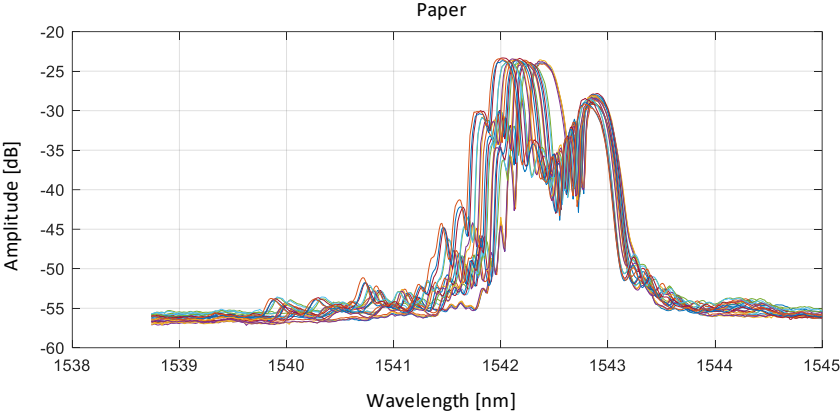


Figure 3-3: Spectrum of SH-1 FBG, under uniform load applied through a paper sheet

Distance between peaks changes, but no peak distortion is present. Application of the uniform load did not compromise possibility to successfully determine both Bragg wavelengths. Cases when load is applied through the single sheet of the non-crimp fabric (NCF) textile is shown in Figure 3-4:

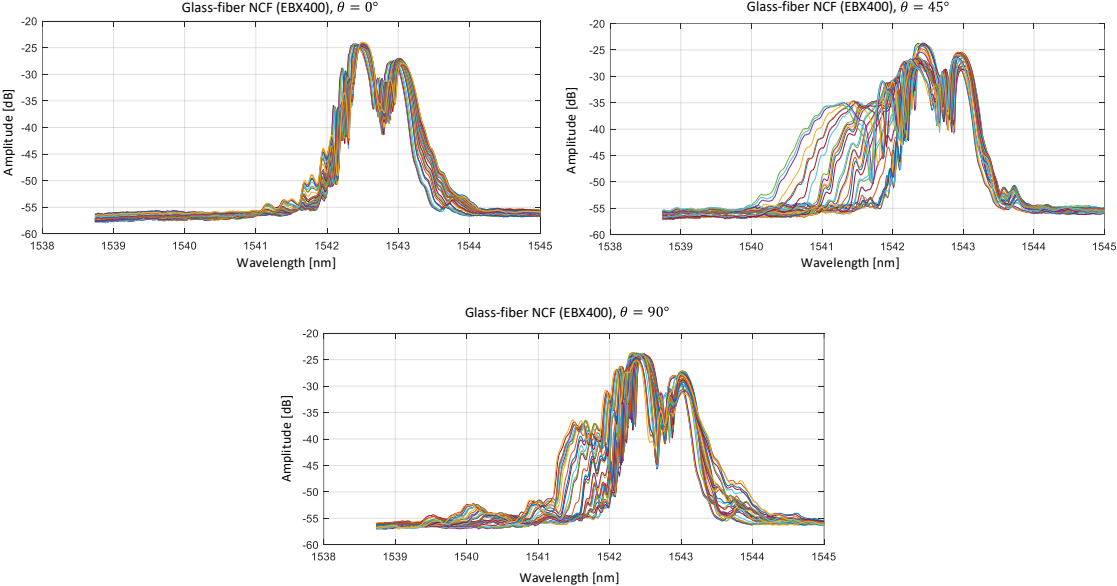


Figure 3-4: Spectra shape when FBG is loaded through the textile aligned at various angles to the optical fiber.

When reinforcing fibers were placed along the FBG sensor, no particular change in the spectrum was observed. Reinforcing fibers protected the optical fiber from the influence of load. No significant change in birefringence was observed. On the other hand, when the sensor was placed at 45 or 90 degrees to the textile direction, spectrum degradation was observed. In the case of 45°, a significant change in the width of the peak is observed. In the case of 90° peak, a side peak forms along with increasing of the load. Consequently, higher loads could lead to domination of the second new peak, causing huge errors in the readings. This is also important to mention, that the misalignment of caused degradation of spectra due to the microbending, not only changing the birefringence

The comparison of spectra for various angles at the same force level is also shown in Figure 3-5.

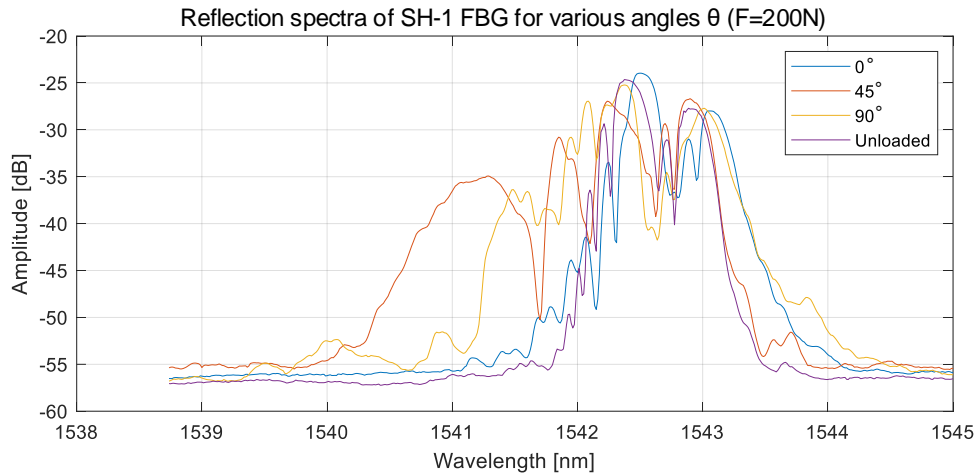


Figure 3-5: Reflection spectra for various angles θ at the same load level ($F=200N$).

The main conclusion that could be drawn from this study is that FBG should be placed along the reinforcing fibers. However, in the case of this test, the FBG is placed on top of the aluminum stamp. In the case of real-time application, the optical fiber is placed between two sheets of reinforcing textiles, which can combine the effects shown to mitigate them.

In addition, as the resin cures, the reinforcing fibers are aggregated by the resin, which can smooth out the pressure distribution along the fiber. In this case, even though the optical is not placed along the optical fiber, the spectrum does not necessarily have to be degraded. It is worth noting that papers [103,121] have shown that induced birefringence is present after curing of a composite.

3.1.2. Compaction using the textile compaction setup

In the previous sub-chapter, it was shown that the relative alignment between optical fiber and reinforcing fibers can influence the performance of FBG sensors, but compaction conditions used there does not precisely match the conditions during the RTM process. In the RTM process more layers of textiles are usually used, first, FBG sensor are often placed between the fabrics, second, the RTM mold is stiff. For this reason, further tests to find limiting for application of optical fibers were done.

To test the maximum allowable fiber volume fraction (FVF), a testing machine adapted for compaction of textiles was used (Figure 3-6). This is a Hegewald & Peschke Universal Testing Machine, with two parallel plates to compress stack of textiles. It is equipped in 200 kN load cell (Z12, HBM, Darmstadt, Germany) with sensitivity tolerance $\leq 0.1\%$, and linear variable differential transformer (LVDT) sensor (WA/10 mm, HBM, Darmstadt, Germany) for measurement of distance between plates.

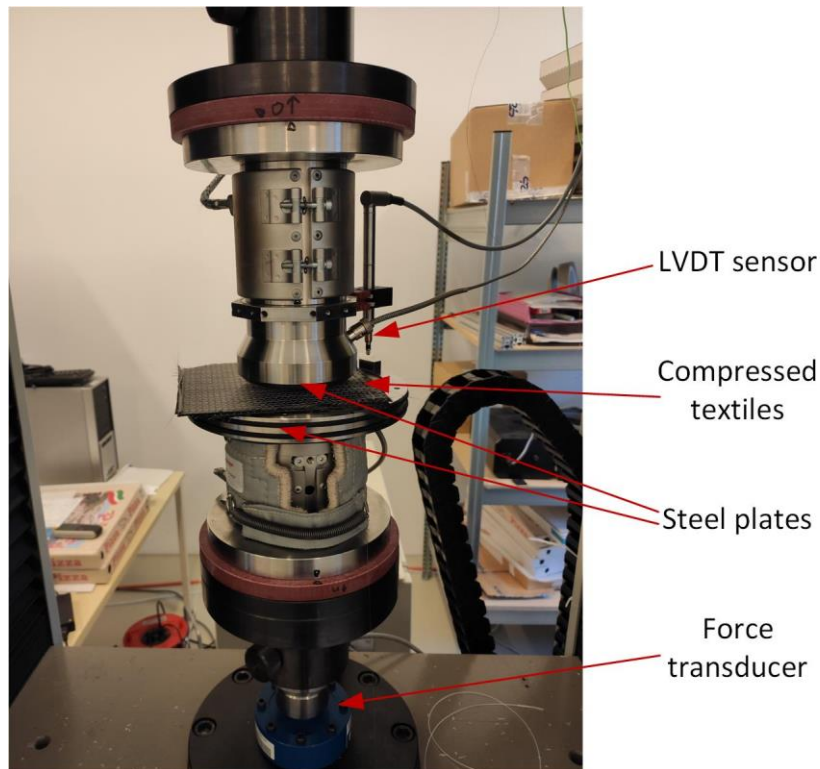


Figure 3-6: Testing machine adapted for compaction of textiles.

Compaction pressure during closing of the mold causes that the whole stack is compressed, and some reinforcing fibers can cause local undulations of the optical fiber [162]. Such undulations cause degradation of FBG spectra, through variations of strain along the FBG, but also reduce the strength of the signal passed through the optical fiber (similar to microbending sensors [25]).

In case of the optical measurement method used (FBG in reflection mode), degradation can be tested in the setup shown in Figure 3-7. An FBG is placed outside the compression area, and compression influences only the bare optical fiber. Compression is controlled with a machine, while the amplitude of the signal can be measured with an optical interrogator. Variations in the amplitude of the reflected signal can indicate the potential threat to the performance of FBG sensors, which would be integrated instead.

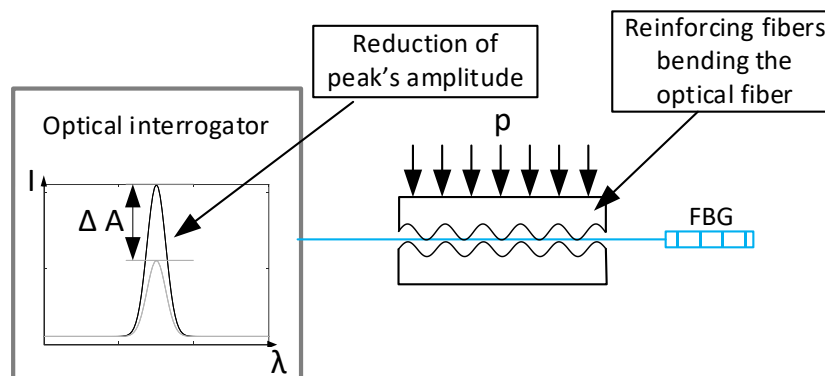


Figure 3-7: Scheme of measurement of transmission signal strength reduction caused by microbending.

Optical fibers were placed into the compaction zone with use of an aluminum octagon fixture. Each side of the octagon had wooden clamps to fix the fiber. When it was stretched between the sides of the octagon, it was fixed underneath a stamp. The distance between the internal side of an octagon was 120 mm, while the diameter of the stamp was 100 mm, so the whole compression was done in the middle of the internal octagon. Inside of the rim octagonal samples cut from fabrics were placed. This setup allowed one to rotate the fibers relatively to stack of textiles at $[0,45,90]^\circ$ with the same shape of samples. In Figure 3-8 the constructed fixture is shown.

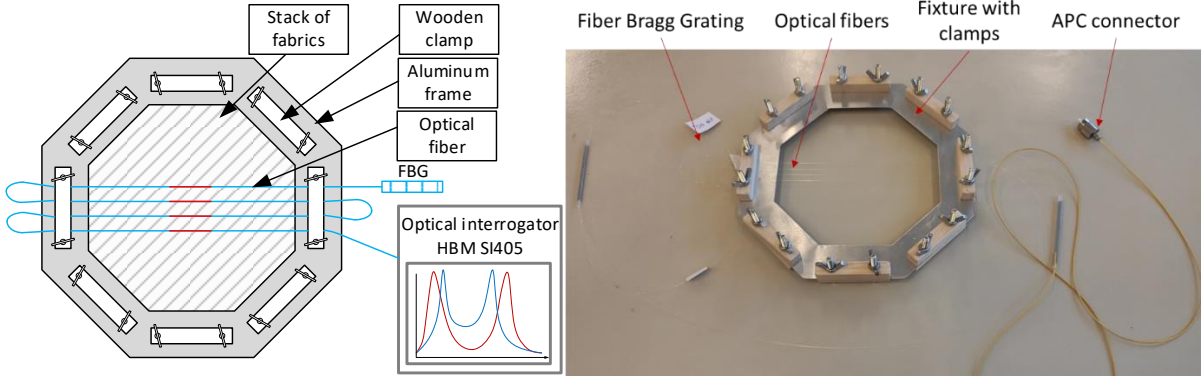


Figure 3-8: Fixture for compaction tests with optical fibers.

FVF resulting in destroying an optical fiber was determined in compaction tests of textile stack with stripped telecommunication fiber. Optical fiber was attached to the frame in such a way, that four parallel sections of one optical fiber were located in the compaction zone. To mimic fragile stripped part where FBG on HB fibers are located, fibers were stripped at the length of 5 cm in the middle of the zone. Outside of the testing area, to one end of a fiber FBG was welded while the other had a connector. This way, light transmitted through the compacted fiber was reflected from FBG and measured with interrogator. If pressure applied to the stack compromises the transmission in the fiber, drop in the signal strength will be observed. A view of compaction zone with fixture is shown in Figure 3-9:

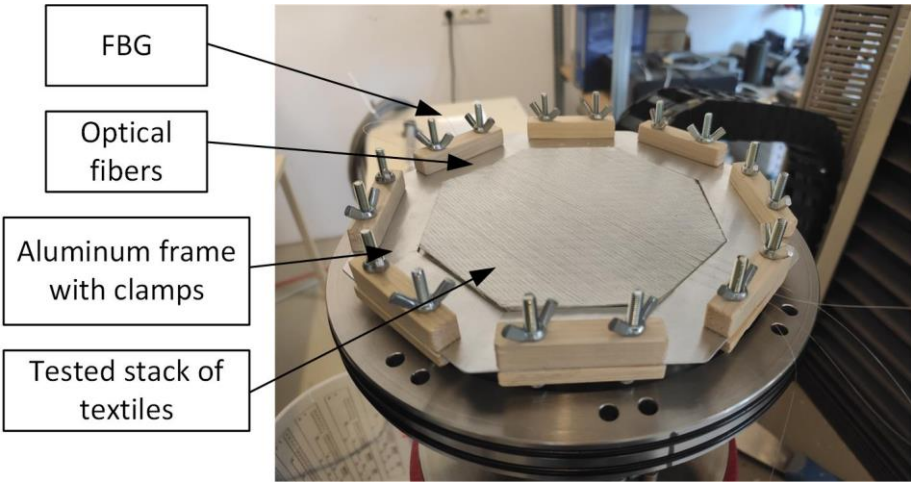


Figure 3-9: Optical fibers fixed on the compaction testing machine.

The signal strength parameter used in this test was signal to noise ratio (SNR) of the received signal. Signal to noise ratio was calculated as ratio between the amplitude of the Bragg peak, and mean amplitude of the noise. Four sections of an optical fiber increased the chance

for the degradation of SNR. If SNR doesn't drop in this test, an optical fiber should survive with even higher probability.

In the compaction zone, a stack of EBX400 NCF was placed in all possible configurations allowed by this approach (sensor 0/45/90°, adjacent layers - 0/45/90°). The notation used for stacking is explained in Figure 3-10.

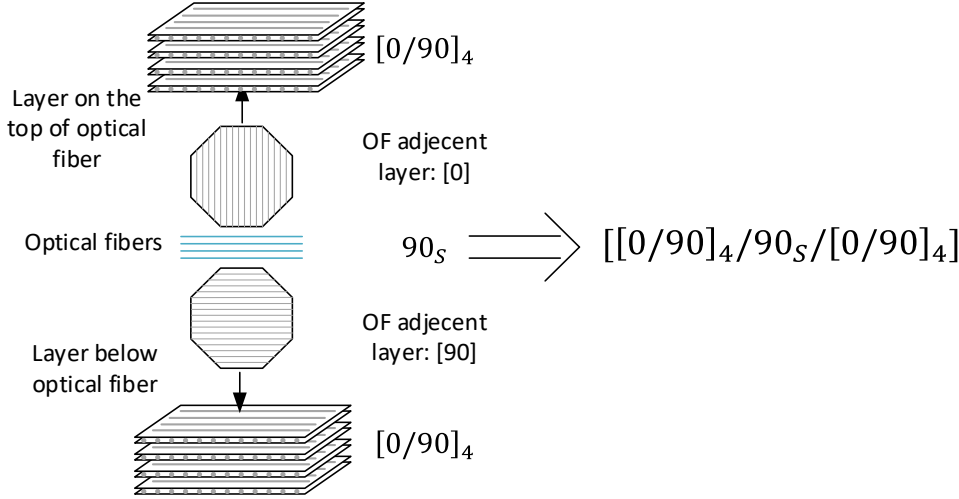


Figure 3-10: Explanation of the notation used for compression stack description.

All configurations considered in the tests are shown in Table 3-1. Due to the symmetry of the textiles, the configurations marked with X already have a corresponding stacking, so it was not necessary to repeat these tests. Three separate tests were performed for each test case.

Table 3-1: Stacking sequence of tested stacks with optical fibers.

Alignment of fibers between on the top and on the bottom of the optical fiber	Optical fibers parallel to reinforcing fibers below	Optical fibers perpendicular to reinforcing fibers below	Optical fibers at 45°
Symmetrical [[0/90]4/Xs/[90/0]4]	[[0/90]4/90s/[90/0]4]	[[0/90]4/0s/[90/0]4]	[[0/90]4/45s/[90/0]4]
Cross-ply [[0/90]4/Xs/[0/90]4]	[[0/90]4/90s/[0/90]4]	X - the same case as OF parallel, cross-ply	[[0/90]4/45s/[0/90]4]
+/- 45 – repeats with 45s for symmetrical and cross-ply	X	X	X

In each test force was increased in the pyramid-like shape. In each step force was increased by 500N and held stable for 15 seconds. Later on, following 500N step was done. Force was increased until FVF=0.62 was achieved. Later on, the stack was unloaded in the similar steps. For each SNR versus FVF was analyzed. Example plot is shown in figure below:

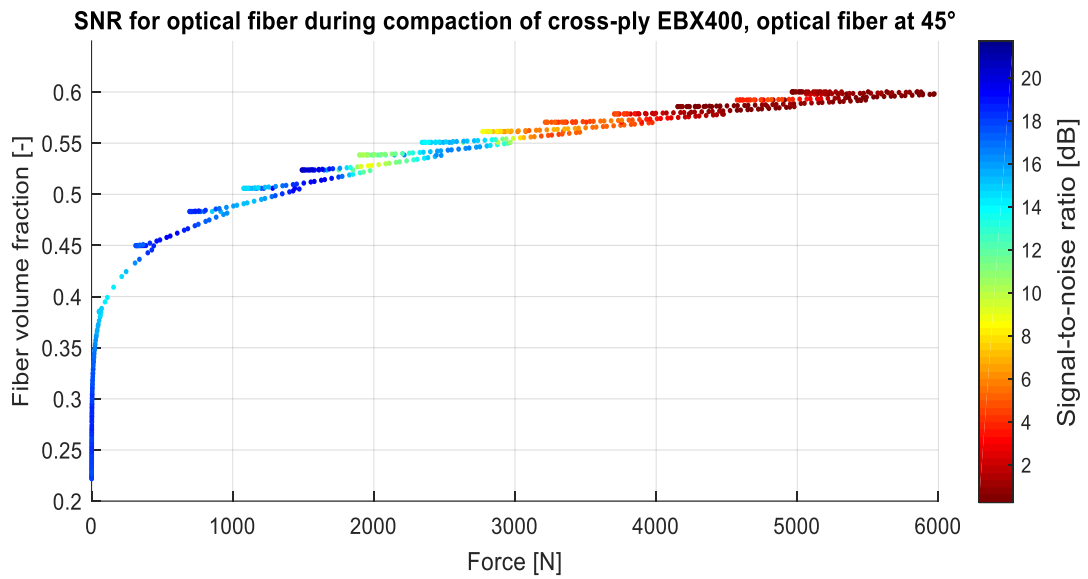


Figure 3-11: Signal to noise ratio (SNR) in the signal transmitted through the optical fiber during the compression of the stack.

From the figure it can be concluded that increasing force applied to the stack caused decrease in SNR of light reflected from an FBG. Plotting SNR versus the FVF allows easier to determine which FVF causes significant drop in the amplitude. Such a plot is shown in Figure 3-12:

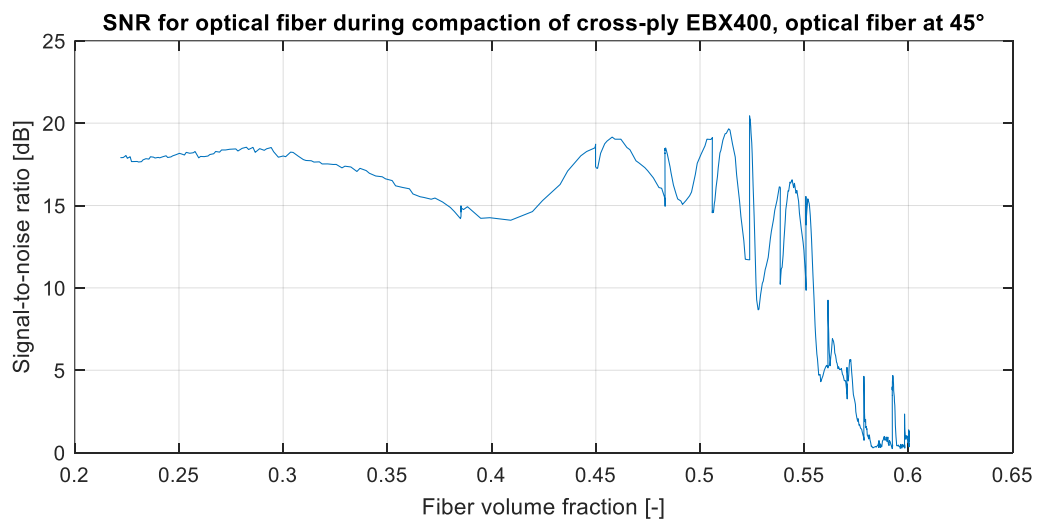


Figure 3-12: SNR vs. FVF in compaction test of NCF textile with a stripped optical fiber.

Tests were repeated for each configuration given in the Table 3-1. The SNR for FBGs used in this research was at least 18 dB, it was assumed that drop in SNR of 6 dB would not compromise measuring possibilities. For this reason, FVF resulting in 6dB drops was found for each testing case (Table 3-2):

Table 3-2: Fiber volume fraction resulting in -6dB drop in SNR.

Alignment of fibers between on the top and on the bottom of the optical fiber	Optical fibers parallel to reinforcing fibers below	Optical fibers perpendicular to reinforcing fibers below	Optical fibers at 45°
Symmetrical [[0/90] ₄ /X _s /[90/0] ₄]	0.56	0.56	0.52
Cross-ply [[0/90] ₄ /X _s /[0/90] ₄]	0.52	X	0.52
+/- 45 – repeats with 45 _s for symmetrical and cross-ply	X	X	X

The highest FVF which resulted in -6dB drop in SNR was observed when the optical sensor was placed in a symmetrical sample (when layer on the top and bottom of the optical fiber were in the same direction as the sensor). In the case when fiber is placed along the fibers, it is quite intuitive, since fibers will be surrounded by the textile. In the case of the perpendicular case, it could be possible due to the quasi-uniform force distribution along the fiber. When an optical fiber was placed in the cross-ply stack or placed at 45 degrees to the adjacent textile fibers, the maximum allowable FVF was 0.52.

It is also important, that such a compaction test was performed with slowly increasing force. In the regular process, mold would compress in order of magnitude faster than during this test. Such slow increase allowed relaxation of the textiles. If relaxation is not possible, breakage can occur with lower FVF than measured here. It is assumed that in the RTM process, the maximum FVF used for this textile and FBG sensors will be 0.52.

3.1.3. Spectrum changes due to textile compaction

After determination of the maximum allowable FVF, actual fiber optic sensors were compressed to investigate effect on the spectrum due to textile-sensor interaction. In total, four FBG sensors were mounted in the fixture shown in Figure 3-8. Two of them were regular FBG sensors (FFA-01, Sylex, Bratislava, Slovakia), with stripped 5 cm long sections in the compaction zone. Two others were HB FBG (HB1500 fiber), which were oriented in such a way that the highest sensitivity was in compaction direction. Orientation was fixed with small drops of paraffin on both sides of the sensors, and drops of X60 glue were placed in such a way they will be on the top of aluminum rim. When FBG sensors were fixed at desired orientation, paraffin was removed by heating up with a heat gun. Fibers arrangement before testing is shown in Figure 3-13.

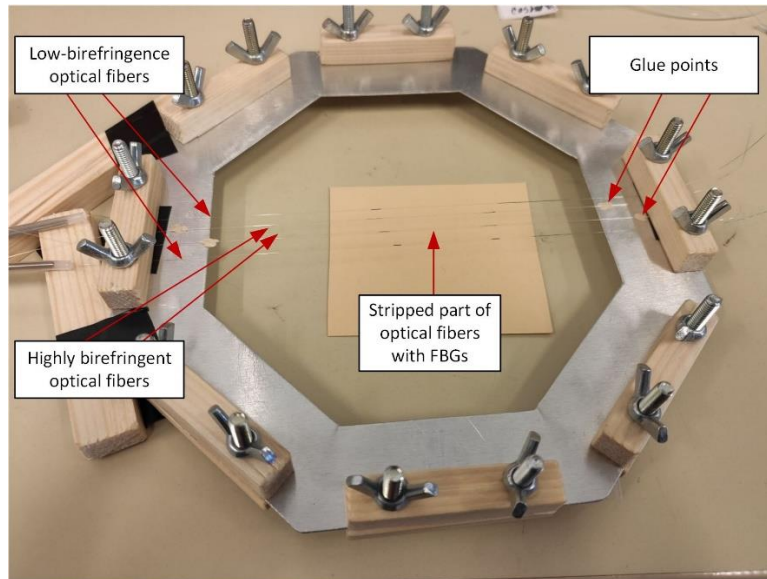


Figure 3-13: The arrangement of FBG sensors in the compaction zone.

Compaction tests performed on rig for testing of optical fiber sensors (section 3.1.1) shown that influence of optical fibers, which are not aligned with any reinforcing fibers can lead to degradation of spectra. Because of this reason, it was decided that final stacking for RTM will include at least layer of reinforcing fibers below or on the top of FBG to be parallel. Because of this reason, following tests were tested in two cases:

- $[0/90]_4/90_S/[0/90]_4$ – cross-ply stacking, with sensor aligned with bottom reinforcing fibers
- $[0/90]_4/90_S/[90/0]_4$ – symmetrical stacking, with sensor aligned with bottom and top reinforcing fibers

Tests were performed for FVF up to 0.52 as was concluded from previous tests. Loading scheme was the same as for compaction tests (increasing in 500N steps until achieving desired FVF).

In Figure 3-14, optical spectra of un-loaded and fully loaded HB FBGs are shown.

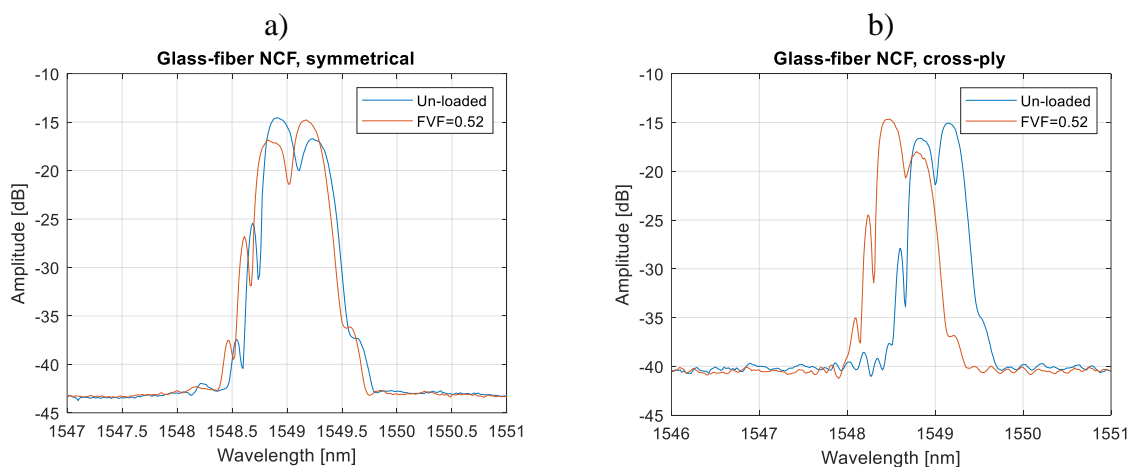


Figure 3-14: Exemplary optical spectra of full-loaded optical fibers when FBG sensor was: a) Parallel to the reinforcing fibers above and below; b) Parallel to the reinforcing fibers below FBG.

As can be concluded, found stacking conditions did not negative influence the performance of FBG sensors. Shape of the peak slightly changed. Amplitude of peaks changed due to variation in the strength of signal for each polarization in stacking cases, but these variations did not compromise the performance of FBG sensors at all. For regular FBG sensors (not shown), neither peak splitting nor its degradation occurred.

Separation of peaks for HB FBG was also investigated. It is presented in Figure 3-15:

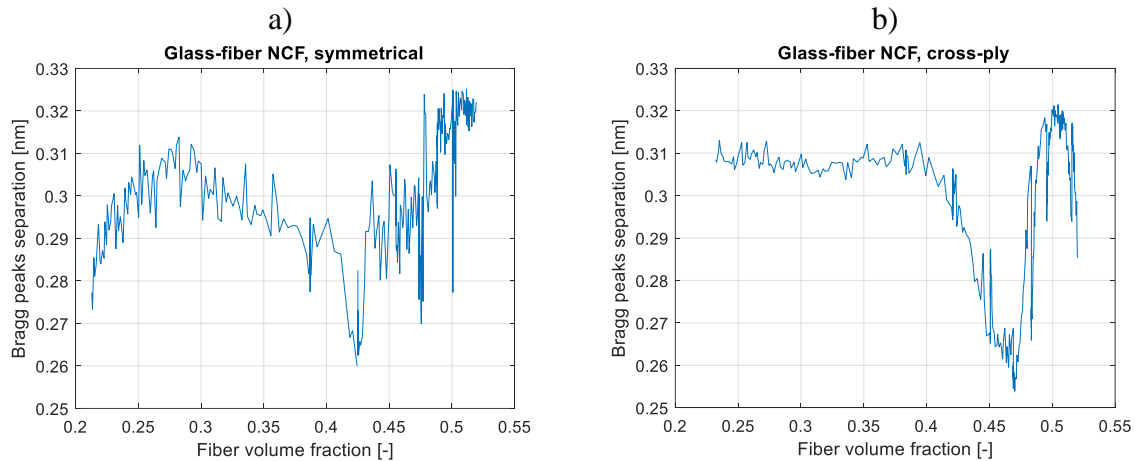


Figure 3-15: Peak separation of FBG inscribed in loaded optical fiber.

Compaction of fibers caused changes in the peak separation. Changes were not monotonic. Peak separation for FBG which had reinforcing fibers on both top and bottom parallel to the optical fiber (symmetrical, Figure 3-15a), peak separation varied between [0.259 nm; 0.324 nm]. However, in the case where only top layer was parallel to the optical fiber (cross-ply, Figure 3-15b), peak separation varied between [0.254 nm; 0.321 nm], so in both cases amplitude of peak separation variations was comparable. It means, that HB FBG sensors can be applied in both stacking conditions and they should perform well during monitoring of RTM process.

3.1.4. Summary of the study of textile-sensor interaction during compression

The textile-sensor interaction during compression can result in non-uniform strain, which can be a challenging environment for FBG sensors. It can cause spectral degradation, which can reduce the applicability of FBG sensors. Fiber orientation and maximum compressive force limits should be considered.

Compression of optical fibers along with multiple layers of fabric can increase transmission losses through the optical fiber. Therefore, if optical fibers are to be used in high performance composites where significant compressive pressure is applied, possible transmission losses through the integrated optical fibers should be considered. Alignment with reinforcing fibers can increase this limit, but is impossible for textiles such as twill. For specific textiles, the limits of optical fiber application with specific fabrics can be found with a compression testing machine.

FBG sensors compressed between layers of the composite (within the limits found in compression tests) were not negatively affected by the load. This can be explained by the fact that multiple layers of textiles mitigated the negative effect on the sensors by some movement

of the reinforcing fibers. When FBG sensors had a layer of reinforcing fibers aligned with the FBG, the FBG sensors could be surrounded by these fibers during compression, protecting them from the negative influence of the force. However, this was not possible if the FBG was placed at an angle to the reinforcing fibers of both adjacent textiles.

On the other hand, due to the relatively small thickness of a stack, the compressive force could be concentrated on the unstripped section of the fiber, which is 20% thicker than the stripped sensor section. This could cause most of the load to be concentrated on the covered, bare fiber and only a small portion of the load to be distributed along the sensor itself. This could explain the lack of influence on the spectra and also increase the probability of survival of the sensors during RTM, since the closing of the mold will act in the same way.

It is also worth noting that although compression of textiles with HB FBG sensors did not cause the sensors to respond, transverse shrinkage during resin curing during RTM may be observable. As the resin cures, the reinforcing fibers are packed, and as the resin shrinks, a uniform load that affects the FBG birefringence may occur. This may explain why researchers report birefringence or microbending induced by the manufacturing process [8,83,103].

3.2. RESIN CURING MONITORING

The next step in the research conducted was to investigate the applicability of the FBG sensor for monitoring the curing of neat epoxy resin. Resin in composites binds fibers together, provides the shape of the manufactured part, protects fibers from the environment, and contributes to the strength of the part (especially in compression and shear) [163].

Resin is curing transiting from liquid to solid state. If a manufactured composite part is demolded before full cure, produced part may not achieve predicted mechanical properties, or have defects, which may be impossible to be repaired [7,69]. On the other hand, too long curing of each sample can lead to a negative economic aspect because each part will be manufactured longer than needed. In this case, to obtain the proper manufacturing time, cure monitoring can be used. For curing monitoring, usually in mold sensors are used (e.g. dielectric analysis sensors - DEA). They do not require manual integration, can be used for industrial processes. However, if it is required to equip specific structure in sensors intended for future SHM, the same sensors can be used for process monitoring. In this application, FBG sensors were shown to be applicable [7–9,70,90,94,95].

As was described in section 1.2.2, FBG sensors were used for gel point detection and measuring of overall residual strain. In gel point detection, gel point is often described as a moment when resin is stiff enough to transfer strain to the optical fiber. This means, that theoretically by the moment of gelation, no residual-strain should be detected. Consequently – rapid changes in the strain measured with sensors are considered as gel point [9,93,95,97].

When curing of the composite ends, residual strain gets its final value and becomes stable. When it is achieved, FBG sensors are used to measure the residual strain, chemical (keeping isothermal conditions when measured [9,95,164]), or final (after cooling down) to the room temperature [95,101].

The influence of reinforcing fibers on the curing process causes that monitoring of process is not easily reproducible and reduces the precision of monitoring [9,165]. For this reason, often researchers focus on curing of neat resin for determination of various measurement methods [97,98].

Regarding the objectives of the thesis, identification of each component of the process was required and measurements were performed with neat resin. Three aluminum cups with FBG sensor and thermocouple in each cup and one outside were used. Optical fiber was placed inside the cups through holes punctured on both sides of the aluminum cup, which were sealed with tack tape. In the vicinity of FBG sensor, a thermocouple was placed. The FBG reflection spectrum was collected with the HBM SI405 interrogator. The thermocouples were connected to the Omega TC-08 thermocouple logger. To the cup, a mixture of EPIKOTE RIMR135 (Hexion, Columbus, USA) and EPIKURE RIMH1366 (Hexion, Columbus, USA) in a mass ratio of 100:30 [166]. The cure was performed at room temperature. After 45 hours, the samples were postcured on a heating plate at 80°C. A cup with a visible location FBG sensor and thermocouple is presented in Figure 3-16:

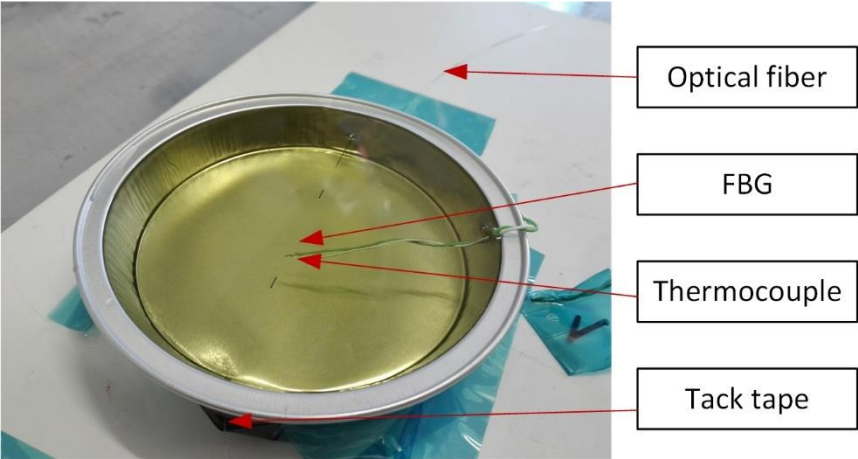


Figure 3-16: A cup with poured resin during the curing with location of sensors.

During first 45 hours data collected for the resin curing is shown in Figure 3-17:

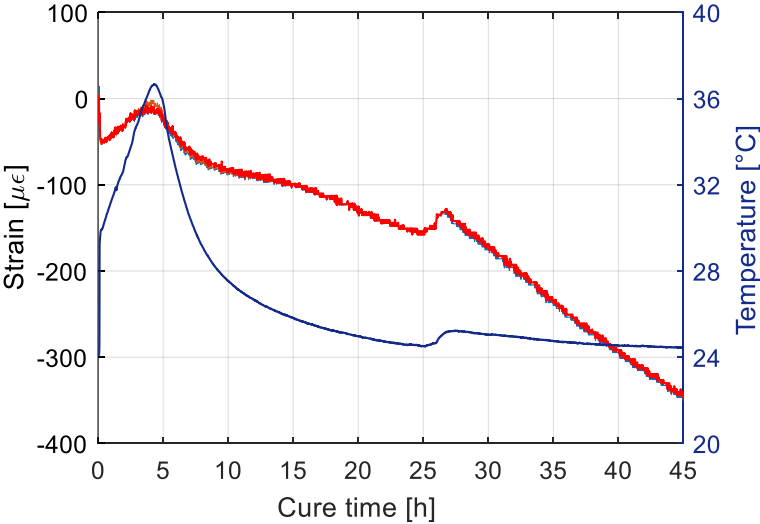


Figure 3-17: Monitoring of epoxy resin (RIMR135+RIMH1366) curing with FBG sensor in room temperature.

In the beginning, resin was poured into cups, which could be seen as a temperature variation. Subsequently, the temperature slowly increased for 4.5h when a maximum temperature of 37°C was achieved. Around the same time, strain began to drop, which could be associated with the

gel point. After this time, compressive strain arises getting to $-350 \mu\epsilon$ after 45h. The increase in temperature at 26h from the start was associated with sunlight, which was heating the samples. After whole 45h, strain drop was still observed, so cure was still not completed.

The gel point is described as the moment from which resin can transfer stress to the optical fiber, so before that point, strain measured by FBG sensors should be approximately zero. However, curing is an exothermal process, thus before the gel point temperature increased up 37°C . Since FBG sensors were punctured through the cup and fixed on the ends, thermal expansion of cup influenced FBG as well. CTE for aluminum is around $22 \cdot 10^{-6} \mu\epsilon/^\circ\text{C}$ [167], so a variation of 8°C (29°C to 37°C) caused the expansion of a optical fiber comparable to measured with FBG sensors.

After 45 hours curing, samples were post cured using the heat plate. Results of monitoring is shown in Figure 3-18.

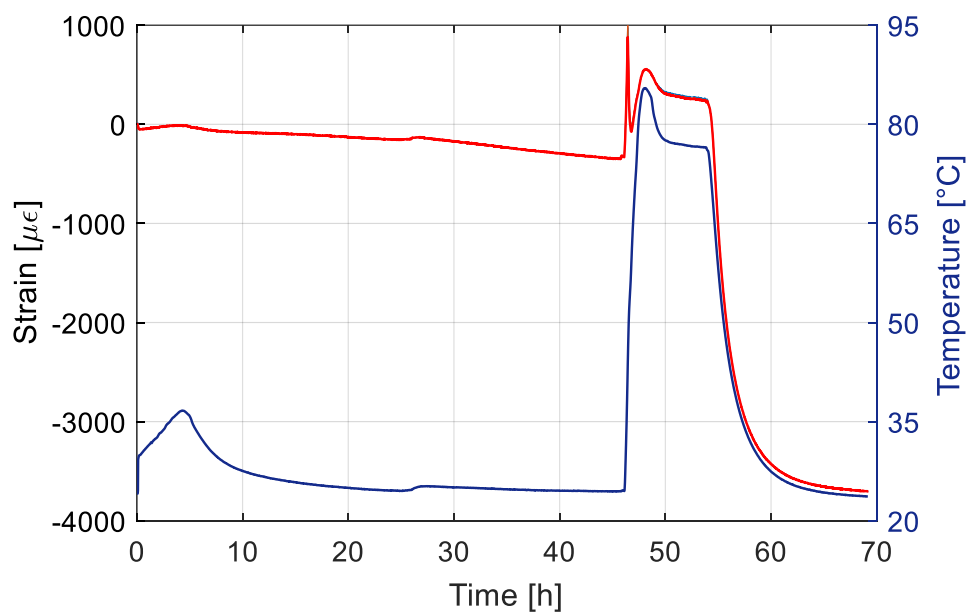


Figure 3-18: Monitoring of epoxy resin (RIMR135+RIMH1366) curing and post-curing with FBG sensor.

During post curing, the chemical reaction proceeded more rapidly, resulting in a temperature increase to 90°C . After reaching the maximum heat emission, the cup containing the resin was cooled down to the hotplate temperature (75°C). After the entire post-cure, when the resin was cooled down, it showed a final resin shrinkage of $3500 \mu\epsilon$, which is 10 times more than during the curing process.

From this part of the study, it can be concluded that FBG sensors are capable of detecting the gel point, but during the process the strain amplitudes during gelation are small (comparable to the thermal expansion of the vessel), so the gel point determination has to be carefully planned and performed. In addition, FBG sensors can measure residual strain after the entire cure process.

3.3. RTM PROCESS MONITORING

In the previous parts of this chapter, the parts of RTM process were examined to get an understanding about the process itself. Textiles are reinforcement of the composite. They increase mechanical properties of composite, but also can negatively influence a performance of integrated FBG sensors, so they should be kept aligned to reinforcing fibers. An epoxy resin curing results in residual strain, which can be measured with FBG sensors. Since gel point is the moment when residual strain begins to arise, they can be used to find this point as well. Part of this chapter is published in paper [168].

In case of this study, not only regular FBG sensors will be used for process monitoring, but also HB FBG sensors. Since they can measure radial load of the fiber, they could be also used to measure through-thickness strain [23,101,102].

3.3.1. RTM conditions and measurement setup for process monitoring

The RTM was performed in a closed mold with a cavity in shape of square, flat plate with dimensions of 270x270x2 mm. The tool temperature was $100\text{ C} \pm 0.5\text{ }^{\circ}\text{C}$ and was controlled with cooling/heating channels positioned in both halves of the mold. The mold was preheated to $100\text{ }^{\circ}\text{C}$ and preform was inserted. As a reinforcement six layers of NCF carbon fiber textile (Saertex-X-C-PB-555) were used. For this preform, calculated FVF was 0.47, which is lower than critical level found for another NCF in previous chapters. Although this different NCF is used, the compression pressure needed to compress the stack to this FVF was substantially lower than during previous tests with EBX400.

After placing of preform into cavity, the mold was closed and locked with a force of 40 kN, ensuring a sealing during the injection. Data collection from all sensors began. A mixture of preheated ($50\text{ }^{\circ}\text{C}$) Epinal 77.55-A1 resin and Epinal 77.55-B1 hardener in 100:32 ratio was injected into a cavity at a mass flow rate of 0.30 kg/min until complete filling. When resin began to overflow, injection was continued for 10 more seconds to ensure complete filling without voids in laminate. Afterwards, the injection was stopped and an injection hose was clamped.

To monitor the process, FBG sensors (commercial and highly-birefringent), but also in-mold sensors were used. FBG sensors were placed between two top layers (fifth and sixth) to ensure maximum bending sensitivity during further mechanical tests. Sensors were placed at corners of the square, 170 mm apart. Each of FBG sensors was 50 mm from the edge of the plate. FBG sensors inscribed in SMF fibers used in these tests were commercial polyimide coated sensors (FFA-01, Sylex, Bratislava, Slovakia). Highly-birefringent fibers were side-hole 2 fibers.

The optical interrogator SI405 (HBM GmbH, Darmstadt, Germany) was used to measure Bragg wavelength. During monitoring with SMF FBG sensors, Bragg wavelength were measured with 1 Hz sampling rate, with optical resolution of 1 pm. In the case HB FBG sensors, during first 30 min of process, optical spectra were collected with sampling rate of 0.1 Hz, and peak detection was performed afterwards with cross-correlation method. After 30 minutes, automatic peak tracking at 1 Hz was used. Temperature compensation was based on the in-mold temperature sensors.

Since RTM process is done in closed mold and FBG sensors had to be connected with measurement equipment, some way of egress mold had to be used. In literature egress point protection was shown to be done in various different methods [2,8,169]. In the case of this

work, an aluminum plate with groves to lead optical fibers was used. The aluminum plate was 2 mm thick, which increased the height of a cavity to 4 mm. To seal the cavity and protect the egress points, silicone foam tape was placed around the cavity. In total, three layers of 2 mm thick tape were used: two underneath optical fiber and one on top, ensuring there is no leakage. In Figure 3-19 view of a cavity with plate with groves is shown.

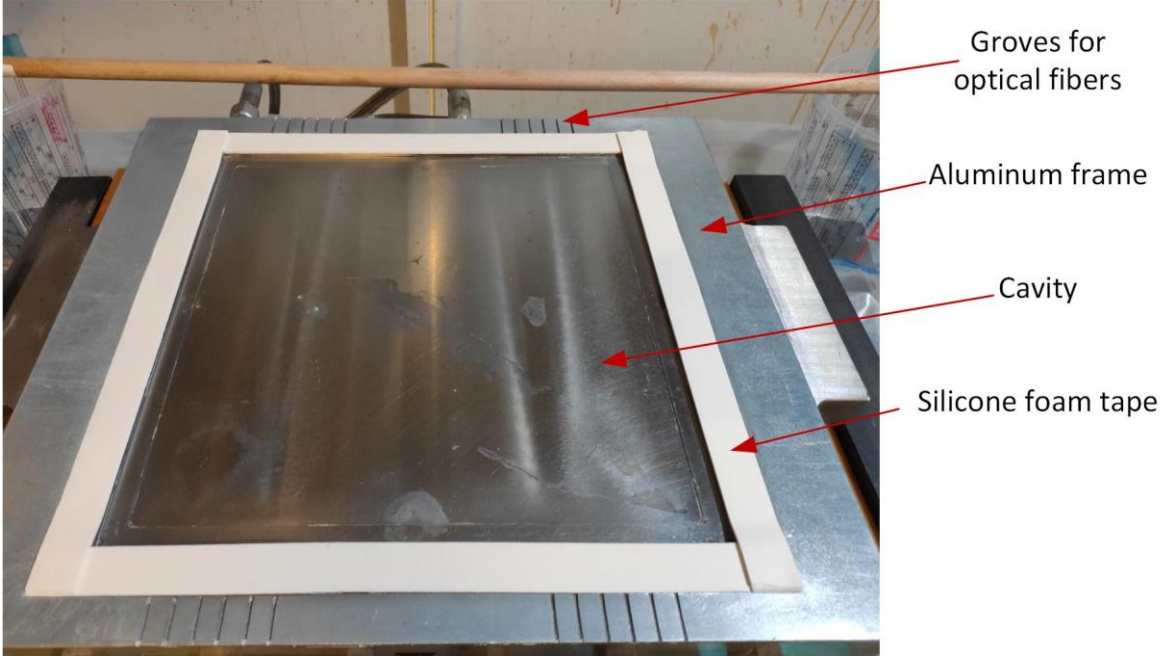


Figure 3-19: View of a cavity of mold without preform.

Optical fibers were fixed to the textile with cyanoacrylate glue on one side of FBG sensor. Egress points of optical fibers were protected with PTFE tubing. To enable movement and seal the tubing, a little amount of cyanoacrylate glue was dropped on each end of tubing. Schematically placement of sensors in the mold is shown in Figure 3-20.

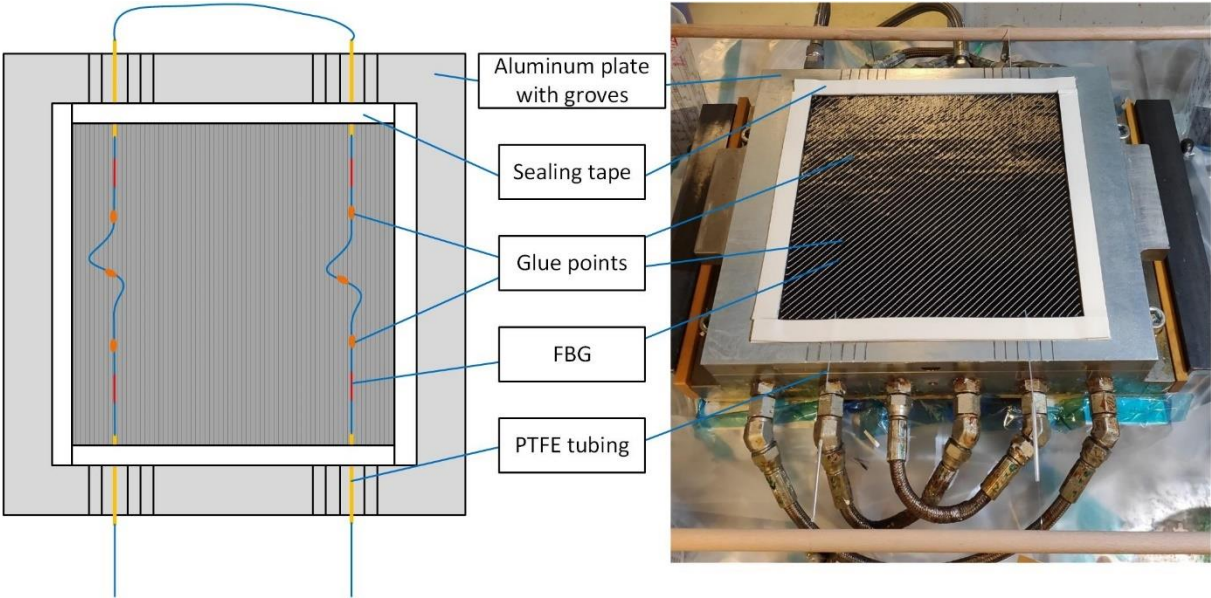


Figure 3-20: Integration of FBG sensors into the mold; a) Top view of the mold with preform.

To cause pretension of optical fibers, they were hung over wooden cylindrical bars placed outside of the mold (Figure 3-21). Combination of fixing method, outside pretension applying to the fiber and protective silicon foam tape allowed precise placement with pretension and proper protection of egress points.

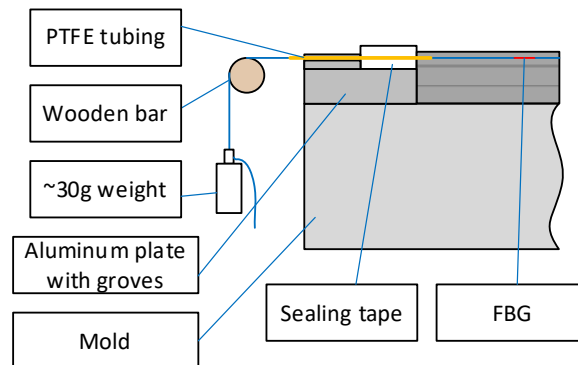


Figure 3-21: Method of integration of FBG into the mold – side view.

The plate mold used for these measurements is integrated into a Langzauner LZT-OK-80-SO mold carrier (Lambrechten, Austria). The plate mold was designed to monitor RTM process during closing, injection and curing. For this reason, top part has 21 slots, where different sensors can be mounted (grey spots on Figure 3-22). During this research following sensors were integrated:

- Three combined pressure/temperature sensors (p/T) – detects flow front arrival,
- Combined DC/temperature (type K thermocouple) sensor - detects changes in resistance from dry to saturated preform state
- Two temperature sensors (Pt100)
- The DC-sensor (Synthesites optimold) - detects chances in the matrix material e.g., the degree of cure.
- Near Infra-Red (NIR) – detects changes in the molecular composition of the resin and degree of cure.
- Dielectric analysis sensor (INASCO cure monitor) - detects gel point, reactivity and diffusion properties

The data from sensors can be correlated with results from FBG sensors to attribute points measured with sensors with data from FBG integrated in the textile. Placement of in-built sensors along with FBG sensors is shown in Figure 3-22.

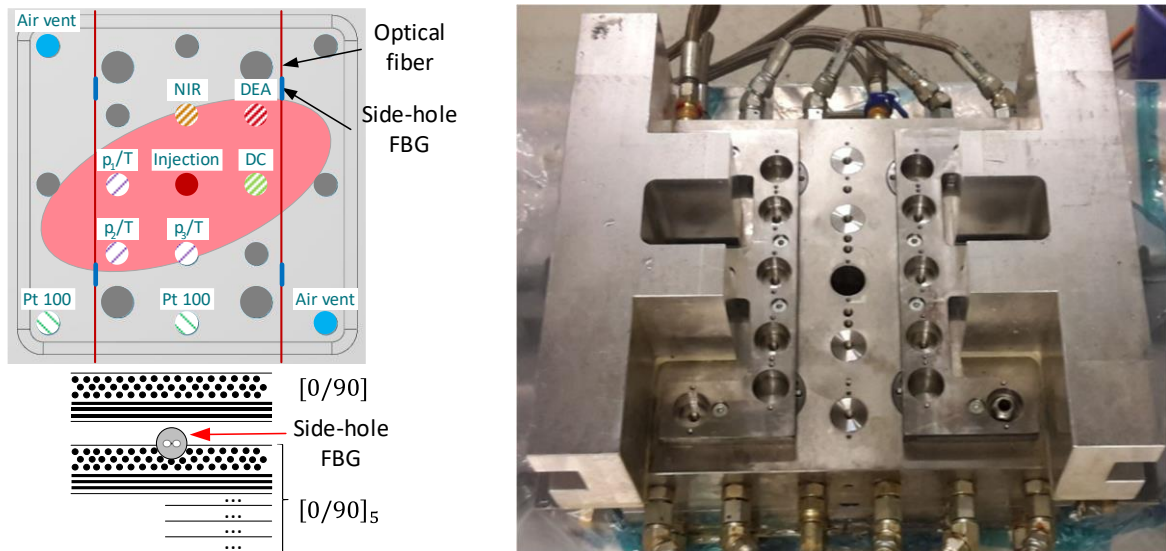


Figure 3-22: FBG sensors placement along with in-mold sensors [168].

In this part of the study, the main focus of FBG and HB FBG sensors for process monitoring is residual strain measurement and gel point detection. Residual strain measurement is based on the optical response of the FBG sensors, which is converted into strain using opto-mechanical coefficients obtained from the manufacturer (regular SMF fibers) or calibrated in mechanical tests (HB FBG sensors).

The gel point detection is compared with the results measured by sensors built into the mold. For this reason, data from a DC/temperature sensor is used. The method is based on the measurement of electrical resistance and temperature, which are later processed to calculate the gel point. The method was described by Patrick Hergan in his PhD thesis [86], while the application to this specific case is described in the author's paper [168].

3.3.2. RTM process monitoring with SMF FBG sensors

In the initial tests, four FBG sensors embedded in regular (low birefringence) optical fibers were integrated into the composite. Results of strain measurements for a plate with four sensors are shown in Figure 3-23.

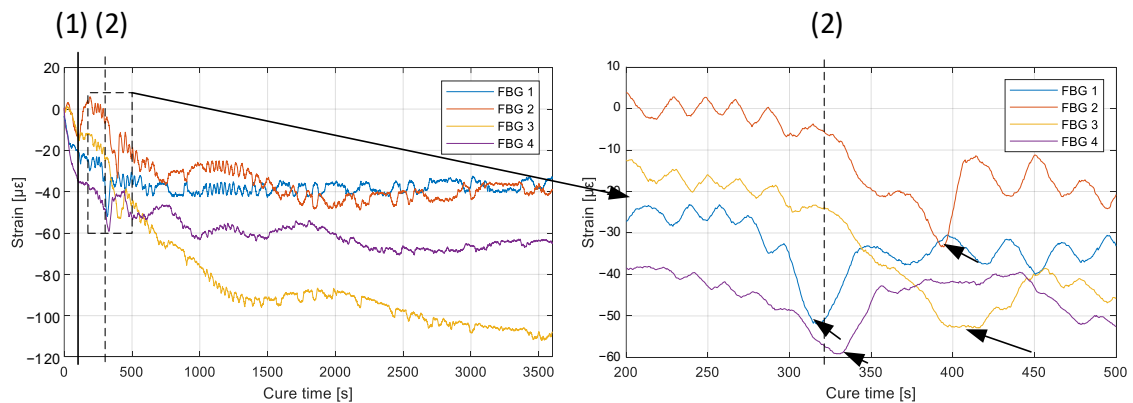


Figure 3-23: Strain during the curing process measured with SMF FBG sensors; (1) – clamping of inlet hose, (2) – gel point estimated with DC sensor [168].

When the inlet hose was clamped (point (1)), a rapid change in strain measured with FBG was observed. The gel point determined with DC sensors (point (2)) was 322 s. Around this time, rapid changes in strain can be seen in all sensors. They are not synchronized due to the relatively slow injection rate. Throughout the process, period variations of the strain plot can be observed. This can be explained by the temperature variation during the process. Active temperature control maintained the temperature with a tolerance of 0.5°C, which caused the same effect as 5µε of strain. The temperature was not measured at the location of the sensor, but by the in-mold sensors, so these variations could not be completely eliminated.

The strain slowly changes to compressive strain as the resin shrinks. The shrinkage stabilizes around 2400 s (full cure time for this resin system [170]). The measured residual strain after the full cure varied between -(40-120) µε between sensors. The panel was held in the mold at processing temperature for another 2 hours, and then cooled and demolded. In total, the final residual strain after cooling was about -1100 µε. After the process, neither microbending nor birefringence affected the FBG performance. The shape of the Bragg peaks was well preserved. This means that the integration method was well chosen for the process.

3.3.3. Process monitoring with HB FBG sensors

In the next test HB FBG (side-hole 2) sensors were integrated into the composite. In this case after clamping the injection hose data from FBG sensors were collected. Sensors were inserted in two orientations: one, when highest sensitivity was in out-of-plane direction and one where it was in-plane.

A. HB FBG with highest sensitivity in out-of-plane direction (slow axis out-of-plane)

Bragg wavelengths and peak separation for case where FBG was inserted in out-of-plane direction is presented in Figure 3-24.

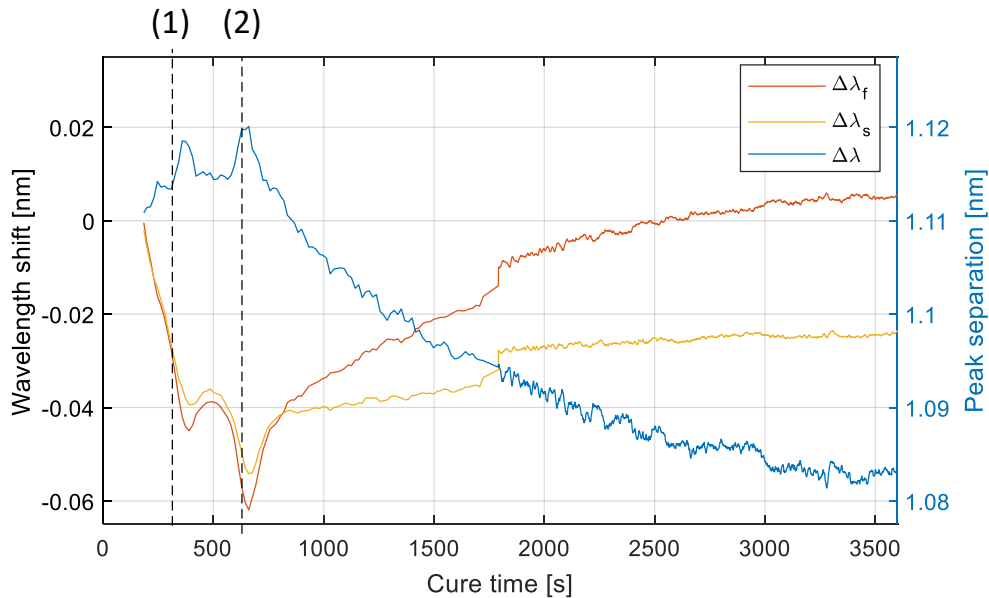


Figure 3-24: Peak shifts and separation variation observed with FBG inscribed in side-hole 2 fiber in the case when highest sensitivity was out-of-plane (slow-axis out-of-plane); (1) – gel point calculated from DC sensor's data ; (2) – deadhesion of a plate from the mold [168].

Before the gel point, both Bragg peaks move parallelly in a decreasing trend. Around the gel time mark (350 s, point (1)), trend of peak separation forms. Beginning at 550 s timestamp, a monotonic trend of decreasing peak separation is visible, which can be associated with through-thickness shrinking of composite. Around 700 s mark, distinct peak separation change can be observed, which could be associated with the detachment of the laminate from the mold. A visible sudden change in the data around 1800 s is associated with a change of optical response data collection method. During first 30 minute of the process, unprocessed FBG spectra were collected, while after 1800 s the detection mechanism built into the interrogator was used.

Data from the peak separation can be calculated into through-thickness strain measurement based on the sensitivity coefficient $k_\epsilon = 0.12 \text{ pm}/\mu\epsilon$ [128] which was determined during mechanical testing (chapter 3.4). This coefficient is an approximation, because stress transfer from composite to optical fiber varies during the manufacturing process. Calculated strain during whole manufacturing process is shown in Figure 3-25:

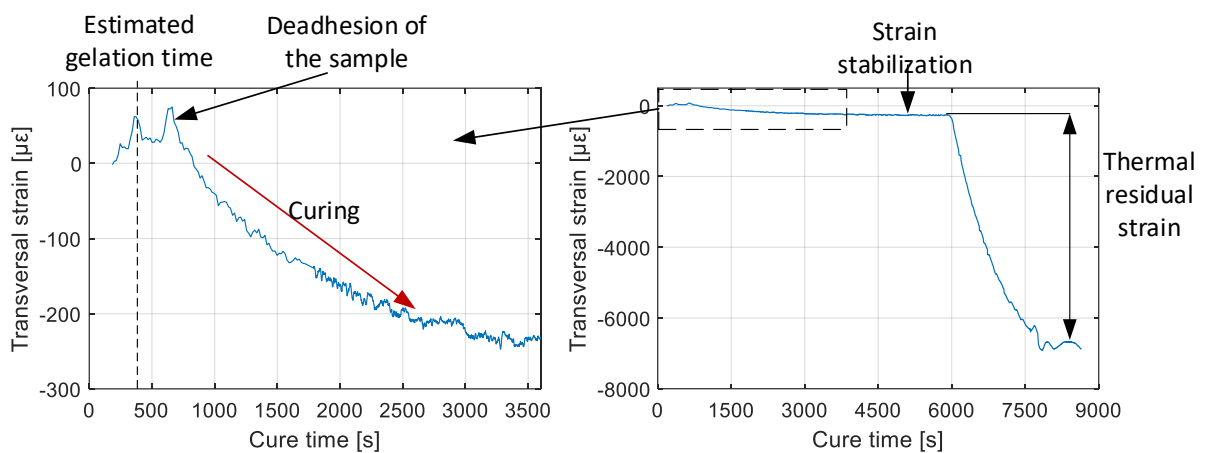


Figure 3-25: Through-thickness strain during the RTM process [168].

Trend of decreasing strain during the curing stabilizes around 2800 s indication the end of cure, which is comparable to the data from the resin system manufacturer [170]. On this time, value of residual strain (chemical) was $-250 \mu\epsilon$. After 6000 s, mold's heating was turned off and laminate was cooled. After complete cooling of a plate, the final transversal residual strain was $-7000 \mu\epsilon$.

The angular orientation of FBG sensor was confirmed by microscopic images of the cross-section (Figure 3-26a) and difference in intended angle was less than 5° . Manufacturing process also did not compromise the reflection spectrum of the sensor (Figure 3-26b), so it can be still used for further mechanical tests. It is however worth to mention, that compressive strain during the process reduced the peak separation (down to 150 pm), thus limiting further compressive strain measurement in this direction. When strain is to be measured in compression, strain causing merging of peaks will be in the range of $1250 \mu\epsilon$ (0.125%).

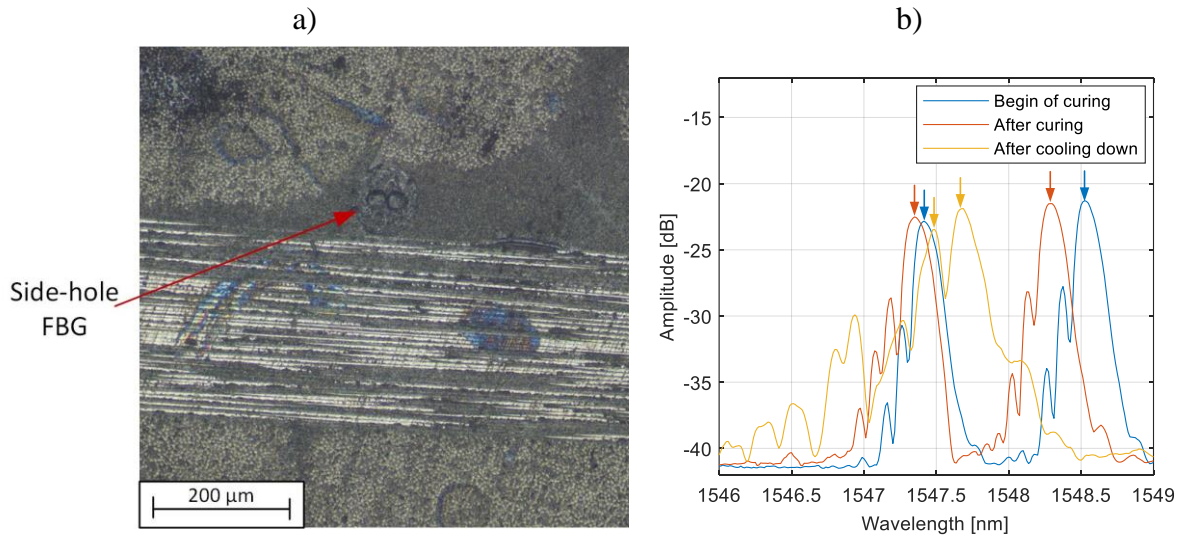


Figure 3-26: a) View of the vicinity of SH2 FBG; b) Reflection spectra of a HB FBG sensor at: the beginning of the curing, after the curing and after cooling down [168].

The detachment of plate from the mold was previously reported in literature. Paper [95], where regular FBG sensors were used to monitor the RTM process, reported on deadhesion of the mold manufactured part, which was visible in FBG sensor data and occurred between gelation and vitrification of the composite. The hypothesis of detached laminate can also be supported by pressure data registered during the process. The results of the pressure measurement from the closest to the FBG pressure sensor are shown in Figure 3-27.

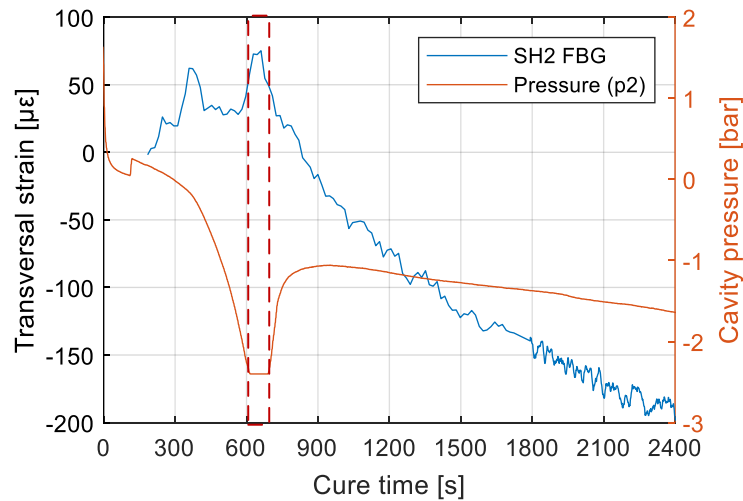


Figure 3-27: Pressure and peak separation during the RTM process.

After gelation (around 350 s), distinct drop in the cavity pressure is observed (-2.4 bar), which after 700 s mark, it goes back to (-1.0 bar). A schematic explanation of this behavior by plate detachment is shown in Figure 3-28. A pressure sensor has a membrane, which adheres to the manufactured part. During curing, the plate shrinks through the thickness, causing the pressure in the cavity to drop. When the pressure sensor is pulled to the maximum by the shrinking composite (minimum pressure), it stays on the place. After some time, the shrinkage progresses and the plate is detached from the upper part of the mold. The pressure sensor returns

to the normal measurement range. At the same time, SH2 FBG indicates the increase in transverse strain, resulting in transverse tension of the fiber, which is in accordance with collected data.

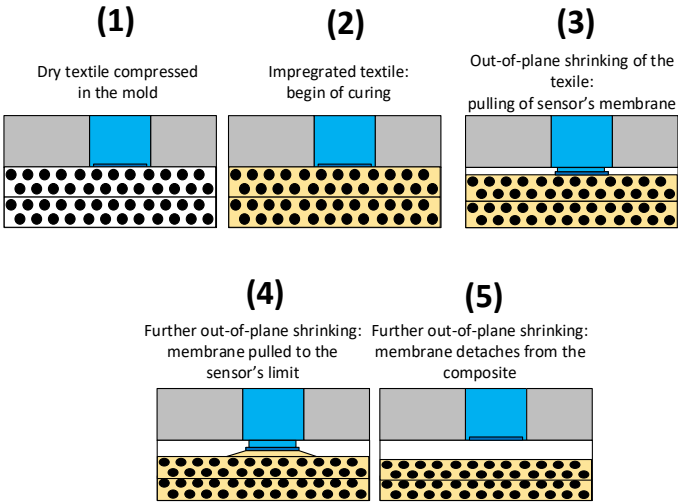


Figure 3-28: A possible behavior of pressure sensors during plate's detachment due to through-thickness shrinking.

B. HB FBG with highest sensitivity in in-plane direction (slow axis in-plane)

In the same manufacturing conditions, a SH2 FBG was inserted in orientation when highest sensitivity was in plane of laminate. Results are presented in Figure 3-29.

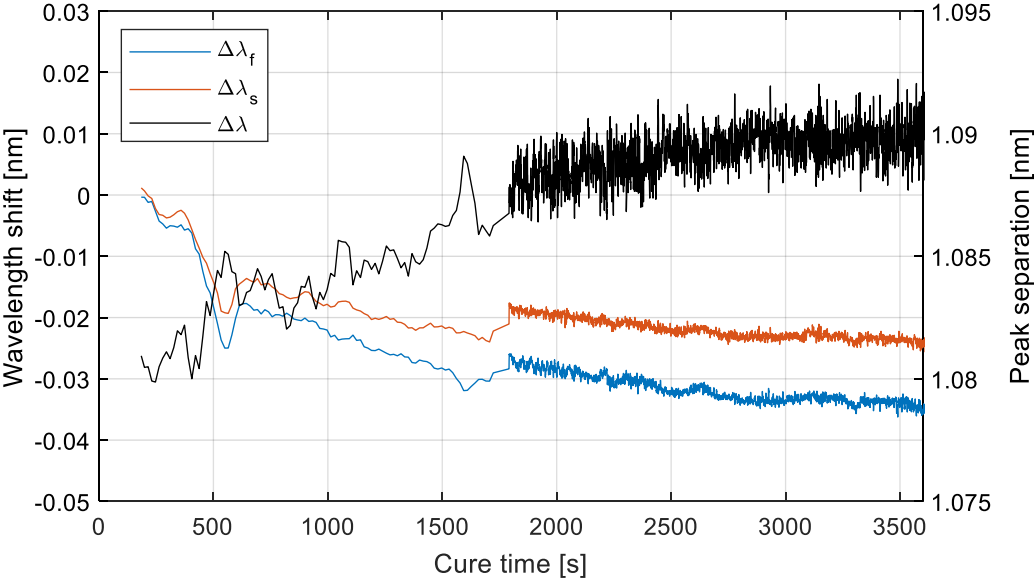


Figure 3-29: Wavelength shifts are separation changes during the RTM process, when highest transversal sensitivity of SH2 fiber was in in-plane direction (slow-axis in-plane of laminate).

In this case, a visible decrease of both Bragg wavelengths is observed after the gel point (350 s), similar to regular FBG sensors. However, the trend of the peak separation does not indicate the progress of curing as in the case of SH2 integrated for out-of-plane measurement. The peak separation increases monotonically and no significant change in trend was observed,

unlike the previous setup (SH2 with highest sensitivity in out-of-plane direction). The peak separation changed by 10 pm after the whole cure, while in the case where the maximum sensitivity was out-of-plane, the maximum separation changed by 28 pm. The difference in the measurements may be due to a smaller in-plane strain, but it may also be due to the influence of the out-of-plane strain on the total peak separation.

3.3.4. Summary of RTM process monitoring with FBG and HB FBG sensors

The above-described trials of using SMF FBG and HB FBG sensors to monitor the RTM process, for residual strain measurement and gel point detection, lead to the following conclusions:

1. Production of composite plates with embedded sensors, both SMF FBG and HB FBG, was performed in RTM process. The problem of locating the sensors between the reinforcing textiles, positioning them and getting the cables out of the mold was solved. Validation of sensor data was supported by temperature, dielectric and resistive property and pressure sensors integrated into the mold,
2. SMF FBG sensors allow determination of the gel point and measurement of residual strain along the fiber:
 - Gel point determination with conventional (SMF) FBG sensors was performed by analyzing the deformation measured by the sensor. A change in the strain trend was observed around the reference gelation time measured by the DC sensor. However, it should be noted that this trend could be affected by temperature variations. In the case of standard FBGs, a 1°C change in temperature causes a similar change in Bragg wavelength corresponding to a strain of 10 $\mu\epsilon$. Despite precise process control, the temperature sensors integrated into the mold measured temperature changes of 1°C during the process, and the temperature changes inside the wafer were probably even greater. The strain changes recorded by the sensor, indicating the point of gelation, had an amplitude of about 20 $\mu\epsilon$, which is not much larger than the oscillations caused by temperature fluctuations. Therefore, even with temperature control, a sensor of this type requires an additional integrated sensor placed as close as possible to the FBG sensor to allow temperature compensation.
 - SMF FBG sensors were used to measure residual strain after curing and after cooling of the composite. After the process, the deformations had a mean value of -100 $\mu\epsilon$ and after cooling -1100 $\mu\epsilon$.
3. HB FBG sensors with highest sensitivity in out-of-plane direction (slow axis out-of-plane) allowed determination of the gel point, and measurement of deformation in the direction perpendicular to the optical fiber:
 - Starting from the gel point of the resin, a monotonic build-up of strain in the direction perpendicular to the plane of the laminate was observed. Importantly, this measurement was not affected by temperature variations inside the mold. This lack of influence related to the fact that the determination of the gelation point is based on the reading of the change in Bragg peak separation, which, in the case of SH2 sensors, is almost insensitive to temperature changes. This makes the gel point determination more precise and does not require additional temperature compensation.
 - Set in this orientation, the sensor mainly measures deformation in the direction perpendicular to the plane of the plate. After the fabrication process, the Bragg peak separation changed by 30 pm. Based on the calibration of the embedded sensor during the bending test, this corresponded to a strain of 250 $\mu\epsilon$. In contrast, it was -7000 $\mu\epsilon$ (0.7%) after the whole process.

4. HB FBG sensors with highest in-plane direction (slow axis in-plane) show worse ability to determine the gel point than for the out-of-plane system, but can still be used to measure residual strain:
 - The peak separation change signal did not show a clear change in trend that would indicate progressing curing of the composite. At a time corresponding to the gelation time of the resin (350 s), a change was observed indicating a parallel shift of the reflections, similar to that measured with SMF FBG sensors, so that the gel point can be determined using the same approach
 - In the case of this arrangement, the total change in peak separation after the fabrication process changed by 10 pm, which is 36% of that recorded by HB FBG in the second arrangement. This change in separation corresponds to a strain of about $110 \mu\epsilon$, which is comparable to the in-plane strain measured with SMF FBG.

In summary, the use of HB FBG sensors perpendicular to the plane of the composite is particularly useful in this case. Such an arrangement allows the most effective method of determining the gel point of the composite. Measurement of residual strain is possible with any of the arrangements presented.

3.4. MULTI-AXIAL STRAIN MEASUREMENT IN A PLATE ELEMENT

A significant part of the products manufactured by the RTM method are plates. Measurement of the components of the strain state inside a fiber-reinforced composite plate with complex geometry is a generally difficult issue. Therefore, the possibility of using HB FBG sensors for this purpose was considered in this chapter.

FBG sensors inscribed in highly birefringent fibers are capable of measuring transversal strain or force [21,23,59,100,140,142,157]. Birefringence induced in fiber causes two distinct Bragg peaks to appear in the reflection spectrum. Because of the photoelasticity effect, when stress is applied transversally to the optical fiber, the birefringence changes, and so the peak separation changes as well. In some articles, application of two HB FBG allowed measurement of complex strain [19,22,118]. To achieve it, two HB FBG sensors are placed at different orientation angles which allows us to measure strain in three dimensions, two in-plane axial strain components and out-of-plane axial strain (more in section 1.3.4).

However, in some cases, measurement of out-of-plane strain is not as important as measurement of components of in-plane strain. For this reason, possibility of application of a single FBG sensor inscribed in side-hole highly birefringent fiber for two-directional strain measurements will be tested in a two-directional four-point bending test of composite with integrated side-hole fiber. Parts of this chapter were published in [128].

3.4.1. Four point bending of a composite plate with embedded HB FBG

The following section describes the feasibility of applying the HB FBG sensor to determine strains in a composite plate under four-point bending manufactured using RTM method. Tests were conducted for different loading configurations and sensor locations.

During bending, loaded material is partially in tension and in compression. Between them there is a zero plane. The further from the neutral plane, the greater axial strain is. If FBG sensor is placed parallelly to the supports close to top surface, it will be transversally compressed (Figure 3-30a), which is similar to loading in testing rig for optical fibers (Figure 2-7).

Moreover, if sample is rotated by 90°, the same sensor will be in axial compression (Figure 3-30b). Consequently, if the sample is flipped, sensors will be subjected to transversal/axial tension. Using this approach, a strain sensing capability of an FBG can be measured for both: strain along the fiber, and in-plane strain, which is transversal to the optical fibers. Both of cases can be measure in tension and compression.

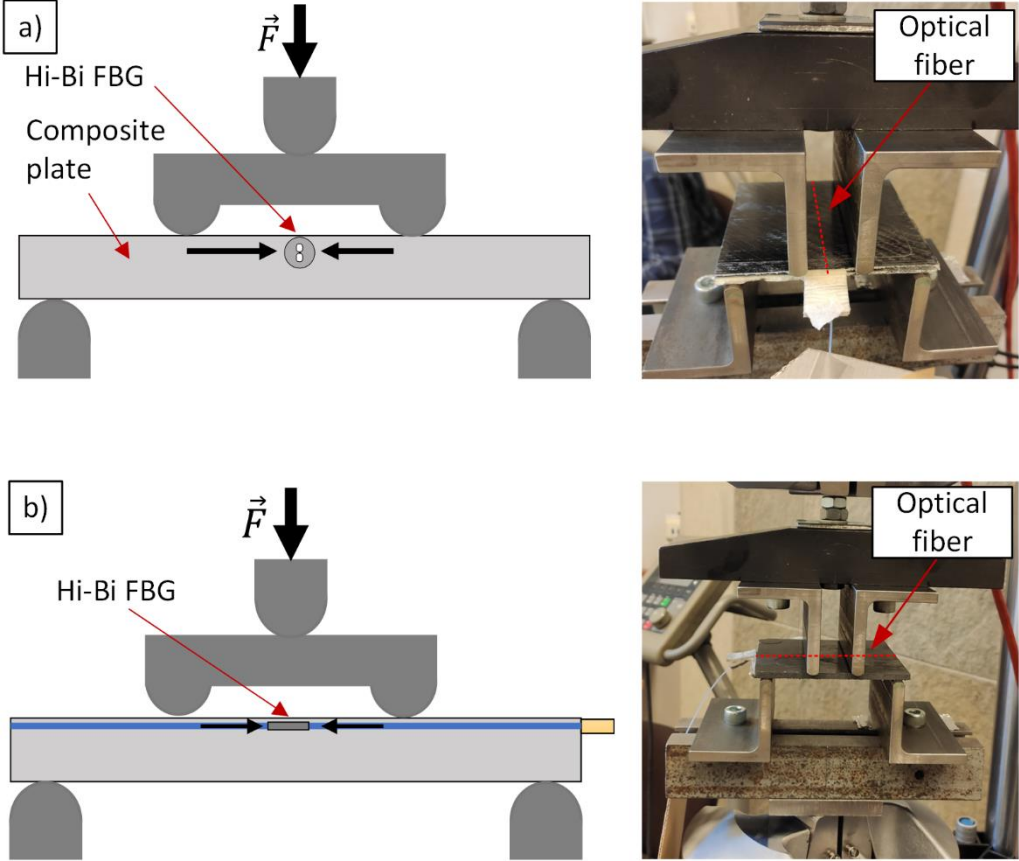


Figure 3-30: Scheme of an FBG sensor subjected to the four-point-bending, a) transversal to the optical fiber, b) along the optical fiber [128].

In the RTM process laminates with integrated FBG sensors were manufactured. Whole manufacturing process is described in the section 3.3. HB FBG sensors were integrated into 270x270x4 mm³ plate, containing 6 layers of carbon fiber non-crimp-fabric. Sensors were integrated on the top of 5th layer, so as close to the top of the plate as possible. Fibers were arranged in such a way that FBG sensors were in a middle of 100x100 mm² samples cut from corners of the plate (Figure 3-31).

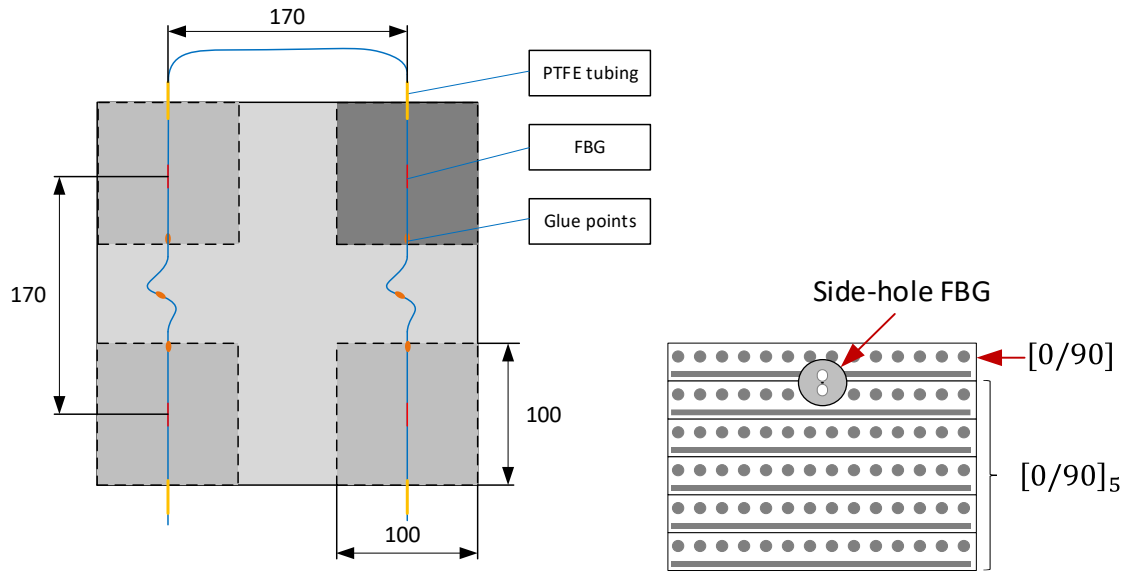


Figure 3-31: An arrangement of samples with FBG sensors cut from the plate manufactured in RTM process.

The samples were tested with a universal testing machine (810, MTS, MN, USA). The distance between the supports was 84 and 28 mm for the lower and higher supports. The distance was chosen in accordance with the ASTM D6272 standard [171]. In the standard, samples should be rectangular, but in case of such a biaxial bending test, square shape is better. Loading was performed to achieve strain of 0.4%, which was in elastic region for this composite. Strain in the location of sensor was calculated from the crosshead displacement. Since stacking was $[0/90]_6$, it was assumed that zero plane was in the middle of a sample, so strain in the location of sensor was calculated from strain in the outer fibers (from standard), and distance from the middle of a sample (measured post-mortem in microscopic images). Bragg peaks were detected from optical spectra collected with an optical interrogator (SI405, HBM, Darmstadt, Germany).

3.4.2. Analysis of the effect of load configuration and HB FBG sensor location on strain measurement sensitivity

Sensors were integrated in two different arrangements – with the slow optical axis in-plane (highest sensitivity in-plane) and out-of-plane of composite (highest sensitivity out-of-plane). Both cases are presented in this subchapter.

A. Slow axis in-plane of composite

First, samples were tested in the case where the load was applied along the optical fiber. Samples were placed in such a way that an optical fiber was compressed, a later sample was flipped, and FBG was subjected to tension. Figure 3-32 shows the combined results of Bragg wavelength shifts.

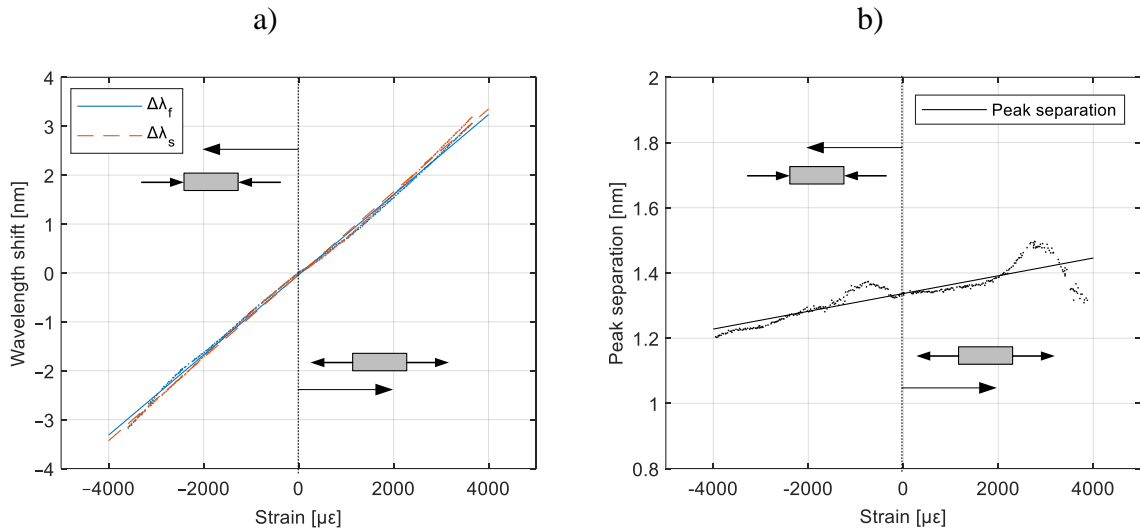


Figure 3-32: Response of SH2 FBG in four-point bending: a) Bragg wavelengths shifts; b) Peak separation; in the case the load is applied along the optical fiber and slow-axis is in-plane of composite [128].

The results of the Bragg wavelength variation $\Delta\lambda$ (ϵ) were linear with $R^2 > 0.99$ for both axes. Strain sensitivity were $k_f=0.819$ pm/ $\mu\epsilon$ and $k_s=0.848$ pm/ $\mu\epsilon$ for fast and slow axis respectively. The difference in the sensitivity between both axes was around 3%. The separation changes due to the axial load were $k_{SEP}=0.028$ pm/ $\mu\epsilon$ with linear fitting of $R^2=0.72$.

After these tests, plate with sensor was rotated in such a way, that bending caused the strain in the direction transversal to the optical fiber. The combination of tension and compression in the transverse direction is shown in Figure 3-33.

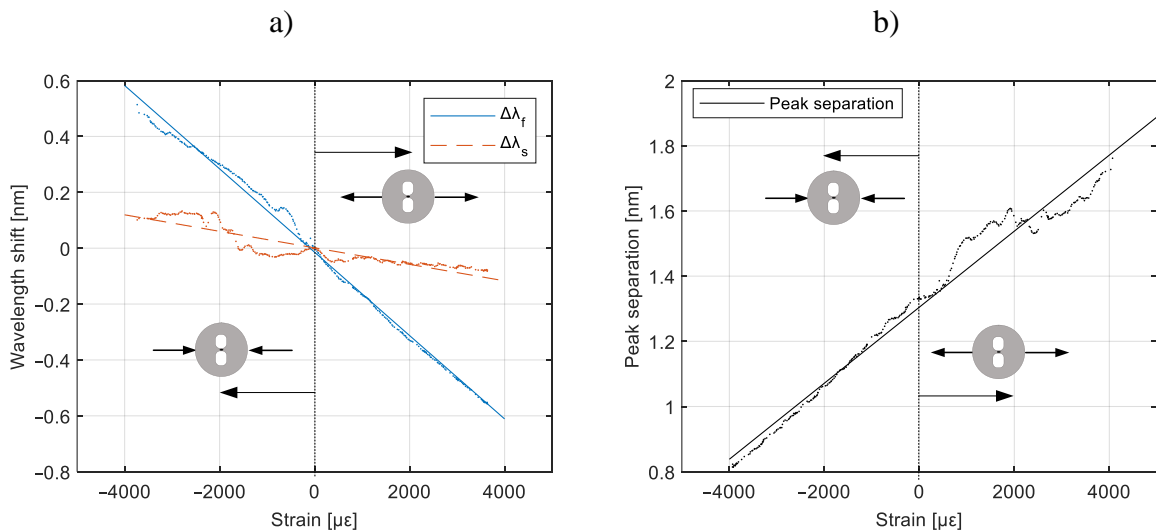


Figure 3-33: Response of SH2 FBG in four-point bending: a) Bragg wavelengths shifts; b) Peak separation; the load is applied transversally to the optical fiber and slow-axis is in-plane of composite [128].


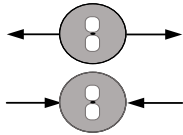
The transverse strain caused the response of the FBG sensor with the following sensitivities (Figure 3-33a) $k_f=-0.149$ pm/ $\mu\epsilon$; $k_s=0.0295$ pm/ $\mu\epsilon$. Peak separation (Figure 3-33b) dependent on strain with a strain-separation coefficient of $k_{SEP}=0.120$ pm/ $\mu\epsilon$. Linear fitting resulted in R^2

coefficient of $R^2 > 0.99$ and $R^2 = 0.81$ for fast and slow axis respectively. For the peak separation correlation coefficient was $R^2 = 0.96$.

Worse correlation coefficient for the slow axis in comparison to the fast axis was caused by small amplitude of Bragg peak shift. Worse fitting coefficient was also observed for the peak separation in longitudinal direction than in transversal direction. In that case, the separation variations were also small, which caused the same issue.

All the sensitivities are collected in the Table 3-3.

Table 3-3: Strain sensitivities of a side-hole 2 FBG integrated into the composite in the case when axis is in-plane of composite [128].

Load state		k_f [pm/ $\mu\epsilon$]	k_s [pm/ $\mu\epsilon$]	k_{SEP} [pm/ $\mu\epsilon$]
Along the optical fiber		0.819	0.848	0.0288
Perpendicular to the fiber		-0.149	-0.0295	0.120

B. Slow axis out-of-plane of composite

The same type of tests were carried out with HB FBG integrated in the composite plate so that the orientation of the fiber slow axis was in the out-of-plane direction. Results for the longitudinal loading of the optical fiber are shown in Figure 3-34.

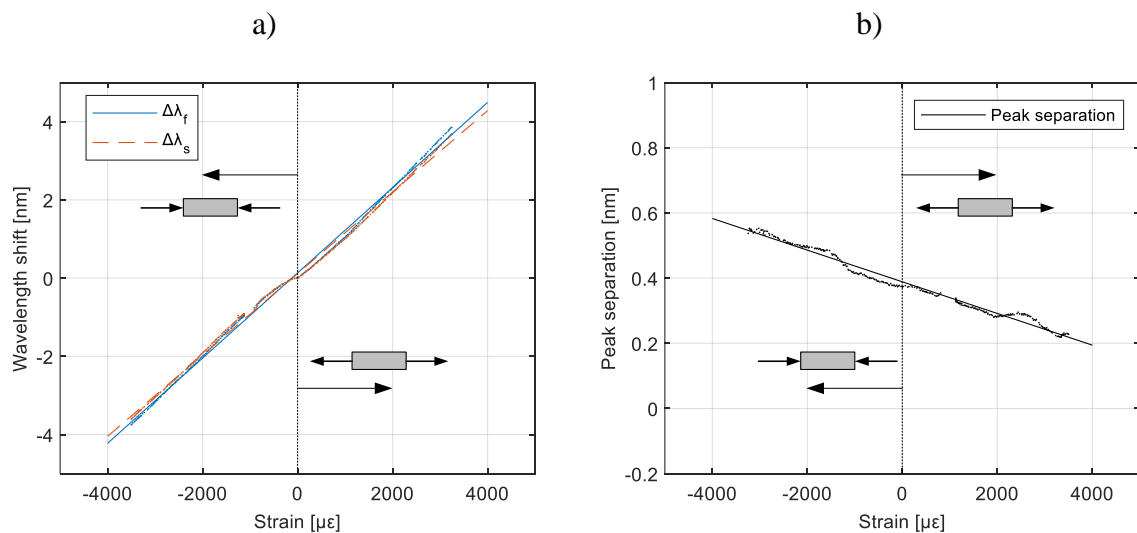


Figure 3-34: Response of SH2 FBG in four-point bending: a) Bragg wavelengths shifts, (b) Peak separation; the load is applied along the optical fiber and slow-axis is out-of-plane of composite.

Longitudinal strain caused the movement of both peaks with comparable sensitivity. It was $k_f=1.089$ pm/ $\mu\epsilon$ and $k_s=1.041$ pm/ $\mu\epsilon$ with $R^2>0.99$ for both axes. The difference in sensitivity for both polarization modes was 4.6%. Peak separation changed by $k_{SEP}=-0.0486$ pm/ $\mu\epsilon$ with linear fitting with $R^2=0.98$.

Transversal loading of the optical sensor resulted in following plots (Figure 3-35):

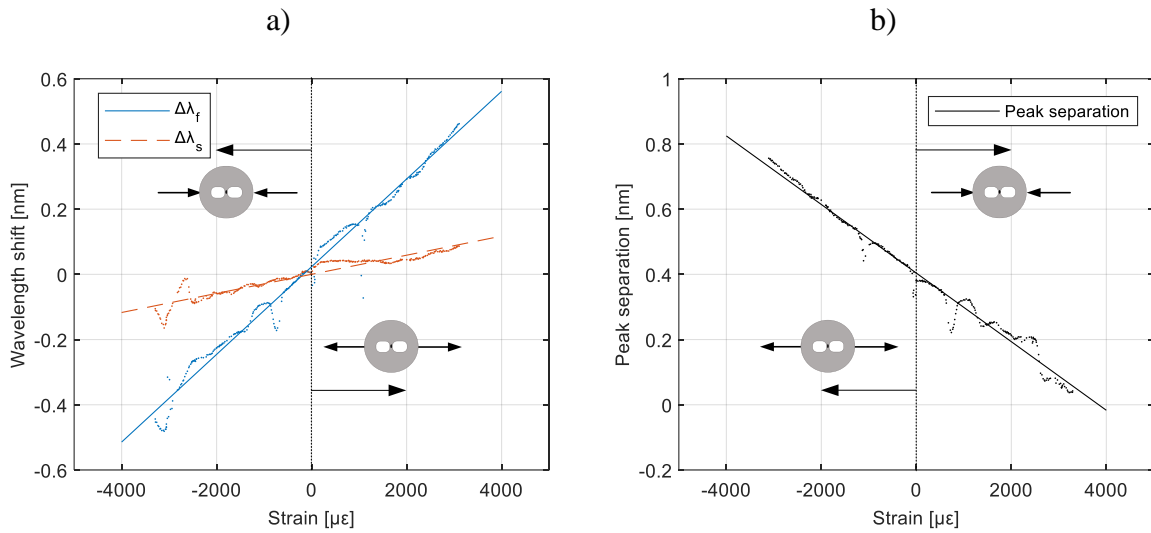


Figure 3-35: Response of SH2 FBG in four-point bending: a) Bragg wavelengths shifts, b) Peak separation; the load is applied transversally to the optical fiber and slow-axis is out-of-plane of composite.

In this case, peak wavelength shift for both axes shown slopes of $k_f=0.1345$ pm/ $\mu\epsilon$ and $k_s=0.0293$ pm/ $\mu\epsilon$ resulting in peak separation sensitivity of $k_{SEP}=-0.1052$. Linear coefficients were $R^2=0.98$, $R^2=0.89$ and $R^2=0.98$ for fast, slow axes, and separation respectively.

All the results for these tests are collected in the Table 3-4

Table 3-4: Strain sensitivities of a side-hole 2 FBG integrated into the composite in the case when axis is out-of-plane of composite.

Load state		k_f [pm/ $\mu\epsilon$]	k_s [pm/ $\mu\epsilon$]	k_{SEP} [pm/ $\mu\epsilon$]
Along the optical fiber		1.089	1.041	-0.0486
Perpendicular to the fiber		0.1345	0.0293	-0.1052

3.4.3. Summary on the application of FBG (HB FBG) sensors to plates produced by the RTM process

The research described above demonstrates the applicability of HB FBG sensors to the testing of plates subjected to four-point bending, which were produced by the RTM process. The main conclusions are summarized below, namely:

1. The sensitivity of the measurement system to deformation in the direction perpendicular to the optical fiber for the two configurations of HB FBG sensors was $0.120 \text{ pm}/\mu\epsilon$ for the system when the sensor was in the arrangement that showed the highest sensitivity to deformation in the plane of the board, and $-0.105 \text{ pm}/\mu\epsilon$ for the system with the sensor whose highest sensitivity was in the direction perpendicular to the laminate, respectively.
2. HB FBG sensors, when loaded along the fiber, exhibited behavior similar to SMF FBG sensors, that is, both Bragg peaks moved in parallel with the increase in strain. The sensitivity in this case was, $0.834 \text{ pm}/\mu\epsilon$ for the system where the highest sensitivity was in the plane of the composite, and $1.065 \text{ pm}/\mu\epsilon$ for the system where the direction of maximum sensitivity was in the direction perpendicular to the laminate.
3. The difference in sensitivity to the composite deformation state in the two systems indicates that the use of two HB FBG sensors can be applied to measure deformation in three directions, i.e. two directions in the plane of the plate and in the direction perpendicular to the plate.
4. The mechano-optical calibration coefficients determined in this study made it possible to measure strain changes during the resin curing in the RTM process

In addition, it should be noted that the sensitivity of strain measurement with SH2 sensors in the presented study is lower than the sensitivity reported in the literature for a "butterfly" type sensor [19], despite the fact that in mechanical calibration tests, the SH2 sensor showed higher sensitivity. This difference can be explained by analyzing the difference in load and strain states during calibration and presented strain measurement.

The transverse force during the compression of an optical fiber on the calibration stand can cause a large deformation in the fiber core, which results in high sensitivity to such a loading variant. On the other hand, in the case where the fiber is embedded in a composite, the deformation of the fiber is limited by the surrounding material. In the case of sensor calibration tests, the parameter describing its sensitivity does not depend on the strain, but on the applied force. Thus - a particular optical fiber design (material, cross-section) may exhibit high sensitivity to the transverse force, but at the time undergo a large deformation, which will not be encountered in the target composite. Thus, high force sensitivity does not necessarily go together with high strain measurement sensitivity.

3.5. SUMMARY ON THE APPLICATION OF HB FBG SENSORS FOR MONITORING RTM PROCESS KINETICS AND DETERMINATION OF STRAIN STATE IN PLATE COMPONENTS

Chapter 3 of the dissertation deals with the use of HB FBG fiber optic sensors to monitor the kinetics of the RTM manufacturing process, as well as the determination of the complex strain field in carbon fiber reinforced plates manufactured using this technology.

The main conclusions related to the performed tasks are summarized below:

1. Regarding the effect of compression in the mold on the sensors embedded in the reinforcing fibers and the possible degradation of the reflection spectrum. The study showed that there is no negative effect on the HB FBG sensors used during compression of the sensor with fabrics in which the reinforcing fibers of at least one of the reinforcing layers directly adjacent to the sensor are arranged in the same direction as the optical fiber. In this arrangement, the optical fiber is fitted between the reinforcing fibers, which protect it from direct compression and prevent spectral degradation. Preliminary tests have shown that compression of the HB FBG sensor placed between the solid die surface and the reinforcing fibers positioned at a 45-degree angle could result in degradation of the grating's measurement characteristics. This means that, as with conventional (SMF) Bragg gratings, the optical fiber should be placed along the reinforcing fibers if possible, and the mechanism that negatively affects the measurement capability is microbending rather than induced birefringence. Thus, the use of FBG on SH2-type birefringent fibers does not allow for more flexibility in the arrangement of the fiber relative to the reinforcing fibers.
2. In terms of investigating the kinetics of the RTM process, including gel point determination and strain changes due to the resin curing process. The study showed that HB FBG sensors can be integrated into the composite in the RTM process and used to monitor the process. The study solved the problem of integrating the sensors into the composite. The gel point measurement results were validated with a dedicated process monitoring sensor (DC sensor). The HB FBG sensor allowed the determination of the gel point of the resin based on the measurement of deformations perpendicular to the plane of the sheet. It was observed that, from the gel point, there is a continuous monotonic trend in the change of the separation of the Bragg peaks, which indicates the build-up of transverse deformations. This measurement, unlike the method used in the SMF FBG, is almost independent of temperature. For this reason, the SMF FBG requires an additional sensor integrated into the FBG sensor location, which is not required for the HB FBG sensor.
3. In terms of determining the complex strain field in a plate element produced by the RTM process. The test object in this case was a plate-shaped specimen, which was subjected to four-point bending. The tests showed that HB FBG sensors allow measurement of the multiaxial strain field. The sensitivity of strain measurement in the direction perpendicular to the fiber was $0.120 \text{ pm}/\mu\epsilon$ for the system when the sensor was in an arrangement where the direction of its maximum force sensitivity was in the plane of the plate, and $-0.105 \text{ pm}/\mu\epsilon$ for the system with the sensor where the direction of sensor's maximum force sensitivity was perpendicular to the laminate, respectively. These values imply the ability to measure strain at $8.33 \mu\epsilon$ and $9.52 \mu\epsilon$, respectively, for the typical resolution of available interrogators, i.e., 1 pm.

The different measurement sensitivities depending on the direction of deformation indicate that the HB FBG two-sensor system can be used to measure deformation in three directions, i.e., two directions in the plate shell and in the direction perpendicular to the plate.

4. In terms of the composite manufacturing method, this study is the first example known to the author of the use of FBG inscribed in highly birefringent fiber for monitoring of a closed-form (RTM) process.
5. In terms of the loading condition analyzed, the embedded sensors of HB FBG were used for the first time to measure the deformation of a composite in a bending test. This approach made it possible to demonstrate its multidirectional measurement capabilities, using a single sample. It only had to be bent along different directions.

The research conducted is among the few in the field of applying HB FBG to the thermoset composites in terms of monitoring their manufacturing process and measuring their strain at the exploitation stage.

In summary, the full suitability of HB FBG sensors for monitoring the RTM process in terms of detecting the gel point and measuring residual strain, as well as measuring the composite's complex strain state during its operation was demonstrated, moreover, their significant advantage in measurements compared to typical SMF FBG sensors was shown.

4. AUTOMATED TAPE LAYUP (ATL). MONITORING WITH FIBER OPTIC SENSORS

Automated tape layup (ATL) is a process for manufacturing thermoplastic composites from unidirectional tape. An incoming composite tape is bonded to previously laid-up layers and consolidated under heat and locally applied pressure. The layup can be performed at different angles, which allows the fabrication of parts with desired properties [172,173].

A schematic of the ATL process is shown in Figure 4-1. A composite tape is melted by heat and fed under the roller. The roller applies pressure to bond the tape to the already deposited composite. Movement of the tool (or placement head) allows layup.

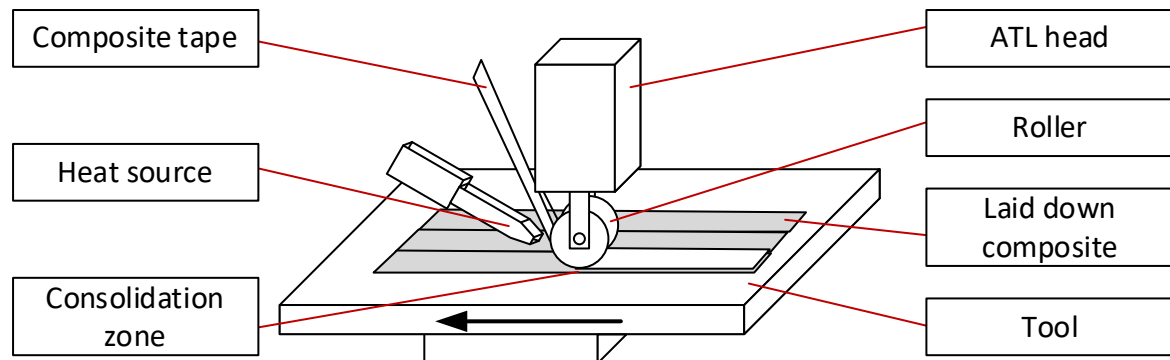


Figure 4-1: Scheme of ATL process.

There are a few cases in the literature where FBG sensors have been used to monitor the ATL process [174–176]. They are used to monitor residual strain during layup [174,176], or for defect detection. However, to the best of the authors' knowledge, there is no case of HB FBG sensors being used for this technology.

In this chapter, preliminary tests are performed to identify the problems with the integration of FBG sensors (section 4.1). Later - HB FBG sensors will be used for in-process (section 4.2) and exploitation monitoring (section 0).

4.1. INFLUENCE OF THE ATL PROCESSING PARAMETERS ON FBG SENSORS PERFORMANCE

During the ATL process, the sensors to be integrated into the composites are affected by the manufacturing conditions, resulting in a reduction in sensor performance. The process consists of melting the composite tape and later consolidating it with the compression roller. There are two main sources that can affect their performance: compression by the roller and high temperature.

The influence of the compression force on the FBG sensors has not been investigated in detail before. There are few papers showing the applicability of FBG sensors for ATL process [174–176], however, they did not investigate the influence of processing conditions on the sensor performance. In the paper [174], the authors reported that the quality of the sensor's reflection spectrum was not affected after the whole process, but there was no information about the direct influence of phenomena on the reflection spectrum quality during the consolidation itself..

Regarding the temperature, the FBG sensors used in published studies [174–176] were coated with polyimide, which allows temperature resistance of up to 350°C [174]. This is more

than melting temperature of CF/PEEK (carbon-fiber/polyetheretherketone) tapes (about 343 °C [176]). The optical fiber is only affected by temperature for a few seconds per layup, so even if the temperature limits are exceeded, no negative effects should occur.

In this sub-section, the preliminary tests using FBG sensors inscribed in conventional (single-mode) fibers are described. The main focus is on the thermal and mechanical resistance of the optical fiber.

The specimens were produced on an ATL test stand built by the Chair of Processing of Composites at Leoben University (Figure 4-2). The test stand consists of three main parts: ATL head, motorized tool, and heat source. The ATL head is equipped with a tape feeder, and a compaction roller. The tape is fed through the ATL head and heated with a pulsed light heat source (Humm3, Heraeus Noblelight GmbH, Hanau, Germany). The melted tape is compacted with the composite placed on the tool below. The tool moves in the X-Y plane to allow layup along the desired paths.

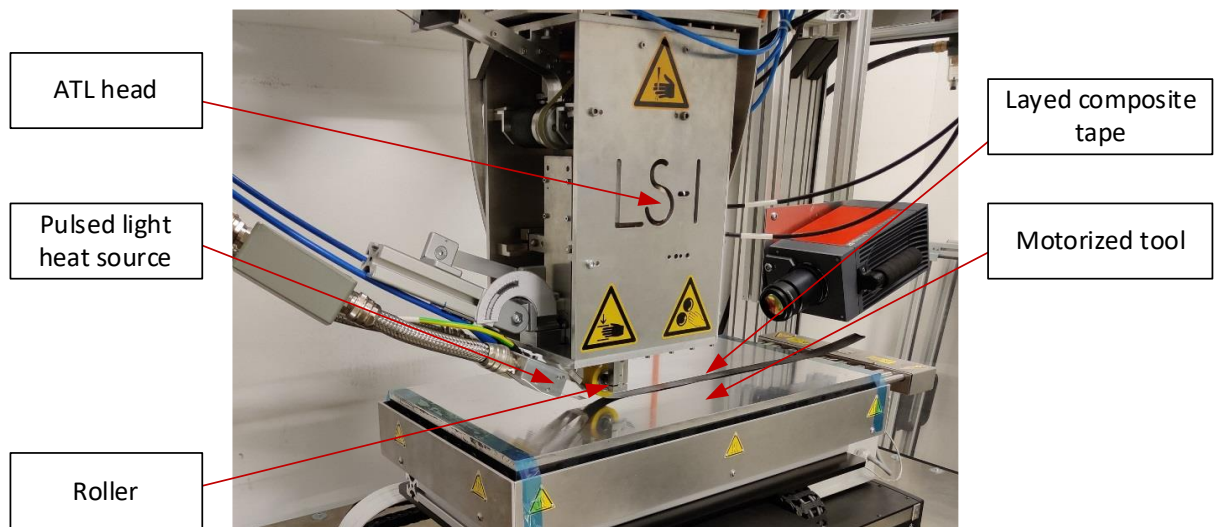


Figure 4-2: ATL test stand used in study.

4.1.1. Investigation of the compaction force on the spectrum of regular FBGs

In the first step, the influence of the compression force on the optical fiber was investigated. No heat was applied and the laying speed was kept low (2 mm/s) in order to allow the measurement of the optical spectra as the roller passes the FBG. A rubber roller of 50 mm diameter and 70 shore hardness was used. The applied consolidation pressure caused the roller to deform, resulting in a contact length of 10 mm. A CF/PP (carbon fiber and polypropylene) tape was used in this test. The position of the roller was recorded at a sampling rate of 10 Hz. Four FBG sensors (FFA-01, Sylex, Slovakia) with a base length of 6 mm were attached to the surface with tape (Flashtape, ECF Composite LTD, United Kingdom) at the measurement locations (Figure 4-3). During the roller passage, reflection spectra were collected with 0.5 Hz sampling rate (maximum sampling rate available for optical interrogator - SI405, HBM, Germany). Due to the lack of hardware triggers to simultaneously collect data on the position of the roller and the optical spectra, the measurement results were manually aligned based on the video recorded for each roller passage.

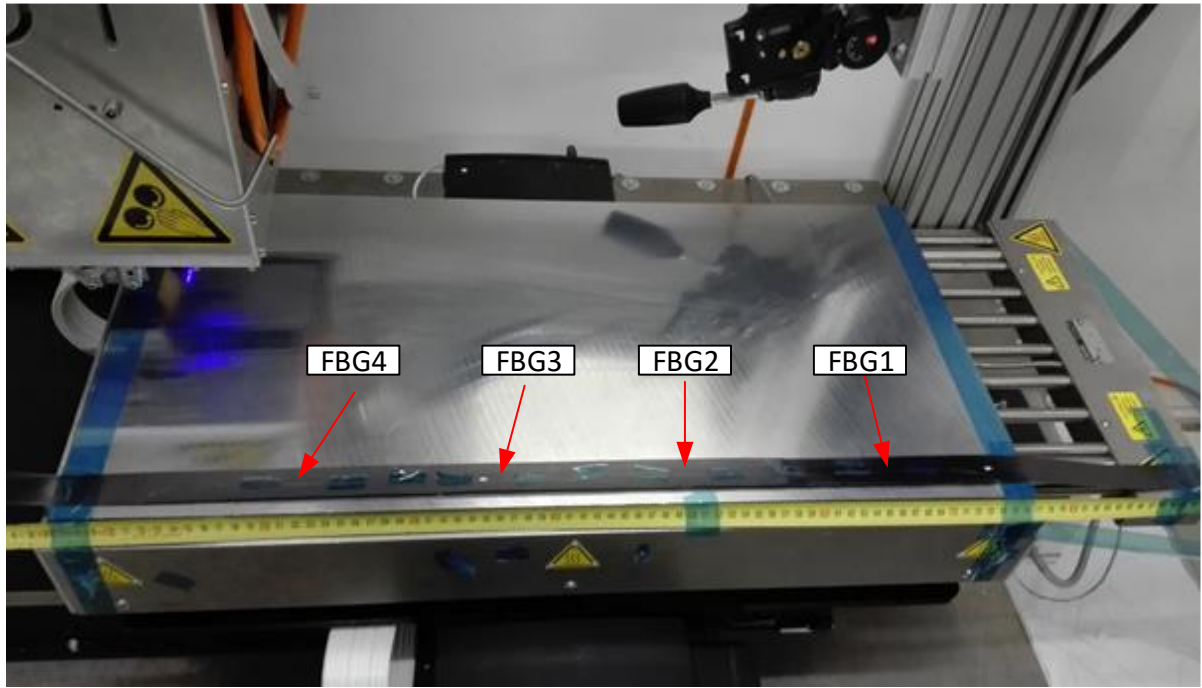


Figure 4-3: FBG sensors attached to the CF/PP tape for the force influence testing.

Based on the position of the roller and the measured position of the FBG sensors, the relative distance at the current time was determined. Using this approach, it was possible to correlate the optical spectra with the distance to the center of the FBG sensor. Combined data of roller position and spectral shape for a selected FBG are shown in Figure 4-4.

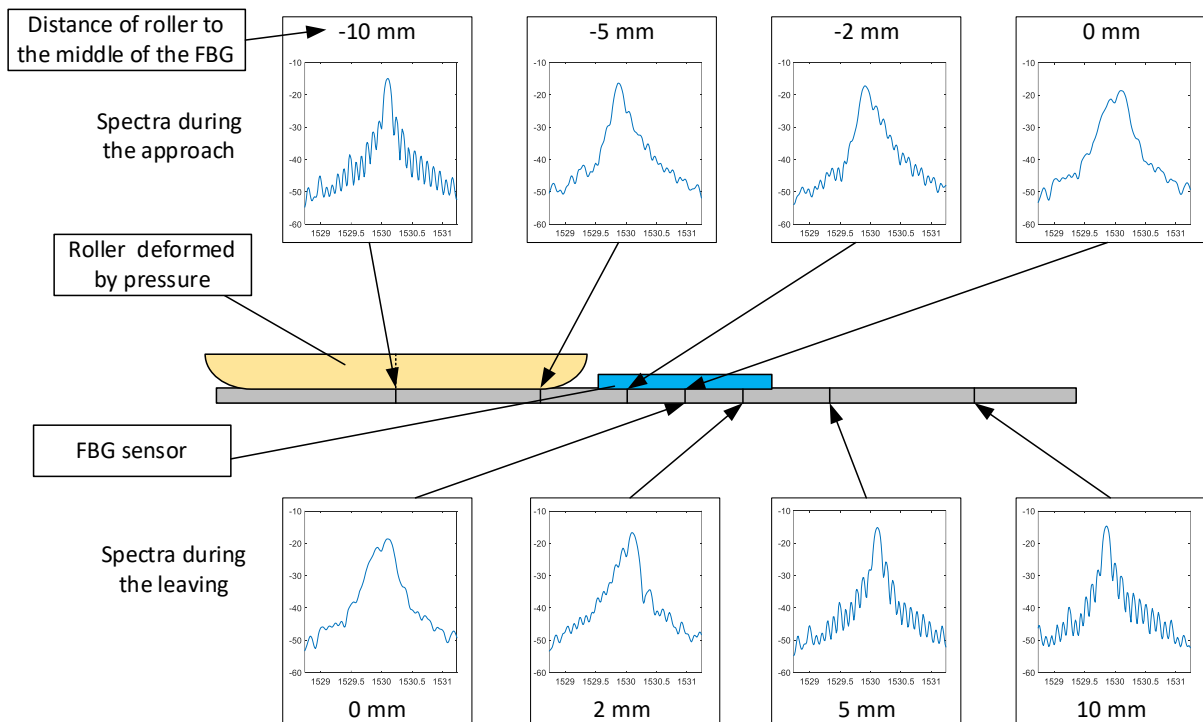


Figure 4-4: Optical spectra of selected FBG during the passage of the roller.

Before approaching the FBG sensor, the peak is not deformed. At the point when the roller is moving on the top of the FBG, reflection spectra begin to split. The deformation is visible in the range of 5 mm before and after the center of the FBG, which is half of the contact distance of the deformed roller. During the passage, the width of the peak increases, and at the center of the FBG, the reflection peak splits into two. This may be due to differences in strain along the roller contact, or induced birefringence caused by roller pressure transversely compressing the fiber, or microbending due to misalignment between the FBG and fibers in the tape. This is important because the interpretation of strain calculated from simple peak tracking, as is often done in the literature [174–176], may be inaccurate in the consolidation zone. The most important observation is the fact that the FBG sensors were not destroyed by the applied force.

4.1.2. Monitoring of ATL process with SMF FBG sensors

As previously mentioned, residual stresses generated during the manufacturing process can cause damage and weakening of composite structures. Residual stresses are highly dependent on the processing environment. For this reason, the use of FBG sensors has been proposed to measure residual strains during consolidation and build-up during the lay-up of successive layers. One of the most important factors influencing residual stresses is the temperature cooling rate during the process [74,75], which depends on several parameters, including the temperature of the tool on which the composite is being placed. For this reason, the tests were carried out under different tool temperature conditions. This part of the work is described in detail in [73].

For this reason, unidirectional one-tape-wide beams with integrated FBG sensors were fabricated. Carbon fiber PA6 tapes (SGL Carbon [177], melting temperature 220°C) of 25.4 mm width were fabricated into 15-layer beams. The compaction force was kept at 200N. The lay-up speed was 50 mm/s, and the heat was adjusted to achieve good adhesion to the tool at 30°C. The tool temperatures used in the tests were 30°C, 60°C, and 120°C, respectively. All parameters except tool temperature were kept constant.

The FBG sensors used in the tests were polyimide coated with an 8 mm grating length and an outer diameter of 145 μm (Sylex, Slovakia). The polyimide coating can withstand temperatures up to 350°C, so its resistance is higher than the temperature that occurs during the process. Both temperature and strain cause shifts in Bragg wavelengths. Therefore, a method is needed to distinguish between the two effects. In this work, the strain of the temperature measurements could be divided by integrating two FBG sensors close to each other such that one FBG was aligned with the carbon fibers (straight) and the other at 15° to the first (angled). The same sensor arrangement was used in the article [174]. This approach is schematically shown in Figure 4-5.

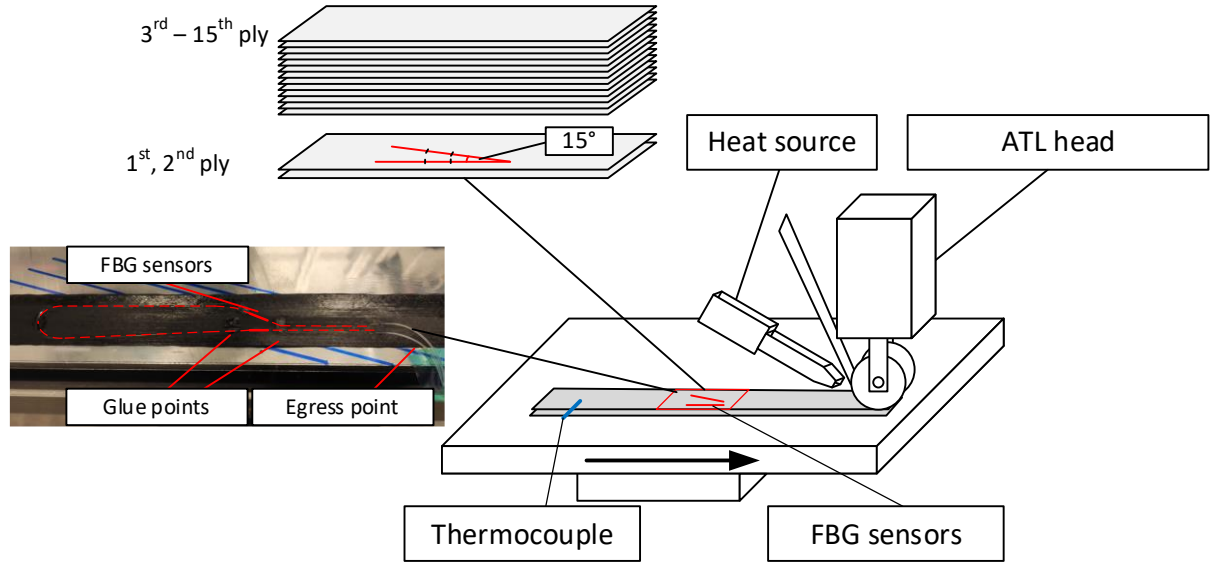


Figure 4-5: Process scheme to measure the residual strain along with temperature using the FBG (based on [73]).

The difference in angle relative to the material causes both FBG sensors to have different sensitivities to strain and temperature [176]. The longitudinal strain sensitivity is different due to the orientation with the composite, while the dependence of the strain sensitivity due to the angle is aligned with the laminate, while the temperature sensitivity is caused by the difference in the coefficients of thermal expansion of the fibers and the thermoplastic matrix of the composite.

Strain and temperature can be calculated using the following equation [73,174,178]:

$$\begin{bmatrix} \Delta\lambda_{BS} \\ \Delta\lambda_{BA} \end{bmatrix} = \begin{bmatrix} K_{\varepsilon_S} & K_{T_S} \\ K_{\varepsilon_A} & K_{T_A} \end{bmatrix} \begin{bmatrix} \varepsilon \\ \Delta T \end{bmatrix} \quad (4.1)$$

$$\begin{bmatrix} \varepsilon \\ \Delta T \end{bmatrix} = \left(\begin{bmatrix} K_{\varepsilon_S} & K_{T_S} \\ K_{\varepsilon_A} & K_{T_A} \end{bmatrix} \right)^{-1} \begin{bmatrix} \Delta\lambda_{BS} \\ \Delta\lambda_{BA} \end{bmatrix} \quad (4.2)$$

where:

ε – axial strain,

ΔT – temperature variation,

$\Delta\lambda_{BS,A}$ – wavelength shift of Bragg peaks of straight and aligned FBG,

$K_{\varepsilon_{S,A}}$ – strain sensitivity coefficients for straight and angled FBG,

$K_{T_{S,A}}$ – temperature sensitivity coefficients for straight and angled FBG,

Data from FBG sensors were collected using two optical interrogators: Benchtop BraggSCOPE FS5500 (FiberSensing, Portugal) and SI405 (HBM, Germany). The use of two different interrogators was due to the fact that the FS5500 could measure the Bragg wavelength with a high sampling rate, but did not provide data on the quality of the reflection spectra. Therefore, for quality assessment, SI405 was used to collect the spectra after each analysis to confirm that no spectra degradation occurred. The inline measurement was performed with a sampling rate of 1 kHz and a resolution of 0.1 pm, which corresponds to a resolution of 0.12 μe or 0.01 $^{\circ}\text{C}$ for the FBG sensor in air. Between layups, the SI405 allowed the spectra to be

exported with a resolution of 7.5 pm, with a peak detection resolution of 1 pm (resolution of 1.2 $\mu\epsilon$ or 0.1°C for the FBG sensor in air). Temperature readings were validated with the thermocouple integrated into the tape at the known location, but not directly at the sensor location. It was assumed that the temperature shift caused by heat would cause the same temperature shift along the entire layup path, so the thermocouple results were matched to the corresponding location of the FBG sensors.

FBG sensors were attached to the composite on the top of the second layer of composite to separate from direct tool influence, but could measure the strain buildup caused by as many layers as possible. Sensor fixation was done with Loctite 406 cyanoacrylate glue applied on both sides of the FBG sensors. During the fixing, FBG sensors were pre-tensioned ensuring no undulation of optical fiber after the integration.

4.1.3. Calibration of integrated FBG sensors

To determine the sensitivities of the FBG sensors to calculate the real strain and temperature of the FBG sensors, the calibration of samples after the manufacturing process was performed. For this reason, sample was subjected to axial tension on the MTS 793 testing machine. Strain measurement was performed with MTS extensometer with a 50 mm gauge length (Figure 4-6b). A test procedure was performed for each specimen for temperature levels of 30°C, 60°C and 120°C.

From the test procedure, the sensitivity of both sensors to axial strain was determined as the slope of the regression line (Figure 4-6a). In each case, the regression was possible with $R^2 > 0.99$. The sensitivities are shown in the Table 4-1.

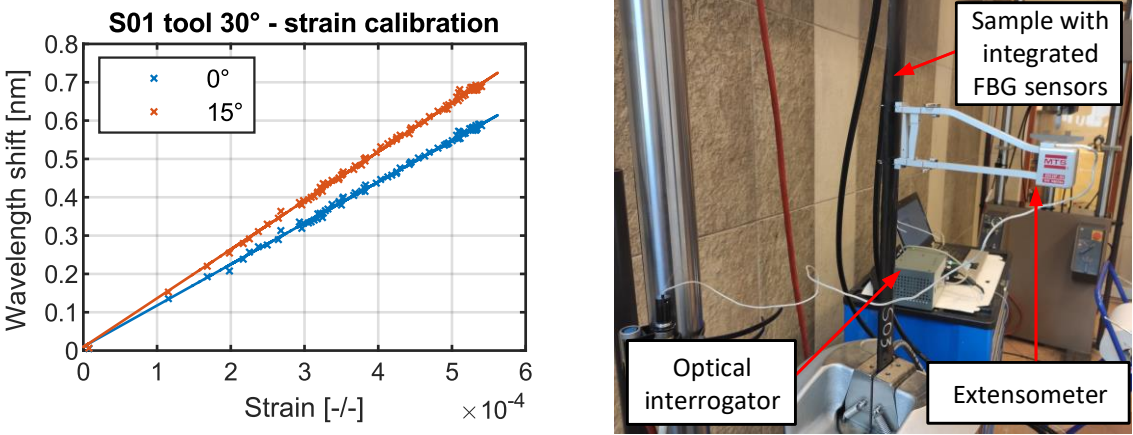


Figure 4-6: Determination of sensitivities of FBG sensors embedded into composite samples, left – exemplary results, right – sample on the testing machine [73].

FBG sensors were also calibrated under the temperature variations. To determine the sensitivities, samples with integrated FBG sensors were placed in the heating oven and the temperature was changed in steps of 25°C, 55°C, and 85°C. At each temperature level, the temperature was held stable for 5 minutes. From this point, spectral data was collected for 30 seconds at a sampling rate of 0.5 Hz. Based on this, the sensitivity was determined. The sensitivity results are summarized in Table 4-1.

Table 4-1: Sensitivity of the sensors to the axial strain and to the changes in temperature [73].

Sample (tool temperature)	$K_{\epsilon_S} [\frac{pm}{\mu\epsilon}]$	$K_{\epsilon_A} [\frac{pm}{\mu\epsilon}]$	$K_{T_S} [\frac{pm}{^\circ C}]$	$K_{T_A} [\frac{pm}{^\circ C}]$
S01 (30°C)	1,074	1,273	8,650	17,399
S02 (60°C)	1,102	1,169	8,890	18,448
S03 (120°C)	1,166	1,163	9,116	14,686

The results of the in-line monitoring of the tape layup were separated using equation 4.2. Since temperature measurements were taken not only with FBG sensors but also with thermocouples, the data calculated from the FBG response were validated with results from the integrated thermocouple. One of the parameters is the maximum temperature recorded during each layup (Figure 4-7).

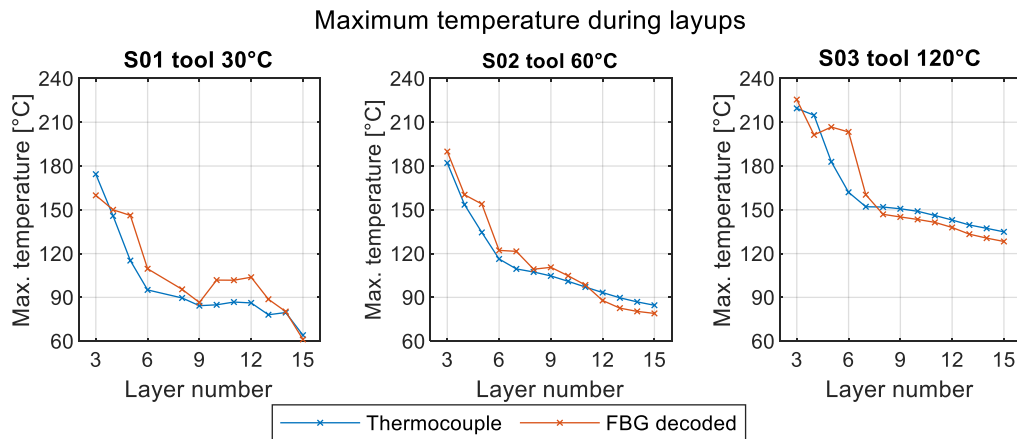


Figure 4-7: Maximum temperature during the tests for various tool temperatures [73].

In all cases, the trend of decreasing temperature is similar for both methods. There is some variation between the FBG and thermocouple readings (highest at 120°C). An example of the results of layup monitoring using TC and FBG is shown in Figure 4-8a. The gray area indicates the area where the roller was compressing the FBG, i.e. the compaction zone.

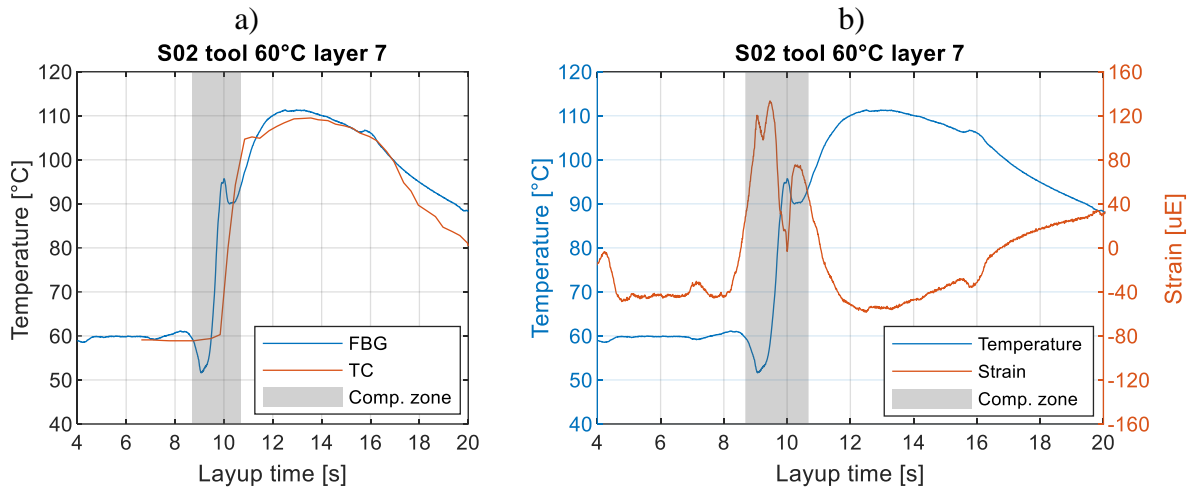


Figure 4-8: Results of in-line consolidation monitoring; a) Temperature readings decoded from fiber optic sensors, validated with readings from thermocouples, b) Temperature and strain readings during the consolidation of a selected layer [73].

The temperature increases during consolidation and 2 seconds after the compression zone. This delay can be explained by the heat transfer through the layers of the composite (this is the layup of the seventh layer, so the whole stack is about 1.4 mm thick). The temperature readings from both sensors are comparable. The difference in temperature measurements does not exceed 5 degrees.

In addition to temperature, strain was also calculated and plotted with temperature in Figure 4-8b. During compaction, rapid changes in strain are observed with an amplitude of $150 \mu\epsilon$ in tension. After the roller passes through the compaction zone, the strain drops to compression, which tends to return to tension during cooling. It is worth noting that variations in the results in the compaction zone can be influenced by the compression of the roller. This compression can cause peak splitting, which can be misinterpreted by the measuring device (as shown in Figure 4-4).

One of the most important pieces of information from monitoring is the residual strain built up during the installation of the subsequent layers of tapes. For this reason, the strain values were measured after 30 seconds, decoded from the FBG data (so-called in-line residual strain), and the strain was measured after the tape had cooled down, i.e., when the temperature measured with the integrated TC did not change for 30 seconds (so-called "before next layup" strain). The mean value was calculated from both results. The results are shown in Figure 4-9.

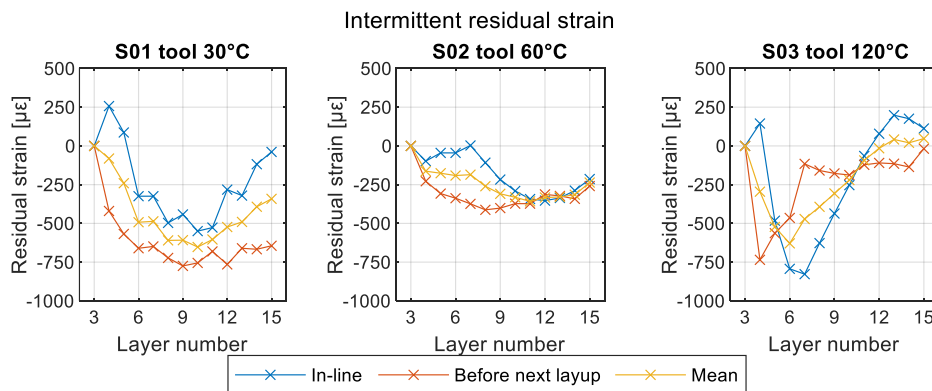


Figure 4-9: Residual strain along with increasing number of layers of composite.

From the end user's point of view, the most important thing is the total residual stress after the entire manufacturing process. The dependence of the calculated global longitudinal residual stress on the tool temperature is shown in Figure 4-10.

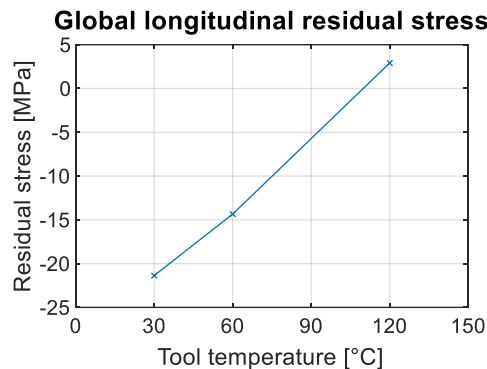


Figure 4-10: Dependency of residual stress calculated as a function of tool temperature.

It can be seen that the residual stress decreases as the temperature increases. For a temperature of 120°C this value is less than 5 MPa. This is in agreement with the literature where it is said that the longitudinal strain is asymptotically close to zero with decreasing cooling rate [179,180].

4.1.4. Summary of tests on ATL processing parameters on FBG sensor performance

Investigation on the ATL processing parameters on FBG sensors performance lead to the following conclusions:

1. FBG sensors inscribed in low birefringence optical fibers are capable of measuring longitudinal strain and temperature during the ATL process. The influence of process conditions on the FBG sensor was identified, and processing conditions did not degrade the sensing capabilities of FBGs for monitoring strain build-up, so the sensors can be used for monitoring the subsequent exploitation stage.
2. During consolidation, the force applied by the roller can cause a broadening of the Bragg peak, leading to errors in strain measurement when the FBG is under the roller. The reason for this peak broadening can be attributed to the induced birefringence caused by the pressure or the strain gradient.
3. The temperatures that occurred during the tests were much lower than the resistance of the polyimide-coated sensors. Thus, temperature did not affect the performance of the FBG sensors.

It should be noted that the highly birefringent side-hole fiber 2 used in this work was not coated with a non-heat resistant coating. This fiber is the unique construction manufactured at the Optical Fibers Technology, Institute of Chemical Sciences, Maria Curie-Skłodowska University in Lublin, and the author did not have the opportunity to use a different coating.

However, during the author's test of SH2 fiber, it was observed that the coating was not damaged in a few hours at a temperature of 150°C. Moreover, preliminary tests presented in this section showed that during the manufacture of the CF/PA6 composite, such a high temperature was exceeded only during the layup of two layers on top of FBG (tool temperature 30°C). Furthermore, this temperature limit was only exceeded for less than 3 seconds per layup. Therefore, it should be possible to use FBGs with this particular type of HB fiber in the ATL process for the same material.

4.2. MONITORING OF RESIDUAL STRAIN IN THE ATL PROCESS WITH HB FBG SENSORS

One of the main objectives of the thesis was to monitor the ATL process with HB FBG sensors. Their unique feature is their sensitivity to transverse strain. During the ATL process, layup of successive layers causes changes in residual strain, which can lead to deformation and degradation of mechanical properties of the composite. HB FBG sensors could measure this strain buildup and allow future optimization of the process. This section describes the technique of integrating HB FBG into a thermoplastic composite and the results of strain monitoring during composite manufacturing.

4.2.1. ATL process conditions and measurement setup for process monitoring

The preliminary tests in the ATL process showed that the technological conditions occurring during the process should not damage the HB FBG sensors, even though their coating is not optimized to operate at temperatures around the melting point of the PA6/CF composite, so the same manufacturing conditions were used. In particular, the speed was kept at 50 mm/s, the heat source emitted the same power as in the previous tests, and the tool temperature was 30°C. The main difference was the stacking of the final object. In this case, instead of the unidirectional beam, an 8-layer cross-ply plate (stacking $[0_4/90_4]$) was used. The measurement of the buildup after each stacking is based on the spectra collected after each layer. The optical signals were measured with an SI405 (HBM, Germany) optical interrogator, and the Bragg wavelengths were then determined using the centroid method.

HB FBGs were integrated on top of the second layer to reduce the influence of the tool. The optical fibers were parallel to the carbon reinforcing fibers. Two FBG sensors were used in each sample so that the highest sensitivity of the first FBG was in the out-of-plane direction and the second was in the in-plane direction. The orientation of the FBG sensors was determined using the diffraction-based setup described in section 2.5. To fix the intended orientation of an FBG, small drops of X60 adhesive were placed on both sides of the sensor. Their flat bottom surfaces indicated the intended orientation. A schematic representation of the FBG sensor orientation is shown in Figure 4-11

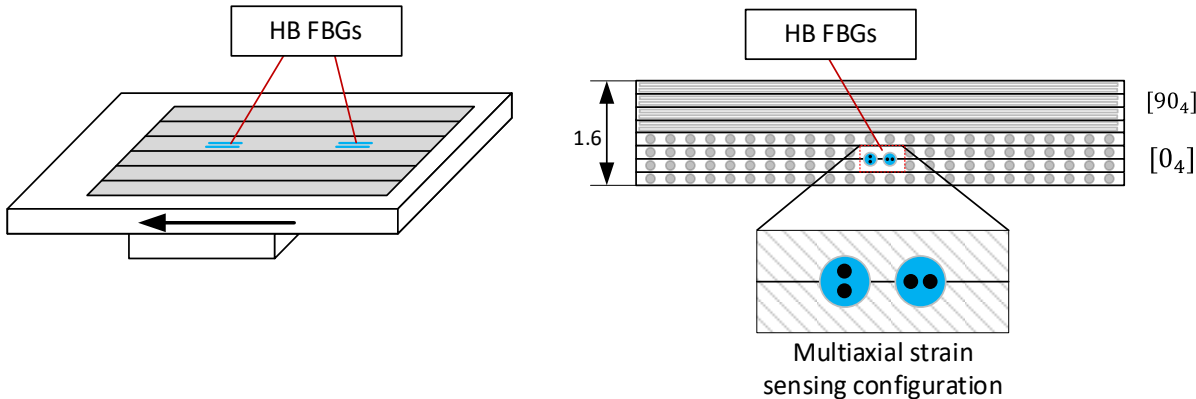


Figure 4-11: Configuration of HB FBG sensors used for multiaxial strain measurement during the ATL process.

In previous tests, sometimes the cyanoacrylate adhesive holding sensors got melted because of the temperature during the layup. To ensure this would not occur in these tests, FBG sensors

were fixed with of EP310 (HBM, Germany) hot curing glue dedicated for long last high temperature tests. The only issue was the need for curing of the adhesive before the tests. However, the design of this ATL machine’s tool allowed demounting of the top part of the tool with already laid-up composite. The two layers of composite with fixed FBG sensors could be transported to the heating oven without need of peeling off of the composite. Curing was performed in temperature of 140°C for 4 hours. After this step, tool was fixed back to the machine and layup was continued. FBG sensors attached to the composite after curing of the glue are shown in Figure 4-12.

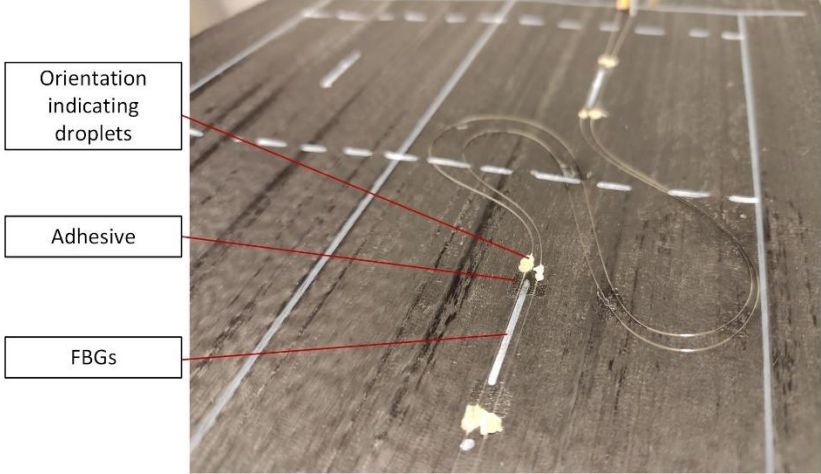


Figure 4-12: View of FBGs attached to the two bottom layers for the FBG sensors integration.

4.2.2. In-plane and out-of-plane residual strain measured with HB FBG sensors

The strain sensitivity of FBG sensors depends on the strain transfer in the particular material and optical fiber, so the sensitivity had to be determined in the quasi-static tests. Sensitivity was determined in bending tests as described in the next section (4.3.1). Strain was calculated by multiplying the peak separation changes by the sensitivity of the FBG to transverse strain (0.0571 $\mu\epsilon/\text{pm}$), namely in-plane strain was calculated from the peak separation changes of the HB FBG whose axis of highest force sensitivity was in-plane of the composite, while out-of-plane strain results were calculated from the HB FBG with the most sensitive axis out-of-plane. Residual strains calculated after each layer are shown in Figure 4-13.

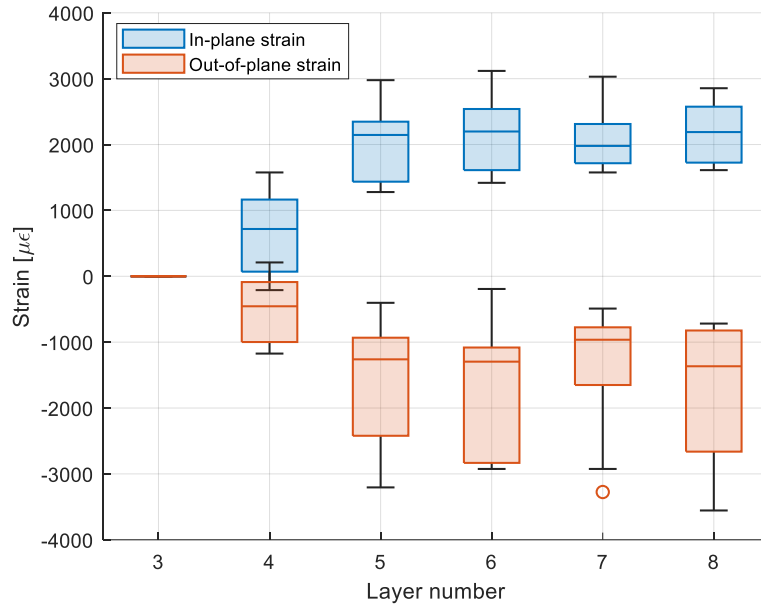


Figure 4-13: Residual in-plane and out-of-plane strain measured from transversal response of HB FBG sensors.

The strain in the out-of-plane direction had a compressive behavior, while the strain transverse to the optical fiber (as well as to the reinforcing fibers) in the plane of the composite was positive. The median final residual strains between the second and third layers were 2189 $\mu\epsilon$ and -1366 $\mu\epsilon$ for in-plane and out-of-plane, respectively. The strain buildup occurred mostly during the layup of the fifth layer (the first layer perpendicular to the optical fiber). After this point, it stabilizes for both strain directions and remains at approximately the same level. This means that perpendicular layers of the composite caused stabilization of the residual strain that occurred in that directions.

4.2.3. Summary of ATL process monitoring with HB FBG sensors

Results regarding the application of HB FBG sensors for monitoring of residual strain build-up presented in the above subchapter lead to the following conclusions:

1. Plates with embedded HB FBG sensors inscribed in SH2 fibers were manufactured in ATL process. Protection and embedded method of fiber optic sensors was developed and successfully applied resulting in well consolidated plates with fully functional sensors.
2. HB FBG sensors allowed measurement of the residual strain in transverse direction to the optical fibers. Effect of the build-up of residual strain both for in-plane and out-of-plane strain in the location of the sensor (between the second and third layer of the composite) was recorded.

4.3. QUASI-STATIC AND CYCLIC TESTING OF COMPOSITE MANUFACTURED IN ATL PROCESS

In this process, 200x200mm composite plates were fabricated. Around the edge of the plate were 20 millimeters long pieces of unconsolidated tape. Typically, these tapes are trimmed to size, but fiber optic sensors were entering into the composite at this location. For this reason, as much of the unconsolidated tape as possible was removed manually. As a result, less than 5 mm of unconsolidated tape was left on these sides. Each plate was then cut into four 75x100 mm samples with the FBG in the center between the second and third layers. The shape of the specimen is shown in Figure 4-14.

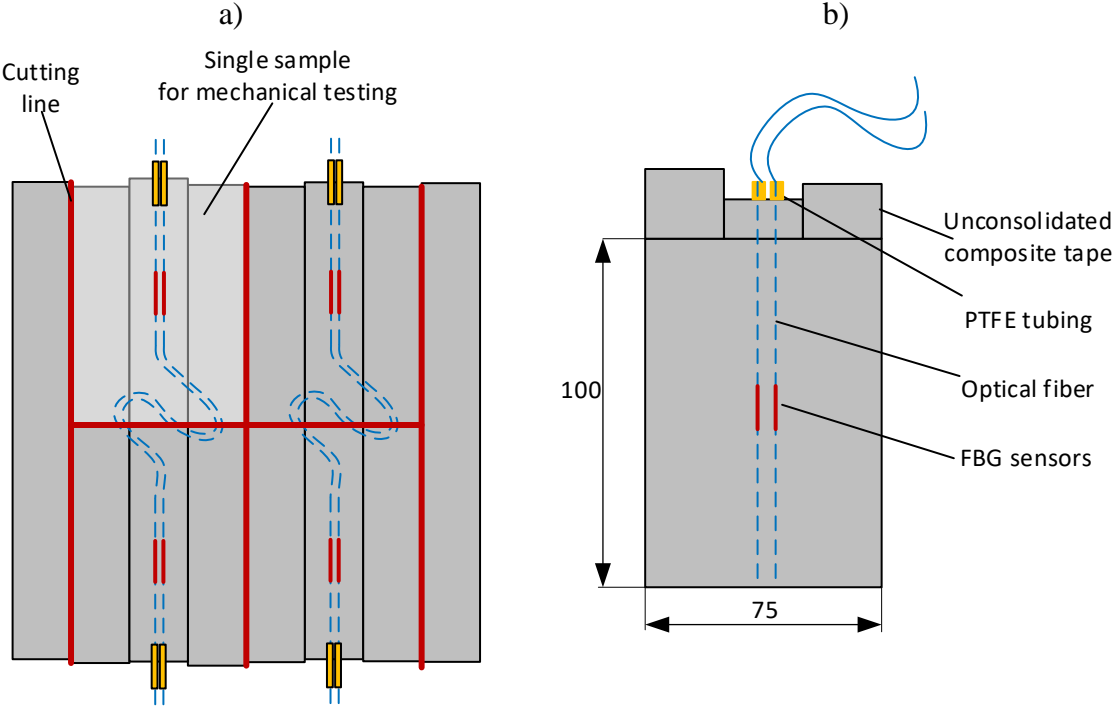


Figure 4-14: Samples used for mechanical testing cut from the manufactured plate, a) Cutting scheme; b) A single sample.

The samples were tested in the four-point bending setup. The main focus of this research was the transversal sensing capability of the HB FBG, so specimens were tested in the case where the FBG sensor was transversally compressed during bending. The specimens were flipped according to the manufacturing so that the FBG sensors were on the top side of the specimen (Figure 4-15).

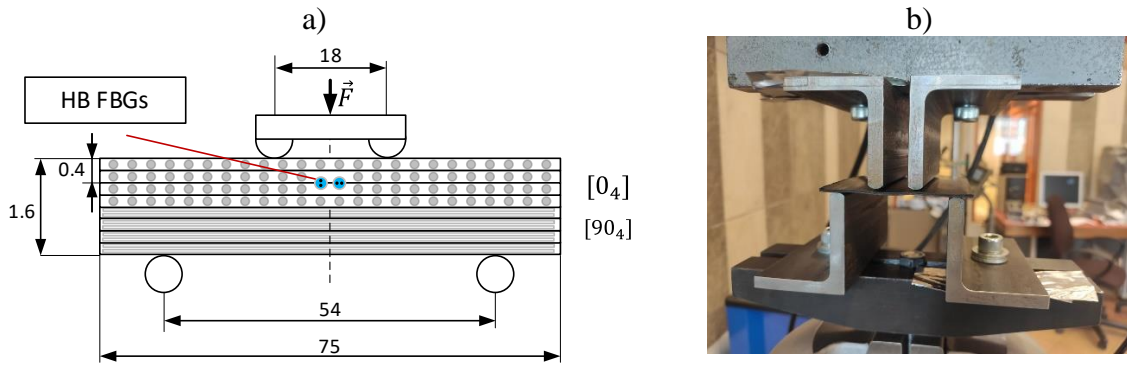


Figure 4-15: Arrangement for mechanical testing of specimens produced by ATL; a) Scheme of loading; b) View of the specimen on the testing machine.

The span of the supports was selected based on the ASTM D6272 standard [171]. The span of the upper supports was 18 mm, while the span of the lower supports was 54 mm. The supports were rounded with radius $R=5$. In all cases, FBG spectra were collected during the test at a sampling rate of 5 Hz, and peak determination was performed afterwards with developed scripts.

4.3.1. Quasi-Static tests of ATL samples with integrated HB FBG sensors

Quasi-static tests of the specimens were used to determine the sensitivity to transverse deformation, which was used to calculate the residual strain from manufacturing and further cyclic tests. Tests were performed on each specimen in the elastic range of the specimens (force up to 800N). The elastic range was determined from the samples without sensors that were tested prior to the HB FBG sensor tests.

To calculate the strain in the composite based on the results from the sensors, it is necessary to correlate the position of the crosshead with the strain at the location of the sensor. The specimens were made with $[0_4/90_4]$ stacking, so the neutral zone is not in the middle of the laminate. To determine the strain at the sensor location, finite element analysis (FEA) was performed.

FEA was performed with LS-Dyna software with implicit solver. Geometry was meshed with solid elements, with 16 elements in thickness. Half of them was corresponding to the $[0_4]$ part of the composite and second to $[90_4]$ part, so of half of the model had material properties of composite along the reinforcing fibers, the other half – perpendicular to the carbon fibers. In this analysis, composite was considered as linear elastic material with material properties based on the datasheet provided by manufacturer [177]. The fine tuning was done to fit the experimental data collected during four-point bending. Results of the FEA for stress and strain are shown in Figure 4-16.

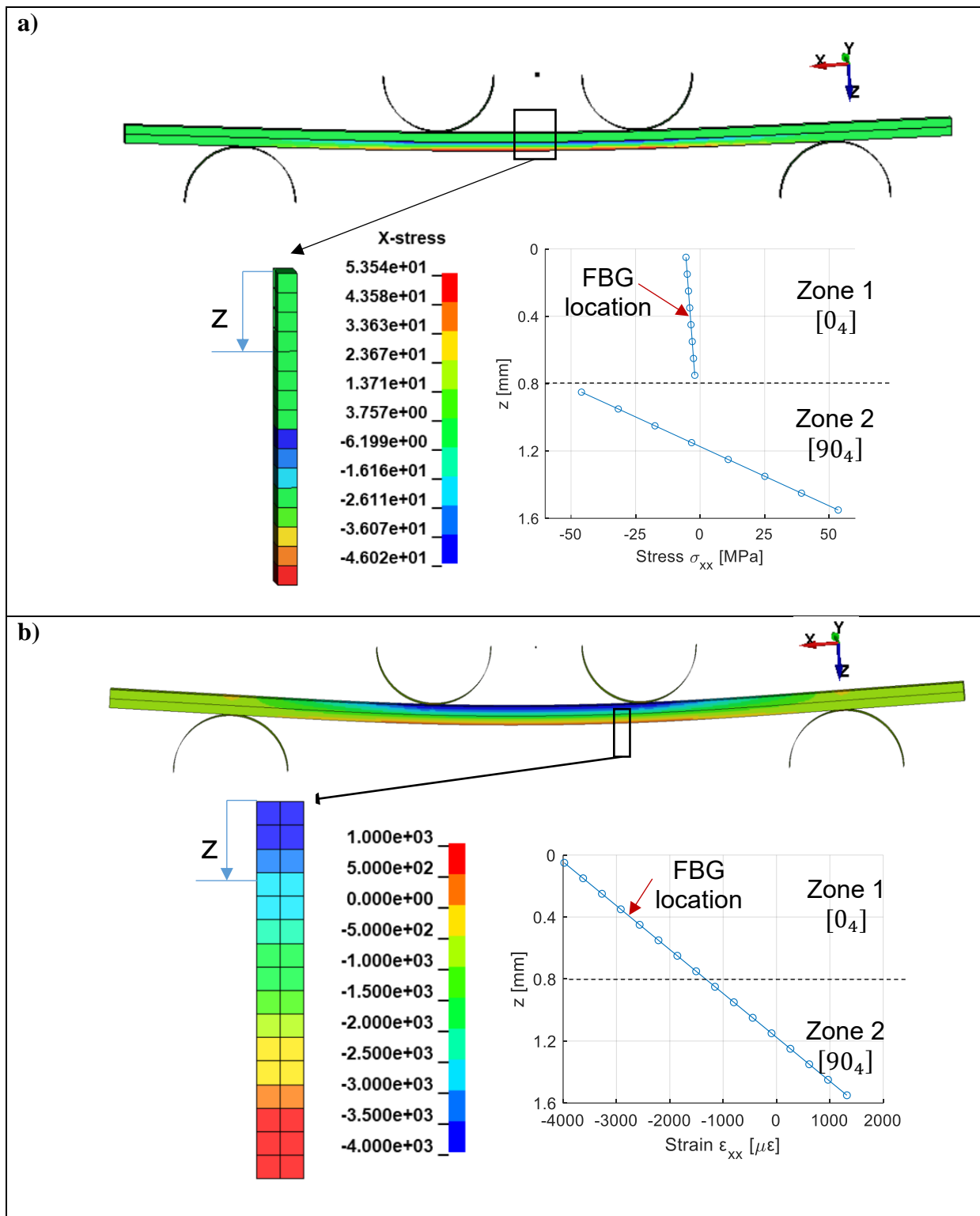


Figure 4-16: Through-thickness distribution of calculated:
 a) Stress σ_{xx} caused by 100N load,
 b) Strain ϵ_{xx} caused by 1 mm of displacement.

From the presented analysis it was found that loading with force of 100 N resulted in strain of -3.529 MPa in the sensor location, and displacement of the supports by 1 mm caused 2800 $\mu\epsilon$ strain at the location of the sensors.

The displacement-strain coefficient evaluated previously was used to calculate the strain in the location of HB FBG sensors. This strain along with optical response of HB FBG sensors is presented in figures below. Results are shown separately for HB FBG with axis most sensitive to force in-plane of composite (Figure 4-17), and out-of-plane of laminate (Figure 4-18):

In-plane

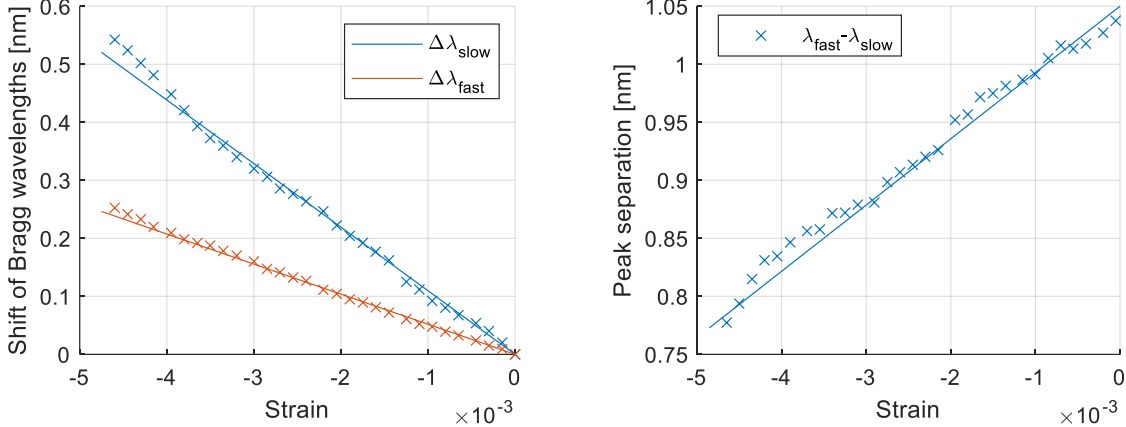


Figure 4-17: Response of the FBG sensors to the transversal load applied to the FBG sensor, which main sensing direction was in-plane of the composite.

Out-of-plane

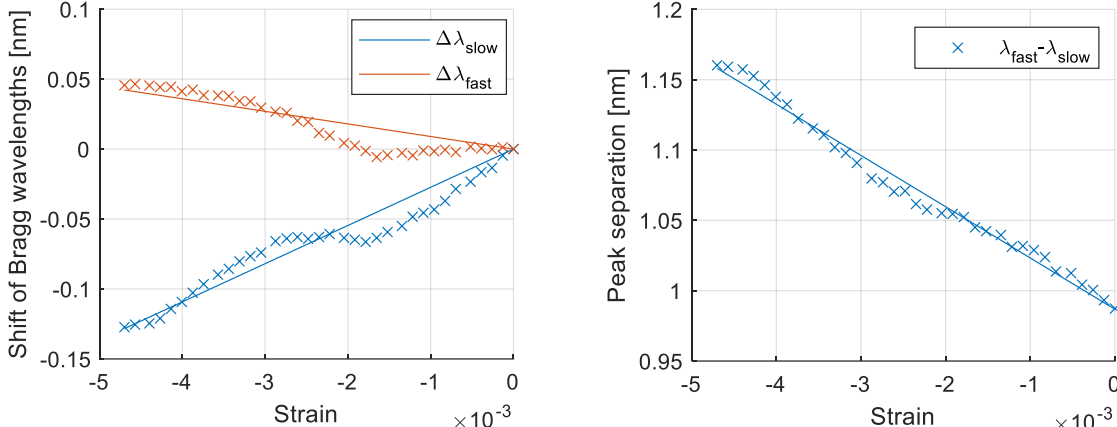


Figure 4-18: Response of the FBG sensors to the transversal load applied to the FBG sensor, which main sensing direction was out-of-plane of the composite.

Using the linear regression, sensitivity of sensor to the transversal strain was determined (Table 4-2):

Table 4-2: Sensitivity of the FBG sensors to the transversal strain.

Main measuring direction of the sensor		Sensitivity [$pm/\mu\epsilon$]
In-plane	Slow axis	-0.109
	Fast axis	-0.0519
	Peak separation	0.0571
Out-of-plane	Slow axis	0.0271
	Fast axis	-0.0090
	Peak separation	-0.0365

The sensitivities determined for these embedded sensors are lower than those presented in the previous paper on HB FBGs used for RTM fabricated composite [128]. This difference can be explained by the properties of the material surrounding the FBG. The stress induced in the core of an optical fiber depends on the strain transfer from the composite; the lower the stiffness of the surrounding composite, the lower the strain sensitivity. In the case of the paper [128], FBG sensors were integrated into the composite with a stacking of $[0/90]_4$, so the reinforcing fibers were not only along the optical fiber, but also perpendicular to the FBG, which increased the stiffness of the material around the sensor. Moreover, overall stiffness of the material (especially when optical fibers were aligned with the reinforcing fibers) is also dependent on the matrix material. The epoxy used in RTM process [170] has higher flexural modulus than PA6 [181,182], which further supports the possible explanation.

4.3.2. Monitoring of composite plates with integrated HB FBG sensors during cyclic four-point bending test

The results in previous section showed that HB FBG sensors can be effectively used to measure strain during quasi-static tests, but their application to cyclic testing has not yet been reported more extensively in the literature. The only application known to the author for cyclic testing was reported in [20], where the HB FBG was integrated into an adhesive joint of two laminates. The sensor allowed monitoring the delamination growth that propagated in this layer. The lack of other applications in this area and the proven ability to measure quasi-static strains was the reason to investigate the presented sensors for assessing the condition of the material during fatigue testing.

For this purpose, cyclic tests were conducted on ATL-made specimens with embedded sensors, loading them with a cyclic sinusoidal load with a constant amplitude of force. The range of force was selected during the initial cyclic tests of specimens without sensors in such a way that material failure would occur after about 10,000 cycles. A force range of 0.12 kN to 1.2 kN was selected for this setup. During the test, the specimens were loaded at a frequency of $f=2$ Hz. Due to the limitations of the maximum sampling frequency of the optical interrogator, it was impossible to correctly collect measurement data at such a loading frequency. For this reason, every 1,000 cycles, the loading rate was reduced for two cycles to a frequency of $f=0.02$ Hz and then recorded data from the fiber optic sensors. Due to the lack of a hardware trigger in optical interrogator, the force and piston displacement data from the testing machine

were manually synchronized with the data from the fiber optic sensors. The force-time loading scheme is shown in Figure 4-19.

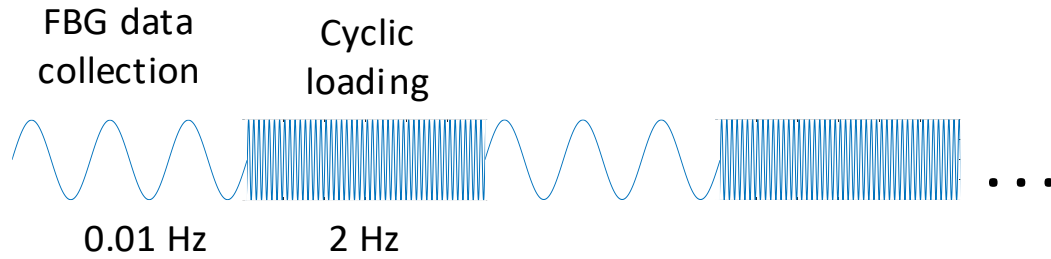


Figure 4-19: A schematic representation of the force versus time curve during cyclic loading of composite plates with embedded HB FBG sensors manufactured using the ATL process.

Hysteresis loops recorded during bending of the composite specimens were plotted from the data collected from the testing machine and HB FBG sensors. At the same time, the stress value was determined using the measured force value and the numerical model of the specimen. The hysteresis loops for the selected specimen are presented on the Figure 4-20.

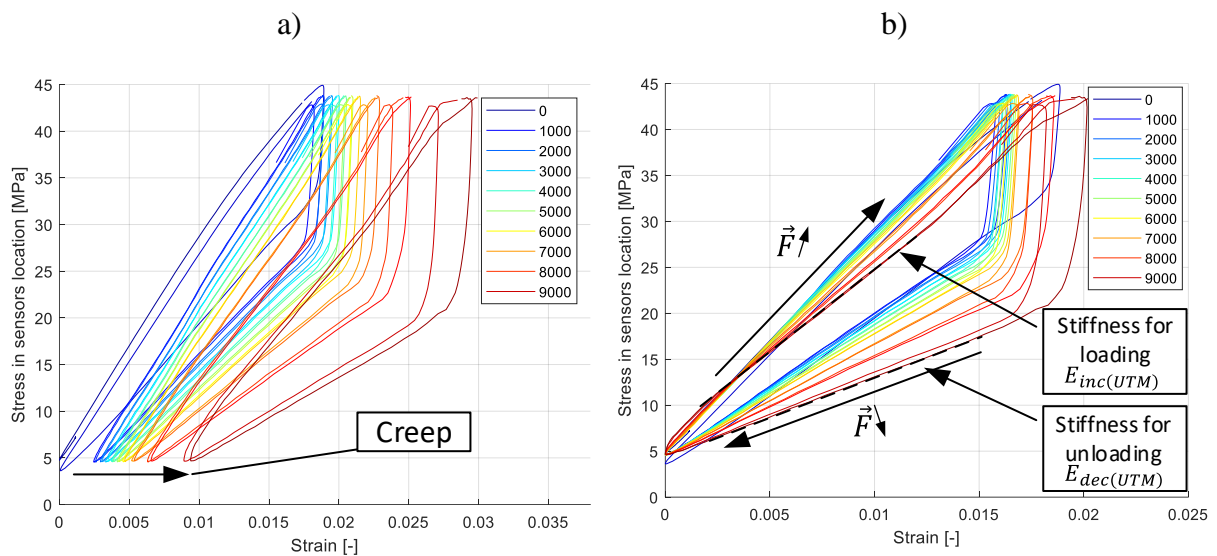


Figure 4-20: Hysteresis loops during fatigue of the specimen based on the data from the testing machine, a) with visible creep; b) after compensation of creep, with the stiffness difference visible in both cases for loading and unloading

Figure 4-20a shows the hysteresis loops for consecutive logging points counted in thousands of cycles. The creep visible in the figure, appearing as progressive strain for the minimum force value, is marked with an arrow. After compensating for the creep that occurs, it is easier to analyze the change in the shape of the hysteresis loop with increasing number of cycles and fatigue progression (Figure 4-20b). The figure also shows the different stiffness of the specimen during loading and unloading, and that both stiffnesses change with the number of cycles. By stiffness here is meant the angle of slope of the rectilinear part of the stress-strain diagram, separately for the half-cycle of loading and half-cycle of unloading the specimen. In addition - as the number of cycles increases, the area of the hysteresis loop changes, indicating progressive energy cumulation and material degradation.

Similar results can be presented for HB FBG sensor data. Due to the higher strain sensitivity of this sensor, which had maximum sensitivity in the plane of the sample, it was assumed that this sensor would be used in the cyclic tests. The waveforms for the same sample collected from the HB FBG sensor are presented in Figure 4-21.

Similar results can be given for HB FBG data. In the following analysis, data from a sensor that showed greater sensitivity to in-plane strain, i.e. a sensor whose axis of greatest sensitivity to perpendicular force was in the plane of the laminate, was examined. The waveforms for the same sample, collected from the HB FBG sensor, are presented in Figure 4-21.

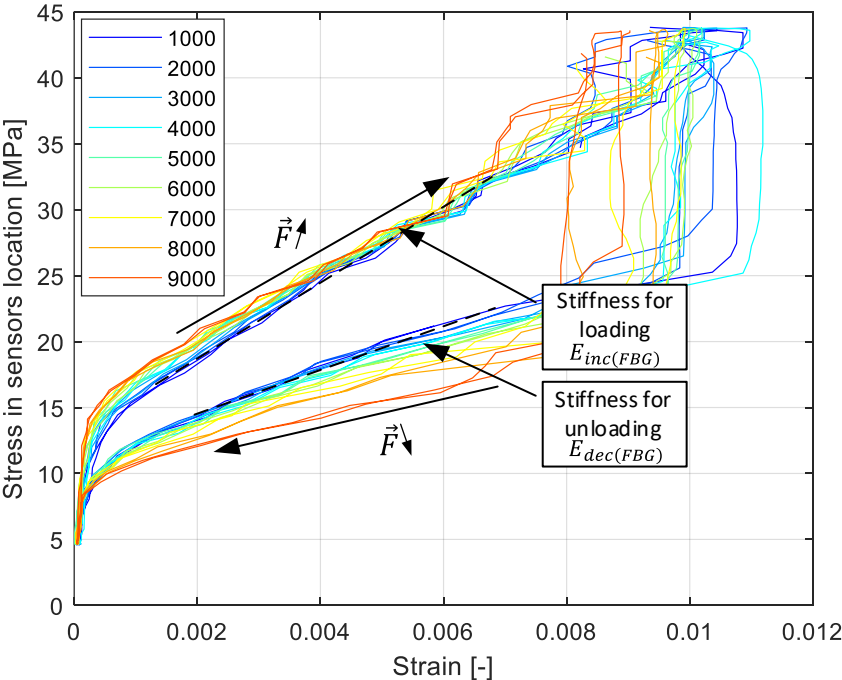


Figure 4-21: Hysteresis loops for an example specimen with strain measured with HB FBG sensors

The hysteresis loop diagrams for HB FBG also show the change in stiffness when the specimen is loaded and unloaded, as well as the change in hysteresis loop area as the fatigue process progresses. It is worth noting that no creep was observed here, in contrast to the data from the testing machine. It is possible, therefore, that the occurrence of this effect was mainly caused by the gradual change in the arrangement of the sample on the supports, or by creep occurring at a different location than the location of the sensor. Moreover - as the number of cycles increased, the HB FBG sensors showed a decreasing strain amplitude. One of the explanations can be the failure mechanism observed for the tested samples. A view of the damaged sample is shown in Figure 4-22.

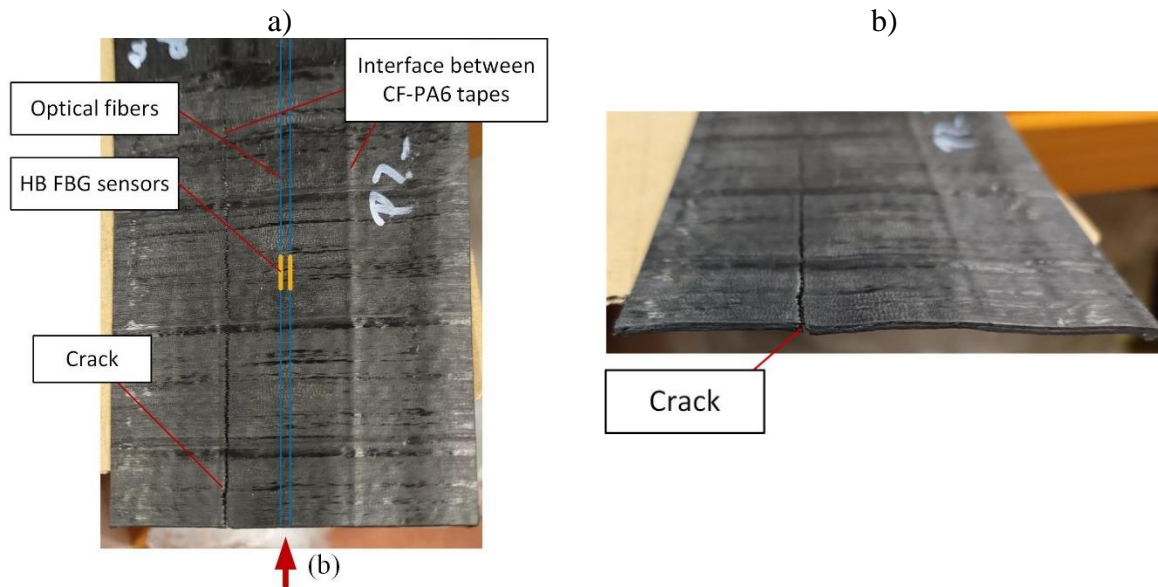


Figure 4-22: An image of a sample after cyclic testing; a) Top view; b) Side view

Figure 4-22a shows that the crack formed near the interface between the two composite tapes, while the fiber optic sensors were located in the center of the tape, approximately 10 mm from the crack. Such a location of damage may have caused most of the stress to accumulate around the crack, reducing the strain in the area of the sensor. This type of failure could be caused by the overlapping of tapes formed during the manufacturing process [183,184].

Another explanation for the decrease in amplitude could be the progressive debonding of the optical fiber from the host material. During cyclic loading, the interface between the optical fiber and the material transferred strain from the host material to the sensor. If the cyclic loading causes a weakening of the bond between the materials, the strain transfer from the host to the sensor will be compromised. As a result, the same strain in the host material would cause a smaller change in Bragg peaks separation and could be misinterpreted as a reduction in the transverse strain. However, optical fiber detachment would also reduce the sensitivity to strain during loading and unloading itself, so the stiffness measured for loading and unloading would not decrease during fatigue in the same way as for the whole sample.

On the other hand, the fact that there was no increase in the measured strain amplitude does not mean that such damage cannot be detected with a given sensor. The HB FBG sensor detected a decrease in strain amplitude at a given point even though the load amplitude did not change. Such behavior may also indicate that damage is occurring elsewhere and strain is accumulating there.

Nevertheless, the most important conclusion is that the parameters characterizing the process of local material damage caused by cyclic loading can be determined from the hysteresis plotted from HB FBG sensor data. In this case, the analyzed parameters were:

- change in stiffness during loading/unloading of the composite,
- the area of the hysteresis loop (energy accumulation per cycle related to the unit volume of the material)

A. Change of composite stiffness under loading and unloading during cyclic tests of composite produced by ATL process

As thermoplastic composites degrade, a reduction in material stiffness is observed. In this section, the results of monitoring the change in stiffness of the composite during loading and unloading, using HB FBG sensors, will be presented. For comparison, data from a testing machine measuring the "global" change in stiffness of the specimen were used.

For specimens subjected to cyclic loading, the corresponding hysteresis was determined, and the loading and unloading stiffnesses were calculated. The stiffnesses determined were normalized against the "reference" stiffness measured after 1,000 cycles, while the cycles were normalized against the life of the entire specimen. A value of 1,000 cycles was taken as a reference, due to the fact that in the first cycles the position of the specimen in the holders changed until a stable position was reached. The results of relative stiffness measurement during loading and unloading during fatigue are presented in Figure 4-23.

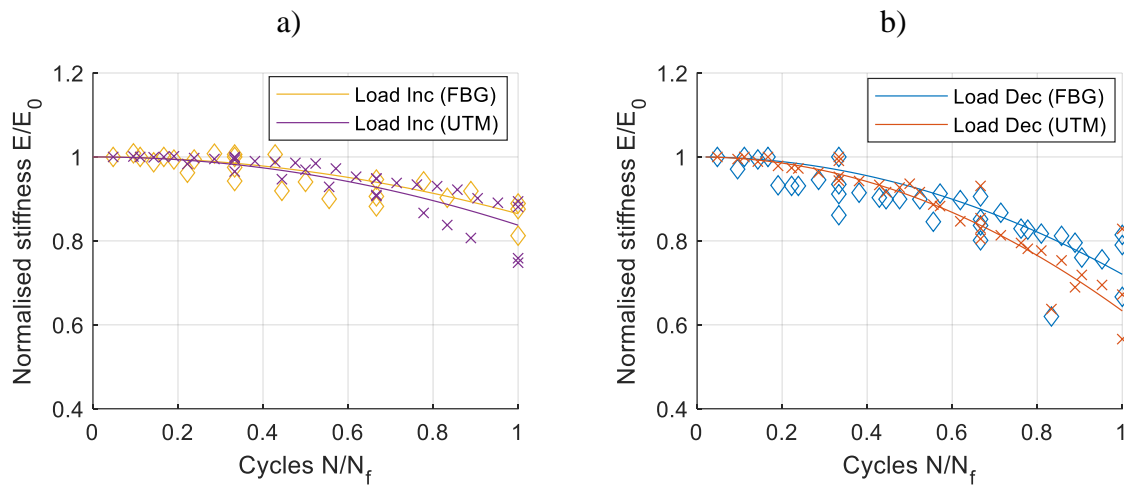


Figure 4-23: Change in stiffness relative to reference stiffness based on data from the testing machine and sensors; (a) loading the composite; (b) unloading the composite; Results labeled FBG - results from HB FBG sensors, UTM - data from the testing machine.

As fatigue progresses, a decrease in material stiffness is observed. This effect is observable with fiber optic sensors, and confirmed by readings from the testing machine. At the end of life, the stiffness for the loading half-cycle dropped by 12% and 18%, as measured by sensors and UTM data, respectively. For unloading, the drop is greater than for loading. According to HB FBG measurements, the decrease was 28%, while for UTM data it was 34%. The differences in the results may be due to the different measurement mechanism - the sensors measured local changes in the material, while the results based on crosshead displacement averaged material degradation over the entire sample.

Thus, if the damage generally occurred at a certain distance from the sensor, the stiffness degradation for a local sensor-based measurement should be smaller than for a global measurement for the specimen. This conclusion agrees with the presented results. Since the trend of decreasing stiffness was observed for both UTM and FBG results, the deadhesion was not dominating effect.

B. Area of mechanical hysteresis loop during fatigue of composite manufactured by ATL method based on data from HB FBG sensors and testing machine

One of the parameters that can be used to describe the ongoing degradation of the material during the cyclic loading process is the plastic strain energy cumulated during fatigue. Its value is calculated as the area of mechanical hysteresis loop for consecutive loading cycles of the composite.

For the present study, it is possible to determine the hysteresis loop using data from the testing machine and data from HB FBG sensors embedded inside the composite. Examples of hysteresis loops for one specimen are shown in Figure 4-20 for the data from the testing machine and in Figure 4-21 for the data from the fiber optic sensors.

To remove noise, the sensor data was filtered using a low-pass filter with a cutoff frequency above the tenth harmonic of the load frequency. Then - the filtered signal was reconstructed using the inverse fast Fourier transform (IFFT).

The hysteresis loops for the testing machine and sensor data (before and after filtering), for the long life sample (approximately $N_f=21,800$ cycles) are shown in Figure 4-24, while for the shorter life sample (approximately $N_f=9,100$ cycles) are shown in Figure 4-25.

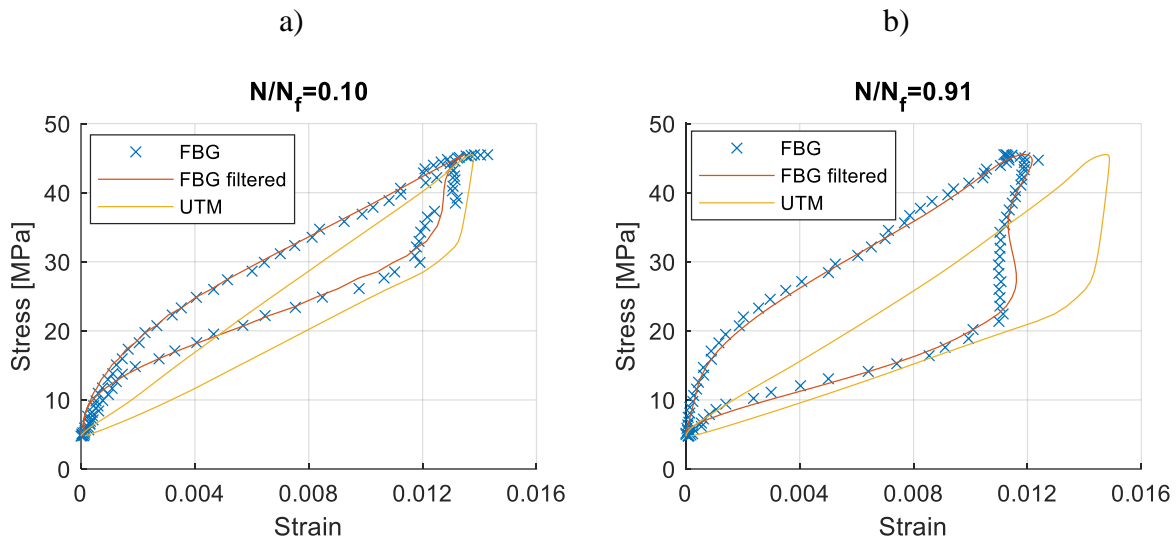


Figure 4-24: Hysteresis loops for the selected long-life specimen ($N_f=21,800$ cycles) measured by the testing machine and HB FBG sensor; a) at the beginning of the fatigue process; b) at the end of life.

In the figure, it can be observed that with the number of cycles, the amplitude of strain recorded by the sensor changes in relation to the amplitude resulting from the crosshead displacement. In the initial cycles (Figure 4-24a), the value of the amplitude from the two measurements is comparable, while at the end of life (Figure 4-24b) the HB FBG registers an amplitude that is 15% lower than the reading from the testing machine. This is most likely due to the fact that the damage did not occur at the location of the sensor, but developed near the interface between CF/PA6 tapes, which is around 10 mm away from the sensor. Deadhesion of FOS from the host material could be a factor in his changes, but since HB FBG sensors shown similar trend of stiffness degradation, degradation of the interface between the optical fiber and host material was not dominating factor.

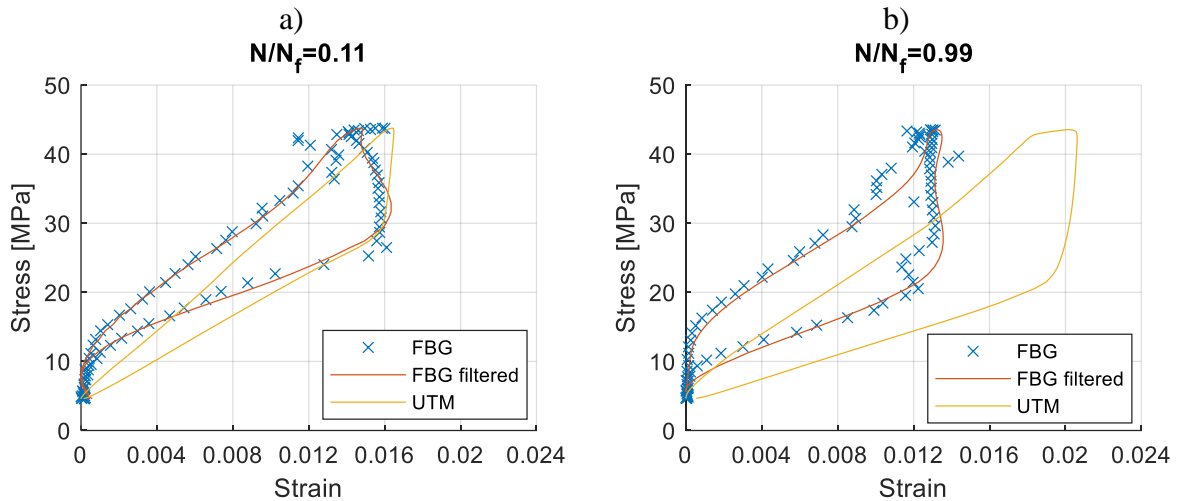


Figure 4-25: Hysteresis loops for the selected short-life specimen ($N_f=9,100$ cycles) measured by the testing machine and HB FBG sensor; a) at the beginning of the fatigue process; b) at the end of life.

It can be observed in the figure that as the number of cycles progressed, the global strain recorded by the testing machine increased, but the amplitude of the measurements from the HB FBG decreased. As in the case of the long-lived sample, an increasing difference between the strain measured with the HB FBG sensors and that calculated from the piston displacement can be observed. On the other hand, the difference in strain amplitudes is greater than that of a specimen with higher fatigue strength. In the case of the shorter fatigue life specimen, the maximum strain recorded with the HB FBG sensor was 59% of the strain calculated from the crosshead displacement, while in the case of the longer-lived specimen it was 85%.

An important parameter indicating the progression of material degradation is the area of the hysteresis loop, i.e. the energy introduced in one cycle, and its cumulation throughout the test. Figure 4-26 shows these parameters for a specimen with a high fatigue strength, while Figure 4-27 shows them for a specimen with a short fatigue life.

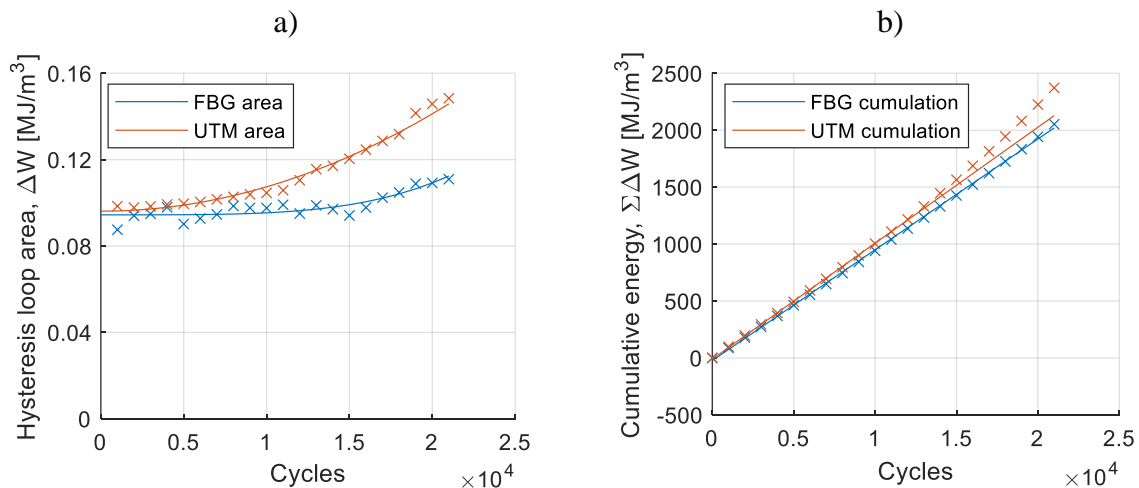


Figure 4-26: Energy (ΔW) in consecutive cycles and its cumulation ($\Sigma \Delta W$) determined using HB FBG sensors and measurement data from the testing machine; specimen with higher fatigue strength.

In Figure 4-26a it can be observed that the areas of hysteresis loops calculated from both the HB FBG sensor and the testing machine gradually increase with the number of cycles. Around 11,000 cycles, there is a significant increase in the hysteresis loop area calculated from the "global" data (for the entire sample), while a slower increase is seen for the local data, i.e. from the HB FBG. It is likely that from this point the faster defect cumulation in the material structure begins.

In the energy cumulation plot (Figure 4-26b), the cumulative energy initially grows linearly, meaning that the amount of energy introduced into the material in each cycle is approximately constant. However, from the point where the hysteresis loop area, as measured by the data from the testing machine, increases, an increase in the rate of energy accumulation in the material is observed, which deviates significantly from the regression line.

The increase in the hysteresis loop field is smaller for HB FBG sensor data than for UTM. A possible explanation for this is that the damage occurred at the interface of the tapes laid by the ATL process, which is about 10 mm from the sensor. Deadhesion could also contribute, but was not the main factor. As a result, despite the increase in loop width (as seen in Figure 4-24), the reduction in strain amplitude ultimately caused the change in hysteresis loop area to be smaller.

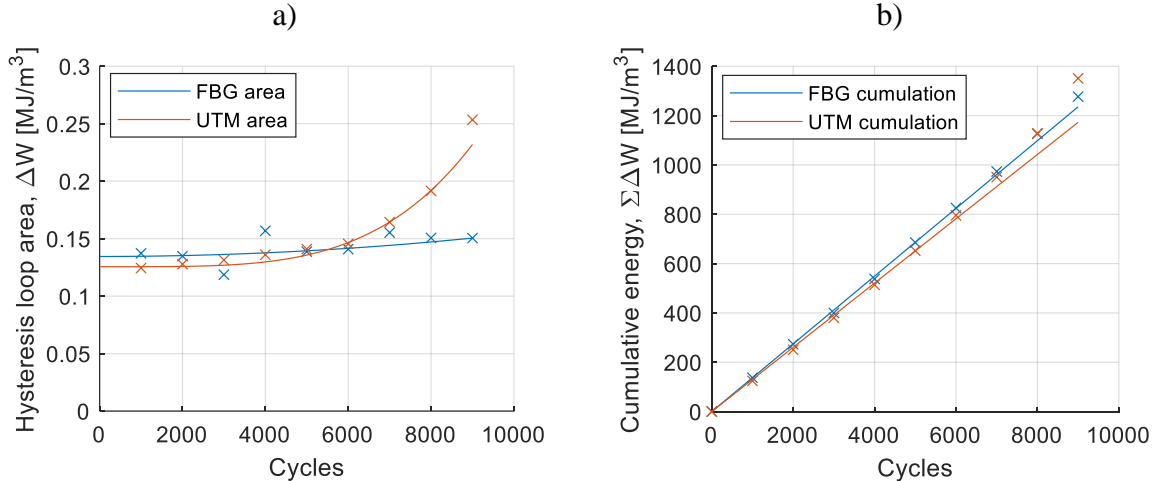


Figure 4-27: Energy (ΔW) in consecutive cycles and its cumulation ($\Sigma \Delta W$) determined using HB FBG sensors and measurement data from the testing machine; specimen with lower fatigue strength.

For a sample with a lower life ($N_f=9,100$ cycles), a similar trend can be observed as for a sample with a longer fatigue life. The area of the hysteresis loops (Figure 4-27a) was approximately constant up to 7,000 cycles, where a significant increase appeared for the UTM data. The HB FBG data does not show a similar trend. The difference is also visible in the energy cumulation plot (Figure 4-27b). The explanation for this effect is identical to that of the long-life specimen.

4.3.3. Summary of the application of HB FBG to monitor the plate produced in the ATL process in terms of quasi-static and cyclic bending

The research presented above describes the feasibility of using HB FBG sensors to monitor composite plates made by the ATL method under quasi-static and cyclic four-point bending. The main conclusions are presented below, namely:

1. HB FBG sensors embedded in an ATL thermoplastic composite were used to measure strain during a static four-point bending test. FEA was used to determine the strains occurring at the sensor location as a function of beam deflection. This approach allowed the determination of the sensitivity of the HB FBG to measure strain in the direction perpendicular to the optical fiber axis. The sensitivity for measuring strain in the plane of the specimen, in the direction perpendicular to the sensor, was studied in two arrangements of the sensor. One - in which the direction of maximum sensitivity of the sensor to the perpendicular force was in the plane of the specimen. This resulted in strain sensing sensitivity of 0.0571 pm/ $\mu\epsilon$. In the second setup, the direction of maximum sensitivity of the HB FBG to force was perpendicular to the plane of the laminate. This resulted in a strain measurement sensitivity of -0.0365 pm/ $\mu\epsilon$.
2. The HB FBG sensor, which showed higher sensitivity to in-plane strain, was used to measure strain in the process of cyclic bending of the specimen. Thus, the sensors were shown to be able to measure local strain in the fatigue of the composite.
3. In cyclic tests, the use of HB FBG sensors allowed the determination of parameters related to material degradation, namely the change in stiffness (independently in the loading and unloading half-cycles) and the mechanical hysteresis loop area and its changes as a function of cycles. It was found that, on the one hand, the HB FBG results show similar trends to the "global" results calculated from the measurement data of the testing machine. On the other hand, the HB FBG results show how much the damage process differs locally from the process "averaged" for the whole sample.

It is worth noting that the HB FBG sensors for this composite showed less sensitivity to strain than for the composite produced by the RTM method. While the highest strain sensitivity measured for the composite produced by RTM technology was 0.120 pm/ $\mu\epsilon$, for the composite manufactured by ATL technology it was to 0.0571 pm/ $\mu\epsilon$. A possible explanation is the fact that the material surrounding the FBG had higher stiffness in the composite made by RTM than by ATL. In the case of the RTM-manufactured composite, the material surrounding the FBG sensor was reinforced in two directions (reinforcing fibers were along and perpendicular to the optical fiber). The sensor integrated in the ATL process, on the other hand, was placed along the reinforcing fibers within the zone where the composite was unidirectional. The bending of this material was performed by compressing the optical fiber transversely (along its diameter). Since the stiffness of the bent composite was less than that of the sensor material, the "transfer" of strain from the material to the sensor was worse.

In summary, the possibility of using HB FBG sensors in thermoplastic composites made by the ATL method for local strain measurements in quasi-static tests and for possible monitoring of material degradation during cyclic loading was demonstrated.

4.4. SUMMARY OF THE APPLICATION OF HB FBG SENSORS FOR MONITORING A COMPOSITE MANUFACTURED BY ATL PROCESS

The conducted tests described in the above subchapter allowed to draw the following conclusions:

1. Preliminary tests with SMF FBG sensors have shown that the conditions of the ATL process, i.e. the roller compaction force and the temperature range, do not have a negative effect on the measurement properties of the SMF FBG sensors in polyimide coating. It was found that during the production of the CF/PA6 composite at the parameters used, the temperature that could be dangerous for HB FBG sensors occurred for such a short time that the sensor did not change its measurement parameters.

2. During the monitoring of the ATL process with HB FBG, the state of residual strain that built up during the application of successive layers of the composite was measured. It was observed that there is tensile strain in the plane of the composite in the direction perpendicular to the reinforcing fibers of the composite, and compressive strain in the direction perpendicular to the laminate. At the same time, it was shown that the absolute value of the measured strain in the direction perpendicular to the plane is higher than that in the plane.
3. It was shown that FBG sensors on SH2 fiber embedded in the composite manufactured by the ATL process can be used to measure strain in the direction perpendicular to the fiber, and their sensitivity is $0.0571 \text{ pm}/\mu\epsilon$ for $-0.0365 \text{ pm}/\mu\epsilon$ depending on the fiber sensor configuration. These measurements were used to calculate the residual strain cumulated during composite manufacturing.
4. In terms of fatigue monitoring, HB FBG sensors were able to record changes in material stiffness and the area of mechanical hysteresis loop, demonstrating the potential applicability for point-wise monitoring of composite structures.

It is worth mentioning that, to the author's knowledge, this is the first application of HB FBG sensors to measure strain in thermoplastic composites.

In summary, the full applicability of HB FBG sensors for monitoring the ATL process in terms of measuring residual strain, as well as for determining the complex strain state of the composite during operation, in terms of static and cyclic testing, was demonstrated.

5. CONCLUSIONS AND FUTURE PERSPECTIVES

The subject of interest, and at the same time the main objective of the dissertation, was the possibility of effective application of embedded Bragg gratings on high birefringence fiber (HB FBG) to measure strain during the manufacturing and exploitation stages of continuous fiber-reinforced composites and composite structures.

An attempt was made to apply HB FBG sensors for two selected modern composite manufacturing methods, namely resin transfer molding (RTM) and automated tape layup (ATL).

The thesis was stated that the proposed generation of HB FBG sensors will enable the monitoring of the manufacturing processes of composites with thermosetting and thermoplastic matrix, and will allow the measurement of the complex strain state inside the composite, under both quasi-static and cyclic loading conditions.

The provided results allow to conclude that the proposed generation of HB FBG sensors, the measurement systems used, the ways of implementing the sensors into the composite, the software used, the adopted method of processing optical signals and overcoming technological limitations, together made it possible to determine the local complex strain state in composites under the assumed loading conditions. Moreover, the suitability of the solution for strain measurements during both RTM and ATL manufacturing processes, as well as for the subsequent operation was confirmed.

Thus, the thesis of the work was confirmed, the main objective was achieved and the detailed tasks were accomplished

The detailed results are further discussed below. Conclusions are arranged into those related to the main objectives and theses of the dissertation, and additional issues relevant to the further development in the field of strain measurement in composites using HB FBG fiber optic sensors.

1. **Building of a measurement system with a fiber Bragg grating inscribed in side-hole highly birefringent optical fiber, including:**

- a. Obtaining a highly-birefringent optical fiber with the required parameters. Commercially available birefringent optical fiber (Fibercore HB 1500, bow-tie type) did not meet expectations in terms of the required sensitivity and was used in a further stage only for performance comparisons. Therefore, it was necessary to obtain a specialized side-hole optical fiber manufactured at the Optical Fibers Technology, Institute of Chemical Sciences, Maria Curie-Skłodowska University in Lublin. It was a highly-birefringent optical fiber with two side holes and an elliptical core. Different fabrication pressures made it possible to obtain two fibers with different geometrical characteristics and different phase birefringence. One of the fibers was chosen as particularly suitable for composite testing applications.
- b. Inscription of fiber Bragg gratings into highly-birefringent optical fibers using the phase mask technique, using custom systems of a team from the Institute of Electronic Systems, Faculty of Electronics and Information Technology, Warsaw University of Technology (WUT). By controlling the grating inscription process, high-quality gratings with equal excitation of both polarization modes were manufactured.
- c. Determination of the sensitivity of the inscribed HB FBG sensors with the developed original test stand. The test stand was calibrated using known parameters of an FBG sensor inscribed in a commercial fiber. Original software was developed to support HB FBGs sensitivity testing. Bragg wavelengths were determined (by various methods) for

both axes of the sensor (so-called fast and slow). The method of peak determination using cross-correlation was found to be particularly useful and was used in further studies, namely side-hole2 (SH2). It was shown that the sensitivity of FBG inscribed in the investigated fiber, to transverse force, was 60% higher than values known from the literature for other HB FBG sensors.

As a result, the full suitability of the measurement system with the original FBG sensor to measure strain while loading the sensor along its length and across its diameter was demonstrated.

2. Application of HB FBG fiber optic sensors for monitoring of the kinetics of composites manufacturing process by RTM technology and testing of composites under bending conditions, including:

- a. Investigation of the effect of compression occurring in the mold on the sensor embedded in the reinforcing fibers and evaluation of the possible degradation of the reflection spectrum. The study showed that there is no negative effect on the HB FBG sensors used during compression of the sensor with fabrics in which the reinforcing fibers of at least one of the reinforcing layers adjacent to the sensor are aligned in the same direction as the optical fiber. In contrast, a different orientation of the optical fiber with respect to the reinforcing fibers can lead to a degradation of the measurement properties of the fiber Bragg grating as a result of micro-bending, but not induced birefringence.
- b. Investigation of composite curing kinetics in the RTM process, including gel point identification and strain changes due to the resin curing process. It was shown that SH2 FBG sensors can be integrated into the composite in the RTM process and used for process monitoring. The research solved the problem of integrating the sensors with the fabrics and embedding them in the composite. Gel point determination results were obtained by measuring strain in the direction perpendicular to the plane of the laminate and validated with results from DC sensors. It was shown that after the gel point occurs, a continuous monotonic trend in the change of the separation of the Bragg peaks is visible, indicating the build-up of transverse strains. The HB FBG transverse strain measurement method is almost independent of temperature and has an advantage over the use of a standard SMF FBG fiber optic sensor, which requires the use of an additional temperature sensor to compensate for temperature effects.
- c. Measurement of triaxial strain field in a plate element manufactured by RTM technology and subjected to four-point bending. It has been shown that HB-FBG sensors allow measurement of the multi-axial strain field. The sensitivity of strain measurement in the direction perpendicular to the fiber was $0.120 \text{ pm}/\mu\epsilon$ for the system when the sensor was in the arrangement which showed the highest sensitivity to the force was in the plane of the plate, and $-0.105 \text{ pm}/\mu\epsilon$ for the system with the sensor whose highest sensitivity was in the direction perpendicular to the laminate, respectively. These values imply a strain resolution of $8.33 \mu\epsilon$ and $9.52 \mu\epsilon$, respectively, assuming the typical resolution of available interrogators, i.e., 1 pm. The response of the sensors to the same strain in both arrangements gives different slow and fast peak shifts, thus the HB FBG two-sensor system can be used to measure strain in three directions, i.e., two directions in the plane of the plate and in the direction perpendicular to the laminate.

As a result, the full suitability of HB FBG sensors for monitoring the RTM process in terms of gel point detection and residual strain measurement, as well as measurement of composite complex strain during its operation was demonstrated. Moreover, their significant advantage over typical SMF FBG sensors was documented.

To the author's knowledge, this research is the first documented example of the use of birefringent sensors to study a closed-mold process (in this case, RTM t is also believed to be the first time that the embedded HB FBG sensor has been used for the first time to measure the composite's complex deformation state in bending tests. In addition, the research conducted is one of the few in the field of HB FBG application for monitoring the manufacturing process of thermoset composites and measuring their deformation in the exploitation stage.

3. Application of HB FBG sensors for monitoring the composite manufactured by the ATL process, including:

- a. Preliminary tests were carried out with SMF FBG sensors, which showed that roller compaction and temperature conditions do not negatively affect the measuring properties of FBG sensors.
- b. The residual strain state built up during the laying of successive composite layers using the ATL process was measured. It was observed that in the plane of the composite there is tensile strain in the direction perpendicular to the reinforcing fibers of the composite and compressive strain in the direction perpendicular to the plane. The absolute value of the measured strains in the direction perpendicular to the plane is higher than that in the plane.
- c. It was shown that FBG sensors on SH2 fiber embedded in the composite produced by the ATL process can be used to measure strains in the direction perpendicular to the fiber, with sensitivities ranging from 0.0571 pm/ $\mu\epsilon$ to -0.0365 pm/ $\mu\epsilon$, depending on the fiber optic sensor configuration. These measurements were used to calculate the residual strain cumulated during composite production.
- d. Measurement of strain under cyclic loads showed that HB FBG sensors can record changes in material stiffness and the area of mechanical hysteresis loop, which allows to examine the local fatigue process of composite structures.

As a result, the full suitability of SH2 HB FBG sensors for monitoring the ATL process in terms of measuring residual strain, as well as measuring the composite's complex state of strain during service, in terms of static and cyclic testing, was demonstrated.

In addition, to the author's knowledge, this is the first example of the application of HB FBG sensors to measure strain in thermoplastic fiber-reinforced polymers.

4. **Scientific output**, including those related to the dissertation, has been published in 14 documents, including 10 journal articles, 3 conference proceedings and 1 abstract in abstract books, of which the doctoral student is the author or co-author. The total Impact Factor of the published works is currently 21.559. Another article for the journal with the working title " Monitoring of composite manufactured with automated tape layup process with fiber Bragg grating inscribed in side-hole fiber with an elliptical core" is currently being prepared.

5. Financial support

The main costs of the works were covered by two sources, namely:

- a. Main project: InterDok – Interdisciplinary Doctoral Studies Projects at Wroclaw University of Science and Technology, project no, POWR.03.02.00-00-I003/16, co-financed by the European Union under the European Social Fund.
- b. Mobility project: Mobility program financed by the Polish National Agency for Academic Exchange (NAWA, project no. PPN/BIL/2018/1/00058) and Austria's Agency for Education and Internationalisation (OeAD, No. PL 05/2019).

5.1. FUTURE PERSPECTIVES

Suggested below are selected issues to be addressed in future work, which are a consequence of the results acquired and the literature review.

1. Study of the interaction between the sensor and the host material

The results presented in the thesis show that one of the factors influencing the ability of the sensor to measure transverse strain is the material in which it is embedded. The same sensor embedded in a lower stiffness composite had a lower sensitivity compared to one embedded in a material with higher stiffness. Currently, before the sensor is embedded, it is not known what the approximate sensitivity will be in the final structure. Modeling such interactions is a complex problem (the optical response of the sensor to a given strain in a core, and furthermore, what strain will occur in the sensor core itself depending on the strain of the surrounding material). This issue has only been addressed in one paper [19], which analyzed the case of one type of sensor embedded in one material.

The research can be focused on analyzing changes in the sensitivity of a given type of optical fiber and sensor, for materials with different stiffness. The same way - to determine the measurement capability for several different sensors in the same material. So far, HB FBG sensors shown in literature have been used to measure strain in various composite materials, which makes it difficult to compare them.

It should be noted that using the HB FBG with the highest sensitivity is not always the best solution. In the case of HB FBG sensors, the measurement range is limited by the separation of the Bragg peaks. If the strain in the material causes the peaks to merge, further separation will be zero, making strain measurement with conventional interrogators impossible. In this case, the dependence of sensor sensitivity on material stiffness may provide a solution. A material with low stiffness will have worse strain transfer to the sensor, and therefore the sensitivity to strain measurement will be lower. Thus, the same sensor with a given measurement range (in terms of optical signals) will allow the measurement of larger strains.

2. The angular orientation of HB FBG sensor during integrating into composite

Due to the dependence of the strain sensitivity on the angular orientation of the sensor, HB FBG sensors require more complex preparation for integration into a composite than typical fiber Bragg gratings. For this reason, their wider application may be limited.

One of the aspects addressed in this dissertation was the acceleration of the angular orientation of the sensor. A system based on a diffraction image to orient the sensor has been proposed, which allows to reduce the time for orienting the optical fiber from one hour (for the mechanical method) to a few minutes for the diffraction method.

However, the integration of the pre-oriented sensor into the composite in the correct orientation remains an open question. Applying droplets of glue or epoxy on both sides of the FBG during calibration to maintain the rotation angle, as suggested in [149], is one method of maintaining orientation, but integrating the sensor into a patch could make integration even easier. An idea of how to achieve this can be seen in the work of a team from Milan [185,186], where fiber optic sensors were integrated into a so-called smart veil, i.e. a polyurethane patch cast in a mold made by 3D printing. This patch allowed the pre-positioning of sensors in the patch, which should also be used to preserve the angular orientation of HB FBG sensors.

3. Testing the applicability of HB FBG sensors to other composite manufacturing techniques

The use of HB FBG sensors has only been demonstrated for a few manufacturing processes. However, there are still many technologies for which these types of sensors have not yet been applied. For example, winding or braiding.

In addition, this dissertation describes the possibility of applying the HB FBG sensors to thermoplastic materials, which opens up the possibility of monitoring a whole new group of composites with them. Thermoplastic matrix composites are an important segment of the composites market due to their ease of recycling and flexibility in manufacturing, e.g. the possibility of automated application of successive composite layers. The research presented here, using the ATL process, has shown that the process conditions (the high temperature occurring for a very short time) do not damage the HB FBG sensors, and the sensors can be used to measure strain after the process for further monitoring of the structure in the operational phase.

4. Usage of HB FBG sensors to measure strain in composite structures

There is probably only one example in the literature where HB FBG sensors have been used to monitor a composite structure. In [23], bow-tie sensors were integrated into an aerospace component to measure strain. All others are for materials testing. Sensors have not been used on a larger scale than individual specimens.

5. Optimization of sensor designs for applications in composites

Numerous microstructured sensor designs have been tested for their ability to measure pressure [5-11], but the strain state of the sensor after integration into the material is different. For this reason, it would be reasonable to develop models in which the sensor is integrated into the material and subjected to strain.

Coating the sensor is also an important consideration. At the moment, all HB FBGs were used as "bare fiber", meaning they do not have any coating to increase their resistance to mechanical damage. This definitely increases their fragility and complicates proper integration. For this reason, it would be an important step to analyze the impact of the layer coating the optical fiber on its measurement capabilities.

LIST OF FIGURES

Figure 1-1: An optical fiber, a) Basic cross section [3], b) working principle (based on [27]).	3
Figure 1-2: A classification of optical fiber sensors by sensing method used for the SHM (based on [2]).	3
Figure 1-3: A diagram of different interferometric optical fiber types; a) Fabry-Perot, b) Mach-Zehnder, c) Michelson, d) Sagnac [29,30].	4
Figure 1-4: A FPI formed in fiber, a) Microscopic view; b) Wavelength shift of the interferometric fringe around 1550 nm to strain [33].	5
Figure 1-5: A Mach-Zehnder interferometer formed with a sections of SMF and four-core-fiber; a) schematic build; b) Response of interferometric fringe to axial strain [40].	7
Figure 1-6: Setup of the SOFO system [45].	8
Figure 1-7: Fiber grating types, a) standard, b) chirped, c) birefringent, d) tilted, and exemplary reflection spectra [50].	9
Figure 1-8: Comparison of refractive index variations along the a) regular FBG; b) A chirped [54].	10
Figure 1-9: Light scattering spectrum in optical fiber [4].	11
Figure 1-10: A diagram of Optical Backscatter Reflectometry [64].	12
Figure 1-11: Scheme of a Fresnel refractometer applied for measurement of resin refractive index variations [91].	15
Figure 1-12: An application of FBGs along with thermocouple to measure the curing of neat resin; a) location of FBG sensors, b) identified stages of the process: A – start of the cure, B – gelation, C – curing, D – end of curing, E – sample cooled down, F - oven shut off, G – room temperature reached [97].	16
Figure 1-13: Through thickness measurement of strain during the curing the process; a) Scheme of a sample, b) Sample with an inserted FBG [99].	17
Figure 1-14: Spectra of FBG sensors inscribed in highly-birefringent and single-mode fibers changed by the transversal shrinking of the composite laminate.	17
Figure 1-15: The microstructured FBG used for the autoclave process monitoring; a) The microstructured optical fiber cross-section, b) peak separation changes due to curing stages [102].	18
Figure 1-16: View of the tail cone of a commercial aircraft monitored with FBG sensors; a) Scheme with localization of sensors, b) View of the composite cone during the production [23].	21
Figure 1-17: The Airbus A380 hinge arm; a) Concept diagram with shown sensors locations, b) Manufactured part [95].	21
Figure 1-18: A composite drag strut monitored with FBG sensors, a) FEA model with sensors locations, b) The drag strut in the testing machine [122].	22
Figure 1-19: Composite wind turbine blade with FOS; a) Locations of sensors, b) View of the loaded blade [4].	22

Figure 1-20: A composite pressure vessel with attached FBG sensors for detection of artificial defects in the vessel. Surface of the vessel is sprayed with a pattern for DIC strain analysis [108].	23
Figure 1-21: A text viewed through the birefringent crystal (calcite) [125].	24
Figure 1-22: Cross-sections of highly-birefringent optical fibers [27].	24
Figure 1-23: Cross-sections of highly-birefringent microstructured optical fibers used for pressure and strain sensing; a) With two rows of holes, [130], b) With triangular sections with air channels (Butterfly) [131] ; c) With two big holes on both side of the core (Side-hole) [128].	25
Figure 1-24: Fiber Bragg grating's operation principle [2].	26
Figure 1-25: A coordinate system of a highly-birefringent optical fiber.	27
Figure 1-26: Stress distribution calculated with FEA of the dual side-hole fiber (DSHF) under transversal load applied along: (a, b) slow axis, and (c, d) fast axis. Diagrams present distribution of stress in (a, c) y direction and (b, d) z direction [136].	29
Figure 1-27: Concept of the mechanical testing rig for an HB FBG; a) testing scheme; b) An exemplary spectrum change due to transversal loading.	30
Figure 1-28: A sensitivity dependency of a bow-tie fiber to the transversal load applied at varying load to the optical fiber [59].	30
Figure 1-29: HB FBG integrated into the neat resin; a) Geometry of the specimen with FBG, b) Specimen in loading fixture for bi-axial loading tests [60].	31
Figure 1-30: An epoxy roller with an integrated compressed FBG on the testing machine [142].	32
Figure 1-31: Placement of MOF FBGs in a form of 3D strain sensor [19].	33
Figure 1-32: Single lap joint monitored with MOF FBGs in shear-sensitive measurement orientation [20].	33
Figure 2-1: SEM image of side-hole 2 optical fiber, a) An entire fiber's cross-section, b) Zoom of a glass bridge between holes with visible fiber's elliptical core [128].	37
Figure 2-2: An exemplary transmission spectrum of fiber Bragg gratings written in SH2 optical fiber [128].	38
Figure 2-3: Mechanical test stand based on the lever-design [133].	39
Figure 2-4: Mechanical testing rig design, using the rotating screw to load fibers [59].	39
Figure 2-5: The testing design directly loading optical fibers [133].	40
Figure 2-6: The fixture used to measure sensitivity of HB FBGs in a universal testing machine [149].	40
Figure 2-7: Testing device used for the mechanical testing of the HB optical fibers with in-written FBG [128].	41
Figure 2-8: Procedure for the determination of the mechanical properties of HB FBG.	42
Figure 2-9: Scheme of measurement results flow.	43
Figure 2-10: Determination of sensitivities of HB loaded in some angular orientation.	44

Figure 2-11: Transverse sensitivity of HB15000 fiber to the transversal load for varying fiber orientation [128].	46
Figure 2-12: The transversal force sensitivity curves for fibers: a) Side-hole 1 (SH1) b) Side-hole 2 (SH2).	47
Figure 2-13: Determination of the PANDA fiber orientation based on the stripes widths [157].	49
Figure 2-14: Scheme of testing setup, a) top view, b) side view.	50
Figure 2-15: A diffraction pattern from the side-hole fiber when illuminated with a laser diode. a) along the fast axis; b) along the slow axis; c) not perfectly aligned with slow axis.	51
Figure 3-1: Scheme of the resin transfer molding (RTM) process [160].	53
Figure 3-2: Testing of FBG sensors compressed indirectly through various materials.	55
Figure 3-3: Spectrum of SH-1 FBG, under uniform load applied through a paper sheet	56
Figure 3-4: Spectra shape when FBG is loaded through the textile aligned at various angles to the optical fiber.	56
Figure 3-5: Reflection spectra for various angles θ at the same load level ($F=200N$).	57
Figure 3-6: Testing machine adapted for compaction of textiles.	58
Figure 3-7: Scheme of measurement of transmission signal strength reduction caused by microbending.	58
Figure 3-8: Fixture for compaction tests with optical fibers.	59
Figure 3-9: Optical fibers fixed on the compaction testing machine.	59
Figure 3-10: Explanation of the notation used for compression stack description.	60
Figure 3-11: Signal to noise ratio (SNR) in the signal transmitted through the optical fiber during the compression of the stack.	61
Figure 3-12: SNR vs. FVF in compaction test of NCF textile with a stripped optical fiber.	61
Figure 3-13: The arrangement of FBG sensors in the compaction zone.	63
Figure 3-14: Exemplary optical spectra of full-loaded optical fibers when FBG sensor was: a) Parallel to the reinforcing fibers above and below; b) Parallel to the reinforcing fibers below FBG.	63
Figure 3-15: Peak separation of FBG inscribed in loaded optical fiber.	64
Figure 3-16: A cup with poured resin during the curing with location of sensors.	66
Figure 3-17: Monitoring of epoxy resin (RIMR135+RIMH1366) curing with FBG sensor in room temperature.	66
Figure 3-18: Monitoring of epoxy resin (RIMR135+RIMH1366) curing and post-curing with FBG sensor.	67
Figure 3-19: View of a cavity of mold without preform.	69
Figure 3-20: Integration of FBG sensors into the mold; a) Top view of the mold with preform.	69
Figure 3-21: Method of integration of FBG into the mold – side view.	70
Figure 3-22: FBG sensors placement along with in-mold sensors [168].	71

Figure 3-23: Strain during the curing process measured with SMF FBG sensors; (1) – clamping of inlet hose, (2) – gel point estimated with DC sensor [168].	71
Figure 3-24: Peak shifts and separation variation observed with FBG inscribed in side-hole 2 fiber in the case when highest sensitivity was out-of-plane (slow-axis out-of-plane); (1) – gel point calculated from DC sensor’s data ; (2) – deadhesion of a plate from the mold [168]. ...	72
Figure 3-25: Through-thickness strain during the RTM process [168].	73
Figure 3-26: a) View of the vicinity of SH2 FBG; b) Reflection spectra of a HB FBG sensor at: the beginning of the curing, after the curing and after cooling down [168].	74
Figure 3-27: Pressure and peak separation during the RTM process.	74
Figure 3-28: A possible behavior of pressure sensors during plate’s detachment due to through-thickness shrinking.	75
Figure 3-29: Wavelength shifts and separation changes during the RTM process, when highest transversal sensitivity of SH2 fiber was in in-plane direction (slow-axis in-plane of laminate).	75
Figure 3-30: Scheme of an FBG sensor subjected to the four-point-bending, a) transversal to the optical fiber, b) along the optical fiber [128].	78
Figure 3-31: An arrangement of samples with FBG sensors cut from the plate manufactured in RTM process.	79
Figure 3-32: Response of SH2 FBG in four-point bending: a) Bragg wavelengths shifts; b) Peak separation; in the case the load is applied along the optical fiber and slow-axis is in-plane of composite [128].	80
Figure 3-33: Response of SH2 FBG in four-point bending: a) Bragg wavelengths shifts; b) Peak separation; the load is applied transversally to the optical fiber and slow-axis is in-plane of composite [128].	80
Figure 3-34: Response of SH2 FBG in four-point bending: a) Bragg wavelengths shifts, (b) Peak separation; the load is applied along the optical fiber and slow-axis is out-of-plane of composite.	81
Figure 3-35: Response of SH2 FBG in four-point bending: a) Bragg wavelengths shifts, b) Peak separation; the load is applied transversally to the optical fiber and slow-axis is out-of-plane of composite.	82
Figure 4-1: Scheme of ATL process.	86
Figure 4-2: ATL test stand used in study.	87
Figure 4-3: FBG sensors attached to the CF/PP tape for the force influence testing.	88
Figure 4-4: Optical spectra of selected FBG during the passage of the roller.	88
Figure 4-5: Process scheme to measure the residual strain along with temperature using the FBG (based on [73]).	90
Figure 4-6: Determination of sensitivities of FBG sensors embedded into composite samples, left – exemplary results, right – sample on the testing machine [73].	91
Figure 4-7: Maximum temperature during the tests for various tool temperatures [73].	92
Figure 4-8: Results of in-line consolidation monitoring; a) Temperature readings decoded from fiber optic sensors, validated with readings from thermocouples, b) Temperature and strain readings during the consolidation of a selected layer [73].	93

Figure 4-9: Residual strain along with increasing number of layers of composite.....	93
Figure 4-10: Dependency of residual stress calculated as a function of tool temperature.....	94
Figure 4-11: Configuration of HB FBG sensors used for multiaxial strain measurement during the ATL process.	95
Figure 4-12: View of FBGs attached to the two bottom layers for the FBG sensors integration.	96
Figure 4-13: Residual in-plane and out-of-plane strain measured from transversal response of HB FBG sensors.....	97
Figure 4-14: Samples used for mechanical testing cut from the manufactured plate, a) Cutting scheme; b) A single sample.....	98
Figure 4-15: Arrangement for mechanical testing of specimens produced by ATL; a) Scheme of loading; b) View of the specimen on the testing machine.	99
Figure 4-16: Through-thickness distribution of calculated: a) Stress σ_{xx} caused by 100N load, b) Strain ϵ_{xx} caused by 1 mm of displacement.	100
Figure 4-17: Response of the FBG sensors to the transversal load applied to the FBG sensor, which main sensing direction was in-plane of the composite.....	101
Figure 4-18: Response of the FBG sensors to the transversal load applied to the FBG sensor, which main sensing direction was out-of-plane of the composite.	101
Figure 4-19: A schematic representation of the force versus time curve during cyclic loading of composite plates with embedded HB FBG sensors manufactured using the ATL process. ..	103
Figure 4-20: Hysteresis loops during fatigue of the specimen based on the data from the testing machine, a) with visible creep; b) after compensation of creep, with the stiffness difference visible in both cases for loading and unloading	103
Figure 4-21: Hysteresis loops for an example specimen with strain measured with HB FBG sensors	104
Figure 4-22: An image of a sample after cyclic testing; a) Top view; b) Side view.....	105
Figure 4-23: Change in stiffness relative to reference stiffness based on data from the testing machine and sensors; (a) loading the composite; (b) unloading the composite; Results labeled FBG - results from HB FBG sensors, UTM - data from the testing machine.....	106
Figure 4-24: Hysteresis loops for the selected long-life specimen ($N_f=21,800$ cycles) measured by the testing machine and HB FBG sensor; a) at the beginning of the fatigue process; b) at the end of life.	107
Figure 4-25: Hysteresis loops for the selected short-life specimen ($N_f=9,100$ cycles) measured by the testing machine and HB FBG sensor; a) at the beginning of the fatigue process; b) at the end of life.	108
Figure 4-26: Energy (ΔW) in consecutive cycles and its cumulation ($\Sigma \Delta W$) determined using HB FBG sensors and measurement data from the testing machine; specimen with higher fatigue strength.	108
Figure 4-27: Energy (ΔW) in consecutive cycles and its cumulation ($\Sigma \Delta W$) determined using HB FBG sensors and measurement data from the testing machine; specimen with lower fatigue strength.	109

LIST OF TABLES

Table 2-1: Geometrical features of the side-hole fibers [128].	37
Table 2-2: Peak separation and effective sensitivity to the transversal load [128].	48
Table 3-1: Stacking sequence of tested stacks with optical fibers.	60
Table 3-2: Fiber volume fraction resulting in -6dB drop in SNR.	62
Table 3-3: Strain sensitivities of a side-hole 2 FBG integrated into the composite in the case when axis is in-plane of composite [128].	81
Table 3-4: Strain sensitivities of a side-hole 2 FBG integrated into the composite in the case when axis is out-of-plane of composite.	82
Table 4-1: Sensitivity of the sensors to the axial strain and to the changes in temperature [73].	92
Table 4-2: Sensitivity of the FBG sensors to the transversal strain.	102

REFERENCES

1. Abbas, S.; Li, F.; Qiu, J. A Review on SHM Techniques and Current Challenges for Characteristic Investigation of Damage in Composite Material Components of Aviation Industry. *Mater. Perform. Charact.* **2018**, *7*, 20170167, doi:10.1520/mpc20170167.
2. Di Sante, R. Fibre optic sensors for structural health monitoring of aircraft composite structures: Recent advances and applications. *Sensors (Switzerland)* **2015**, *15*, 18666–18713, doi:10.3390/s150818666.
3. Rocha, H.; Semprimoschnig, C.; Nunes, J.P. Sensors for process and structural health monitoring of aerospace composites: A review. *Eng. Struct.* **2021**, *237*, doi:10.1016/j.engstruct.2021.112231.
4. Sierra-Pérez, J.; Torres-Arredondo, M.A.; Güemes, A. Damage and nonlinearities detection in wind turbine blades based on strain field pattern recognition. FBGs, OBR and strain gauges comparison. *Compos. Struct.* **2016**, *135*, 156–166, doi:10.1016/j.compstruct.2015.08.137.
5. Gąsior, P.; Rybczyński, R.; Kaleta, J.; Villalonga, S.; Nony, F.; Magnier, C.; Gąsior, P.; Rybczynski, R.; Kaleta, J.; Villalonga, S.; et al. High pressure composite vessel with integrated optical fiber sensors. Monitoring of manufacturing process and operation. *Am. Soc. Mech. Eng. Press. Vessel. Pip. Div. PVP* **2018**, *5*, doi:10.1115/PVP2018-85157.
6. Giurgiutiu, V. Introduction. In *Structural Health Monitoring of Aerospace Composites*; Elsevier, 2015; pp. 1–23 ISBN 9780124096059.
7. Konstantopoulos, S.; Fauster, E.; Schledjewski, R. Monitoring the production of FRP composites: A review of in-line sensing methods. *Express Polym. Lett.* **2014**, *8*, 823–840, doi:10.3144/expresspolymlett.2014.84.
8. Kinet, D.; Mégret, P.; Goossen, K.W.; Qiu, L.; Heider, D.; Caucheteur, C. Fiber Bragg grating sensors toward structural health monitoring in composite materials: Challenges and solutions. *Sensors (Switzerland)* **2014**, *14*, 7394–7419, doi:10.3390/s140407394.
9. Blöbl, Y.; Hegedüs, G.; Szebényi, G.; Tábi, T.; Schledjewski, R.; Czigany, T. Applicability of fiber Bragg grating sensors for cure monitoring in resin transfer molding processes. *J. Reinf. Plast. Compos.* **2021**, *40*, 701–713, doi:10.1177/0731684420958111.
10. Szebényi, G.; Blöbl, Y.; Hegedüs, G.; Tábi, T.; Czigany, T.; Schledjewski, R. Fatigue monitoring of flax fibre reinforced epoxy composites using integrated fibre-optical FBG sensors. *Compos. Sci. Technol.* **2020**, *199*, 108317, doi:10.1016/j.compscitech.2020.108317.
11. Qing, X.; Li, W.; Wang, Y.; Sun, H. Piezoelectric Transducer-Based Structural Health. *Sensors (Switzerland)* **2019**, *19*, 1–27, doi:10.3390/s19030545.
12. Jiao, P.; Egbe, K.I.; Xie, Y.; Matin Nazar, A.; Alavi, A.H. Piezoelectric Sensing Techniques in Structural Health Monitoring: A State-of-the-Art Review. *Sensors* **2020**, *20*, 3730, doi:10.3390/s20133730.
13. Qing, X.P.; Beard, S.J.; Kumar, A.; Li, I.; Lin, M.; Chang, F. Stanford Multiactuator-Receiver Transduction (SMART) Layer Technology and Its Applications. In *Encyclopedia of Structural Health Monitoring*; Boller, C., Chang, F.-K., Fujino, Y., Eds.; John Wiley & Son, 2009 ISBN 978-0-470-05822-0.

14. Boztepe, S.; Liu, H.; Heider, D.; Thostenson, E.T. Novel carbon nanotube interlaminar film sensors for carbon fiber composites under uniaxial fatigue loading. *Compos. Struct.* **2018**, doi:10.1016/j.compstruct.2018.01.033.
15. Klein, L. Sensor Systems for FRP Lightweight Structures: Automotive Features Based on Serial Sensor Products. *Sensors* **2019**, *19*, 3088, doi:10.3390/s19143088.
16. Wang, G.; Wang, Y.; Zhang, P.; Zhai, Y.; Luo, Y.; Li, L.; Luo, S. Structure dependent properties of carbon nanomaterials enabled fiber sensors for in situ monitoring of composites. *Compos. Struct.* **2018**, doi:10.1016/j.compstruct.2018.04.052.
17. Soman, R.; Wee, J.; Peters, K. Optical Fiber Sensors for Ultrasonic Structural Health Monitoring: A Review. *Sensors* **2021**, *21*, 7345, doi:10.3390/s21217345.
18. Kang, I.; Schulz, M.J.; Kim, J.H.; Shanov, V.; Shi, D. A carbon nanotube strain sensor for structural health monitoring. *Smart Mater. Struct.* **2006**, *15*, 737–748, doi:10.1088/0964-1726/15/3/009.
19. Sonnenfeld, C.; Luyckx, G.; Sulejmani, S.; Geernaert, T.; Eve, S.; Gomina, M.; Chah, K.; Mergo, P.; Urbanczyk, W.; Thienpont, H.; et al. Microstructured optical fiber Bragg grating as an internal three-dimensional strain sensor for composite laminates. *Smart Mater. Struct.* **2015**, *24*, 055003, doi:10.1088/0964-1726/24/5/055003.
20. Sulejmani, S.; Sonnenfeld, C.; Geernaert, T.; Luyckx, G.; Mergo, P.; Urbanczyk, W.; Chah, K.; Thienpont, H.; Berghmans, F. Disbond monitoring in adhesive joints using shear stress optical fiber sensors. *Smart Mater. Struct.* **2014**, *23*, doi:10.1088/0964-1726/23/7/075006.
21. Geernaert, T.; Luyckx, G.; Voet, E.; Nasilowski, T.; Chah, K.; Becker, M.; Bartelt, H.; Urbanczyk, W.; Wojcik, J.; De Waele, W.; et al. Transversal load sensing with fiber Bragg gratings in microstructured optical fibers. *IEEE Photonics Technol. Lett.* **2009**, *21*, 6–8, doi:10.1109/LPT.2008.2007915.
22. Luyckx, G.; De Waele, W.; Degrieck, J.; Van Paepegem, W.; Vlekken, J.; Vandamme, S.; Chah, K. Three-dimensional strain and temperature monitoring of composite laminates. *Insight Non-Destructive Test. Cond. Monit.* **2007**, *49*, 10–16, doi:10.1784/insi.2007.49.1.10.
23. Chehura, E.; James, S.W.; Staines, S.; Groenendijk, C.; Cartie, D.; Portet, S.; Hugon, M.; Tatam, R.P. Production process monitoring and post-production strain measurement on a full-size carbon-fibre composite aircraft tail cone assembly using embedded optical fibre sensors. *Meas. Sci. Technol.* **2020**, *31*, doi:10.1088/1361-6501/ab8a7b.
24. Güemes, J.A.; Sierra-Pérez, J. Fiber Optics Sensors. In *New Trends in Structural Health Monitoring*; Ostachowicz, W., Güemes, J.A., Eds.; Springer Vienna: Vienna, 2013; pp. 265–316 ISBN 978-3-7091-1390-5.
25. Udd, E.; Spillman, W.B. *Fiber Optic Sensors*; Udd, E., Spillman, W.B., Eds.; John Wiley & Sons, Inc.: Hoboken, NJ, USA, 2011; ISBN 9781118014103.
26. Peters, K. Polymer optical fiber sensors - A review. *Smart Mater. Struct.* **2011**, *20*, doi:10.1088/0964-1726/20/1/013002.
27. Thévenaz, L. *Advanced Fiber Optics*; Thévenaz, L., Ed.; 1st ed.; EPFL Press: Lousanne, 2011; ISBN 9781482247039.

28. Shivakumar, K.; Emmanwori, L. Mechanics of Failure of Composite Laminates with an Embedded Fiber Optic Sensor. *J. Compos. Mater.* **2004**, *38*, 669–680, doi:10.1177/0021998304042393.
29. Lee, B.H.; Kim, Y.H.; Park, K.S.; Eom, J.B.; Kim, M.J.; Rho, B.S.; Choi, H.Y. Interferometric fiber optic sensors. *Sensors* **2012**, *12*, 2467–2486, doi:10.3390/s120302467.
30. Montazerian, H.; Rashidi, A.; Milani, A.S.; Hoorfar, M. Integrated Sensors in Advanced Composites: A Critical Review. *Crit. Rev. Solid State Mater. Sci.* **2019**, *0*, 1–52, doi:10.1080/10408436.2019.1588705.
31. Leng, J.; Asundi, A. Structural health monitoring of smart composite materials by using EFPI and FBG sensors. *Sensors Actuators, A Phys.* **2003**, *103*, 330–340, doi:10.1016/S0924-4247(02)00429-6.
32. Miliou, A. In-Fiber Interferometric-Based Sensors: Overview and Recent Advances. *Photonics* **2021**, *8*, 265, doi:10.3390/photonics8070265.
33. Liu, S.; Yang, K.; Wang, Y.; Qu, J.; Liao, C.; He, J.; Li, Z.; Yin, G.; Sun, B.; Zhou, J.; et al. High-sensitivity strain sensor based on in-fiber rectangular air bubble. *Sci. Rep.* **2015**, *5*, 1–7, doi:10.1038/srep07624.
34. Chen, K.; Yang, B.; Deng, H.; Guo, M.; Zhang, B.; Yang, Y.; Liu, S.; Zhao, Y.; Peng, W.; Yu, Q. Simultaneous measurement of acoustic pressure and temperature using a Fabry-Perot interferometric fiber-optic cantilever sensor. *Opt. Express* **2020**, *28*, 15050, doi:10.1364/oe.387195.
35. Lim, J.H.; Jang, H.S.; Lee, K.S.; Kim, J.C.; Lee, B.H. Mach–Zehnder interferometer formed in a photonic crystal fiber based on a pair of long-period fiber gratings. *Opt. Lett.* **2004**, *29*, 346, doi:10.1364/ol.29.000346.
36. Shao, M.; Qiao, X.; Fu, H.; Liu, Y.; Zhao, X.; Yao, N. High sensitivity refractive index sensing of Mach-Zehnder interferometer based on multimode fiber core sandwiched between two waist-enlarged fiber tapers. *Opt. Commun.* **2013**, *311*, 359–363, doi:10.1016/j.optcom.2013.08.090.
37. Kim, M.J.; Kim, Y.H.; Mudhana, G.; Lee, B.H. Simultaneous measurement of temperature and strain based on double cladding fiber interferometer assisted by fiber grating pair. *IEEE Photonics Technol. Lett.* **2008**, *20*, 1290–1292, doi:10.1109/LPT.2008.926889.
38. Kowal, D.; Urbanczyk, W.; Mergo, P. Twin-Core Fiber-Based Mach Zehnder Interferometer for Simultaneous Measurement of Strain and Temperature. *Sensors* **2018**, *18*, 915, doi:10.3390/s18030915.
39. Naeem, K.; Kwon, I.B.; Chung, Y. Multibeam interferometer using a photonic crystal fiber with two asymmetric cores for torsion, strain and temperature sensing. *Sensors (Switzerland)* **2017**, *17*, doi:10.3390/s17010132.
40. Li, C.; Ning, T.; Zhang, C.; Li, J.; Zhang, C.; Wen, X.; Lin, H.; Pei, L. All-fiber multipath Mach–Zehnder interferometer based on a four-core fiber for sensing applications. *Sensors Actuators, A Phys.* **2016**, *248*, 148–154, doi:10.1016/j.sna.2016.07.031.
41. Liu, S.; Meng, H.; Deng, S.; Wei, Z.; Wang, F.; Tan, C. Fiber Humidity Sensor Based on a Graphene-Coated Core-Offset Mach–Zehnder Interferometer. *IEEE Sensors Lett.*

- 2018**, 2, 1–4, doi:10.1109/lensens.2018.2849750.
42. Sun, H.; Shao, M.; Han, L.; Liang, J.; Zhang, R.; Fu, H. Large core-offset based in-fiber Michelson interferometer for humidity sensing. *Opt. Fiber Technol.* **2020**, *55*, 102153, doi:10.1016/j.yofte.2020.102153.
 43. Park, K.S.; Choi, H.Y.; Park, S.J.; Paek, U.; Lee, B.H. Temperature Robust Refractive Index Sensor Based on a Photonic Crystal Fiber Interferometer. *IEEE Sens. J.* **2010**, *10*, 1147–1148, doi:10.1109/JSEN.2009.2037510.
 44. Rong, Q.; Qiao, X.; Du, Y.; Feng, D.; Wang, R.; Ma, Y.; Sun, H.; Hu, M.; Feng, Z. In-fiber quasi-michelson interferometer with a core-cladding-mode fiber end-face mirror. *Appl. Opt.* **2013**, *52*, 1441–1447, doi:10.1364/AO.52.001441.
 45. Inaudi, D.; Casanova, N.; Vurpillot, S.; Kronenberg, P.; Martinola, G.; Steinmann, G.; Jean-Francois, M. SOFO: Structural monitoring with fiber optic sensors. In Proceedings of the Monitoring and Safety of Existing Concrete Structures; Vienna, 1999; pp. 1–13.
 46. Smartec SA SOFO Lite Reading Unit Datasheet 2015, 4.
 47. Li, A.; Wang, Y.; Hu, Q.; Shieh, W. Few-mode fiber based optical sensors. *Opt. Express* **2015**, *23*, 1139, doi:10.1364/oe.23.001139.
 48. He, X.; Ma, C.; Wang, X.; Wang, Z.; Yuan, L. Pressure vector sensor based on an orthogonal optical path Sagnac interferometer. *Opt. Express* **2020**, *28*, 7969, doi:10.1364/oe.388821.
 49. Campanella, C.E.; Cuccovillo, A.; Campanella, C.; Yurt, A.; Passaro, V.M.N. Fibre Bragg Grating based strain sensors: Review of technology and applications. *Sensors (Switzerland)* **2018**, *18*, doi:10.3390/s18093115.
 50. Allwood, G.; Wild, G.; Hinckley, S. Fiber bragg grating sensors for mainstream industrial processes. *Electron.* **2017**, *6*, 1–19, doi:10.3390/electronics6040092.
 51. Sylex s.r.o. Calibration coefficients of FFA-01 FBG sensor 2020.
 52. Han, K.J.; Lee, Y.W.; Kwon, J.; Roh, S.; Jung, J.; Lee, B. Simultaneous Measurement of Strain and Temperature Incorporating a Long-Period Fiber Grating Inscribed on a Polarization-Maintaining Fiber. *IEEE Photonics Technol. Lett.* **2004**, *16*, 2114–2116, doi:10.1109/LPT.2004.833081.
 53. Esposito, F.; Srivastava, A.; Iadicicco, A.; Campopiano, S. Multi-parameter sensor based on single Long Period Grating in Panda fiber for the simultaneous measurement of SRI, temperature and strain. *Opt. Laser Technol.* **2019**, doi:10.1016/j.optlastec.2018.12.022.
 54. Okabe, Y.; Tsuji, R.; Takeda, N. Application of chirped fiber Bragg grating sensors for identification of crack locations in composites. *Compos. Part A Appl. Sci. Manuf.* **2004**, *35*, 59–65, doi:10.1016/j.compositesa.2003.09.004.
 55. Rito, R.L.; Crocombe, A.D.; Ogin, S.L. Health monitoring of composite patch repairs using CFBG sensors: Experimental study and numerical modelling. *Compos. Part A Appl. Sci. Manuf.* **2017**, *100*, 255–268, doi:10.1016/j.compositesa.2017.05.012.
 56. Chehura, E.; James, S.W.; Tatam, R.P. Temperature and strain discrimination using a single tilted fibre Bragg grating. *Opt. Commun.* **2007**, *275*, 344–347, doi:10.1016/j.optcom.2007.03.043.

57. Albert, J.; Shao, L.Y.; Caucheteur, C. Tilted fiber Bragg grating sensors. *Laser Photonics Rev.* **2013**, *7*, 83–108, doi:10.1002/lpor.201100039.
58. Gafsi, R.; El-Sherif, M.A. Analysis of Induced-Birefringence Effects on Fiber Bragg Gratings. *Opt. Fiber Technol.* **2000**, doi:10.1006/ofte.2000.0333.
59. Chehura, E.; Ye, C.C.; Staines, S.E.; James, S.W.; Tatam, R.P. Characterization of the response of fibre Bragg gratings fabricated in stress and geometrically induced high birefringence fibres to temperature and transverse load. *Smart Mater. Struct.* **2004**, *13*, 888–895, doi:10.1088/0964-1726/13/4/027.
60. Bosia, F.; Giaccari, P.; Botsis, J.; Facchini, M.; Limberger, H.G.; Salathé, R.P. Characterization of the response of fibre Bragg grating sensors subjected to a two-dimensional strain field. *Smart Mater. Struct.* **2003**, *12*, 925–934, doi:10.1088/0964-1726/12/6/009.
61. Barnoski, M.K.; Rourke, M.D.; Jensen, S.M.; Melville, R.T. Optical time domain reflectometer. *Appl. Opt.* **1977**, *16*, 2375, doi:10.1364/AO.16.002375.
62. Farahani, M.A.; Gogolla, T. Spontaneous Raman scattering in optical fibers with modulated probe light for distributed temperature Raman remote sensing. *J. Light. Technol.* **1999**, *17*, 1379–1391, doi:10.1109/50.779159.
63. Sierra-Pérez, J. Smart Aeronautical Structures: Development And Experimental Validation Of A Structural Health Monitoring System For Damage Detection, Universidad Politecnica De Madrid, 2014.
64. Luna Inc. Optical Backscatter Reflectometry (OBR) - Overview And Applications Available online: <https://lunainc.com/sites/default/files/assets/files/resource-library/OBR - Overview and Applications.pdf>.
65. Soller, B.J.; Gifford, D.K.; Wolfe, M.S.; Froggatt, M.E. High resolution optical frequency domain reflectometry for characterization of components and assemblies Abstract : *Opt. Express* **2005**, *13*, 666–674, doi:10.1364/OPEX.13.000666.
66. OptaSense OptaSense QuantX™ Data Sheet 2022.
67. Luna Inc. ODiSI 6000 Series 2019, 6.
68. Konstantopoulos, S.; Hueber, C.; Antoniadis, I.; Summerscales, J.; Schledjewski, R. Liquid composite molding reproducibility in real-world production of fiber reinforced polymeric composites: a review of challenges and solutions. *Adv. Manuf. Polym. Compos. Sci.* **2019**, *5*, 85–99, doi:10.1080/20550340.2019.1635778.
69. Hueber, C.; Konstantopoulos, S.; Hergan, P.; Höfler, J.; Horejsi, K.; Schledjewski, R. Influence of Cure Monitoring on the Curing Cycle Time and the Associated Economic Impact. **2017**.
70. Torres, M. Parameters' monitoring and in-situ instrumentation for resin transfer moulding: A review. *Compos. Part A Appl. Sci. Manuf.* 2019.
71. Atkinson, G.A.; Nash, S.O.; Smith, L.N. Precision fibre angle inspection for carbon fibre composite structures using polarisation vision. *Electron.* **2021**, *10*, doi:10.3390/electronics10222765.
72. Rufai, O.; Chandarana, N.; Gautam, M.; Potluri, P.; Gresil, M. Cure monitoring and structural health monitoring of composites using micro-braided distributed optical fibre.

- Compos. Struct.* **2020**, *254*, 112861, doi:10.1016/j.compstruct.2020.112861.
73. Yadav, N.; Wachtarczyk, K.; Gašior, P.; Schledjewski, R.; Kaleta, J. In-line residual strain monitoring for thermoplastic automated tape layup using fiber Bragg grating sensors. *Polym. Compos.* **2022**, 1–13, doi:10.1002/pc.26480.
 74. Parlevliet, P.P.; Bersee, H.E.N.; Beukers, A. Residual stresses in thermoplastic composites-A study of the literature-Part I: Formation of residual stresses. *Compos. Part A Appl. Sci. Manuf.* **2006**, *37*, 1847–1857, doi:10.1016/j.compositesa.2005.12.025.
 75. Parlevliet, P.P.; Bersee, H.E.N.; Beukers, A. Residual stresses in thermoplastic composites-A study of the literature-Part I: Formation of residual stresses. *Compos. Part A Appl. Sci. Manuf.* **2006**, doi:10.1016/j.compositesa.2005.12.025.
 76. Parlevliet, P.P.; Bersee, H.E.N.; Beukers, A. Residual stresses in thermoplastic composites - a study of the literature. Part III: Effects of thermal residual stresses. *Compos. Part A Appl. Sci. Manuf.* **2007**, *38*, 1581–1596, doi:10.1016/j.compositesa.2006.12.005.
 77. Seers, B.; Tomlinson, R.; Fairclough, P. Residual stress in fiber reinforced thermosetting composites: A review of measurement techniques. *Polym. Compos.* **2021**, *42*, 1631–1647, doi:10.1002/pc.25934.
 78. Luo, G.; Liou, G.; Xiao, H. Using a Fiber Bragg Grating Sensor to Measure Residual Strain in the Vacuum-Assisted Resin Transfer Molding Process. *Polymers (Basel)*. **2022**, *14*, 1446, doi:10.3390/polym14071446.
 79. Tsukada, T.; Minakuchi, S.; Takeda, N. Identification of process-induced residual stress/strain distribution in thick thermoplastic composites based on in situ strain monitoring using optical fiber sensors. *J. Compos. Mater.* **2019**, *53*, 3445–3458, doi:10.1177/0021998319837199.
 80. Waris, M.; Liotier, P.J.; Drapier, S. Effect of the mold on the residual strain field monitored with optical fibers sensors in resin transfer molding processes. *J. Compos. Mater.* **2014**, *48*, 2589–2601, doi:10.1177/0021998313501532.
 81. Rocha, H.; Semprimoschnig, C.; Nunes, J.P. Small-diameter optical fibre sensor embedment for ambient temperature cure monitoring and residual strain evaluation of CFRP composite laminates produced by vacuum-assisted resin infusion. *CEAS Sp. J.* **2021**, *13*, 353–367, doi:10.1007/s12567-021-00357-5.
 82. Prussak, R.; Stefaniak, D.; Hühne, C.; Sinapius, M. Evaluation of residual stress development in FRP-metal hybrids using fiber Bragg grating sensors. *Prod. Eng.* **2018**, *12*, 259–267, doi:10.1007/s11740-018-0793-4.
 83. Lammens, N.; Kinet, D.; Chah, K.; Luyckx, G.; Caucheteur, C.; Degrieck, J.; Mégret, P. Residual strain monitoring of out-of-autoclave cured parts by use of polarization dependent loss measurements in embedded optical fiber Bragg gratings. *Compos. Part A* **2013**, *52*, 38–44, doi:10.1016/j.compositesa.2013.05.005.
 84. Matsuzaki, R.; Kobayashi, S.; Todoroki, A.; Mizutani, Y. Full-field monitoring of resin flow using an area-sensor array in a VaRTM process. *Compos. Part A Appl. Sci. Manuf.* **2011**, *42*, 550–559, doi:10.1016/j.compositesa.2011.01.014.
 85. Hardis, R.; Jessop, J.L.P.; Peters, F.E.; Kessler, M.R. Cure kinetics characterization and monitoring of an epoxy resin using DSC, Raman spectroscopy, and DEA. *Compos. Part*

- A Appl. Sci. Manuf.* **2013**, *49*, 100–108, doi:10.1016/j.compositesa.2013.01.021.
86. Hergan, P. Entwicklung einer modellbasierten Fertigungstechnik zur intrinsischen Herstellung von hybriden Verbundwerkstoffen, Montanuniversität Leoben, Leoben, Austria, 2019.
 87. Afromowitz, M.A.; Lam, K.Y. The optical properties of curing epoxies and applications to the fiber-optic epoxy cure sensor. *Sensors Actuators A. Phys.* **1990**, *23*, 1107–1110, doi:10.1016/0924-4247(90)87097-3.
 88. Hirota, I.; Takeda, S.; Ogasawara, T. Evaluation of thermosetting resin curing using a tilted fiber Bragg grating. *Compos. Part A Appl. Sci. Manuf.* **2022**, *158*, 106956, doi:10.1016/j.compositesa.2022.106956.
 89. Fazzi, L.; Struzziero, G.; Dransfeld, C.; Groves, R.M. A single three-parameter tilted fibre Bragg grating sensor to monitor the thermosetting composite curing process. *Adv. Manuf. Polym. Compos. Sci.* **2022**, *8*, 33–41, doi:10.1080/20550340.2022.2041221.
 90. Wong, R.Y.N.; Chehura, E.; James, S.W.; Tatam, R.P. Resin Directional Flow and Degree of Cure Sensing Using Chirped Optical Fiber Long Period Gratings. *IEEE Sens. J.* **2017**, *17*, 6605–6614, doi:10.1109/JSEN.2017.2739422.
 91. Sampath, U.; Kim, H.; Kim, D.; Kim, Y.; Song, M. In-Situ Cure Monitoring of Wind Turbine Blades by Using Fiber Bragg Grating Sensors and Fresnel Reflection Measurement. *Sensors* **2015**, *15*, 18229–18238, doi:10.3390/s150818229.
 92. Keulen, C.J.; Yildiz, M.; Suleman, A. Multiplexed FBG and etched fiber sensors for process and health monitoring of 2- & 3-D RTM components. *J. Reinf. Plast. Compos.* **2011**, *30*, 1055–1064, doi:10.1177/0731684411411960.
 93. Keulen, C.; Rocha, B.; Yildiz, M.; Suleman, A. Embedded fiber optic sensors for monitoring processing, quality and structural health of resin transfer molded components. *J. Phys. Conf. Ser.* **2011**, *305*, doi:10.1088/1742-6596/305/1/012135.
 94. Yildiz, M.; Ozdemir, N.G.; Bektas, G.; Keulen, C.J.; Boz, T.; Sengun, E.F.; Ozturk, C.; Menciloglu, Y.Z.; Suleman, A. An experimental study on the process monitoring of resin transfer molded composite structures using fiber optic sensors. *J. Manuf. Sci. Eng. Trans. ASME* **2012**, *134*, 1–6, doi:10.1115/1.4006770.
 95. Chiesura, G.; Lamberti, A.; Yang, Y.; Luyckx, G.; Van Paepegem, W.; Vanlanduit, S.; Vanfleteren, J.; Degrieck, J. RTM production monitoring of the A380 hinge arm droop nose mechanism: A multi-sensor approach. *Sensors (Switzerland)* **2016**, *16*, 1–17, doi:10.3390/s16060866.
 96. Chiesura, G. Interaction of Composites with Various Types of Embedded Sensors and Their Use for Cure and Fatigue Life, Ghent University, 2017.
 97. Hoffman, J.; Khadka, S.; Kumosa, M. Determination of gel point and completion of curing in a single fiber/polymer composite. *Compos. Sci. Technol.* **2020**, doi:10.1016/j.compscitech.2020.107997.
 98. Karalekas, D.; Cugnoni, J.; Botsis, J. Monitoring of process induced strains in a single fibre composite using FBG sensor: A methodological study. *Compos. Part A Appl. Sci. Manuf.* **2008**, *39*, 1118–1127, doi:10.1016/j.compositesa.2008.04.010.
 99. Minakuchi, S. In situ characterization of direction-dependent cure-induced shrinkage in

- thermoset composite laminates with fiber-optic sensors embedded in through-thickness and in-plane directions. *J. Compos. Mater.* **2015**, *49*, 1021–1034, doi:10.1177/0021998314528735.
100. Chehura, E.; Skordos, A.A.; Ye, C.C.; James, S.W.; Partridge, I.K.; Tatam, R.P. Strain development in curing epoxy resin and glass fibre/epoxy composites monitored by fibre Bragg grating sensors in birefringent optical fibre. *Smart Mater. Struct.* **2005**, *14*, 354–362, doi:10.1088/0964-1726/14/2/009.
 101. Collombet, F.; Torres, M.; Douchin, B.; Crouzeix, L.; Grunevald, Y.H.; Lubin, J.; Camps, T.; Jacob, X.; Luyckx, G.; Wu, K.T. Multi-instrumentation monitoring for the curing process of a composite structure. *Meas. J. Int. Meas. Confed.* **2020**, *157*, doi:10.1016/j.measurement.2020.107635.
 102. Sonnenfeld, C.; Luyckx, G.; Collombet, F.; Grunevald, Y.-H.; Douchin, B.; Crouzeix, L.; Torres, M.; Geernaert, T.; Sulejmani, S.; Eve, S.; et al. Embedded fiber Bragg gratings in photonic crystal fiber for cure cycle monitoring of carbon fiber-reinforced polymer materials. In Proceedings of the Micro-structured and Specialty Optical Fibres II; Kalli, K., Kanka, J., Mendez, A., Eds.; SPIE, 2013; Vol. 8775, pp. 1–10.
 103. Singh, A.K.; Berggren, S.; Zhu, Y.; Han, M.; Huang, H. Simultaneous strain and temperature measurement using a single fiber Bragg grating embedded in a composite laminate. *Smart Mater. Struct.* **2017**, *26*, 115025, doi:10.1088/1361-665X/aa91ab.
 104. Boller, C. Structural Health Monitoring -- Its Association and Use. In *New Trends in Structural Health Monitoring*; Ostachowicz, W., Güemes, J.A., Eds.; Springer Vienna: Vienna, 2013; pp. 1–79 ISBN 978-3-7091-1390-5.
 105. Shrestha, P.; Park, Y.; Kim, C.G. Low velocity impact localization on composite wing structure using error outlier based algorithm and FBG sensors. *Compos. Part B Eng.* **2017**, doi:10.1016/j.compositesb.2016.10.068.
 106. Lamberti, A.; Chiesura, G.; Luyckx, G.; Degrieck, J.; Kaufmann, M.; Vanlanduit, S. Dynamic strain measurements on automotive and aeronautic composite components by means of embedded fiber bragg grating sensors. *Sensors (Switzerland)* **2015**, *15*, 27174–27200, doi:10.3390/s151027174.
 107. Mieloszyk, M.; Ostachowicz, W. An application of Structural Health Monitoring system based on FBG sensors to offshore wind turbine support structure model. *Mar. Struct.* **2017**, *51*, 65–86, doi:10.1016/j.marstruc.2016.10.006.
 108. Gašior, P.; Malesa, M.; Kaleta, J.; Kujawińska, M.; Malowany, K.; Rybczyński, R. Application of complementary optical methods for strain investigation in composite high pressure vessel. *Compos. Struct.* **2018**, doi:10.1016/j.compstruct.2018.07.060.
 109. Zhang, W.; Zhang, M.; Wang, X.; Zhao, Y.; Jin, B.; Dai, W. The analysis of FBG central wavelength variation with crack propagation based on a self-adaptive multi-peak detection algorithm. *Sensors (Switzerland)* **2019**, *19*, doi:10.3390/s19051056.
 110. Shrestha, P.; Kim, J.H.; Park, Y.; Kim, C.G. Impact localization on composite structure using FBG sensors and novel impact localization technique based on error outliers. *Compos. Struct.* **2016**, *142*, 263–271, doi:10.1016/j.compstruct.2016.01.088.
 111. Majewska, K.; Opoka, S.; Kudela, P.; Ostachowicz, W. Novel FBG rosette for determining impact location in thin plate-like structure. *J. Phys. Conf. Ser.* **2015**, *628*,

- 012118, doi:10.1088/1742-6596/628/1/012118.
112. Takeda, S.; Okabe, Y.; Takeda, N. Detection of delamination in composite laminates using small-diameter FBG sensors. **2002**, *4694*, 138–148.
 113. Zhang, G.; Tang, L.; Zhou, L.; Liu, Z.; Liu, Y.; Jiang, Z. Principal component analysis method with space and time windows for damage detection. *Sensors (Switzerland)* **2019**, *19*, doi:10.3390/s19112521.
 114. Lu, S.; Jiang, M.; Wang, X.; Yu, H. Damage detection method of CFRP structure based on fiber Bragg grating and principal component analysis. *Optik (Stuttg.)*. **2019**, doi:10.1016/j.ijleo.2018.10.055.
 115. Sierra-Pérez, J.; Torres-Arredondo, M.A.; Alvarez-Montoya, J. Damage detection methodology under variable load conditions based on strain field pattern recognition using FBGs, nonlinear principal component analysis, and clustering techniques. *Smart Mater. Struct.* **2018**, *27*, doi:10.1088/1361-665X/aa9797.
 116. Salehi, H.; Burgueño, R. Emerging artificial intelligence methods in structural engineering. *Eng. Struct.* 2018.
 117. Lawrence, C.M.; Nelson, D. V; Udd, E. Measurement of transverse strains with fiber Bragg gratings. In Proceedings of the Proceedings of SPIE; SPIE: San Diego, 1997; Vol. 3042, pp. 218–228.
 118. Goossens, S.; Geernaert, T.; De Pauw, B.; Lamberti, A.; Vanlanduit, S.; Luyckx, G.; Chiesura, G.; Thienpont, H.; Berghmans, F. Dynamic 3D strain measurements with embedded micro-structured optical fiber Bragg grating sensors during impact on a CFRP coupon. *25th Int. Conf. Opt. Fiber Sensors* **2017**, *10323*, 1032360, doi:10.1117/12.2263193.
 119. De Pauw, B.; Goossens, S.; Geernaert, T.; Habas, D.; Thienpont, H.; Berghmans, F. Fibre bragg gratings in embedded microstructured optical fibres allow distinguishing between symmetric and anti-symmetric lamb waves in carbon fibre reinforced composites. *Sensors (Switzerland)* **2017**, *17*, doi:10.3390/s17091948.
 120. Zhang, X.; Chen, R.; Wang, A.; Xu, Y.; Jiang, Y.; Ming, H.; Zhao, W. Monitoring the failure forms of a composite laminate system by using panda polarization maintaining fiber Bragg gratings. *Opt. Express* **2019**, *27*, 17571–17580, doi:10.1364/OE.27.017571.
 121. Luyckx, G.; Voet, E.; Lammens, N.; De Waele, W.; Degrieck, J. Residual strain-induced birefringent FBGs for multi-axial strain monitoring of CFRP composite laminates. *NDT E Int.* **2013**, doi:10.1016/j.ndteint.2012.11.008.
 122. Iadicicco, A.; Natale, D.; Palma, P. Di; Spinaci, F.; Apicella, A.; Campopiano, S. Strain monitoring of a composite drag strut in aircraft landing gear by fiber bragg grating sensors. *Sensors (Switzerland)* **2019**, *19*, 1–13, doi:10.3390/s19102239.
 123. Gaşior, P.; Wachtarczyk, K.; Błachut, A.; Kaleta, J.; Yadav, N.; Ozga, M.; Baron, A. Validation of Selected Optical Methods for Assessing Polyethylene (PE) Liners Used in High Pressure Vessels for Hydrogen Storage. *Appl. Sci.* **2021**, *11*, 5667, doi:10.3390/app11125667.
 124. Born, M.; Wolf, E. *Principles of Optics*; 7th Editio.; Cambridge University Press: Cambridge, 2019; ISBN 9781108769914.

125. Danpl Image of refraction properties of Calcite 2018.
126. Anuszkiewicz, A. Metrologiczne właściwości polaryzacyjnych siatek długookresowych wytworzonych w światłowodach mikrostrukturalnych, Wrocław University Of Science And Technology, 2012.
127. Noda, J.; Okamoto, K.; Sasaki, Y. Polarization-Maintaining Fibers and Their Applications. *J. Light. Technol.* **1986**, *4*, 1071–1089, doi:10.1109/JLT.1986.1074847.
128. Wachtarczyk, K.; Gąsior, P.; Kaleta, J.; Anuszkiewicz, A.; Bender, M.; Schledjewski, R.; Mergo, P.; Osuch, T. In-Plane Strain Measurement in Composite Structures with Fiber Bragg Grating Written in Side-Hole Elliptical Core Optical Fiber. *Materials (Basel)*. **2021**, *15*, 77, doi:10.3390/ma15010077.
129. Sulejmani, S.; Sonnenfeld, C.; Geernaert, T.; Berghmans, F.; Thienpont, H.; Eve, S.; Lammens, N.; Luyckx, G.; Voet, E.; Degrieck, J.; et al. Towards micro-structured optical fiber sensors for transverse strain sensing in smart composite materials. *Proc. IEEE Sensors* **2011**, 109–112, doi:10.1109/ICSENS.2011.6127305.
130. Statkiewicz-Barabach, G. Badania eksperymentalne światłowodów mikrostrukturalnych do zastosowań pomiarowych, Wrocław University of Science And Technology, 2007.
131. Martynkien, T.; Statkiewicz-Barabach, G.; Olszewski, J.; Wojcik, J.; Mergo, P.; Geernaert, T.; Sonnenfeld, C.; Anuszkiewicz, A.; Szczurowski, M.K.; Tarnowski, K.; et al. Highly birefringent microstructured fibers with enhanced sensitivity to hydrostatic pressure. *Opt. Express* **2010**, *18*, 15113, doi:10.1364/oe.18.015113.
132. Kashyap, R. *Fiber Bragg Gratings*; Optics and Photonics; Elsevier Science, 2009; ISBN 9780080919911.
133. Guemes, J.A.; Menéndez, J.M. Response of Bragg grating fiber-optic sensors when embedded in composite laminates. *Compos. Sci. Technol.* **2002**, doi:10.1016/S0266-3538(02)00010-6.
134. Bertholds, A.; Dändliker, R. Deterination of the Individual Strain-Optic Coefficients in Single-mode Optical Fibers. *J. Light. Technol.* **1988**, *6*, 17–20, doi:10.1109/50.3956.
135. Sonnenfeld, C.; Sulejmani, S.; Geernaert, T.; Eve, S.; Lammens, N.; Luyckx, G.; Voet, E.; Degrieck, J.; Urbanczyk, W.; Mergo, P.; et al. Microstructured optical fiber sensors embedded in a laminate composite for smart material applications. *Sensors* **2011**, *11*, 2566–2579, doi:10.3390/s110302566.
136. He, J.; Xu, B.; Ju, S.; Hou, M.; Guo, K.; Xu, X.; Wang, Y.; Liu, S.; Wang, Y. Temperature-insensitive directional transverse load sensor based on dual side-hole fiber Bragg grating. *Opt. Express* **2021**, *29*, 17700, doi:10.1364/oe.415082.
137. Luyckx, G.; De Waele, W.; Degrieck, J.; Van Paepegem, W.; Vlekken, J.; Verbeke, T. Feasibility study of an embedded multi-axial fibre Bragg grating sensor. *Opt. Sens. Technol. Appl.* **2007**, 6585, 65850E, doi:10.1117/12.722863.
138. Martynkien, T.; Wojcik, G.; Mergo, P.; Urbanczyk, W. Highly birefringent polymer side-hole fiber for hydrostatic pressure sensing. *Opt. Lett.* **2015**, *40*, 3033, doi:10.1364/ol.40.003033.
139. Anuszkiewicz, A.; Martynkien, T.; Olszewski, J.; Mergo, P.; Urbańczyk, W. Polarimetric sensitivity to hydrostatic pressure and temperature in a side-hole fiber with

- squeezed microstructure. *J. Opt. (United Kingdom)* **2015**, *17*, doi:10.1088/2040-8978/17/12/125609.
140. Lawrence, C.M.; Nelson, D. V.; Udd, E.; Bennett, T. A fiber optic sensor for transverse strain measurement. *Exp. Mech.* **1999**, *39*, 202–209, doi:10.1007/BF02323553.
 141. Xie, H.M.; Okamoto, K.; Dabkiewicz, P.; Ulrich, R. Side-hole fiber for fiber-optic pressure sensing. *Opt. Lett.* **1986**, *11*, 333, doi:10.1364/ol.11.000333.
 142. Gouws, A.; Ford, K.R.; Jones, B.H. Transverse strain measurements in polymer-embedded, polarization-maintaining fiber bragg gratings. *Eng. Res. Express* **2020**, *2*, doi:10.1088/2631-8695/abc307.
 143. Anuszkiewicz, A.; Martynkien, T.; Mergo, P.; Makara, M.; Urbanczyk, W. Sensing and transmission characteristics of a rocking filter fabricated in a side-hole fiber with zero group birefringence. *Opt. Express* **2013**, *21*, 12657, doi:10.1364/oe.21.012657.
 144. Sadeghi, J.; Latifi, H.; Murawski, M.; Mirkhosravi, F.; Nasilowski, T.; Mergo, P.; Poturaj, K. Group polarimetric pressure sensitivity of an elliptical-core side-hole fiber at telecommunication wavelengths. *IEEE J. Sel. Top. Quantum Electron.* **2016**, *22*, 49–54, doi:10.1109/JSTQE.2015.2435896.
 145. Wójcik, J.; Urbańczyk, W.; Bock, W.J.; Janoszczyk, B.; Mergo, P.; Makara, M.; Poturaj, K.; Spytek, W. Prototype of the side-hole HB optical fiber. In Proceedings of the Optical Fibers and Their Applications VI; Dorosz, J., Romaniuk, R.S., Eds.; 1999; Vol. 3731, pp. 88–93.
 146. Shlyagin, M.G.; Khomenko, A. V; Tentori, D. Birefringence dispersion measurement in optical fibers by wavelength scanning. *Opt. Lett.* **1995**, *20*, 869–871.
 147. Calvani, R.; Caponi, R.; Cisternino, F. Polarization measurements on single-mode fibers. *J. Light. Technol.* **1989**, *7*, 1187–1196, doi:10.1109/50.32381.
 148. Geernaert, T.; Becker, M.; Mergo, P.; Nasilowski, T.; Wójcik, J.; Urbańczyk, W.; Rothhardt, M.; Chojetzki, C.; Bartelt, H.; Terryn, H.; et al. Bragg grating inscription in GeO₂-doped microstructured optical fibers. *J. Light. Technol.* **2010**, *28*, 1459–1467, doi:10.1109/JLT.2010.2043414.
 149. Luyckx, G. Multiaxial Strain Monitoring of Fibre Reinforced Thermosetting Plastics Using Embedded Highly Birefringent Optical Fibre Bragg Sensors, Ghent University, 2009.
 150. Ye, C.C.; Staines, S.E.; James, S.W.; Tatam, R.P. A polarisation maintaining fibre Bragg grating interrogation system for multi-axis strain sensing. *2002 15th Opt. Fiber Sensors Conf. Tech. Dig. OFS 2002* **2002**, *4694*, 179–182, doi:10.1109/OFS.2002.1000531.
 151. Lamberti, A.; Vanlanduit, S.; De Pauw, B.; Berghmans, F. Influence of fiber bragg grating spectrum degradation on the performance of sensor interrogation algorithms. *Sensors (Switzerland)* **2014**, *14*, 24258–24277, doi:10.3390/s141224258.
 152. Huang, C.; Jing, W.; Liu, K.; Zhang, Y.; Peng, G. Demodulation of Fiber Bragg Grating Sensor Using Cross-correlation Algorithm. *IEEE Photonics Technol. Lett.* **2007**, *19*, 707–709, doi:10.1109/LPT.2007.895422.
 153. Lamberti, A.; Vanlanduit, S.; Pauw, B. De; Berghmans, F. A novel fast phase correlation algorithm for peak wavelength detection of fiber Bragg grating sensors. *Opt. Express*

2014, 22, 7099–7112, doi:10.1364/OE.22.007099.

154. Fernandez, A.F.; Ottevaere, H.; Ierschot, C. Van; Panajatov, K. Multi-parameter force sensing with fiber Bragg grating sensors. *Symp. A Q. J. Mod. Foreign Lit.* **2002**, 139–142, doi:10.1109/TNET.2017.2653102.
155. He, J.; Xu, B.; Ju, S.; Hou, M.; Guo, K.; Xu, X.; Wang, Y.; Liu, S.; Wang, Y. Temperature-insensitive directional transverse load sensor based on dual side-hole fiber Bragg grating. *Opt. Express* **2021**, 29, 17700, doi:10.1364/OE.415082.
156. Pannell, C.N.; Tatam, R.P.; Jones, J.D.C.; Jackson, D.A. Fibre-optic frequency shifter utilizing travelling flexure waves in birefringent fibre. *J. Inst. Electron. Radio Eng.* **1988**, 58, doi:10.1049/jiere.1988.0042.
157. Hao, P.; Yu, C.; Feng, T.; Zhang, Z.; Qin, M.; Zhao, X.; He, H.; Yao, X.S. PM fiber based sensing tapes with automated 45° birefringence axis alignment for distributed force/pressure sensing. *Opt. Express* **2020**, 28, 18829, doi:10.1364/oe.391376.
158. Zheng, W. Automated fusion-splicing of polarization maintaining fibers. *J. Light. Technol.* **1997**, 15, 125–134, doi:10.1109/50.552120.
159. Hindersmann, A. Confusion about infusion: An overview of infusion processes. *Compos. Part A* **2019**, 126, 105583, doi:10.1016/j.compositesa.2019.105583.
160. Advani, S.G.; Sozer, E.M. *Process Modeling in Composites Manufacturing*; Advani, S.G., Sozer, E.M., Eds.; CRC Press: Boca Raton, 2010; ISBN 9780429166235.
161. Jensen, D.W.; Pascual, J. Degradation of graphite/bismaleimide laminates with multiple embedded fiber optic sensors. In Proceedings of the Fiber Optic Smart Structures and Skins; Claus, R.O., Udd, E., Eds.; 1990; Vol. 1370, p. 228.
162. Chen, C.; Wu, Q.; Xiong, K.; Zhai, H.; Yoshikawa, N.; Wang, R. Hybrid temperature and stress monitoring of woven fabric thermoplastic composite using fiber bragg grating based sensing technique. *Sensors (Switzerland)* **2020**, 20, doi:10.3390/s20113081.
163. Sozer, E.M.; Simacek, P.; Advani, S.G. Resin transfer molding (RTM) in polymer matrix composites. In *Manufacturing Techniques for Polymer Matrix Composites (PMCs)*; Elsevier, 2012; pp. 245–309.
164. Khoun, L.; De Oliveira, R.; Michaud, V.; Hubert, P. Investigation of process-induced strains development by fibre Bragg grating sensors in resin transfer moulded composites. *Compos. Part A Appl. Sci. Manuf.* **2011**, 42, 274–282, doi:10.1016/j.compositesa.2010.11.013.
165. Tsai, J.T.; Dustin, J.S.; Mansson, J.A. Cure strain monitoring in composite laminates with distributed optical sensor. *Compos. Part A Appl. Sci. Manuf.* **2019**, 125, 105503, doi:10.1016/j.compositesa.2019.105503.
166. Hexion Inc. Technical Data Sheet EPIKOTE Resin and EPIKURE Curing Agent 2022, 5.
167. Kaye, G.W.C.; Laby, T.H. *Tables of physical & chemical constants, 16th Edition*; Longman Science & Tech: Middlessex, England, 1995; ISBN 0-582-22629-5.
168. Wachtarczyk, K.; Bender, M.; Fauster, E.; Schledjewski, R.; Gašior, P.; Kaleta, J. Gel Point Determination in Resin Transfer Molding Process with Fiber Bragg Grating Inscribed in Side-Hole Elliptical Core Optical Fiber. *Materials (Basel)*. **2022**, 15, 6497,

doi:10.3390/ma15186497.

169. Ramakrishnan, M.; Rajan, G.; Semenova, Y.; Farrell, G. Overview of fiber optic sensor technologies for strain/temperature sensing applications in composite materials. *Sensors (Switzerland)* **2016**, *16*, doi:10.3390/s16010099.
170. bto-epoxy GmbH Datasheet: Epinal IR 77.55-A1 - IH 77.55-B1 2015, 1–3.
171. ASTM ASTM D6272 Standard Test Method for Flexural Properties of Unreinforced and Reinforced Plastics and Electrical Insulating Materials by Four-Point Bending. *Annu. B. ASTM Stand.* **2017**, *02*, 1–9, doi:10.1520/D6272-17E01.1.
172. Sonmez, F.O.; Akbulut, M. Process optimization of tape placement for thermoplastic composites. *Compos. Part A Appl. Sci. Manuf.* **2007**, *38*, 2013–2023, doi:10.1016/j.compositesa.2007.05.003.
173. Lukaszewicz, D.H.J.A.; Ward, C.; Potter, K.D. The engineering aspects of automated prepreg layup: History, present and future. *Compos. Part B Eng.* **2012**, *43*, 997–1009, doi:10.1016/j.compositesb.2011.12.003.
174. Oromiehie, E.; Gangadhara Prusty, B.; Compston, P.; Rajan, G. In-situ simultaneous measurement of strain and temperature in automated fiber placement (AFP) using optical fiber Bragg grating (FBG) sensors. *Adv. Manuf. Polym. Compos. Sci.* **2017**, *3*, 52–61, doi:10.1080/20550340.2017.1317447.
175. Oromiehie, E.; Prusty, B.G.; Compston, P.; Rajan, G. Characterization of process-induced defects in automated fiber placement manufacturing of composites using fiber Bragg grating sensors. *Struct. Heal. Monit.* **2018**, *17*, 108–117, doi:10.1177/1475921716685935.
176. Saenz-Castillo, D.; Martín, M.I.; Calvo, S.; Güemes, A. Real-time monitoring of thermal history of thermoplastic automatic lamination with FBG sensors and process modelling validation. *Smart Mater. Struct.* **2020**, *29*, 115004, doi:10.1088/1361-665x/abaa97.
177. SGL Carbon Sigrapreg®TP Unidirectional tape based on carbon fiber-reinforced polyamide 6, C U157-0/NF-T340/46% 2018.
178. Frazão, O.; Ferreira, L.A.; Araújo, F.M.; Santos, J.L. Simultaneous measurement of strain and temperature using fibre Bragg gratings in a twisted configuration. *J. Opt. A Pure Appl. Opt.* **2005**, *7*, 427–430, doi:10.1088/1464-4258/7/8/014.
179. Chapman, T.J.; Gillespie, J.W.; Pipes, R.B.; Manson, J.A.E.; Seferis, J.C. Prediction of Process-Induced Residual Stresses in Thermoplastic Composites. *J. Compos. Mater.* **1990**, *24*, 616–643, doi:10.1177/002199839002400603.
180. Fricke, D.; Raps, L.; Schiel, I. Prediction of warping in thermoplastic AFP-manufactured laminates through simulation and experimentation. *Adv. Manuf. Polym. Compos. Sci.* **2022**, *8*, 1–10, doi:10.1080/20550340.2021.2015212.
181. Zhu, S.; Guo, Y.; Chen, Y.; Liu, S. Low water absorption, high-strength polyamide 6 composites blended with sustainable bamboo-based biochar. *Nanomaterials* **2020**, *10*, 1–15, doi:10.3390/nano10071367.
182. BASF Technical datasheet Polyamide 6 (Ultramid® 8202 HS) 2023.
183. Böckl, B.; Wedel, A.; Misik, A.; Drechsler, K. Effects of defects in automated fiber placement laminates and its correlation to automated optical inspection results. *J. Reinf.*

Plast. Compos. **2023**, *42*, 3–16, doi:10.1177/07316844221093273.

184. Woigk, W.; Hallett, S.R.; Jones, M.I.; Kuhtz, M.; Hornig, A.; Gude, M. Experimental investigation of the effect of defects in Automated Fibre Placement produced composite laminates. *Compos. Struct.* **2018**, *201*, 1004–1017, doi:10.1016/j.compstruct.2018.06.078.
185. Sciamé, G.; Rigamonti, D.; Bettini, P.; Tagliabue, P.; Sala, G. An Integrated Fiber Optic Based SHM System for Structural Composite Components: Application to a Racing Motorbike Fork. In Proceedings of the European Workshop on Structural Health Monitoring; Rizzo, P., Milazzo, A., Eds.; Springer International Publishing: Cham, 2023; pp. 933–942.
186. Rigamonti, D.; Bettini, P. Enabling FO-Based HUMS Applications Through an Innovative Integration Technique: Application to a Rotor Blade Mockup. In Proceedings of the European Workshop on Structural Health Monitoring; Rizzo, P., Milazzo, A., Eds.; Springer International Publishing: Cham, 2023; pp. 921–932.